

THE UNIVERSITY
of EDINBURGH

This thesis has been submitted in fulfilment of the requirements for a postgraduate degree (e.g. PhD, MPhil, DClinPsychol) at the University of Edinburgh. Please note the following terms and conditions of use:

This work is protected by copyright and other intellectual property rights, which are retained by the thesis author, unless otherwise stated.
A copy can be downloaded for personal non-commercial research or study, without prior permission or charge.
This thesis cannot be reproduced or quoted extensively from without first obtaining permission in writing from the author.
The content must not be changed in any way or sold commercially in any format or medium without the formal permission of the author.
When referring to this work, full bibliographic details including the author, title, awarding institution and date of the thesis must be given.

Reconstruction of the San Lorenzo Ice Cap during the Last Glacial Cycle: Insights into the build-up and demise of the last Patagonian Ice Sheet

Monika Mendelová



THE UNIVERSITY
of EDINBURGH

Thesis submitted in fulfilment of the requirements for the degree of
Doctor of Philosophy
to the
University of Edinburgh
2020

Declaration

The work presented in this thesis is original and my own, unless indicated otherwise as part of collaborative publications. I declare that this thesis, either in whole or in part, has not been submitted for any other degree or professional qualification.

Monika Mendelová
January 2020

Abstract

Patagonia in southernmost South America is situated in a climatically sensitive region of the Southern Hemisphere. It is the only stretch of land to fully intersect the southern westerly wind belt, an important component of the global climate system. Robust glacial chronologies from this region can help unravel the interhemispheric (a-)synchronicity of climate events and the underlying drivers of glaciation and climate change. Despite exceptional preservation of moraine records in Patagonia, little is known about the build-up and the evolution of the last Patagonian Ice Sheet (PIS) throughout the entire last glacial cycle. The response of glaciers to abrupt climate events during the last deglaciation and glacier change during the Holocene remain poorly resolved in many parts of Patagonia. This thesis reconstructs the extent and timing of glacial advances and the evolution of palaeolakes on the eastern side of Monte San Lorenzo. This site was chosen for its well preserved geomorphological record and the potential to yield new insights in the glacial and climate history of the region.

Geomorphological mapping revealed three landform assemblages. In the Belgrano valley, the geomorphology is dominated by three large moraine systems and associated outwash terraces deposited during advances of the former Belgrano glacier. Once the Belgrano glacier retreated to within its trough, the geomorphology is dominated by glaciolacustrine landforms documenting a formation of a higher, palaeolake Belgrano. Nearer the mountains, moraines, flutes and active outwash tracts evidence recent, Holocene mountain glaciation. Cosmogenic nuclide exposure dating reveals that the maximum extent of the Belgrano glacier occurred at $\sim$ 75 ka, towards the end of Marine Isotope Stage (MIS) 5. The second advance dated at $\sim$ 25 ka, coincident with the global Last Glacial Maximum (gLGM), was significantly smaller. Third advance of the Belgrano glacier was dated at $\sim$ 13 ka, coeval with Antarctic Cold Reversal (ACR). Subsequent rapid ice retreat, accompanied by a palaeolake development, was interrupted by a short ice marginal stabilisation during the Northern Hemisphere (NH) Younger Dryas (YD). After this, glaciers withdrew to the mountains and the palaeolake drained, marking the final demise of the PIS. Finally, a Holocene advance/still-stand of the San Lorenzo glacier is constrained to 2.8 $\pm$ 0.2 ka. An ELA lowering of 221 - 271 m relative to the present was required to match this limit, which translates to a temperatures decrease of $\sim$ 1.3 - 1.6 $^{\circ}$ C assuming an adiabatic lapse rate of 0.6 $^{\circ}$C / 100 m and no change in precipitation. The late Holocene advance coincided

with a climatic deterioration observed regionally and worldwide, and may have been caused by reduced solar activity at the time.

The main implications of this work are as follows: 1) Glaciation of the Patagonian Andes initiated early in the last glacial cycle. 2) The topography, catchment size and the shifting ice divides played an important role in determining the magnitude of glacier advances. 3) During the last glacial-interglacial transition (LGIT), glaciers in the region responded to a dominant Antarctic climate signal, and to lesser extent to the NH YD signal. 4) During the Holocene, glaciers in Patagonia achieved greater extent prior to the last millennium and the overall pattern of Holocene glacier change contrasts with that observed in New Zealand.

Lay summary

Patagonia in southernmost South America was once covered by an ice sheet over 2,000 km long. Glaciers extended from the Andean mountains to the Pacific Ocean in the west and the Patagonian plains in the east. Glaciers grew and shrank with a changing climate and left an imprint in the landscape. Landforms left behind by glaciers serve as archives of past climate and environmental change. In this thesis, I extract information from these archives to document how glaciers in Patagonia changed during the last ice age. This helps us to better understand how the climate was changing during the last ice age and what was causing it, how sensitive glaciers were to small, but rapid changes in climate in the past and how they may respond to present and future climate change.

This thesis revealed that an extensive mountain ice cap developed over the Patagonian Andes at the beginning of the last ice age, about 75,000 years ago. This the first evidence for the expansion of ice during the first half of the last ice age in Patagonia. While we know relatively a lot about ice extent around the world during the peak of the last ice age, it is much harder to find evidence during earlier stages. The growth of ice at this time was likely caused by the Southern Hemisphere receiving less energy from the Sun. As the world was emerging from the last ice age, glaciers were retreating rapidly but were very sensitive to small, rapid changes in climate. The results presented in this thesis show that a brief cooling in Antarctica and the Southern Ocean enabled glaciers to expand about 13,000 ago. Glaciers then disappeared from the Patagonian plains due to a warming climate and large lakes formed in the valleys that had been carved by glaciers. During the last 10,000 years, the so-called Holocene, glaciers were confined to the mountains valleys, much like today, but grew and shrunk several times.

Acknowledgements

I dedicate this thesis to my grandmother who always supported me and sadly could not see this thesis come to completion.

* * *

First of all, I would like to thank my supervisor Andy Hein for his support and guidance throughout my PhD, for his company in the field and for introducing me to the art of rock hammering, for his prompt comments on grant applications and manuscript draft, and for supporting my ventures outside of the PhD.

Many thanks go to Ángel Rodés for teaching me the chemistry of cosmogenic nuclides and his positive spirit in the days of rock crushing and lab work in East Kilbride. I wish to thank Bob McCulloch who became a co-author on a review paper that came out of this PhD; I benefited from his extensive knowledge of Quaternary environmental change in Patagonia. Special thanks go to David Sugden for his wisdom and enthusiasm. I extend my thanks to the laboratory technicians Elaine at the University of Edinburgh and Jenny Bradley at the University of Liverpool.

During my time in Edinburgh, I was lucky to teach on undergraduate fieldtrips to Iceland in three consecutive years. I am thankful to Andy Dugmore for sharing his knowledge of Iceland and for making these trips such a blast. I would like to thank everyone in the Lower Lewis office (past and present) for creating an enjoyable atmosphere. Many thanks go to Boris, Laura, Rosie, Charlie, Polly, Delf, Josh, Louis, Luca, Damon and Fiona for keeping me entertained and sane, for beers, chats and great fieldtrips. Special thanks go to Lauren for her friendship and her *'girl's power'* which continues to inspire me.

I am indebted to an endless number of friendly people I met during my fieldwork in Argentina. Special thanks go to Patricio Parada for his enormous effort in arranging paper work for exporting my samples two hours before my flight. The number of signatures from the country's export custom office testifies what a mission it was! Thank you also to Mary-Jo and Guillermo from Instituto

de Arqueología in Buenos Aires for invaluable logistical advice and for storing 120 kg of rock samples in their office while I traveled. I am grateful to the national park authorities of Argentina for granting permission to work in the Perito Moreno National Park. I appreciate support from park rangers, in particular the occasional opportunity to take a shower and wash off Patagonian dust. The director of the Geological Institute of Argentina kindly provided a letter of support when I knocked on his door. Thanks also to that person who stopped to help when I was changing a wheel by myself at dusk in the middle of nowhere. Muchas gracias. I hope that one day I can return these favors. Patagonia and Argentina will always have a place in my heart.

A v neposlednom rade by som sa chcela pod'akovat' mojím rodičom, Lucke, Zdenke, Lýdii a Milanovi, starkej a starkému za neutíchajúcu podporu, aj ked' sa možno často pýtali čo to vlastne robím a na čo mi je tol'ko diplomov.

Finally, and most importantly, I would like to thank my partner Andrew, for always being there for me, for supporting me through the hardest times and sharing adventures with me. I would have not completed this thesis without him by my side.

* * *

The work presented in this thesis would have been impossible without generous funding from various sources. The Natural Environment Research Council (NERC) and the University of Edinburgh provided me with a full stipend (NE/L002558/1) through the E3 Doctoral Training Program. The cosmogenic nuclide analysis was funded through the NERC Cosmogenic Isotope Analysis Facility Grant to Andy Hein (CIAF.9167.0416). Funding for my fieldwork was provided by the British Society for Geomorphology, Quaternary Research Association, Royal Geographical Society (with IBG), and the Explorers Club. Presenting my research at the INQUA 2019 conference was made possible by funding from the Scottish Alliance for Geoscience, Environment and Society.

Contents

Declaration iii

Abstract v

Lay summary vii

Acknowledgements ix

1 Introduction 1
- 1.1 Rationale . . . 2
- 1.2 Study area . . . 5
- 1.3 Aim and objectives . . . 6
- 1.4 Thesis structure . . . 6

2 Background 11
- 2.1 Physiography of central Patagonia . . . 12
- 2.2 Glacial history and palaeoclimate of central Patagonia . . . 14
  - 2.2.1 Glacial extent . . . 14
  - 2.2.2 Glacial dynamics . . . 15
  - 2.2.3 Timing of glacial advances . . . 19
  - 2.2.4 Proglacial lake evolution . . . 26
  - 2.2.5 Terrestrial palaeoenvironmental proxies . . . 27
  - 2.2.6 Marine proxies . . . 32
  - 2.2.7 Dust record . . . 34
  - 2.2.8 Previous work at Lago Belgrano and around Monte San Lorenzo . . . 35
- 2.3 Synthesis of knowledge gaps and motivation for this thesis . . . 38

3 Glacial geomorphology 41
- 3.1 Introduction . . . 42
- 3.2 Methods . . . 42
- 3.3 Glacial geomorphology . . . 45
  - 3.3.1 Moraine ridges and complexes . . . 46
  - 3.3.2 Hummocky terrain . . . 50
  - 3.3.3 Glacigenic sediment . . . 52

3.3.4 Glacial lineations . . . 52
3.3.5 Ice-scoured bedrock . . . 52
3.3.6 Meltwater channels . . . 53
3.3.7 Glaciofluvial outwash . . . 53
3.3.8 Palaeoshorelines . . . 53
3.3.9 Glaciolacustrine deposits . . . 54
3.3.10 Raised deltas . . . 54
3.3.11 Alluvial fan deposits . . . 54
3.4 Interpretation . . . 54
3.5 Conclusion . . . 55

4 Extensive mountain glaciation in central Patagonia during Marine Isotope Stage 5 63
4.1 Introduction . . . 64
4.2 Physical setting . . . 65
4.3 Glacial history and previous work . . . 68
4.3.1 Previous work at Lago Belgrano . . . 68
4.3.2 Pre- gLGM glacial history of Patagonia . . . 68
4.4 Methods . . . 70
4.4.1 Geomorphic mapping . . . 70
4.4.2 Dating approach and sampling . . . 70
4.4.3 Preparation . . . 71
4.5 Results . . . 74
4.5.1 Moraine Record . . . 74
4.5.2 Exposure ages . . . 78
4.6 Discussion . . . 78
4.6.1 The age of the Klementek outwash . . . 78
4.6.2 The age of Menelik moraines and outwash . . . 81
4.6.3 The last glacial cycle at Lago Belgrano . . . 82
4.6.4 Evidence for MIS 5 glaciation . . . 82
4.6.5 gLGM and deglaciation in Patagonia . . . 83
4.6.6 Causes of glaciation . . . 84
4.7 Conclusion . . . 87

5 Glacier advance in central Patagonia during the Antarctic Cold Reversal followed by retreat and stabilisation during the Younger Dryas 91
5.1 Introduction . . . 92
5.2 Study area and previous work . . . 94
5.2.1 Physical setting . . . 94
5.2.2 Previous work . . . 96
5.3 Methods . . . 98
5.3.1 Surface exposure dating . . . 98
5.3.2 OSL dating . . . 101

5.4 Results . . . 105
5.4.1 Geomorphology . . . 105
5.4.2 Chronology . . . 111
5.5 Discussion . . . 118
5.5.1 LGIT at Lago Belgrano . . . 118
5.5.2 Deglaciation of the central sector of the PIS . . . 118
5.5.3 Factors controlling the relative magnitude of glacier advances 121
5.5.4 Regional view . . . 122
5.6 Conclusions . . . 124

6 Holocene glacial dynamics 125
6.1 Introduction . . . 126
6.2 Study site and previous work . . . 127
6.2.1 The moraine sequence . . . 130
6.3 Methods . . . 130
6.3.1 Exposure dating . . . 130
6.3.2 Glacier reconstruction . . . 134
6.4 Results and discussion . . . 137
6.4.1 ^{10}Be chronology . . . 137
6.4.2 Glacier reconstruction and ELAs . . . 137
6.4.3 Regional comparison . . . 139
6.5 Conclusion . . . 144

7 Conclusions 145
7.1 Synthesis of findings . . . 146
7.1.1 Geomorphological map . . . 146
7.1.2 Early glaciation and the gLGM . . . 146
7.1.3 Glacier response to millennial-scale cold reversals and palaeolake evolution. . . . 147
7.1.4 Holocene dynamics . . . 148
7.2 Implications . . . 149
7.2.1 The role of topography, catchment size and ice-divides . . . 149
7.2.2 How extensive was the mountain glaciation during MIS 5? 150
7.3 Future research directions . . . 151

References 155

Appendix:
Mendelová et al., 2017 187

List of Tables

2.1 Published recalibrated radiocarbon ages from the Lago Belgrano valley 36

3.1 Landform identification criteria, modified from previous studies in Patagonia (e.g. Glasser et al., 2008; Darvill et al., 2014; Bendle et al., 2017b; Chandler et al., 2018) 44

4.1 Sample details and nuclide concentrations 72
4.2 Exposure ages 79

5.1 Sample details and nuclide concentrations 100
5.2 Luminescence dating results 104
5.3 Exposure ages 115
5.4 Summary statistics for moraine ages 116

6.1 Sample details and nuclide concentration 133
6.2 Exposure ages 137
6.3 Palaeo-ELAs (m asl) for the M1 (2.8 ka) terminal position of the Lacteo glacier calculated using different AARs and the median glacier elevation method. 139

List of Figures

1.1 Location of Patagonia in the Southern Hemisphere, the study site is indicated with a circle. Approximate contemporary location of the core of the southern westerly winds (SWW) (Kilian and Lamy, 2012) is shown along with position of the Polar Front (PF), the Subantarctic Front (SAF) and the Subtropical Front (STF) (Orsi et al., 1995) 3

1.2 Map of central Patagonia showing the location of the study site, large over-deepened basins of Lago Pueyrredón and Lago Buenos Aires, and the Northern and Southern Patagonian Icefields. Shaded relief map was derived from SRTM DEM. 7

2.1 A) Map of Patagonia and B) enlarged map of central Patagonia showing the approximate extent of the PIS at the gLGM (after Davies et al., 2020), key places names discussed in the text and the location of marine cores ODP 1233 (Kaiser et al., 2005; Lamy, 2004) and MD07 3088 (Siani et al., 2010; Montade et al., 2013). . 12

2.2 A section of the original map of Caldenius (1932) showing the glacial limits at Lago Buenos Aires, Lago Pueyrredón and Lago Belgrano. He correlated these limits to glacial events identified in Scandinavia. 16

2.3 Deglaciation of the central sector of the Patagonian ice sheet as modelled by Hubbard et al. (2005), forced by the Vostok temperature record. 18

2.4 Simulation of the inception of the Patagonian ice sheet as modelled by Sugden et al. (2002). 19

2.5 Empirical reconstruction of the central sector of the PIS, i.e. area centred on the NPI presented by Davies et al. (2020). 21

2.6 Overview map of published chronologies showing: 1) Main ice limits in Lago Buenos Aires and Lago Pueyrredón valleys. Exposure ages are presented as a range for each moraine system (not differentiating individual advances), taking the youngest and the oldest age with internal uncertainty. 2) Moraine ^{10}Be ages spanning the ACR and YD/Holocene transition. Only ages which have not been affected by submergence in a regional palaeolake are shown (cf. Thorndycraft et al., 2019). Present day glaciers are from the GLIMS database. 23
2.7 The model of palaeolake evolution in the LBA, LP and Chacabuco valleys, from Thorndycraft et al. (2019). 28
2.8 The location of palaeoenvironmental proxies in central Patagonia spanning the Late Glacial. The records, which document the ACR signal are shown with a full orange circle, while the ones which do not document either ACR or YD are depicted with an empty circle. 30
2.9 A summary figure of marine and Antarctic proxies. A: SST record from off Chile (ODP1233) (Kaiser et al., 2005; Lamy, 2004). B: EDC dust record (Lambert et al., 2012). C: EDC deuterium record (EPICA Community Members, 2004) plotted on AICC2012 timescale (Veres et al., 2013). 34
2.10 A map of San Lorenzo and the Belgrano valley showing published radiocarbon and surface exposure ages. 37
2.11 The palaeolake evolution in the Belgrano valley based on Horta et al. (2017). Palaeolakes are depicted in blue (a & c) and green (b), and moraines in pink. 38

3.1 A map of the study area showing approximate field checking area and the extent of previous mapping. ML: Monte Leon, BP: Belgrano peninsula. Geomorphological mapping by Glasser et al. (2008) covered the entire study area. 42
3.2 The geomorphological map of the Belgrano valley. 47
3.3 A) Satellite image (Sentinel-2) and B) mapped moraine ridges of the Klementek moraine system and the associated hummocky terrain. 48
3.4 A) Photograph showing part of the hummocky terrain, with a vehicle in the bottom left corner for scale. B) Photograph showing the outermost Klementek moraine ridges. 49
3.5 Satellite images (Sentinel-2) A) snow-free and B) with snow cover highlighting moraine ridges of the Menelik moraine system and C) a corresponding geomorphological map. 50
3.6 A) View of a medial moraine (pink dashed lines) formed by the coalescence of the Belgrano and Burmeister glaciers. B) Photograph showing the lateral moraines on Cerro Mie and the medial moraine. 51

3.7 A) Satellite image (ESRI World Imagery) and B) mapped landforms near the present day margin of the Lacteo glacier. 57
3.8 A) Satellite image (Sentinel-2) and B) mapped glacial lineations and meltwater channels within the glacigenic sediment. 58
3.9 A) Satellite images (ESRI World Imagery) and B) mapped ice-scoured bedrock and bedrock lineations in the Lacteo valley. Bedrock is in many place overlain by diamict. C) Striated bedrock in the Lacteo valley, location of the photograph is shown in A). D) Photograph of a roche moutonnée on the Belgrano peninsula. . . 59
3.10 A - B) A prominent shoreline (dotted yellow line) at 885 - 882 m asl above the modern Lago Belgrano. Fine pale sediments interpreted as glaciolacustrine deposits are visible in B) below the shoreline. . 60
3.11 A) Satellite image (Google Earth) and B) mapped raised deltas above Lago Belgrano, palaeo shorelines, and glaciolacustrine deposits. C) Photograph of a raised delta. 61

4.1 A) Location of Patagonia in the southern hemisphere along with Southern Ocean and Antarctic proxies discussed in the text and approximate location of the southern westerlies (SWW). B) Location of our study site in Patagonia and approximate extent of the Patagonian Ice Sheet during the gLGM (Singer et al., 2004). Image: ESRI World Imagery. (LBA: Lago Buenos Aires, TdP: Torres del Paine, UE: Última Esperanza, BI-SS: Bahí Inútil-San Sebastián lobe). C) A map showing the topography of central Patagonia and location of the San Lorenzo massif. Blue arrows depict drainage directions described in the text, blue dotted line represents hydrological drainage divide.The hillshade basemap: (SRTM). Glacier outlines are from the GLIMS database (Falaschi et al., 2017; De Angelis et al., 2015). 66
4.2 Geomorphological map showing the main moraine systems in the Belgrano valley, informally named the Klementek, Menelik and Belgrano moraines from the oldest to youngest. Sample locations are also shown. The hillshade basemap: SRTM. 67
4.3 A) Satellite image (Sentinel-2) and B) mapped moraine ridges of the Klementek moraine system and the associated hummocky terrain. Sample locations and ^{10}Be exposure ages are also shown. C) Photograph showing part of the hummocky terrain, with a vehicle in the bottom left corner for scale. D) Photograph showing the outermost Klementek moraine ridges. E) Photograph showing the outermost Klementek moraine ridges and the associated outwash in foreground that was sampled for surface exposure analysis. F) An example of an outwash cobble sampled, which still exhibits fluvial shape, but some surface erosion is evident (maximum 3 mm). . . . 75

4.4 A) Photograph showing the Menelik moraines (dashed yellow lines) draped on higher ground. B-E) Photographs showing the outermost Menelik moraines (dashed yellow lines) along with examples of sampled boulders. F) Example of a cobble sampled from the outwash associated with Menelik moraines. Ventifacts on the surface suggest long surface exposure (cf. Hein et al., 2011). . 76

4.5 Enlarged geomorphological map showing the Menelik moraine system along with sample locations and ^{10}Be exposure ages. . . . 77

4.6 Probability density diagrams ('camelplots') for A) the Klementek cobble ages, A) Menelik boulder ages, and C) Menelik cobble ages. Thin purple curves represent Gaussian curves for individual samples. Thick purple curve represent the summed probability distribution for the data, excluding outliers. Outliers are represented by dashed curves. Vertical lines denote an arithmetic mean (dark green, excluding outliers), and 1 and 2 σ (paired brown and yellow lines respectively) confidence intervals of the mean. Wmean: uncertainty-weighted mean. 80

4.7 Comparison of our ^{10}Be ages and other proxies. A: July insolation intensity for 60° N (Berger and Loutre, 1991). B: July (orange) and December (blue) insolation intensity for 50° S (Berger and Loutre, 1991). C: EDC dust record (Lambert et al., 2012). D: SST (Mg/CA) record from off New Zealand (MD97-2120) (Pahnke et al., 2003). E: EDC deuterium record (EPICA Community Members, 2004) plotted on AICC2012 timescale (Veres et al., 2013). F: Oxygen isotope record from Byrd ice core (Johnsen et al., 1972) plotted on GISP2 timescale (Blunier, 2001). G: Summed probability density functions ('camelplots') for the Klementek outwash, and the Menelik boulders and outwash cobbles combined (plotted on individual y-axis; dashed curves represent outliers). Circles indicate the arithmetic means of the Klementek and Menelik ages (after outliers have been excluded) and error bars indicate uncertainty of the mean, which includes propagated individual internal uncertainties of the ^{10}Be ages and production rate uncertainty (Kaplan et al., 2011). 88

4.8 89

4.8 A conceptual model of the build-up of the last Patagonian Ice Sheet (PIS). A) The initial inception of the Patagonian Ice Sheet begins with nucleation centres over the present day North and South Patagonian Icefields (NPI, SPI), and the San Lorenzo massif (SL), likely triggered by reduced summer insolation in the southern hemisphere. At this time, the Southern Westerly Winds (SWW) can freely penetrate through the topographic depression between the present icefields to bring snowfall east to the San Lorenzo ice cap. Ice expansion is greatest down the high-elevation eastern Belgrano valley, since glaciers draining to the south, west and north of the massif descended into deep valleys. B) The individual ice masses coalesce, causing reorganization of ice (and fluvial) drainage routes, and reducing ice flux down the Belgrano valley. C) Under peak glacial conditions, the ice-divide increased in elevation, and migrated westward towards the precipitation source. This caused snow starvation to the San Lorenzo massif, and significant reorganization of ice-drainage routes to focus ice flow into the major outlets of the Patagonian Ice Sheet that surround the San Lorenzo massif (LP and SM). These processes limited ice expansion in the Belgrano valley when the major outlet to its north, LP (and also LBA, which is not shown) was near its maximum last glacial extent indicated by the Río Blanco moraines (Hein et al., 2010). 90

5.1 A) Location of Patagonia in the southern hemisphere with approximate location of the Southern Westerly Winds. B) Location of the study area in Patagonia, with an approximate extent of the PIS at the global Last Glacial Maximum (pink line). Image: ESRI World Imagery. C) Map of central Patagonia showing contemporary ice fields and ice caps (outlines were downloaded from the GLIMS database (Falaschi et al., 2017; De Angelis et al., 2015)), modern drainage divide and location of Monte San Lorenzo and Lago Belgrano valley. Magenta arrows indicate former ice discharge routes from the San Lorenzo. Basemap: SRTM DEM. 95

5.2 Map showing Monte San Lorenzo, Lago Belgrano and Lacteo valleys, along with published chronologies (black curves indicate dated ice margins). Where more than 2 ages exist for a landform, uncertainty-weighted means with 1 σ standard deviation are presented. Otherwise, individual ages are given with 1 σ uncertainty (internal in case of ^{10}Be ages). Green shading indicates our study area, and ice margins dated in this study are highlighted in pink. Glacier outlines were downloaded from the GLIMS database (Falaschi et al., 2017; De Angelis et al., 2015). River drainage directions are indicated with blue arrows. 97

5.3 Abanico plots of the D_e values determined for OSL dating, where the grey shading shows the MAM D_e for each distribution. Note that sample LBSH0101 was analysed using microhole analysis rather than single grains (i.e. up to four grains in each hole due to a grain size of 125 180 μm) but it is likely that the OSL signal was dominated by one brighter grain. 103

5.4 The geomorphological map of the Belgrano and Lacteo valleys. Sample locations are also shown (white circles). The hillshade basemap: SRTM DEM. 106

5.5 Examples of moraine boulders sampled for surface exposure analysis. (A & B) Boulders on the innermost Belgrano moraine, a former shoreline is visible in the background (A, dashed line). (C & D) Boulders on the outermost Belgrano moraine. 107

5.6 Enlarged geomorphology map showing the Belgrano and Rincon moraines. The locations of moraine boulder samples, shoreline samples and OSL samples collected from glaciolacustrine deposits are also shown. The area where the Belgrano moraines cross-cut older recessional moraines is indicated with a box (Fig. 5.7). The ^{10}Be ages presented here are individual ages with 1 σ internal uncertainty. The approximate area of the palaeolake is indicated. This is based on 882 m asl elevation extracted from an SRTM DEM with resolution of 30 m. 108

5.7 (A) Photograph showing the area where the Belgrano moraines cross-cut older moraines. (B & C) Satellite images showing the cross-cutting relationship (Image: Google Earth). 109

5.8 (A & B) Photographs showing the Rincon moraines and an outwash plain grading from the moraines to the SE. The outwash terrace was incised by meltwater creating a series of stepped terraces. (C & D) Photographs showing the multi-crested lateral moraine in the Lacteo valley, about 7 km from the present day margin of the Lacteo glacier. 110

5.9 Enlarged geomorphology map of the Lacteo valley. Locations of samples collected from the Lacteo lateral moraine and along a transect in the valley are shown. The ^{10}Be ages presented here are individual ages with 1 σ internal uncertainty. 112

5.10 (A) Photograph showing raised shorelines above the modern Belgrano lake. (B) Photograph showing a palaeoshoreline with the location of surface exposure (black hexagon) and OSL (square) samples. The valley bottom below the shoreline is infilled with glaciolacutrine sediments. (C) Photograph showing the surface of a shoreline where sample BSH1801 was taken. (D) Photograph of a shoreline where sample BSH1803 was taken. 113

5.11 Normal kernel density diagrams for exposure ages from moraines: (A) the Belgrano inner moraines,(B) the Belgrano outer moraines, (C) the Rincon, and (D) the Lacteo lateral moraine. Thin purple curves represent Gaussian curves for each age and thick purple curves the summed probabilities. Outliers are represented by dashed lines. Circles represent uncertainties-weighted mean of ages after excluding the outliers and 1σ standard deviations. 117

5.12 Model of ice and palaeolake evolution (A) during the ACR and (B) during the YD. The extent of the Belgrano and Lacteo glaciers during the ACR, and the extent of the palaeolake Belgrano during the YD are based on our geomorphological mapping and chronology. The extent of the Calluqueo and Tranquilo glaciers, and palaeolakes (pale blue) on the northern flanks of the San Lorenzo is based on published work (Davies et al., 2018; Sagredo et al., 2018; Glasser et al., 2012; Martin et al., 2019; Thorndycraft et al., 2019). Moraines delineating the extent of these glaciers are highlighted in pink. Elevation of the palaeolakes is also indicated in m asl. Darker blue colour indicates modern lakes. 119

5.13 Comparison of our exposure ages to other proxies: *Nothofagus dombeyi* type and *Astelia pumila* pollen record from core MD07-3088 off the Chilean coast (46° S, Montade et al., 2013) plotted on on a scale from Montade et al. (2019), sea surface temperature reconstruction from core ODP 1233 off the Chilean coast (Kaiser et al., 2005) and the δ D record from EDC, east Antarctica (EPICA Community Members, 2004) plotted on AICC2012 timescale (Veres et al., 2013). The exposure ages are plotted after outliers have been removed. *Astelia* is a plant typical of the Magellanic moorland that at present grows south of 48° S. 123

6.1 A 3D view of Monte San Lorenzo and the Lacteo glacier. Source: Google Earth. 128

6.2 Lichenometric ages for the moraines deposited by the Lacteo and Lorenzo glacier (Garibotti and Villalba, 2017) and a maximum radiocarbon age for a moraine of the Lacteo glacier (Mercer, 1984). Moraines are shown with dashed lines as mapped and labelled by Garibotti and Villalba (2017). 129

6.3 Photographs showing the M1 lateral-terminal moraine in the Lacteo valley, from which moraine boulder samples were collected. 131

6.4 Geomorphological map showing the Holocene moraine sequence in the foreground of the Lacteo glacier. Sample locations and exposure ages are also shown. Shaded relief base map was made using the SRTM DEM (30m). 132

6.5 Map showing the central flow-line used in the glacier reconstruction and the extent of the Lacteo glacier and the proglacial lake as captured by the ASTER DEM, which was used as the basis for the glacier reconstruction. This glacier outline was used to calculate bed topography under the extant glacier using the inversion method of Benn and Hulton (2010). 135
6.6 Probability distributions of the exposure ages from the M1 moraine deposited by the Lacteo glacier. Black circle shows the mean and error bar shows 1σ standard deviation. 138
6.7 Modelled ice surface profile for the Lacteo glacier at the M1 terminal position. The modelled glacier surface profile matches the geomorphological constraints well with imposed basal shear stress of 70 kPa. 139
6.8 Reconstructed ice surface of the Lacteo glacier at 2.8 ka (basal shear stress of 70 kPa) and the ELA estimated using the AAR method with 0.5 and 0.65 ratios. Shaded relief base map was made using the SRTM DEM (30m). 140
6.9 Comparison of the exposure ages from the Lacteo valley with other proxy records. A) Kernel probability density diagrams for exposure ages from the Lacteo glacier (this study), Tranquilo glacier (Sagredo et al., 2016) and Colonia glacier (Nimick et al., 2016). Each thin curve represents a Gaussian probability distribution of an individual exposure age, while the thick curves represent summed probabilities for a moraine. B) Reconstructed total solar irradiance (Wu et al., 2018) C) The timing of glacier advances inferred from the terrigenous sediment record off the Chilean coast at 46° S (Siani et al., 2010). D) Non-arboreal pollen taxa record from southern Patagonia (Moreno et al., 2018) and a regime shift analysis showing alternating warm/dry (light pink) and cold/wet events (light blue), linked to the SAM. E) Summed probability distribution of the exposure ages from outlet glaciers of the Southern Patagonian Icefield (Kaplan et al., 2016; Reynhout et al., 2019). F) Summer insolation intensity at 50° S (Berger and Loutre, 1991), and atmospheric CO_2 concentrations from the Dome C Antarctic ice core (Monnin et al., 2001). 142

Chapter 1

Introduction



1.1 Rationale

Patagonia was once covered by an ice sheet 2,000 km long, which waxed and waned many times in the past in response to climate change and left its imprint on the landscape. Glaciers flowed from the Andean crests down to the Pacific Ocean in the west and the Patagonian steppe in the east. Here, herds of guanaco now roam the semi-desert environment and glaciers had long retreated deep into in the mountains. It is the dry climate that preserved what is *'...probably the most complete and intact sequence of Quaternary moraines anywhere in the world'* (Clapperton, 1993, p. 358). This is a unique archive, which enables us to study past climate of the Southern Hemisphere. However, to fully exploit this archive, we need to constrain past glacier change with robust chronologies. This thesis aims to improve our understanding of the glacial history and past climate in Patagonia over the course of the last glacial cycle and the Holocene.

Patagonia in southernmost South America extends through the southern mid-latitudes (40° S - 60° S, Fig. 1.1). It lies in the vicinity of Antarctica and adjacent to south Atlantic and south-east Pacific. It is uniquely sensitive to climate signals from both the high latitudes and the tropics. It is thus well positioned to study Quaternary climate change of the Southern Hemisphere.

Land comprises only a fraction of Earth's surface in the mid-latitudes of the Southern Hemisphere. Southernmost South America, with the Andean mountain range running north to south, is the only significant barrier to the southern westerly winds (SWW; 1.1). Changes in the latitudinal position and intensity of the SWW influence the Southern Ocean carbon sink (Lovenduski et al., 2008; Le Quere et al., 2007), the southern ocean circulation and productivity as well as sea ice extent (Purich et al., 2016). The SWW drive upwelling of deep waters in the Southern Ocean through which CO_2 is released into the atmosphere, a key component of the meridional overturning circulation (Toggweiler and Samuels, 1995; Marshall and Speer, 2012; Meredith et al., 2012). By controlling atmospheric CO_2 concentrations, the SWW played a critical role in the last glacial-interglacial transition (LGIT) and the Holocene climate change (Toggweiler et al., 2006b; Toggweiler and Russell, 2008; Anderson et al., 2009; Denton et al., 2010; Moreno et al., 2010; Fletcher and Moreno, 2012; Saunders et al., 2018). Strengthening of the SWW has been observed since the 1970's (e.g. Marshall, 2003; Swart and Fyfe, 2012; Swart et al., 2015), but global climate models (the Coupled Model Intercomparison Project, CMIP) underestimate this trend (Swart and Fyfe, 2012; Meijers, 2014). Future projections indicate a poleward shift and intensification of the SWW over the next century but models disagree on the magnitude and position change (Bracegirdle et al., 2013; Meijers, 2014). Improving our understanding of the past dynamics of the SWW is therefore a key goal of palaeoclimate research.

Glaciers in southernmost South America are sensitive indicators of past climate. Well-dated records of past glacier change can provide new insights into the past dynamics of the SWW, the interhemispheric phasing of climate change,

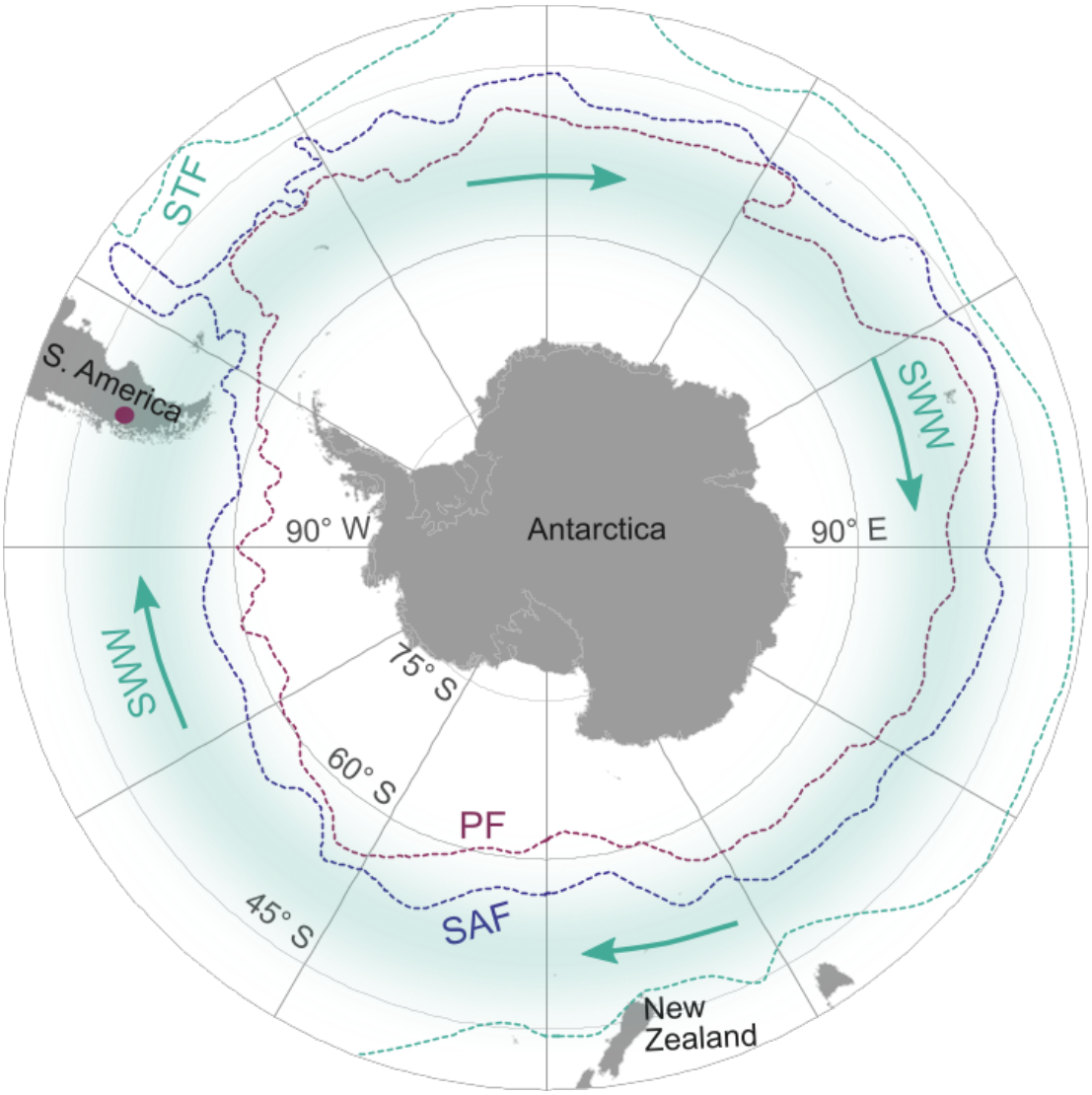

Figure 1.1: Location of Patagonia in the Southern Hemisphere, the study site is indicated with a circle. Approximate contemporary location of the core of the southern westerly winds (SWW) (Kilian and Lamy, 2012) is shown along with position of the Polar Front (PF), the Subantarctic Front (SAF) and the Subtropical Front (STF) (Orsi et al., 1995)

and the drivers of Southern Hemisphere glaciation and climate change (e.g Denton et al., 1999a; Moreno et al., 2001). Mapping the spatial and temporal variability in past climate change is essential for calibrating regional and global climate models and may help to improve future projections. Despite the exceptionally well-preserved geomorphological record, the exact timing and extent of glacier fluctuations remain poorly resolved in many areas. To improve our understanding of the glacial history of Patagonia, this thesis focuses on the following gaps in knowledge:

1) *The development of the last Patagonian Ice Sheet (PIS) and the timing and magnitude of glacial advances throughout the last glacial cycle* are poorly constrained. Increasing number of studies from the southern mid-latitudes demonstrate full glacial conditions well before the global Last Glacial Maximum (gLGM; $\sim$ 26 - 19 ka, Clark et al., 2009). In Patagonia, such evidence is largely restricted to the southernmost outlet glaciers of the PIS, which attained their maximum extent as early as $\sim$48 ka (Darvill et al., 2015; García et al., 2018). In central Patagonia, the existing chronologies from two large outlet lobes do not document glacier expansion prior to $\sim$35 - 30 ka during the last glacial cycle (Hein et al., 2009, 2010; Kaplan et al., 2004, 2005; Smedley et al., 2016). It is unclear if this apparent latitudinal asynchrony is a consequence of 1) a true climatic signal (e.g. latitudinal position of the SWW), 2) a lack of dated pre-gLGM ice limits in central Patagonia, 3) glacial dynamics affecting glacier response to climate, or 4) erosion of the moraine record by geomorphological processes. Lack of robust chronologies spanning the last glacial cycle limits our understanding of the development of the PIS, and hinders examination of ocean-atmosphere-cryosphere interactions and the drivers of Southern Hemisphere glaciation and past climate.

2) *Response of glaciers to millennial scale climate events during the last glacial-interglacial transition (LGIT).* Millennial scale climate events characterised the last glacial period and have been shown to be out-of-phase between the hemispheres by correlating ice cores from Greenland and Antarctica (Blunier et al., 1997; Blunier, 2001; EPICA Community Members, 2006; Pedro et al., 2011; WAIS Divide Project Members, 2015). Although commonly attributed to the bipolar seesaw, the exact oceanic and atmospheric processes governing these abrupt events are still debated (for recent reviews see Pedro et al., 2018; Landais et al., 2015). Recent work has documented a migration of the SWW during theses abrupt events and highlighted the role of atmospheric teleconnections (Markle et al., 2017; Buizert et al., 2018). Mapping the spatial and temporal footprint of millennial-scale climate events across latitudinal gradients can help to uncover the processes responsible for propagation of the climatic signals between the high-, mid-latitudes and the tropics. Expression of these climate signals has, however, been a contentious issue in Patagonia for several decades, in particular the occurrence of the Northern Hemisphere Younger Dryas (YD; $\sim$ 12.9 - 11.7 ka; Blunier et al., 1998) and the Antarctic Cold Reversal (ACR; $\sim$ 14.6 - 12.8 ka, Lemieux-Dudon et al.,

2010). Separating these consecutive events is often problematic due to the low resolution of chronologies. Disentangling climatic and non-climatic factors (e.g. calving, topographic stabilisation) on glacier response to these abrupt events has proven challenging in central Patagonia due to calving into large palaeolakes and the complex topography. Further, large spatial data gaps in dated ice marginal positions (cf. Davies et al., 2020) during the LGIT limit our understanding of the pattern of deglaciation and the break-up of the PIS.

3) While in the Northern Hemisphere, glaciers were restricted in size throughout most of the Holocene and then expanded to their maximum Holocene positions in the last millennium, the emerging evidence in the Southern Hemisphere suggests a more complex story. However, *detailed, well-dated records of the long-term, Holocene glacier change* are still too few in Patagonia (e.g. Kaplan et al., 2016; Strelin et al., 2011; Reynhout et al., 2019; Hall et al., 2019). This hinders our ability to draw a broad picture of millennial to centennial climate variability during the Holocene, elucidate potential hemispheric and regional mechanisms of climate change, and to contextualise the current and future climate change in the region.

1.2 Study area

To address the above gaps in knowledge, an understudied area on the eastern side of Monte San Lorenzo (3706 m asl) in central Patagonia was chosen. New research presented in this thesis focuses on the Belgrano and Lacteo valleys (Fig. 1.2). The site is ideal for addressing the above gaps in knowledge for several reasons:

1) The valleys contain a well-preserved geomorphological record with a potential to track glacier change over the last glacial cycle and through to the Holocene.

2) The former Belgrano glacier was not a major outlet glacier of the PIS (cf. Glasser et al., 2005) and occupied a small and relatively shallow basin sitting at just over 800 m asl (modern lake level). In contrast, the neighbouring valleys of Lago Pueyrredón (LP) and Lago Buenos Aires (LBA), where most chronological work has been done, have been eroded to below sea level ($\sim$ 200 m asl at the lake level, Murdie et al., 1998). Large fast-flowing outlet lobes, which occupied these over-deepened basins drained much of the central sector of the former PIS (Glasser et al., 2005). Fast ice flow and calving into deep proglacial lakes may have, at times decoupled these large outlet lobes from climate (Glasser et al., 2005; Douglass and Bockheim, 2006; Bendle et al., 2019). The Lago Belgrano glacier thus may have been more sensitive to climate than the larger outlet lobes.

3) Based on numerical modeling of the PIS inception, Sugden et al. (2002) suggested that massifs to the east of the main Andean arc, such as the San Lorenzo, which would have been in the precipitation shadow of the PIS during full glacial conditions, likely have preserved a longer geomorphological record.

The Lago Belgrano valley thus may provide clues to the early stages of the last glaciation.

4) Once separated from the PIS, the San Lorenzo, a relatively small ice cap, should have been more sensitive than the larger Patagonian Ice Fields, to climate fluctuations during the LGIT and the Holocene. It thus provides an opportunity to resolve the spatial-temporal footprint and magnitude of cold reversals, in particular, the contested YD and ACR in central Patagonia, as well as the timing of Holocene advances.

1.3 Aim and objectives

This thesis aims to better constrain the glacial history in central Patagonia in order to better understand the drivers of glaciations and the underlying climate change in the southern hemisphere.

The specific objectives are as follows:

1) To map the glacial geomorphology of the area using high resolution satellite imagery and field observations.

2) To determine the extent and timing of the oldest advances in the Belgrano valley using cosmogenic nuclide surface exposure dating of moraines and outwash terraces.

3) To reconstruct the timing and extent of glacier advances and the palaeolake evolution during the LGIT using cosmogenic nuclide surface exposure analysis on moraine boulders and raised shorelines, and optically stimulated luminescence analysis (OSL) of glaciolacustrine sediments.

4) To reconstruct the Holocene glacial history of the Lacteo glacier and determine the Equilibrium Line Altitudes (ELAs).

1.4 Thesis structure

This thesis contains chapters, which have been written as standalone pieces of work, thus necessitating some overlapping content. Chapter 2 is split into two parts and presents background to: 1) the physiography of central Patagonia, and 2) the glacial history and palaeoclimate in central Patagonia. The first part gives a brief description of the physiography of central Patagonia, roughly between 44° S and 49° S. In the second part, I review previous work pertaining to glacial extent, ice dynamics, geochronologies and palaeoenvironmental proxies. I focus on central Patagonia as it provides important context for the work done in this thesis, and draw comparisons to broader regions where necessary. The first two parts of this chapter build on Mendelova et al. (2017) (Appendix 7.3), which is a review of glacial chronologies and palaeoenvironmental proxies spanning the LGM and the Holocene in central Patagonia. Sections 2.1, 2.2.3 and 2.2.5 on the physiography of central Patagonia, the timing of glacial advances and palaeoenvironmental

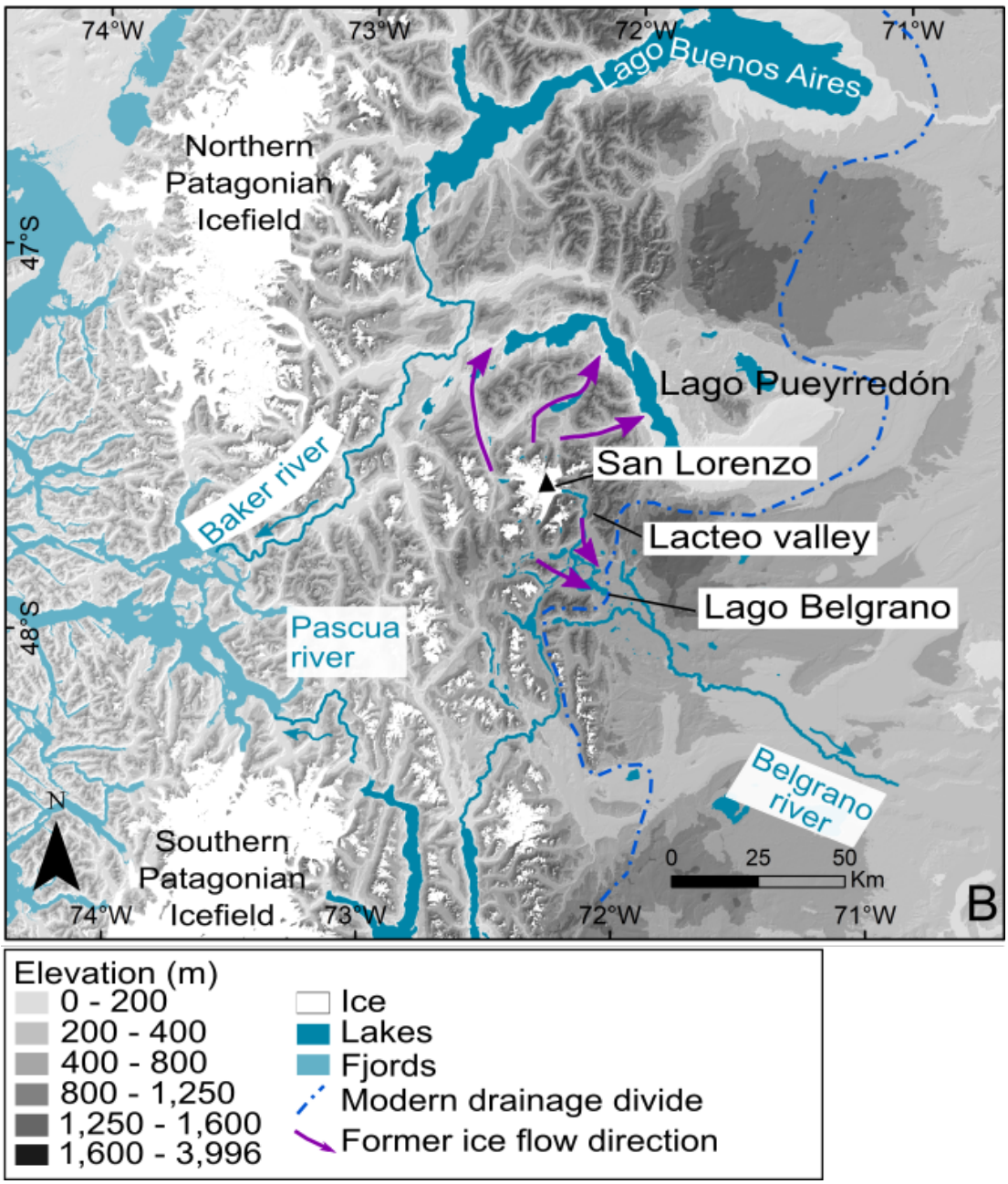

Figure 1.2: Map of central Patagonia showing the location of the study site, large over-deepened basins of Lago Pueyrredón and Lago Buenos Aires, and the Northern and Southern Patagonian Icefields. Shaded relief map was derived from SRTM DEM.

proxies have been adapted from the review paper. Very little work has been done in the Lago Belgrano valley and around Monte San Lorenzo, and I summarize this specifically in section 2.2.8. Chapters 3 - 6 present the main analytical results and discussion of the findings. Chapter 7 synthesizes and evaluates the research presented in this thesis, and outlines avenues for future research. Chapters 4 (Mendelová et al., 2020b) and 5 (Mendelová et al., 2020a) have been published and are a result of collaborative work. Authors contribution statement is given below.

Chapter 4

Mendelová, M., Hein, A.S., Rodés, Á., Xu, S., 2020. Extensive mountain glaciation in central Patagonia during Marine Isotope Stage 5. Quaternary Science Reviews 227, 105996.

This research was conducted as a collaboration with the named co-authors. In this paper, I undertook the fieldwork and most of the laboratory analysis. I wrote the manuscript and made all the figures. Andy Hein assisted with the fieldwork, Ángel Rodés assisted with the laboratory analysis, Sheng Xu conducted the AMS measurements. Andy Hein and Ángel Rodés edited the text and contributed ideas.

Chapter 5

Mendelová, M., Hein, A.S., Rodés, Á., Smedley, R.K., Xu, S., 2020. Glacier expansion in central Patagonia during the Antarctic Cold Reversal followed by retreat and stabilisation during the Younger Dryas. Quaternary Science Reviews 227, 106047.

This research was conducted as a collaboration with the named co-authors. In this paper, I undertook the fieldwork and most of the laboratory analysis. I wrote the manuscript and drew all the figures. Andy Hein assisted with the fieldwork, Ángel Rodés assisted with the laboratory analysis, Rachel Smedley carried out the luminescence analysis, Sheng Xu conducted the AMS measurements. Andy Hein, Ángel Rodés and Rachel Smedley edited the text and contributed ideas.

Review paper

Mendelová, M., Hein, A.S., McCulloch, R., Davies, B., 2017. The Last Glacial Maximum and deglaciation in central Patagonia, 44° S - 49° S. Cuadernos de Investigación Geográfica 43, 719 - 750.

The review paper (Appendix 7.3) was undertaken as a collaboration with the named co-authors. I undertook the literature search, wrote the manuscript and drew all the figures. All authors contributed ideas and edited text.

During my PhD I also contributed to the following two publications:

Hein, A.S., Antoine Cogez, Christopher M. Darvill, Monika Mendelova, Michael R. Kaplan, Frédéric Herman, Tibor J. Dunai, Kevin Norton, Sheng Xu, Marcus Christl, Ángel Rodés, 2017. Regional mid-Pleistocene glaciation in central Patagonia. Quaternary Science Reviews 164, 77 - 94.

Bethan J. Davies, Christopher M. Darvill, Harold Lovell, Jacob M. Bendle, Julian A. Dowdeswell, Derek Fabel, Juan-Luis García, Alessa Geiger,Neil F. Glasser, Delia M. Gheorghiu, Stephan Harrison, Andrew S. Hein, Michael R. Kaplan, Julian R.V. Martin, Monika Mendelova, Adrian Palmer, Mauri Pelto, Ángel Rodés, Esteban A. Sagredo, Rachel K. Smedley, John L. Smellie, Varyl R. Thorndycraft, 2020. The evolution of the Patagonian Ice Sheet from 35 ka to the present day (PATICE). Earth-Science Reviews, 204, 103152.

Chapter 2

Background



2.1 Physiography of central Patagonia

The region of central Patagonia (44° S - 49° S) features the Northern Patagonian Icefield (NPI), the highest mountains of the Patagonian Andes, extended fjord systems on the west coast and large over-deepened basins to the east of the mountain front that are separated by volcanic plateaus (mesetas). Glaciers repeatedly occupied the basins and extended to the low-lying plains known as the Patagonian steppe (Fig. 2.1). The ice flow during successive Quaternary glaciations exploited pre-existing structural faults, and over-deepened and widened the fjords and valleys through selective erosion (Glasser and Ghiglione, 2009). Between 47° S and 48°, the Andean range is interrupted by faulting. As a result, a topographic depression occupies the gap between the NPI and Southern Patagonia Icefield (SPI) and numerous high massifs are offset to the east of the main Andean spine. Among them are Monte San Lorenzo (3706m m asl), the third highest peak of the Patagonian Andes, and Sierra de Sangra, both covered by small ice caps.

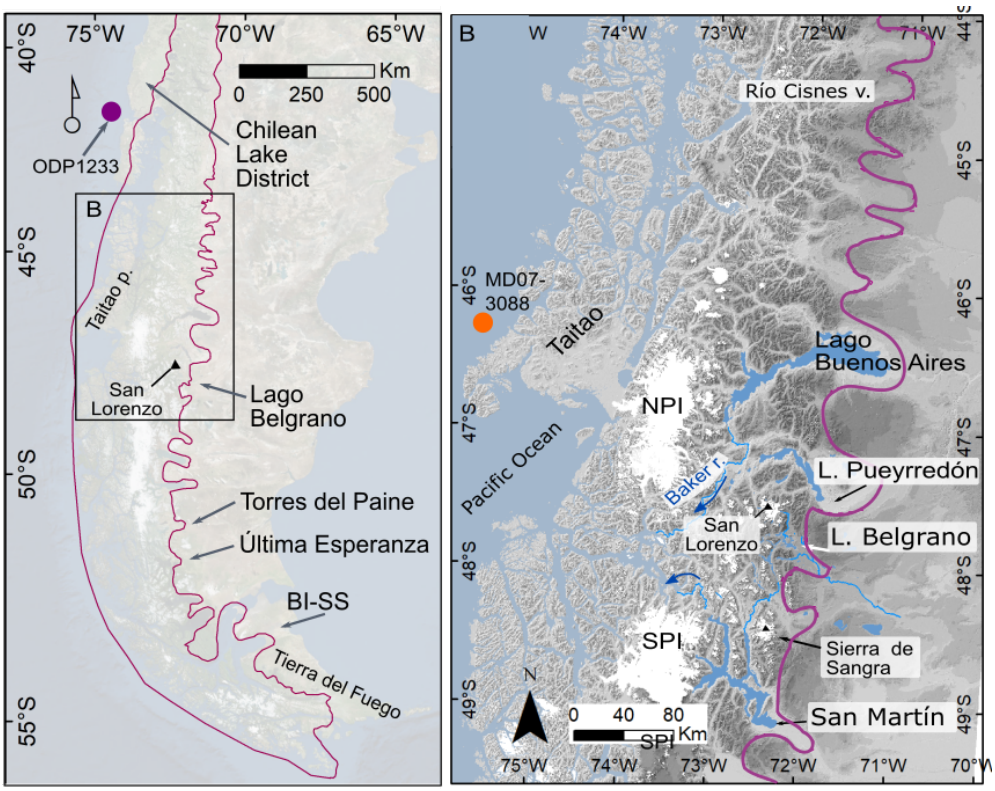

Figure 2.1: A) Map of Patagonia and B) enlarged map of central Patagonia showing the approximate extent of the PIS at the gLGM (after Davies et al., 2020), key places names discussed in the text and the location of marine cores ODP 1233 (Kaiser et al., 2005; Lamy, 2004) and MD07 3088 (Siani et al., 2010; Montade et al., 2013).

The continental divide is unusually located about 170 km to the east of the mountain divide. All major lakes, and all glaciers and icefields drain to the Pacific Ocean via rivers (Río Pascua and Baker), which exploit the topographic gap in the Andes (Fig. 2.1). In the Belgrano valley, the drainage divide runs just east of Lago Belgrano, which drains westward through a series of interconnected lakes and eventually via the Río Pascua to the Pacific Ocean. During glacial times, the growth of ice along the Andes blocked Pacific drainage pathways causing large-scale drainage reversals. Deglaciation is thus associated with Atlantic/Pacific drainage reversals across many parts of Patagonia (Caldenius, 1932; Turner et al., 2005; Bell, 2008; Hein et al., 2010; Glasser et al., 2016; Thorndycraft et al., 2019).

The region features a gap in the active volcanic arc (46.5° S - 49° S), near the Chile Triple Junction, where the Nazca, South American and Antarctic tectonic plates meet (Gutiérrez et al., 2005; Stern, 2004). The regional geology is characterized by intrusions of the Patagonian Batholith within the Andean Cordillera, Mesozoic and Cenozoic volcanics, Mesozoic marine sediments, and a Paleozoic metamorphic complex (Vandekerkhove et al., 2016; Lagabrielle et al., 2004). Basins to the east of the Andes are filled with Pliocene-Quaternary glacial and glaciofluvial sediments (Vandekerkhove et al., 2016; Lagabrielle et al., 2004). San Lorenzo is part of the Patagonian Batholith intrusion (Ramos and Kay, 1992; Ramírez de Arellano et al., 2012). Palaezoic basement rocks outcrop immediately east of the San Lorenzo massif. Jurassic volcanic and Cretaceous sedimentary rocks occur in the Belgrano valley and around Lago Burmeister. Further east in the Belgrano valley, Cenozoic sedimentary rocks and Neogene volcanics are found. The latter is represented by Meseta Belgrano, a high plateau which separates the Belgrano valley from the Pueyrredoón valley.

The SWW exert a dominant influence on the climate of Patagonia. They are strongest in austral summer with the core located between 45° S and 50° S, while in winter they weaken and expand towards the equator (Garreaud et al., 2009). The dominant westerly flow advects moist Pacific air masses, which upon interaction with the Andean mountains produce a strong orographic effect (Aravena and Luckman, 2009; Garreaud et al., 2009). Precipitation can thus reach 5000 - 10 000 mm a^{-1} on the western slopes of the Andes (Garreaud et al., 2013). In the east, precipitation decreases rapidly to less than 300 mm a^{-1} within tens of km downwind of the mountain front (Garreaud et al., 2013). The Andes thus create one of the greatest climate gradients in the world (Schneider et al., 2003). As a consequence of the topographic depression, Monte San Lorenzo is the first orographic barrier to the SWW and has a transitional maritime to continental climate (Falaschi et al., 2013).

The vegetation units in the region, summarized by Villa-Martínez et al. (2012), mirror the climatic and topographic gradients. Hyperhumid islands and fjords on the west side of the Andes are dominated by Magellanic moorland. Further inland, evergreen rainforests (*Nothofagus nitida* and *N. betuloides*) are found, which transition to winter deciduous forests (*Nothofagus pumilio*) on the eastern

mountain slopes. Open and arid lowland areas east of the mountain front are characterized by shrubs and grasses known as the Patagonian steppe. At higher altitude above the tree line, high Andean vegetation communities develop.

Patagonia hosts the largest temperate ice masses in the Southern Hemisphere outside of Antarctica and numerous smaller ice bodies with the NPI covering a total area of 3976 km^2 and the SPI just over 13,200 km^2 (Davies and Glasser, 2012). Between 1961 and 2016, glaciers from the southern Andean region lost a total mass of 1,200 Gt and the region was the third largest contributor to sea level rise after Alaska and Greenland (Zemp et al., 2019). Glaciers in central Patagonia experience a warm and wet climate, they extend well below the mean annual 0 °C isotherm and receive most of their precipitation in austral winter (Sagredo and Lowell, 2012). San Lorenzo and the surrounding mountains constitute the easternmost extensively glaciated area in Patagonia (Falaschi et al., 2013), the San Lorenzo Ice Cap covers $\sim$ 142.9 km^2 (Davies and Glasser, 2012).

Between the LIA ($\sim$ 1870) and 2011, the NPI and San Lorenzo shrank by $\sim$20 % and $\sim$30%, respectively (Davies and Glasser, 2012). Over the recent decades, the Patagonian Icefields experienced an accelerated thinning and mass loss, with intense thinning observed north of 49° S (Rignot et al., 2003; Rivera et al., 2007; Foresta et al., 2018). Between 2011 and 2017, the NPI lost mass at rate of 6.79 $\pm$ 1.16 Gt a^{-1}, an increase of $\sim$70 % and $\sim$134% compared to the periods of 2000-2012 and 1975-2000, respectively (Foresta et al., 2018). Mass balance and mass loss rates for smaller ice caps are less well constrained, in part due to a combination of challenging topography and their smaller size for measurements using radar altimetry (cf. Foresta et al., 2018).

2.2 Glacial history and palaeoclimate of central Patagonia

2.2.1 Glacial extent

First written observations of glaciations in Patagonia were made by Charles Darwin (1842), who described erratic boulders in the Río Santa Cruz valley and correctly assumed their glacial origin. The Swedish geologist Otto Nordenskjöld (1899) was first to make a map of glacial extent in southernmost Patagonia and on Tierra del Fuego (Rabassa, 2008). In his seminal work, Caldenius (1932) mapped moraine sequences across Patagonia and produced the first regional map covering the area between 41° S to 56° S (Fig. 2.2). Across Patagonia, he correlated four glacial limits, which he termed 'Initioglacial, 'Daniglacial', 'Gotiglacial' and 'Finiglacial from the oldest to the youngest following the Scandinavian model. He attributed these glacial limits to the last glaciation, and also identified one younger limit post-dating the LGM. His map was outstanding for his time and laid foundation for research on Quaternary glaciation of Patagonia. Among other early work, Feruglio (1944) described basaltic lava flows interbedded with glacial tills

in the Santa Cruz Province, which he considered Pliocene in age (Rabassa, 2008). In his later work, he described four glacial events, following Caldenius (1932), but based on the position of landforms within the landscape, e.g. near topographic divides vs. valley floor, he clearly distinguished different ages and related some landforms to much older events (Rabassa, 2008; Rabassa and Coronato, 2009). The history of early research on glaciation of Patagonia was summarized by Rabassa (2008) and Rabassa and Coronato (2009). With the advent of modern radiometric dating techniques, the model of glacial phases in Patagonia continues to be refined.

In recent years, Geographical Information System (GIS) and the increased availability of satellite imagery and digital elevation models (DEM) has allowed for large-scale mapping at an increasingly higher resolution. Building on previous Patagonia-wide mapping (Glasser et al., 2008), Davies et al. (2020) presented the most comprehensive map of the glacial geomorphology related to the PIS. High resolution satellite imagery (2.5 m) that since became available enabled mapping at an even greater detail. Supported by field-checking, this has been done for selected parts of Patagonia, for example Tierra del Fuego (Lovell et al., 2012; Darvill et al., 2014), part of the Cordillera Darwin (Izagirre et al., 2018), Lago Viedma (Ponce et al., 2019) and the NPI (Bendle et al., 2017a).

2.2.2 Glacial dynamics

Erosion

Long-term glacial erosion of the landscape can lower the ice-surface elevation and lead to less positive glacier mass balance (MacGregor et al., 2000). Based on preserved glacial limits at LBA in Patagonia, Kaplan et al. (2009) noted that reduced ice extent since $\sim$ 1.2 Ma to the LGM does not mirror palaeoclimate records. They postulated that glacial erosion, rather than climate, may control glacier length. Anderson et al. (2012) then demonstrated this process through numerical modeling, and showed that glacial erosion can reduce ice extent in successive glaciations by lowering the maximum ice surface elevation and reducing the accumulation area, irrespective of climatic forcing. Cogez et al. (2018) also noted that only moraines from alternate glacial cycles are preserved at LBA, similarly to LP (Hein et al., 2009, 2011), and they suggested that a more complex erosion-climate feedback could operate. Over much longer timescales (3.6 Ma), Clague et al. (2020) mapped and dated sequences of tills interbedded with lava flows preserved on high inter-valley plateaus in Patagonia (50° S) and proposed a landscape evolution model, which supports the glacier-erosion feedback concept. They suggested that Pliocene glaciers flowed over low relief landscape. Long-term glacial erosion then incised deep valleys, which entrenched glaciers, isolated high plateaus where these early tills got preserved, and overall reduced glacier length.

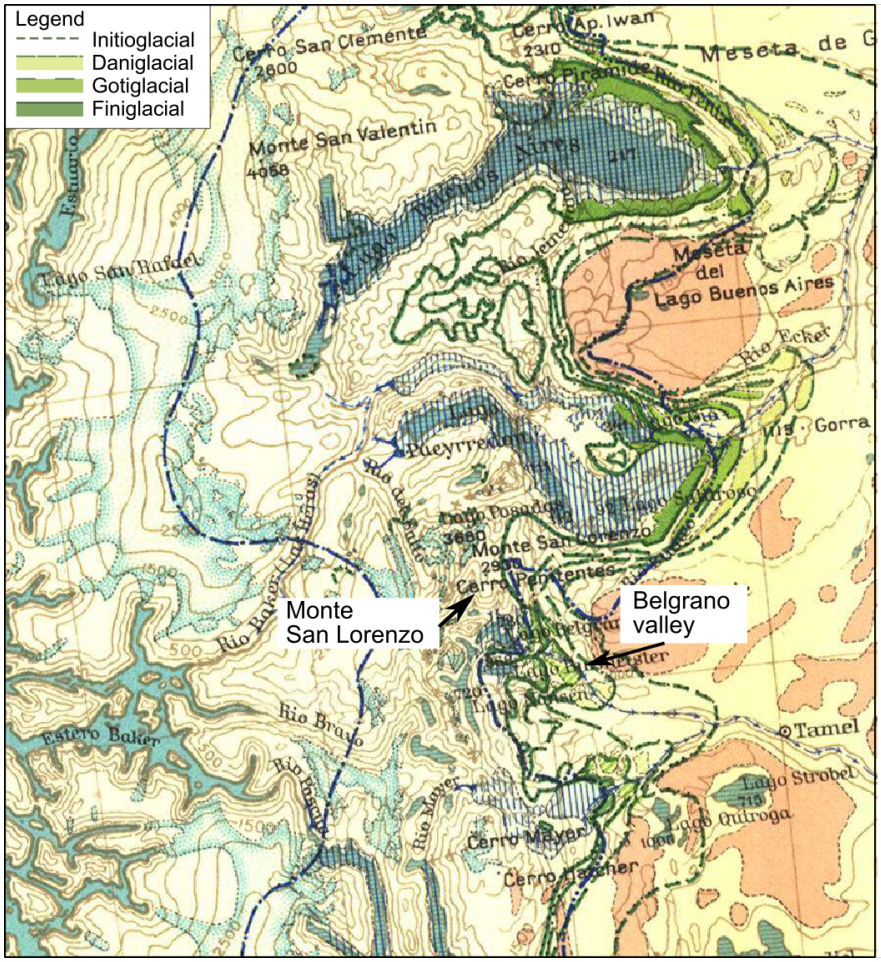

Figure 2.2: A section of the original map of Caldenius (1932) showing the glacial limits at Lago Buenos Aires, Lago Pueyrredón and Lago Belgrano. He correlated these limits to glacial events identified in Scandinavia.

Calving

As the outlet glaciers of the PIS retreated, proglacial lakes developed in over-deepened basins behind moraines (Caldenius, 1932), and led to the establishment of freshwater calving-fronts. Calving can lead to accelerated ice retreat, potential break-up of a glacier tongue (Boyce et al., 2007), and it affects glacier sensitivity to climate (Benn et al., 2007). Calving is thus an important consideration when drawing climatic interpretations from past glacial records. Many present day Patagonian glaciers calve into fjords or lakes, and calving exerts an important control on their mass balance and retreat rates (Warren and Sugden, 1993; Warren and Aniya, 1999; Davies and Glasser, 2012; Sakakibara and Sugiyama, 2014; Foresta et al., 2018). By comparing an annually-resolved varve record from the LBA basin to regional palaeoclimate proxies, Bendle et al. (2019) were able to demonstrate that calving dynamics, more than prevailing climatic conditions,

controlled the retreat rate of the LBA ice lobe once it retreated into its trough and a freshwater calving front had established. Douglass and Bockheim (2006) suggested that a wide calving front and a deep proglacial lake may have affected the LBA outlet lobe during an advance and retreat phase. Similarly, Martin et al. (2019) and Davies et al. (2018) demonstrated that freshwater calving and topographic pinning points exerted a potentially strong control on the response of the central Patagonian glaciers to climate forcing during the Late Glacial.

Fast ice flow

Fast ice flow may decouple glaciers from the prevailing climatic conditions and should be considered when making climatic inferences from the geomorphological record. Fast ice flow has been inferred from landforms evidence in numerous places across Patagonia. Based on mapping of glacial lineations and ice-scoured bedrock east of the NPI, Glasser and Jansson (2005) reconstructed fast flowing, topographically-constrained outlet glaciers. They suggested that these outlet glaciers controlled ice discharge pattern and the position of the ice divide in this sector, and lowered the overall ice elevation profile. Fast ice flow may have decoupled these ice lobes from climate-induced thickness and extent (Glasser and Jansson, 2005). Around the Strait of Magellan, streamlined landforms along with the presence of thrust moraines and deformable bed were interpreted as evidence of rapid ice flow, potentially surge-like activity (Lovell et al., 2012; Darvill et al., 2017). At Lago Viedma (50° S), mapped landforms assemblages, which included crevasse-squeeze ridges, push and over-ridden moraines, and mega flutes, were also interpreted as evidence for surge activity (Ponce et al., 2019).

Numerical modelling

Numerical modelling experiments can provide important insights into the dynamics of former ice sheets. In Patagonia, this proved challenging because of the complex topography (alpine setting underrepresented by coarse model resolution, cf. Hubbard et al., 2005) and a range of climatic regimes encountered by the elongated north-south oriented PIS.

Hulton et al. (2002) used a coupled ice sheet/ climate model to simulate the PIS at the LGM and through deglaciation. The model produces an LGM ice-sheet with steep west-east mass balance gradient: a highly dynamic western ice margin with high mass balance; and an eastern ice margin partly constrained by moisture availability resulting from a precipitation shadow of the ice sheet. They found a good fit with the empirical evidence by lowering temperatures by 6 °C. The model, however, overestimated ice extent in the central sector while under-representing it in the southern parts. It also failed to reproduce large outlet lobes on the eastern side. Forced into deglaciation by stepped increases in temperatures, the northern sector of the PIS collapses rapidly, while the sector between 53° S and 43° S is most resilient.

Hubbard et al. (2005) instead focused on a central sector of the PIS, centred on the NPI. They used a three-dimensional model and a higher resolution grid (2km). The model, tuned to fit the empirical evidence from LBA, reproduced eastern outlet lobes, which are characterised by low ice surface gradients and low basal shear stress. When forced into deglaciation using the Vostok temperature record (Fig. 2.3), the ice sheet initially retreats steadily until a rapid collapse at about 14.5 ka when it loses $\sim$ 85 % of its volume in 800 model years. This may indicate that the ice sheet lost its stable configuration when a certain tipping point was reached. The model also simulates ice-margin stabilization during the ACR (Hubbard et al., 2005).

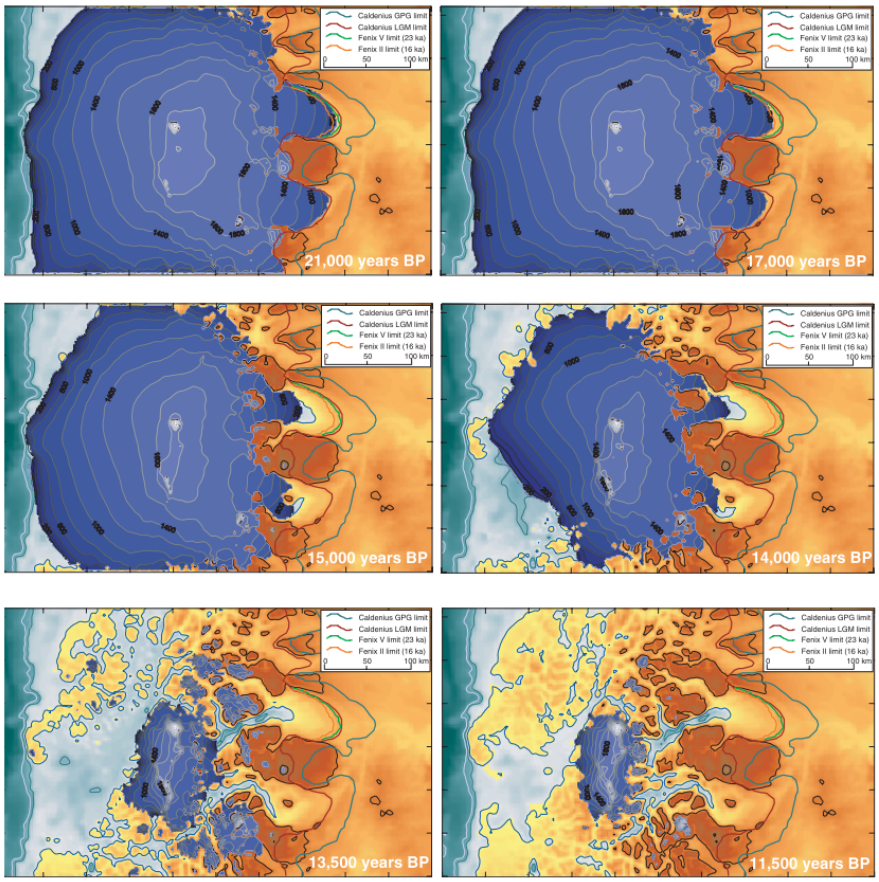

Figure 2.3: Deglaciation of the central sector of the Patagonian ice sheet as modelled by Hubbard et al. (2005), forced by the Vostok temperature record.

Simulating the PIS inception, Sugden et al. (2002) found that the presence of high mountain valleys creates the most favourable topography for ice inception. In contrast, where glaciers descend from narrow mountain crests to deep fjords, it takes longer for ice to build up. The growing ice-sheet also creates a lee-side effect and causes snow starvation over the more easterly massifs. Finally, they found that the increasing elevation of the ice sheet enhances mass-balance

on the western, upwind side and causes the ice-divide to migrate towards the precipitation source.

The wealth of glacial chronologies developed since these earlier modelling experiments provides an opportunity for new modelling work to gain insights into the ice sheet - climate interactions.

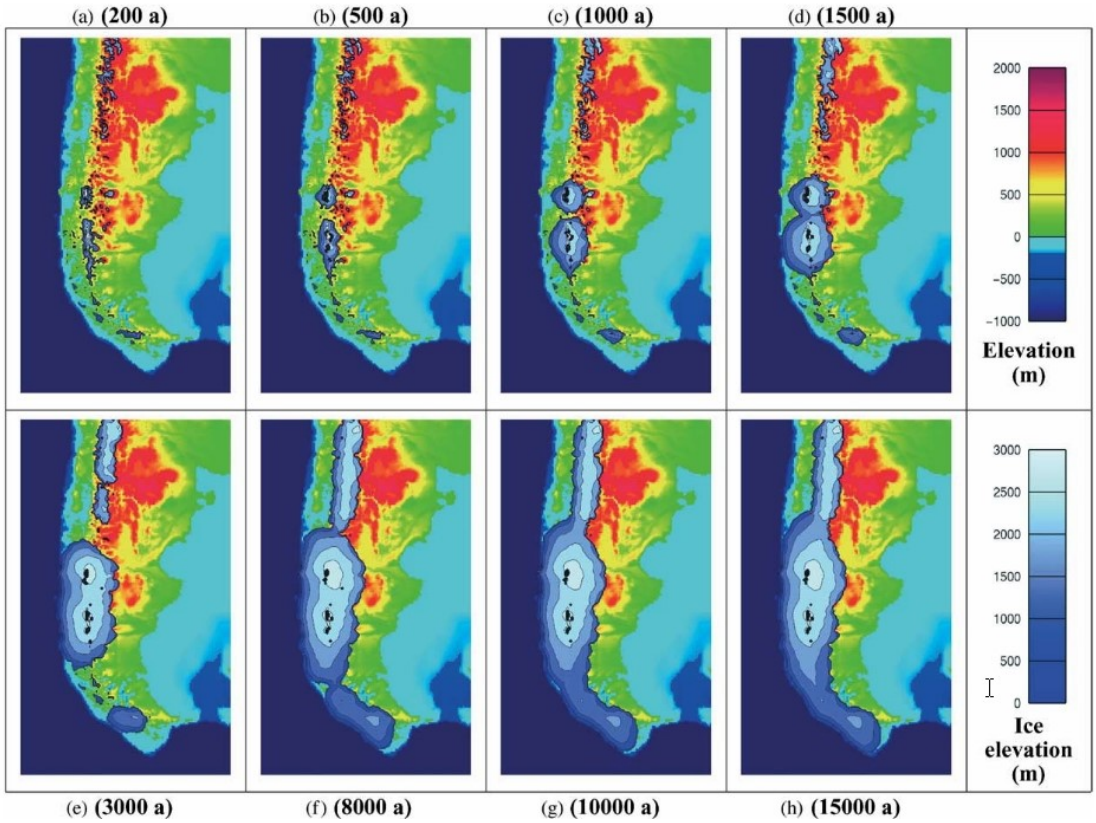

Figure 2.4: Simulation of the inception of the Patagonian ice sheet as modelled by Sugden et al. (2002).

2.2.3 Timing of glacial advances

The development of glacial chronologies using modern radiometric techniques began in the 1960's through the work of John Mercer (e.g. Mercer, 1976, 1982, 1983). Subsequent efforts to develop the glacial history of the PIS have used a wide range of dating techniques and are summarised by several review papers (McCulloch et al., 2000; Rabassa and Clapperton, 1990; Rabassa and Coronato, 2009; Kaplan et al., 2008; Glasser et al., 2004; Rodbell et al., 2009; Clapperton, 1993; Harrison and Glasser, 2011; Rabassa et al., 2000; Mendelova et al., 2017; Davies et al., 2020). Recently, Davies et al. (2020) presented an empirical reconstruction of the PIS from $\sim$ 35 ka to the present based on a compilation of previously published geochronological ages. The reconstruction of the central

sector of the PIS centred on the NPI is shown in Fig. 2.5. In this section, I discuss the chronological data spanning the last glacial cycle ($\sim$ 110 ka) in central Patagonia with references to a wider region where necessary.

Exposure ages presented here were recalculated using the CRONUS-Earth online calculator (version 3, Balco et al., 2008), with the Patagonia production rate (Kaplan et al., 2011) and the Lm time-dependent scaling scheme (Lal, 1991; Stone, 2000). Ages are presented as a mean $\pm 1\sigma$ standard deviation per landform, unless otherwise stated. Interpretations in the original publications were followed and outliers excluded accordingly. Modelled ages for outwash depth profiles are presented as in the original publications.

MIS 5 to the gLGM ($\sim$ 110 - 19 ka)

The evidence for ice expansion in Patagonia prior to MIS 2 is largely restricted to MIS 3 and previous glacial cycles. In southernmost Patagonia (53-54° S), Darvill et al. (2015) dated advances of the Bahía Inútil - San Sebastián ice lobe at 45.6 ($+139.9/-14.3$) ka and 30.1 ($+45.6/-23.1$) ka using outwash depth profile analysis, which were up to 100 km more extensive than the MIS 2 limits (Kaplan et al., 2004; McCulloch et al., 2005b). Similarly, the Torres del Paine and Última Esperanza outlet glaciers (50° S) reached their maximum extent at 48.0 $\pm$ 1.6 ka with subsequent advances/still-stands at 39.2 $\pm$ 2.0 ka, and 34.0 $\pm$ 1.3 ka (García et al., 2018; Sagredo et al., 2011). At 21.5 $\pm$ 1.8 ka, ice extent here was half of its MIS 3 maximum (García et al., 2018). Tentative ^{10}Be ages from Lago San Martín (49° S) suggest a pattern of successively smaller glacier extent from about 100 ka (Glasser et al., 2011). However, a more robust chronology is needed to confirm this. In northwestern Patagonia, stratigraphic evidence and radiocarbon chronology from the Chilean Lake District showed ice expansion at 33.6 $\pm$ 0.2 ka, but this was similar in magnitude or smaller than the MIS 2 ice extent (Denton et al., 1999a; Moreno et al., 2015). Outer moraine belts in three valleys here have been tentatively assigned to MIS 4 (Denton et al., 1999b; Heusser et al., 1999; Mercer, 1976), but further chronology is needed to firmly date these. In northeastern Patagonia (39° S), ^{10}Be ages reveal an advance at $\sim$39 ka Zech et al. (2011a).

In central Patagonia, most of the chronological work has concentrated on just two of the formerly glaciated basins: LBA (46.5° S) and LP (47.5° S) (Fig. 2.6). Here, a range of dating techniques, including argon-argon ($^{40}Ar/^{39}Ar$) dating of basaltic lava flows interbedded with glacial deposits, cosmogenic nuclide surface exposure dating, soil formation rates and OSL dating, have successfully been applied to date glacial advances from $\sim$ 1.2 Ma through to MIS 2 (e.g. Singer et al., 2004; Douglass and Bockheim, 2006; Kaplan et al., 2004, 2005; Smedley et al., 2016; Hein et al., 2009, 2010, 2011; Cogez et al., 2018). In both, LBA and LP valleys the oldest preserved last glacial limits date to MIS3/2 and MIS 2 (Douglass and Bockheim, 2006; Kaplan et al., 2004; Hein et al., 2009, 2010), indicating that these two lobes reached their last glacial maximum extent much

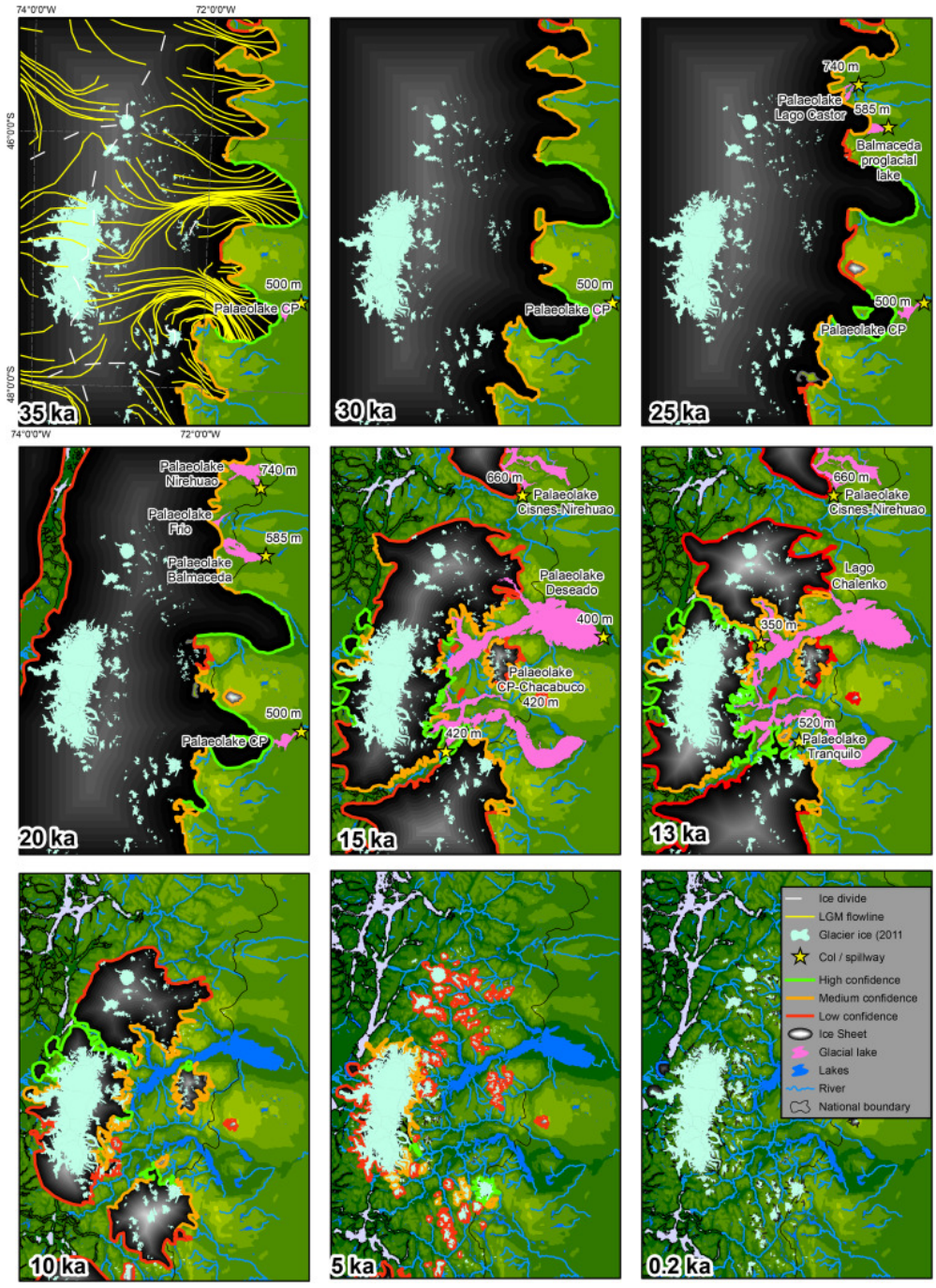

Figure 2.5: Empirical reconstruction of the central sector of the PIS, i.e. area centred on the NPI presented by Davies et al. (2020).

later than the outlet glaciers in southernmost Patagonia (Darvill et al., 2015; García et al., 2018). At LBA, this is marked by the Fenix moraine system with the outermost limit dated at 25.7 ± 1.9 ka followed by four advances/still-stands at 26.1 ± 1.3 ka, 21.6 ± 2.2 ka, 19.8 ± 1.4 ka and 18.5 ± 1.4 ka (Douglass and Bockheim, 2006; Kaplan et al., 2004). In the LP valley, the maximum limit of the last glacial cycle is represented by the Río Blanco moraine system with individual advances/still-stands dated at 28.4 ± 0.8 ka, 24.9 ± 0.4 ka and 20.9 ± 1.0 ka (Hein et al., 2010, 2009). The only evidence for earlier expansion comes from OSL ages (34.0 ± 6.1, 30.8 ± 5.7 ka) of buried glacial outwash at LBA (Smedley et al., 2016), and a single moraine boulder age (35.1 ± 1.2 ka) from Lago Pueyrredón (Hein et al., 2010). In both basins, the next older moraines pre-date the last interglacial (Kaplan et al., 2005; Hein et al., 2017, 2009, 2010; Kaplan et al., 2004; Douglass and Bockheim, 2006). If earlier advances during the last glacial cycle occurred here, they were either less extensive than the MIS 2 limits or of similar magnitude.

Elsewhere in central Patagonia, the MIS 2 ice margins are only assumed or inferred based on minimum radiocarbon ages for ice free conditions (e.g. de Porras et al., 2012; García et al., 2019). In the Río Cisnes valley (44.7° S), a basal radiocarbon age of 19.0 ± 0.1 cal ka BP from an inter-morainic lake (de Porras et al., 2012) provides a minimum age for ice withdrawal from moraines, which likely represent full glacial conditions (García et al., 2019). Ice then retreated by about 35 km, accompanied by a proglacial lake formation, before an advance/still-stand deposited a moraine dated at 21.1 ± 1.2 ka using ^{10}Be (García et al., 2019).

The only published vertical ice reconstruction in central Patagonia was done by Boex et al. (2013) along a mountain transect separating the Lago Pueyrredón and Chacabuco valleys using ^{10}Be ages from boulders and bedrock. Lateral moraines, which are age-equivalent to the Río Blanco moraine system in the LP valley, revealed maximum ice-thickness of ∼ 1100 m, about 40 km from the terminus. This result is consistent with previous modelling (Hubbard et al., 2005).

gLGM to the Holocene (∼ 19 - 10 ka)

Deglaciation

The onset and rate of deglaciation is best constrained at LBA, where a calendar-year anchored varve chronology has been developed (Bendle et al., 2017a). Here, ice retreat initiated at 18.1 ± 0.2 ka based on a Bayesian age model integrating a varve chronology and moraine boulder ages (Bendle et al., 2017a; Douglass and Bockheim, 2006). The retreat, accompanied by a proglacial lake formation, was initially gradual, followed by a short ice stabilisation that deposited the Menucos moraines at 17.7 ± 0.1 ka (Bendle et al., 2017a). Subsequently, ice retreat accelerated due to recession to deeper waters and calving. The formation of varves lasted until 16.9 ± 0.1 suggesting that ice occupied the eastern part of the basin until this time (Bendle et al., 2017a). By 16.0 ± 0.6 ka, the LBA outlet lobe had disintegrated as evidenced by the oldest age from a moraine deposited

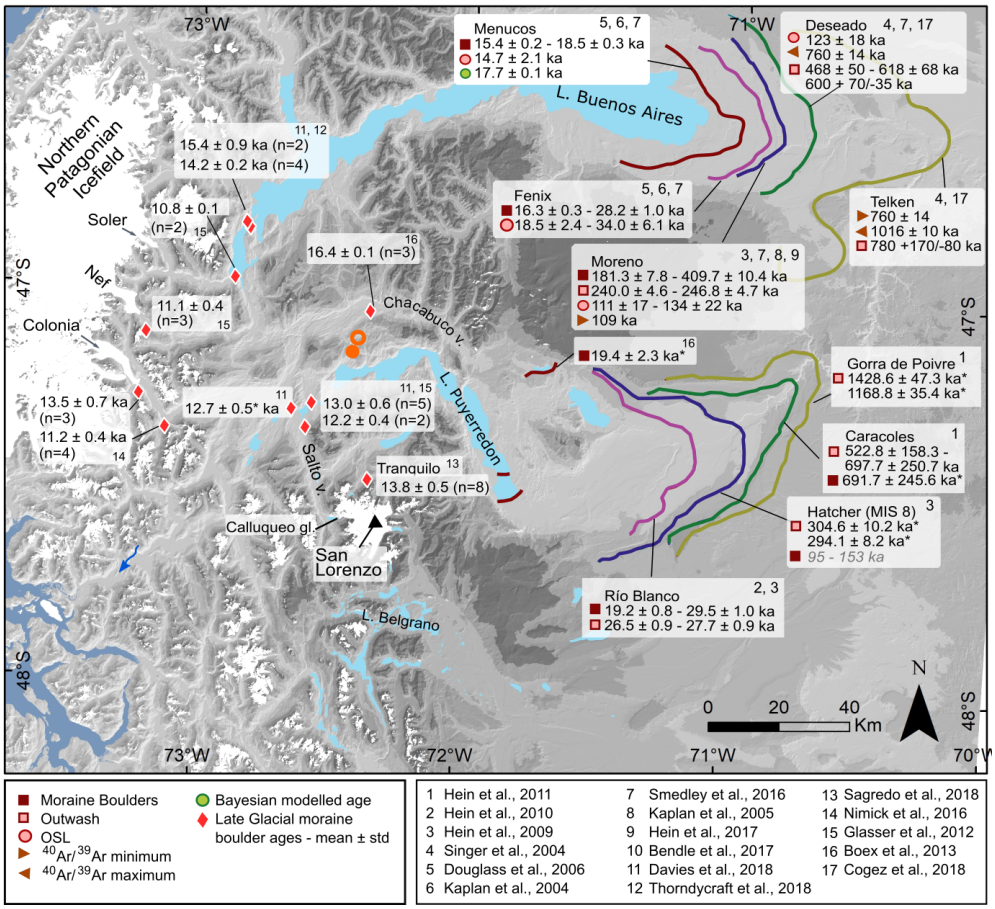

Figure 2.6: Overview map of published chronologies showing: 1) Main ice limits in Lago Buenos Aires and Lago Pueyrredón valleys. Exposure ages are presented as a range for each moraine system (not differentiating individual advances), taking the youngest and the oldest age with internal uncertainty. 2) Moraine ^{10}Be ages spanning the ACR and YD/Holocene transition. Only ages which have not been affected by submergence in a regional palaeolake are shown (cf. Thorndycraft et al., 2019). Present day glaciers are from the GLIMS database.

at the eastern edge of Lago Buenos Aires (Thorndycraft et al., 2019; Davies et al., 2018).

At Lago Pueyrredón, deglaciation started once ice abandoned the innermost LGM moraine, dated with a ^{10}Be age of 19.2 ± 0.8 ka (Hein et al., 2010). Ice retreat was accompanied by a proglacial lake development and was interrupted by ice margin stabilization that deposited moraines in both Lago Pueyrredón and Chacabuco valleys. A tentative age for this stabilisation comes from a single moraine boulder age of 19.4 ± 2.3 ka in the Chacabuco valley (Boex et al., 2013). Hein et al. (2010) inferred a retreat of more than 80 km and proglacial lake lowering in less than 2 ka based on a submerged boulder age (17.3 ± 0.9 ka). Radiocarbon ages from lake sediment cores taken between the Lago Pueyrredón and Chacabuco valleys indicate ice free conditions as early as 19.6 ± 0.1 cal ka BP suggesting separation of the Pueyrredón ice lobe (Henríquez et al., 2017; Villa-Martínez et al., 2012). The ^{10}Be vertical reconstruction revealed rapid thinning equivalent to about 1000 m of ice-surface lowering between ∼ 18 - 17 ka (Boex et al., 2013). Ice may have lingered in the western part of the Chacabuco valley, ∼70 km from the present day margins of the NPI, until about 16.4 ± 0.1 ka (Boex et al., 2013). Rate of deglaciation in the Lago Pueyrredón valley remains poorly constrained, but it is thought that the outlet lobe here also disintegrated by ∼ 16 ka (Turner et al., 2005; Thorndycraft et al., 2019).

Late Glacial advances

Following a period of retreat, glaciers advanced/stabilized during the Late Glacial. There is an ongoing debate on the response of Patagonian glaciers to the southern and northern hemisphere cold reversals, in particular the ACR and YD and their relative magnitudes.

Overall, Late Glacial ice marginal positions are best constrained for the eastern outlet glaciers of the NPI (Fig. 2.6). However, nearly all of theses glaciers calved into regional palaeolakes (cf. Thorndycraft et al., 2019), which may have exerted strong influence on their dynamics and response to cold reversals (Davies et al., 2018). Advances/stillstands during the ACR were documented for the Colonia glacier (13.2 ± 1.0 ka, Nimick et al., 2016) and the Soler glacier (Thorndycraft et al., 2019; Davies et al., 2018). The moraines at the eastern edge of LBA deposited by the Soler glacier yielded two older ages (15.4 ± 0.9 ka, mean) and a cluster of younger ages with a mean of 14.2 ± 0.2 ka (Thorndycraft et al., 2019; Davies et al., 2018). These moraines may mark a longer stabilisation on a topographic pinning point during an overall retreat while the glacier calved into a 400 m deep palaeolake in the LBA basin (Thorndycraft et al., 2019; Davies et al., 2018). The Soler glacier then advanced/stabilised again about 16 km up-valley at the time of the YD (11.0 ± 0.5, 10.7 ± 0.4 ka; Glasser et al., 2012). Stabilisation of the NPI ice margins during the YD is also supported by lateral moraines in the Nef valley (11.1 ± 0.4 ka; Glasser et al., 2012) and in the Colonia valley (11.2 ± 0.4 ka; Nimick et al., 2016). However, the latter age is based on boulders from

low-lying moraines, whose relationship to the regional palaeolake is unconstrained. Some ages from moraine boulders east of the NPI originally interpreted as dating YD advances (Glasser et al., 2012), were submerged in palaeolakes and instead likely date lake level fall (Thorndycraft et al., 2019).

There is evidence from two valleys for glacier advances/still-stands during the ACR on the northern flank of Monte San Lorenzo. In the Salto valley, Davies et al. (2018) obtained a ^{10}Be age of 13.0 ± 0.6 ka from a moraine deposited by the Calluqueo glacier, and in the Tranquilo valley, Sagredo et al. (2018) dated a moraine at 13.8 ± 0.5 ka. The former calved into a 350 m deep palaeolake at this time. Provisional ages from both valleys suggest smaller YD advances/still-stands (Glasser et al., 2012; Sagredo et al., 2018) at the time of the YD.

Late Glacial ice marginal positions remain poorly resolved in central Patagonia, in particular for smaller ice caps. Moraines dated to the YD in most cases rely on small number of ages (< 2). There is a complex interplay between glaciers, topography and palaeolakes in this sector of central Patagonia. Disentangling climatic and non-climatic controls on glacier behaviour is thus a particularly difficult task in this area.

The Holocene (last ∼10 ka)

Our understanding of the Holocene glacier dynamics in central Patagonia is limited owing to a paucity of robust glacier chronologies. Earlier work using radiocarbon dating (e.g. Mercer, 1968; Glasser et al., 2004) has given valuable insights, but only provides minimum/maximum bracketing dates for the timing of glacial advances. Dendrochronology and lichenometry have been helpful in documenting glacier behaviour but often only span the last several centuries (e.g. Glasser et al., 2002; Harrison et al., 2008; Aniya and Naruse, 1999; Winchester and Harrison, 1996; Garibotti and Villalba, 2017). Only a handful of exposure ages have so far been obtained from Holocene moraines in central and northern Patagonia.

There is evidence for glacier expansion in the early Holocene. OSL ages from moraines (9.7 ka, 9.3 ka and 5.7 ka) and glacial outwash (7.7 ka and 7.8 ka) suggested that the Rafael Glacier, a large western outlet of the NPI, was either more extensive between 9.7 ka and 5.7 ka, or advanced multiple times during this time period (Harrison et al., 2012). However, non-climatic factors related to calving dynamics may have driven the Holocene fluctuations of this glacier (Harrison et al., 2012). Previous sedimentological work demonstrated complex composition of these moraines, resulting from sediment reworking by a glacier re-advance into its former proglacial area (Glasser et al., 2006). East of the NPI, two moraines deposited atop of a raised delta above LBA yielded ^{10}Be ages of 10.9 and 8.9 ka (recalculated means) (Douglass et al., 2005), but show a considerable scatter.

The onset of the so-called 'Neoglacial' from the mid-Holocene was originally proposed based on minimum/maximum radiocarbon ages (Aniya, 1995, 1996;

Mercer, 1970, 1976, 1982). The exact timing of glacier advances remains to be established in much of central Patagonia. Mid-Holocene advances/stillstands were only directly dated using ^{10}Be for two glaciers. The Tranquilo glacier on the northern flank of Monte San Lorenzo deposited a moraine at 5.7 ± 0.1 ka (Sagredo et al., 2016), and a lateral moraine in the Colonia valley, east of the NPI, was dated at 5.0 ± 0.2 ka (Nimick et al., 2016). A later advance/stillstand is suggested by three OSL ages from glacio-lacustrine sediments and a terminal moraine of the Leon glacier (2.6 ± 0.2 ka, 2.4 ± 0.5 ka and 3.3 ± 0.9 ka; Harrison et al., 2008). The OSL ages are, however, inconsistent with ^{10}Be ages obtained from the same moraine (1.1 ka and 0.9 ka) (Harrison et al., 2008). More recent glacial history has been investigated extensively around the NPI using historical documents, dendrochronology, lichenometry and radiocarbon dating (e.g. Winchester and Harrison, 1996; Harrison and Winchester, 2000; Winchester et al., 2001; Harrison et al., 2007; Glasser et al., 2002, 2004). These studies demonstrated the onset of ice recession from prominent terminal moraines and trimlines around AD 1870 - 1890. This is considered the end of the Little Ice Age (LIA) in the area (Harrison et al., 2007). Overall, drawing temporal and spatial patterns over the Holocene is problematic and it is not clear when glaciers in central Patagonia were at their Holocene maximum.

In southern Patagonia, more detailed chronologies have been developed, which give insight into the long-term Holocene glacier change. In the Cordillera Darwin, glaciers were similar to, or even smaller than today multiple times in the early and mid-Holocene (Hall et al., 2019). The largest glacier advances then occurred over the last 1.3 ka (Hall et al., 2019). The SPI outlet glaciers also retreated from their Late Glacial maximum to near the present-day limit by ∼ 9.2 ka as documented by stratigraphy and radiocarbon dating (Kaplan et al., 2016; Strelin et al., 2014, 2011). They then achieved their Holocene maximum between 6.1 - 4.5 ka followed by a second phase of advances/stillstands after 2.3 ka (Kaplan et al., 2016; Strelin et al., 2014, 2011). Reynhout et al. (2019) documented decreasing extent of the Torre glacier (SPI) from the early Holocene until the last millennium with advances dated at 9.7 ± 0.4, 6.9 ± 0.2, 6.1 ± 0.3, and 4.5 ± 0.2 ka. The timing of these glacier advances have been linked to the climate variability related to the Southern Annual Mode (SAM) (Reynhout et al., 2019; Kaplan et al., 2016). Reynhout et al. (2019) attributed the pattern of decreasing extent of the Torre glacier to increasing Southern Hemisphere summer insolation.

2.2.4 Proglacial lake evolution

Deglaciation in Patagonia was accompanied by the development of large proglacial lakes and continental drainage reversals. Understanding the evolution of proglacial lakes is important for interpreting the glacial geomorphological record and its palaeoclimatic significance. Thorndycraft et al. (2019) demonstrated that some dated moraines east of the NPI were submerged in regional palaeolakes. Shielding by water would reduce production of cosmogenic nuclides in these sur-

faces and thus boulders from submerged moraines would produce erroneously young exposure ages.

Palaeoshorelines and raised deltas have been mapped extensively in the LP, LBA and Chacabuco basins (Bendle et al., 2017b; Hein et al., 2010; Turner et al., 2005; Glasser et al., 2016; Bell, 2008; Bourgois et al., 2016). Here, proglacial lakes developed in each basin as ice was blocking westward drainage pathways (including the Río Baker valley) and initially drained eastward to the Atlantic Ocean. Retreating ice margins gradually opened up Pacific drainage pathways (Glasser et al., 2016) and also allowed a unified palaeolake to form, which flooded all three valleys. A number of dating techniques have been applied to constrain the evolution of these palaeolakes, including OSL dating of raised deltas and beaches, ^{14}C dating of organic material from spillways, and cosmogenic exposure analysis resulting in a number of different, often competing models of lake evolution (Hein et al., 2010; Glasser et al., 2016; Turner et al., 2005; Bourgois et al., 2016). Recently, Thorndycraft et al. (2019) proposed a refined model of the palaeolake evolution based on an improved high resolution mapping, an altitudinal analysis of existing geochronologies and Bayesian age modelling (Fig. 2.7). They demonstrated a gradual drainage of the paleaolakes over at least six drainage events. Their Bayesian age modeling places the final drainage of the unified palaeolake into the Pacific at 12.4 - 11.8 ka as the lower Río Baker valley opened up. Most outlet glaciers of the NPI and western glaciers of San Lorenzo calved into these regional palaeolakes during most of Late Glacial. Davies et al. (2018) demonstrated that freshwater lakes exerted a strong influence on the dynamics of these glaciers and on their response to climate fluctuations.

Comparatively little work has been done on the evolution of proglacial lakes and drainage reversals in other valleys in the region. For example, García et al. (2019) documented development of a proglacial lake in the Río Cisnes valley (44°) from $\sim$ 19 ka, which extended westwards as the ice margin retreated and flooded multiple basins before draining to the Pacific towards the end of the Late Glacial. Horta et al. (2017) proposed a model of palaeolake evolution in the Belgrano valley. However, geomorphological evidence constraining the palaeolake levels and the relationship of the presented radiocarbon ages to reconstructed palaeolake levels are unclear.

2.2.5 Terrestrial palaeoenvironmental proxies

Terrestrial palaeoenvironmental proxies can yield insights into deglaciation history, palaeoclimate and landscape development. Their distribution in central Patagonia is biased towards the eastern side of the Andes due to easier access, with the exception of the Taito peninsula. This section highlights the major trends in landscape development and palaeoclimatic conditions inferred from different proxies.

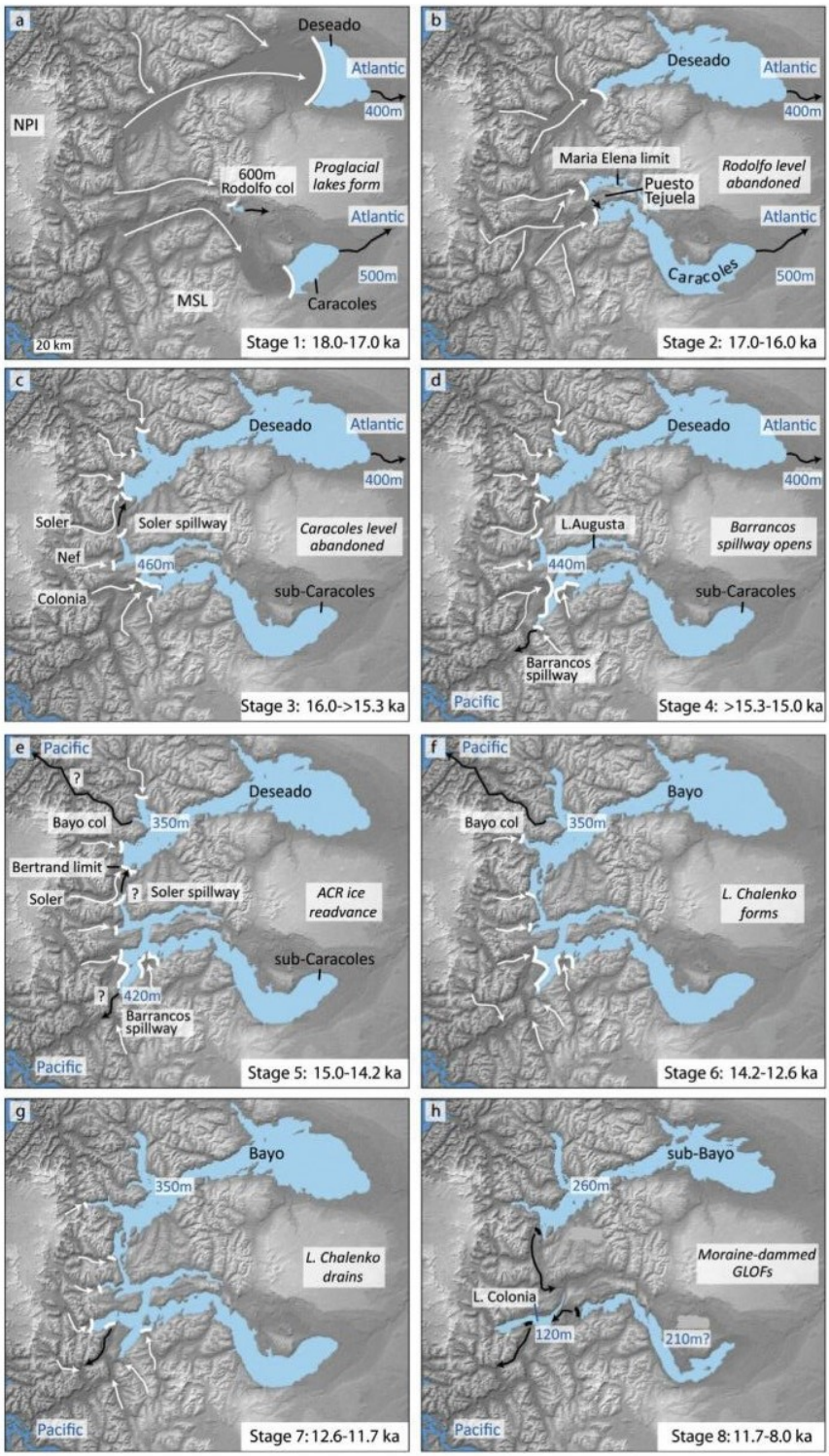

Figure 2.7: The model of palaeolake evolution in the LBA, LP and Chacabuco valleys, from Thorndycraft et al. (2019).

Late Glacial

Following ice retreat, most records from the eastern side of the Andes indicate an open landscape with sparse scrub-steppe dominated by Poacea, Asteraceae, and Ericaceae under persistent cold and dry conditions at most sites until ca. 14 cal ka BP (Markgraf et al., 2007; de Porras et al., 2012; Iglesias et al., 2016). Steppe taxa such as Plantago and Acaena was often present indicating disturbance and unstable post-glacial conditions (de Porras et al., 2012, 2014; Markgraf et al., 2007; Iglesias et al., 2016). Iglesias et al. (2016) inferred $\sim$ 200 mm annual precipitation required to support the reconstructed vegetation community at 44° S 71° W. Subsequently, a gradual increase in Nothofagus taxa suggests grass-steppe vegetation with scattered trees and an increase in effective moisture, but still less than modern values (de Porras et al., 2012, 2014; Markgraf et al., 2007). The pollen record from Lago Los Niños suggests open forest between 14.3 - 13.2 cal ka BP, with a subsequent trend towards more open landscape and drier conditions until 11.5 cal ka BP (Iglesias et al., 2016). Fluctuations of aquatic taxa in pollen records attest for high millennial-scale environmental variability between ca. 14 and 11 cal ka BP (Markgraf et al., 2007; Villa-Martínez et al., 2012).

Contrary to the above, wetter and colder conditions throughout the Late Glacial period are inferred from the Lago Augusta and Lago Edita pollen record on the basis of arboreal taxa, such as Nothofagus, hygrophilous Fitzroya/Pilgerodendron and Drimys present immediately after the onset of sedimentation and persisting until 11.8 cal ka BP (Villa-Martínez et al., 2012; Henríquez et al., 2016). This pollen assemblage reflects patches of evergreen forests in an open landscape, likely a forest refugia in Chacabuco Valley, sustained by the enhanced influence of the SWW at this latitude (Villa-Martínez et al., 2012; Henríquez et al., 2016). A decline in hygrophilous and cold-resistant taxa at ca. 11.8 cal ka BP is concurrent with an increase in Nothofagus and likely reflects warming and reduced precipitation due to the decreased influence of the SWWs (Villa-Martínez et al., 2012).

On the western side of Patagonia, a marine pollen record from 46° S off the Chilean coast (MD07-3088), suggests a gradual Nothofagus forest expansion from $\sim$ 17.6 cal ka BP, representing a first step of warming (Montade et al., 2013). Closed Nothofagus-Pilgerodendron-Podocarpus forest developed across the Chonos Archipelago and Taitao Peninsula between 14 - 13 cal ka BP and showed no reductions in the forest cover once a closed forest became established (Haberle and Bennett, 2004; Bennett et al., 2000; Lumley and Switsur, 1993). Humid rainforests, once established, tend to be insensitive to smaller climatic changes. However, a high-resolution marine pollen record indicated there was an increase in Magellanic moorland (Astelia) at 14.5 cal ka BP, interpreted as a sudden precipitation increase accompanied by a pause in the warming trend and cooling coinciding with the ACR. The subsequent retreat of the Magellanic moorland after 12.8 cal ka BP marks the second warming step during the Late Glacial and provides a strong evidence for the end of the ACR (Montade et al.,

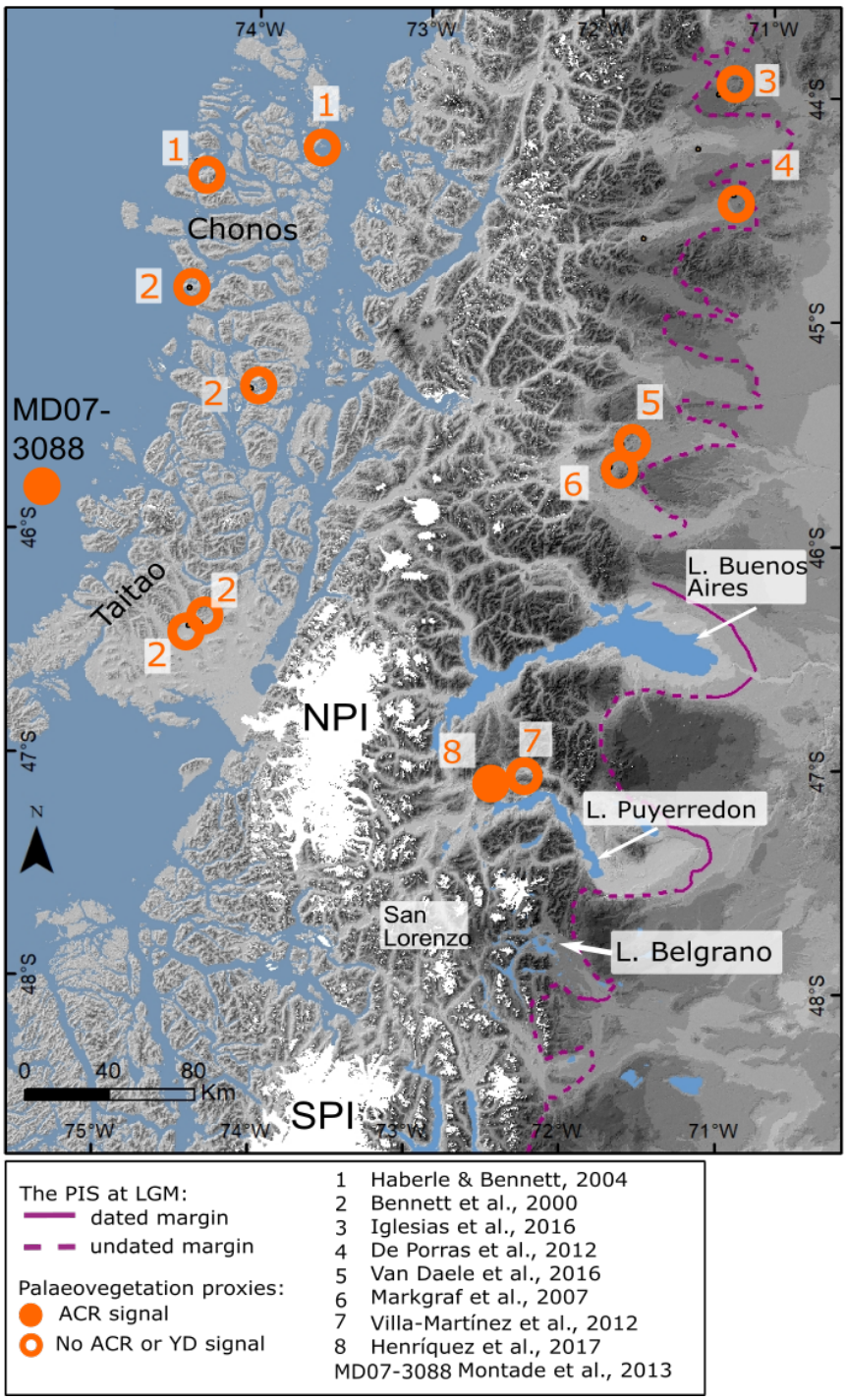

Figure 2.8: The location of palaeoenvironmental proxies in central Patagonia spanning the Late Glacial. The records, which document the ACR signal are shown with a full orange circle, while the ones which do not document either ACR or YD are depicted with an empty circle.

2013). A Chironomid record from Laguna Stibnite on the Taitao Peninsula shows a peak in abundance of Podonominae between 13.1 - 10.5 cal ka BP, interpreted as indicative of cool and oligotrophic lake waters. The changes in the chironomid assemblages were small, however, and any cooling during this period, coeval with the YD would have been minimal (Massaferro and Brooks, 2002).

In summary, with the exception of two pollen records (Henríquez et al., 2017; Montade et al., 2013), palaeovegetation proxies, do not indicate any significant vegetation changes from which cooling contemporaneous with either the ACR or YD may be inferred. Proxies from the eastern side of the Andes show high variability in effective moisture during the Late Glacial (15 - 11 ka), which together with the degree of insensitivity of proxies to minor oscillations in temperature might have masked any less pronounced cooling coeval with either the ACR or YD.

Holocene

During the early Holocene, forests on the Pacific islands were dominated by Tepualia and Weinmannia between 12.4 - 6.7 ka indicating warm and dry conditions ($\sim 1°$ to $2°$ C above present mean temperature) (Haberle and Bennett, 2004). The warmest and driest conditions of the Holocene between 11.5 to 7.4 ka were inferred from a pollen assemblage dominated by heliophytic taxa, such as Myrtacea and Tepualia, in a marine sediment core at 46° S (MD07-3088) (Montade et al., 2013). This is further supported by a chironomid record from the Taitao peninsula, which suggested conditions drier than today between 10.5 - 7.2 cal ka BP (Massaferro and Brooks, 2002).

On the eastern side of the Andes (44° S - 45° S, 71° W), an open Nothofagus woodland developed from $\sim$ 11 ka, accompanied by an increase in the frequency and magnitude of fires signalling increasing effective moisture, but under modern values, and summers drier and/or warmer than present (de Porras et al., 2012, 2014; Markgraf et al., 2007). In the Chacabuco valley (47° S, 72° W), closed Nothofagus forest developed between 11.8 and 9.8 cal ka BP, accompanied by a decline of hygrophilous and cold-resistant taxa, and increased frequency of fires. These changes were interpreted to indicate increased temperatures and declined westerly precipitation (Villa-Martínez et al., 2012). At 49° S, 72° W, on the southern side of Lago San Martin, precipitation lower than today, likely around 200 mm a^{-1}, was inferred based on the pollen assemblage dominated by Poaceae, Ephedra and Chenopodiaceaea between 11.3 - 9.5 cal ka BP (Bamonte and Mancini, 2011).

Precipitation decline and peak fire activity during the early Holocene were recorded in NW Patagonia and SW Patagonia suggesting a regional trend (Moreno and Videla, 2016; Moreno et al., 2010; Whitlock et al., 2007; Villa-Martínez and Moreno, 2007; Moreno and León, 2003; Moreno, 2004; McCulloch and Davies, 2001; Power et al., 2008). This has been attributed to weakening of the SWW and/or their southward displacement (Moreno et al., 2010; Villa-Martínez et al.,

2012; Fletcher and Moreno, 2012; Moreno, 2004). High-resolution reconstruction of the SWW strength based on salt-aerosol input record from a small island in the Southern Ocean supports the SWW weakening between 11.2 and 7.2 ka (Saunders et al., 2018). A major transgression was documented at Lago Cardiel during early Holocene at $\sim$ 11.8 cal ka BP (Gilli et al., 2005, 2001; Markgraf et al., 2003; Stine and Stine, 1990), which may be explained by enhanced easterly moisture advection to the extra-Andean region due to decreased SWW influence (Zolitschka et al., 2013; Villa-Martínez and Moreno, 2007), which would support decreased precipitation within the Andes. On the contrary, Lamy et al. (2010) proposed stronger SWW at their core and weakening at their northern margin in the early Holocene.

During the mid-Holocene, proxies from central Patagonia indicate a shift to cooler and wetter conditions and/or establishment of present day precipitation regime, a decrease in fire activity and establishment of vegetation communities analogous to modern ones on both sides of the Andes (Markgraf et al., 2007; Haberle and Bennett, 2004; de Porras et al., 2014; Montade et al., 2013; Villa-Martínez et al., 2012; Iglesias et al., 2016). de Porras et al. (2012) recorded the easternmost position of the forest-steppe ecotone at 44° S between 8 and 3 cal ka, indicating the highest effective moisture of the record. The chironomid record from the western side suggests a trend towards wetter conditions during the mid-Holocene indicating intermediate precipitation between 7.2 - 5.2 cal ka BP and higher precipitation between 5.2 - 2.4 cal ka BP (Massaferro and Brooks, 2002). Increased humidity and a cooler trend in the mid-Holocene have been inferred based on proxies from NW Patagonia (e.g. Moreno, 2004; Moreno and Videla, 2016). These changes have been attributed to higher intensity of the SWW and/or a northward shift (Moreno et al., 2010). After mid-Holocene, the onset of seasonality and/or high centennial variability is observed in records along with spatial heterogeneity, which has been attributed to centennial contraction/expansion of the SWW and/or high frequency variability associated with the ENSO or SAM (Iglesias et al., 2016; Moreno and Videla, 2016; de Porras et al., 2012; Markgraf et al., 2007; Moreno et al., 2018; Markgraf et al., 2003).

2.2.6 Marine proxies

Sea surface temperature reconstructions

Sea surface temperatures (SST) in the southern mid-latitudes reflect the position of the Antarctic Circumpolar Current and the SWW system (Kaiser et al., 2005; Lamy, 2004). The alkenone-based SST reconstruction at 41° S off the Chilean coast (ODP 1233, Fig. 2.9) provides a continuous record over the last 70 ka with a mean resolution of 320 years (Kaiser et al., 2005; Lamy, 2004). The coldest temperatures of the record (8 °C) occurred between $\sim$ 68 and 62 ka followed by a rapid rise to 12 °C at $\sim$ 61 ka. Subsequently, a cooling trend is observed until $\sim$ 45 ka. Superimposed on the cooling trend are millennial-scale variations of 3

°C, which mirror Antarctic temperature records. Between 45 and 19 ka, the SST are characterized by variability of 2 - 3 °C, and notably the LGM is not clearly resolved by the record. Deglaciation is characterized by two warming steps: the first initiated at 19.2 ka with a temperature rise of 3 °C, and was interrupted by a cooling event of 0.8 °C between 14.8 and 13.3 ka, followed by the second warming step of 2 °C at 12.7 ka.

The alkenone-based SST record from 53° off southernmost Chile showed relatively warm temperatures (up to 9 °C) from ∼ 60 until 55 ka. Minimum temperatures (5 °C) of the record were observed at ∼ 50 ka (Caniupán et al., 2014). Subsequently, a long-term warming trend is observed until 25 ka followed by a cooling trend, which culminated in a minimum at 19 ka. This prolonged cooling trend has been explained by the proximity of the ice margins and high melt-water discharge. Between 50 - 19 ka, a millennial-scale variations with amplitude up to 4 °C are observed, which, together with a two-step warming during the Late Glacial, match ODP 1233 site and Antarctic temperatures (Caniupán et al., 2014).

SST reconstructions spanning the last ∼ 20 ka at sites along the Chilean margin (53° S - 41° S) record a pause in warming/cooling phase coeval with the ACR Haddam et al. (2018) supporting Antarctic timing of millennial-scale climate change during the last deglaciation.

Offshore terrigenous sediment records

Variations in terrigenous sediment composition reaching the Chilean continental margin has been used as a proxy for glacial activity in Patagonia (Siani et al., 2010; Lamy, 2004; Kaiser et al., 2007). For example, high offshore Fe concentrations have been linked to enhanced glacial erosion of the Andean volcanic rocks rich in Fe, at times of the PIS expansion (Lamy, 2004). Comparison of the Fe record and reconstructed SST from the ODP 1233 site revealed that between 40 and 20 ka, and during the cold part of MIS 4, SST led the Fe record by about 700 and 500 years, respectively (Kaiser et al., 2007; Lamy, 2004). The authors relate this to a lagged response of the PIS at times when it was at its largest. The offset disappeared and both records showed synchronous response between 50 and 40 ka. At the MIS4/3 transition and during the Late Glacial the relationship was reversed, Fe values remained high while SST increased, which was attributed to high meltwater and sediment supply from the rapidly wasting PIS (Kaiser et al., 2007; Lamy, 2004).

Similarly, Siani et al. (2010) used Smectite/(illite + chlorite) and Ti/K ratios on a sediment core from site MD07 3088 at 46° S to infer sediment provenance and glacial activity in central Patagonia over the past 22 ka. They infer glacial advances at 21.6 - 20.9 ka, 20.2 - 20 ka, 19.6 - 19.1 ka and 18.5 - 18 ka when the above ratios were lower. After 18 ka, the Smectite/(illite + chlorite) and Ti/K ratios showed a two step increasing trend and a decrease in sediment supply.

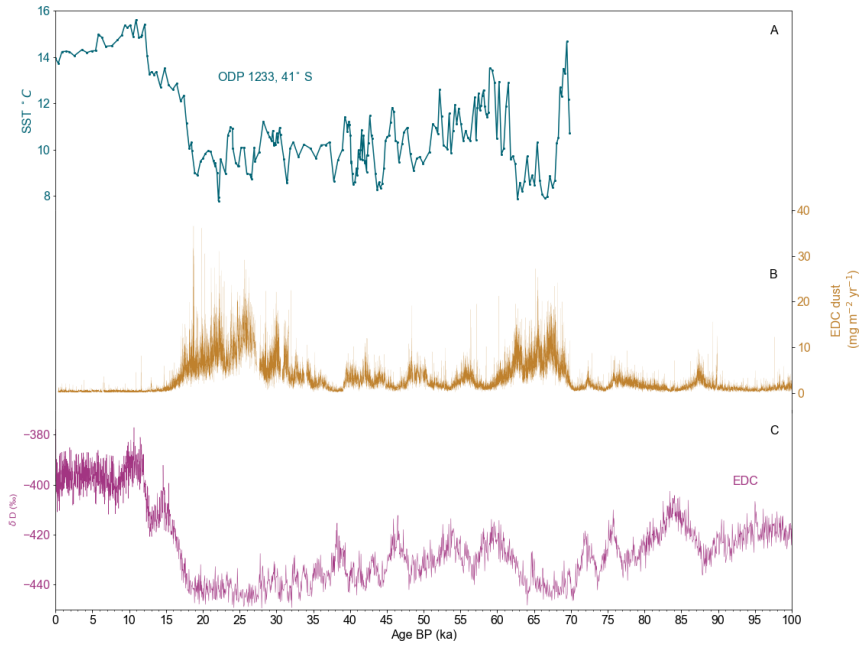

Figure 2.9: A summary figure of marine and Antarctic proxies. A: SST record from off Chile (ODP1233) (Kaiser et al., 2005; Lamy, 2004). B: EDC dust record (Lambert et al., 2012). C: EDC deuterium record (EPICA Community Members, 2004) plotted on AICC2012 timescale (Veres et al., 2013).

During the Holocene, Siani et al. (2010) inferred glacial advances at 10.1 - 9.1 ka, 7.8 - 6.5 ka, 3 - 2.2 ka and 1.5 - 0.7 ka.

2.2.7 Dust record

Dust fluxes to Antarctica (Lambert et al., 2008) are considered a proxy for glacial activity in Patagonia (Sugden et al., 2009; Kaiser and Lamy, 2010), as demonstrated by the similarity in isotopic composition of Antarctic dust and sediments from Patagonia (Sugden et al., 2009). During the glacial times, large outwash plains with braided channels developed on the Patagonian plains east of the Andes, which would provide a large source of dust (Sugden et al., 2009). Interaction of the SWW and the PIS would increase aridity on the eastern, lee side of the Andes and promote foehn winds, which would facilitate dust mobilization from the Patagonian plains (Sugden et al., 2009). Elevated dust values in Antarctic records occurred during MIS 4 (Fig. 2.9, Lambert et al., 2008), coeval with higher Fe concentrations at site ODP1233, also a proxy for glacial activity (Kaiser and Lamy, 2010), suggesting increased glacial activity. However, so far there are no corresponding dated glacial limits in Patagonia at this time. During MIS 3 dust fluxes generally decreased with millennial-scale variability, and began increasing at about 35 ka with a peak at about 30 and then 25 ka

(Lambert et al., 2008). Chronologies from southern Patagonia showed glacial advances at 34.0 ± 1.3 ka (García et al., 2018) and 30.1 (+45.6/−23.1) ka (Darvill et al., 2015), which may correlate to these dust peaks. Comparing high resolution dust records from Antarctica to glacial advances in Patagonia is complicated by the low resolution of dating techniques such as cosmogenic surface exposure analysis to resolve millennial-scale peaks in dust. The Fe concentration record at site ODP1233, a proxy for glacial activity in Patagonia, matches Antarctic dust records at millennial time scales (Kaiser and Lamy, 2010).

2.2.8 Previous work at Lago Belgrano and around Monte San Lorenzo

The San Lorenzo ice cap coalesced with the larger PIS during the full glacial conditions (Caldenius, 1932; Wenzens, 2005; Glasser et al., 2008). Ice from the northern flank of San Lorenzo discharged into the Lago Pueyrredón valley, while the eastern side of the massif sustained an outlet glacier in the Belgrano valley.

The Belgrano valley has received little scientific attention, and as a result little has been done to map the glacial geomorphology in detail and to develop robust chronologies (Fig. 2.10). Caldenius (1932) assumed glacial limits in the Belgrano valley correlate to other valleys in Patagonia, but himself did not visit because of a broken vehicle. Up to this date, the only chronological constraint on the timing of the major fluctuations of the Belgrano outlet glacier comes from two minimum radiocarbon ages of 18.0 ± 0.2 and 12.6 ± 0.1 cal ka BP (Wenzens, 2005 [1]; Table 2). Wenzens (2005) also tentatively attributed the outermost moraine belt in the Belgrano valley to the LGM (Fig. 2.10).

Based on the reconstruction of Wenzens (2005), ice oscillated in the Belgrano valley until the Late Glacial/Holocene transition. Ice on the northern and western flanks of Monte San Lorenzo was confined to mountain valleys by the Late Glacial (∼ 13.7 ka, Fig. 2.10) and no longer interacted with the shrinking PIS as evidenced by geomorphological mapping and surface exposure chronologies from the Salto and Tranquilo valleys (Davies et al., 2018; Sagredo et al., 2018; Martin et al., 2019).

The Holocene history of the San Lorenzo glaciers remains largely unknown as well. Mercer (1968) obtained a maximum radiocarbon age of 5.2 ± 0.2 cal ka BP[1] for an advance of the Lacteo glacier, and ∼15 km down the valley, Wenzens (2005) obtained two minimum radiocarbon ages of 7.5 ± 0.04 and 9.5 ± 0.03 cal ka BP [1]. Garibotti and Villalba (2017) used dendrochronology and lichenometry to date moraines in the forefields of the Lacteo and San Lorenzo glaciers. However, their lichen growth rate curve is partly based on the moraine constrained only by a maximum limiting age, and thus their chronology should be treated with caution. An advance of a glacier in the Burmeister valley, immediately south of

[1]Recalibrated using the OxCal online calibration program (version 4.3; Bronk Ramsey, 2009 and the SHCal13 calibration curve (Hogg et al., 2013)

Table 2.1: Published recalibrated radiocarbon ages from the Lago Belgrano valley

		Cal BP[b]				^{14}C yr BP			
Reference	Location[a]	Cal age range		Median	1 σ	^{14}C age	1 σ	Material	Sample ID
Wenzens (2005)	Kettle within the Belgrano moraines	12683	12436	12597	59	10650	40	rootlets	beta 163 976
Wenzens (2005)	Kettle inboard of the Rincon moraines	9623	9475	9535	34	8610	40	humic material	beta 163 979
Wenzens (2005)	Kettle, south-east of Lago Volcan	7569	7434	7501	40	6650	40	humic material	beta 163 978
Wenzens (2005)	Kettle within the Burmeister moraines	5710	5473	5600	57	4900	40		beta 163 977
Horta et al. (2017)	Glaciolacustrine sediments inboard of the Rincon moraines (-47.779, -72.073)	11082	10515	10722	157	9503	69	organic rich mudstone	X28550
Horta et al. (2017)	Lacustrine sediments inboard of the Rincon moraines (-47.782, -72.073)	11995	11407	11751	141	10169	48	organic rich mudstone	X28551
Mercer (1968)	Overridden tree stump outboards of a moraine	5576	4870	5194	172	4590	115	wood	I-2208

[a] Coordinates are given in parenthesis where they were provided in the original publications.
[b] Ages were calibrated using the online Oxcal v4.3.2 (Bronk Ramsey 2009) and SHCal13 (Hogg et al., 2013) calibration curve, 95.4 % confidence interval

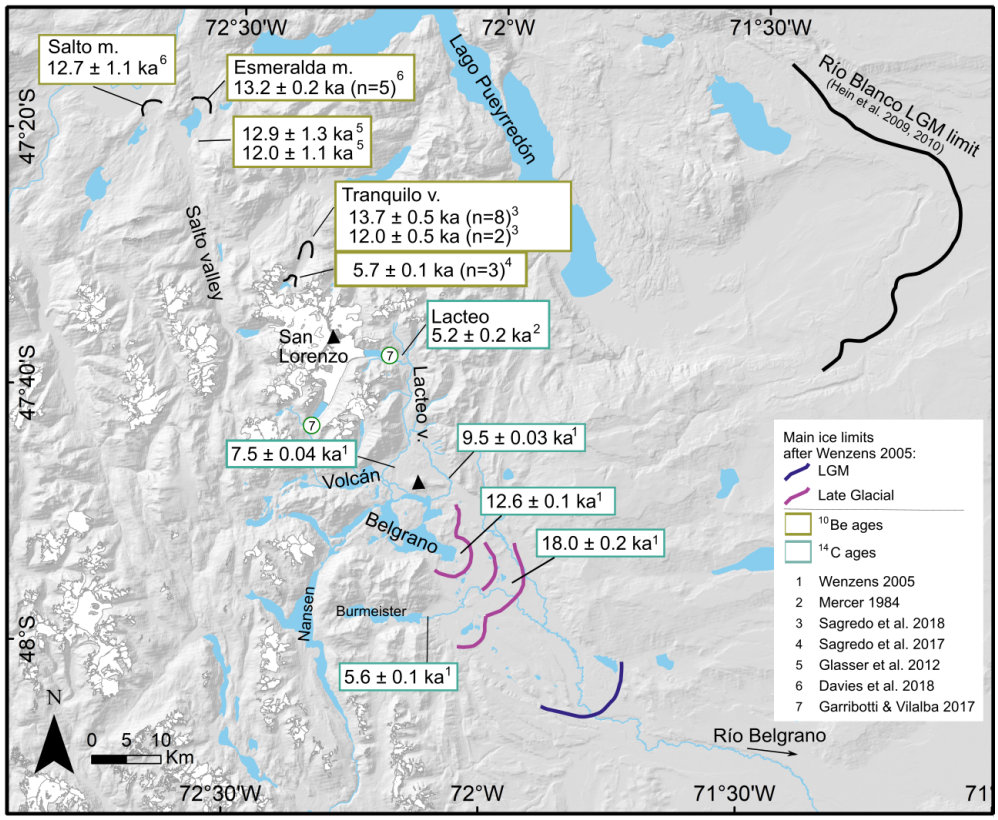

Figure 2.10: A map of San Lorenzo and the Belgrano valley showing published radiocarbon and surface exposure ages.

Lago Belgrano (Fig. 2.10), is constrained by a minimum radiocarbon age of 5.6 ± 0.1 cal ka BP (Wenzens, 2005). Dendrochronology was also used to date recent glacier fluctuations (last 400 years) in other valleys around San Lorenzo (Aravena (2007) and Garca-Zamora et al. (2004)). The only ^{10}Be-dated moraine with an age of 5.7 ± 0.1 ka is found in the Tranquilo valley on the northern flank of Monte San Lorenzo (Sagredo et al., 2016).

The evolution of palaeolakes in the valleys east of San Lorenzo has only been studied by Horta et al. (2017). They proposed a three stage model of palaeolake evolution in the Belgrano valley based on radiocarbon ages from lacustrine deposits (Fig. 2.11). The geomorphological evidence for different lake levels and extent is, however, not presented and the relationship between the radiocarbon ages and the proposed lake levels is not clear.

There is a great capacity for detailed mapping from high-resolution satellite imagery and development of chronologies to reconstruct glacier fluctuations and lake evolution in the Belgrano valley and around San Lorenzo.

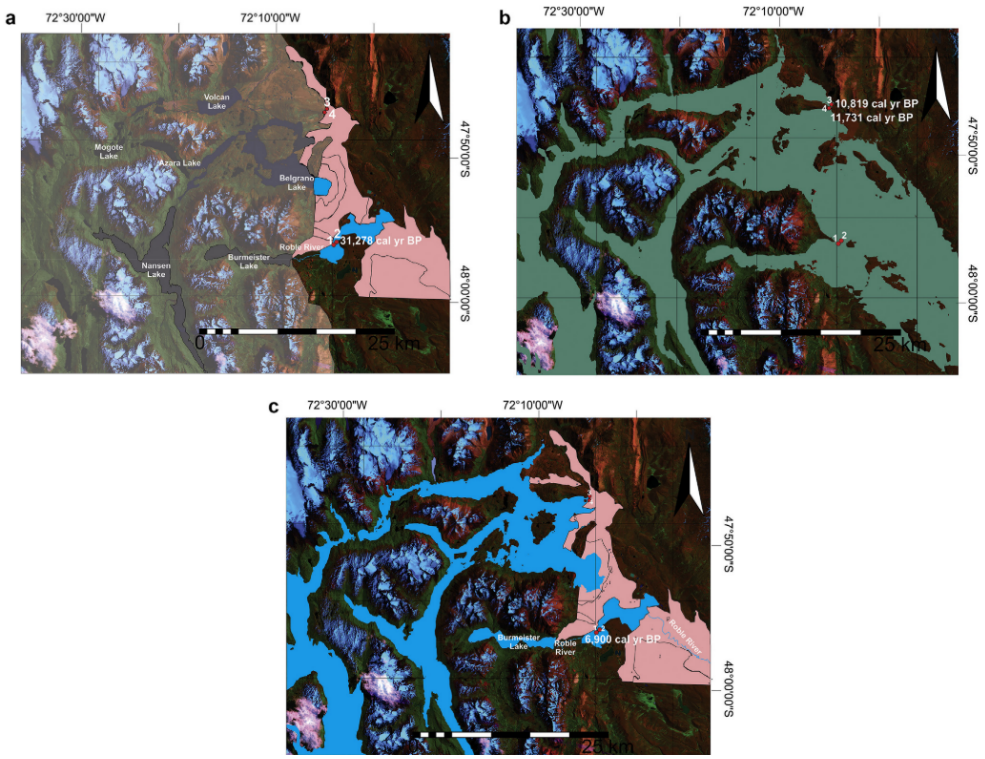

Figure 2.11: The palaeolake evolution in the Belgrano valley based on Horta et al. (2017). Palaeolakes are depicted in blue (a & c) and green (b), and moraines in pink.

2.3 Synthesis of knowledge gaps and motivation for this thesis

Despite several decades of research, there are still gaps in our understanding of the build-up and evolution of the PIS, patterns of deglaciation, the glacier response to abrupt climate events as well as the Holocene glacier dynamics. The following summarises key gaps in knowledge which motivate work done in this thesis.

1) We have limited knowledge of the onset of glaciation and the evolution of the PIS throughout the last glacial cycle. Ice-marginal positions prior to MIS 2 remain poorly resolved in most of central and northern Patagonia. Our understanding of the development of the PIS is thus limited to insights gained from a modelling experiment (Sugden et al., 2002), and the drivers of glacial activity in Patagonia and the southern mid-latitudes throughout the last glacial cycle remain elusive.

The absence of pre-MIS 2 evidence in central Patagonia is puzzling given that glacial maxima occurred during MIS 3 in southernmost Patagonia and in New Zealand (García et al., 2018; Vandergoes et al., 2008; Darvill et al., 2015; Kelley et al., 2014), and during MIS 4 in New Zealand (Schaefer et al., 2015). Antarctic dust record (Lambert et al., 2008) and Fe record off the Chilean coast (Kaiser et al., 2007; Lamy, 2004) support ice expansion towards the end of MIS 3, and pronounced peaks in both records occur during the MIS 4 as well. Conditions

comparable to or colder than the global LGM are observed during MIS 4 in SST records off the Chilean coast (Kaiser et al., 2005) and from the Southern Ocean, and in Antarctic ice cores. Yet, there is no evidence for glacial advances during MIS 4 in Patagonia.

In central Patagonia, the global LGM and deglaciation is only chronologically constrained in the LBA and LP valleys. Both were occupied by large fast-flowing outlet glaciers, whose dynamics was, to an extent, controlled by calving during both advance (Douglass and Bockheim, 2006) and retreat phases (Bendle et al., 2019). Thus, the absence of pre-MIS 2 signal in central Patagonia may, at least in part be explained by large outlet glaciers failing to respond to these climate signals. Alternatively, pre-MIS 2 moraines may have been obliterated by more extensive gLGM advances, or have been removed by focused meltwater erosion in these over-deepened basins (Hein et al., 2017). Robust glacial chronologies from less over-deepened valleys, which hosted smaller outlet glaciers, and which may provide longer geomorphological record (cf. Sugden et al., 2002) are thus required to gain insight into the development of the PIS and to assess the ice sheet - climate interaction over the last glacial cycle.

2) While there is evidence for glacial activity coeval with both the ACR and YD, evaluating the glacier-climate response during this time period in central Patagonia is complicated by calving into large regional palaeolakes and complex topography. It is not clear if there was a reversal in deglaciation during the Late Glacial, or merely a pause in overall ice retreat, likely aided by stabilization at topographic pinning-points. In many cases, in particular for moraines dated to YD (Sagredo et al., 2018; Glasser et al., 2012), the number of exposure ages is too low (< 2) to resolve millennial-scale climate events. Late Glacial ice marginal positions of smaller ice caps, which may provide a more climatically sensitive record, and yield insights into the overall pattern of deglaciation and break-up of the ice-sheet, remain largely unresolved.

3) The timing and extent of Holocene glacier advances are poorly constrained in much of Patagonia, in particular north of 49° S. Radiocarbon dating provides only limiting ages, and beyond the limits of lichenometry and dendrochronology, there are few directly-dated moraines. A paucity of robust glacial chronologies hinders assessment of the spatial coherence of climatic events recorded by glaciers and potential non-climatic factors affecting their behaviour. The Holocene was characterised by high-frequency climate variability and spatial heterogeneity, likely under the influence of different climatic oscillations (e.g ENSO, SAM). Rapid retreat and mass loss of Patagonian glaciers over the recent decades (e.g. Foresta et al., 2018) highlights the need for documenting glacier behaviour during the Holocene in order to contextualise the present and future change, and to elucidate the climatic controls.

Chapter 3

Glacial geomorphology



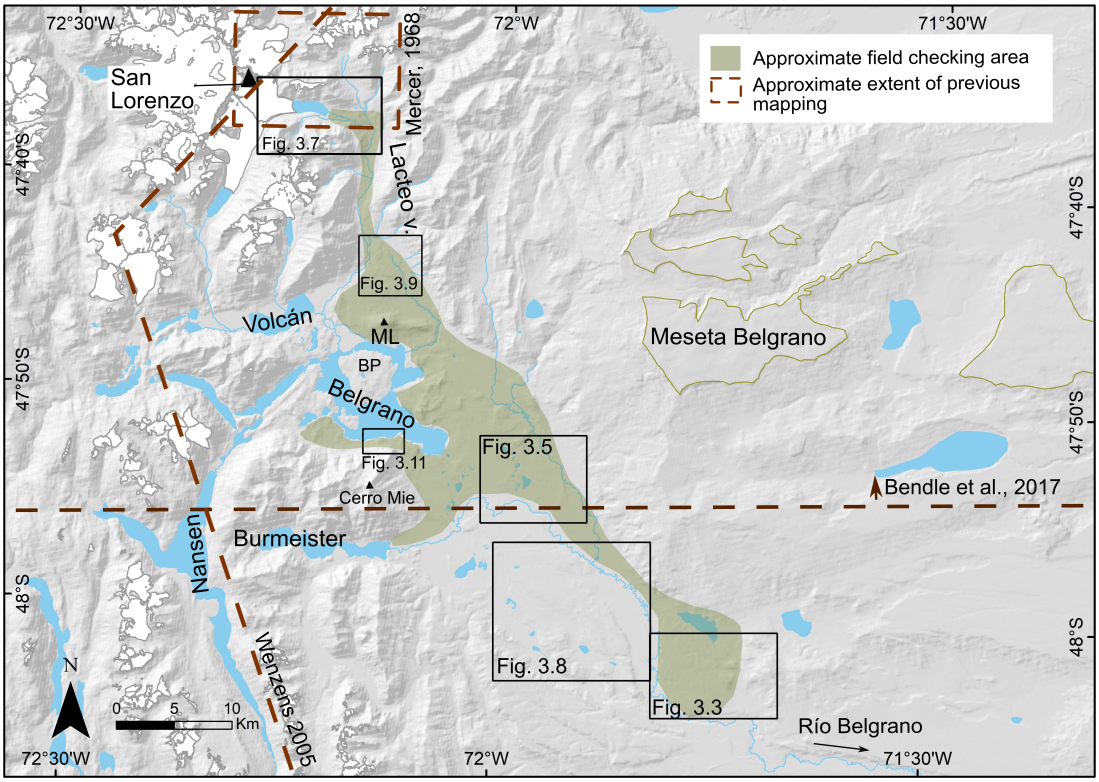

Figure 3.1: A map of the study area showing approximate field checking area and the extent of previous mapping. ML: Monte Leon, BP: Belgrano peninsula. Geomorphological mapping by Glasser et al. (2008) covered the entire study area.

3.1 Introduction

This chapter presents a detailed map of the glacial geomorphology related to the former Belgrano outlet glacier and valley glaciers on the eastern side of Monte San Lorenzo. The geomorphological mapping was used to target sampling for cosmogenic nuclide exposure dating and OSL analysis, results of which are presented in Chapters 4, 5 and 6. Previous studies mapped only localised areas, selected features or used coarse resolution imagery. The geomorphological map produced by Bendle et al. (2017b) covers part of the study area (Fig. 3.1), but it lacks sufficient detail and spatial coverage necessary to understand the glacial history of the Belgrano valley.

3.2 Methods

Geomorphological mappping was done using optical satellite imagery and digital elevation models (DEM), supported by ground-truthing during two field campaigns in 2016 and 2018. High resolution imagery available through the ESRI^{TM} World Imagery (15m TerraColor imagery and 2.5m SPOT Imagery) were used

in conjunction with the 10 m Sentinel-2 imagery (true and infrared band combinations). This was supplemented by viewing imagery via Google Earth^{TM} Pro along with its three-dimensional visualization tool. An ALOS PALSAR radiometrically terrain-corrected DEM with a resolution of 12.5 m and Shuttle Radar Topography Mission (30 m) DEM were used to aid landform identification and to provide background for maps.

Landforms were identified using well established criteria (Glasser et al., 2008; Darvill et al., 2014; Bendle et al., 2017b; Chandler et al., 2018) that were adapted to suit the appearance of landforms at the study site (Table 3.1). Lakes, rivers, modern deltas and mesetas are also mapped to provide further geographic and topographic context. Outlines of contemporary glaciers were downloaded from the GLIMS Glacier database (analysis date Oct 2017; Falaschi and Huber, 2017), and glacier fronts were adjusted based on a Sentinel-2 image acquired on the 24th of March 2019. Landforms were digitised in ArcGIS (10.6.1) and stored as shapefiles georeferenced to the WGS-1984 UTM Zone 18S projection. Final map production was done in the Inkscape graphical software.

Table 3.1: Landform identification criteria, modified from previous studies in Patagonia (e.g. Glasser et al., 2008; Darvill et al., 2014; Bendle et al., 2017b; Chandler et al., 2018)

Landform	Morphology	Appearance in imagery	Potential uncertainties	Significance
Ice marginal				
Moraine ridges	Prominent ridges of positive relief that may be linear, arcuate, sinuous or saw-tooth in planform. Often found parallel or perpendicular to the valley.	Texture/colour difference from adjacent terrain. Crest-lines often appear pale coloured. Shadowing on one side indicative of change in relief.	Possible confusion with trimlines. Difficult to detect in vegetated areas. Low-relief ridges may be less visible.	Mark former position of ice margins.
Moraine system	Undulating terrain with distinct moraine ridges, often with an associated outwash plain on the down-valley side. Often contains intermorainic depressions, and could be cross-cut by meltwater channels	Texture/colour difference from adjacent terrain. Higher relative relief. Presence of distinct ridges within.	Boundaries can be difficult to delimit, especially on the ice-proximal side or where it drapes on the underlying topography.	Marks approximate position of ice extent and ice-marginal deposition.
Hummocky terrain	Less defined, broad ridges and mounds of varying shape often separated by hollows. Unlike moraine ridges, lack distinct crest-lines.	Shadowing indicating positive relief, texture and colour difference from adjacent terrain. Circular hollows can be filled with water.	Boundaries of individual hummock difficult to delimit.	Former ice marginal zone or area of stagnant ice.
Glacigenic sediment	Accumulations of glacigenic sediment, not moulded into any particular shape.	A change in colour and texture from adjacent terrain; could be dissected by meltwater channels or streamlined.	It can only be inferred from satellite imagery.	Indicates areas of glacial deposition.
Trimlines	Sub-horizontal linear feature on valley sides separating non-vegetated and vegetated areas.	A sharp altitudinal change in texture and colour due to a vegetation change.	Possible confusion with lateral moraines, especially where these are not well-defined ridges.	Former vertical limits of glaciers, and potential thermal boundary.
Subglacial				
Ice-scoured bedrock	Exposure of bare or lightly vegetated rock, sometimes with small lakes. In places, it may be covered by glacigenic sediment.	Rough and irregular texture, bedrock rock structures, joints and faults might be visible. Colour varies depending on geology.	Boundaries could be difficult to delimit in areas with vegetation.	Indicative of an area of ice at pressure melting point.
Glacial lineations	Elongate, parallel landforms eroded to bedrock or formed by accumulation of sediment. They could vary in size.	Shadowing indicative of positive relief. Often occur in groups, aligned in the direction of former ice flow.	Misinterpretation of non-glacial structures in bedrock.	Indicative of ice flow direction, and fast ice flow, where they are large in size.
Glaciofluvial				
Outwash	Large flat plains gently grading from moraines, or narrow valley-parallel tracts with modern drainage.	Unvegetated, often homogenous surface with distinct texture/colour. Relict braided channels are often preserved on the surface.	Boundaries could be difficult to delimit in areas with overprinting alluvial deposition.	Indicates major meltwater paths.
Meltwater channels	Linear or sinuous channels eroded by lateral, proglacial or subglacial meltwater. They are often steep sided.	Shadowing due to a change in relative relief. Often distinct colour in near-infrared imagery due to a change in vegetation. Often occur in association with moraines and do not contain modern drainage.		Indicate areas of significant meltwater production, and approximate position of ice margins.

Glaciolacustrine				
Shorelines	Raised terraces, benches or notches cut by wave action into sediment or bedrock.	Linear or curvilinear terraces often run parallel to modern day shorelines, or on the ice proximal side of moraines. Often occur in stepped series.	Could be difficult to identified from imagery especially where cut into bedrock or where discontinuous, usually clear in the field.	Indicate former lake level, or a proglacial lake.
Glaciolacustrine deposits	Accumulation of fine-grained sediments, which can be flat-topped or exhibit positive relief (e.g. mounds).	Appear pale coloured where exposed and not vegetated.	Difficult to identify from satellite imagery alone, and to delaminate boundaries, extent could be underestimated. Field identification necessary to confirm composition.	Indicate approximate former lake extent.
Raised deltas	Gently sloping deposits extending from valley sides, above the valley floor or a modern lake. They often occur upstream of active deltas, and have been incised by modern streams. A break in slope and steeply inclined front side.	Homogenous surface texture and colour, unvegetated.	Could be misinterpreted as a shoreline or ice-contact deposit.	Indicative of former lake level.
Other features				
Alluvial fans	Sediment fans sloping from valley side, fed by a river or small stream. Often occur at the bottom of gullies.	A change in vegetation and a distinct fan shape. Sometimes, multiple fans occur adjacent to each other along valley sides.	Could be misinterpreted as a raised delta but unlikely.	Reworking of unconsolidated material by streams.

3.3 Glacial geomorphology

The main geomorphological map is presented in Figure 3.2. The following sections describe main features mapped.

3.3.1 Moraine ridges and complexes

Prominent cross-valley or valley-parallel ridges are interpreted as moraines marking former glacier margins. East of Lago Belgrano on the Argentine plain, they form large moraine complexes, which extend over 10 km, separated by outwash plains. Three main moraine systems were identified, which delimit the positions of the Belgrano outlet glacier. These are informally named here after local features, Klementek, Menelik and Belgrano, from the oldest to youngest.

The Klementek moraine system comprises of fragmentary outermost moraine ridges with 25 m relief and slopes up to 12°, which transition into an area of hummocky terrain extending for about 10 km on the northern side of the Rio Belgrano (Figs. 3.3 & 3.4). This hummocky terrain was described by Wenzens (2005) as a 'ground moraine' of the terminal moraine ridges. Superimposed on the hummocky terrain, are small narrow ridges of up to one kilometer in length orientated transverse to ice flow, which are interpreted as moraines.

The Menelik moraines system (Fig. 3.5) has a double-lobate shape, which together with a medial moraine (Fig. 3.6) indicates a coalescence of the Belgrano and Burmeister glaciers. The moraine ridges can be linear, arcuate, or sinuous in planform, and exhibit leveled or undulating crests. The outermost moraines are broad-crested, prominent ridges of 30 m relief and slopes up to 15°. They are largely continuous cross-valley, except where they are dissected by meltwater channels and a river. Inboard, the moraine ridges diminish in size and are interspersed with intermorainic depressions. They often occur draped on higher topography. The smaller closely spaced moraines are interpreted as recessional moraines and could be indicative of active gradual ice recession.

On the Cerro Mie, to the south of Lago Belgrano, is a series of prominent lateral moraines at $\sim$ 920 - 1160 m asl (Fig. 3.6 B), which likely relate to advances that deposited the Menelik, and possibly also the Klementek, terminal moraines.

The Belgrano moraine system consists of up to six distinct arcuate moraine ridges bounding Lago Belgrano. The most prominent ridges are about 10 m in height with slopes up to 22° and exhibit undulating crests. The Belgrano moraines cross-cut older moraines north of the lake suggesting that they represent a re-advance of the Belgrano glacier.

Further two sets of moraines were mapped, one bounding Lago Burmeister, and one at the foot of the Lacteo valley, which occupy the same morphostratigraphic position as the Belgrano moraines. The Burmeister moraines delimit the position of the former Burmeister glacier after it retreated and separated from the Belgrano glacier. The moraines vary from small ridges of 1 - 2 m in relief and gentle slopes of up to 6° and more distinct ridges of 6 - 14 m in relief and slopes up to 17°. The lateral-terminal moraines in the Lacteo valley were deposited along the northern side of Monte Leon and extend to the western side of the Lacteo valley. The lateral moraines are well preserved, in particular on the side of Monte Leon, whereas, the terminal moraines only occur as fragments cut by meltwater channels.

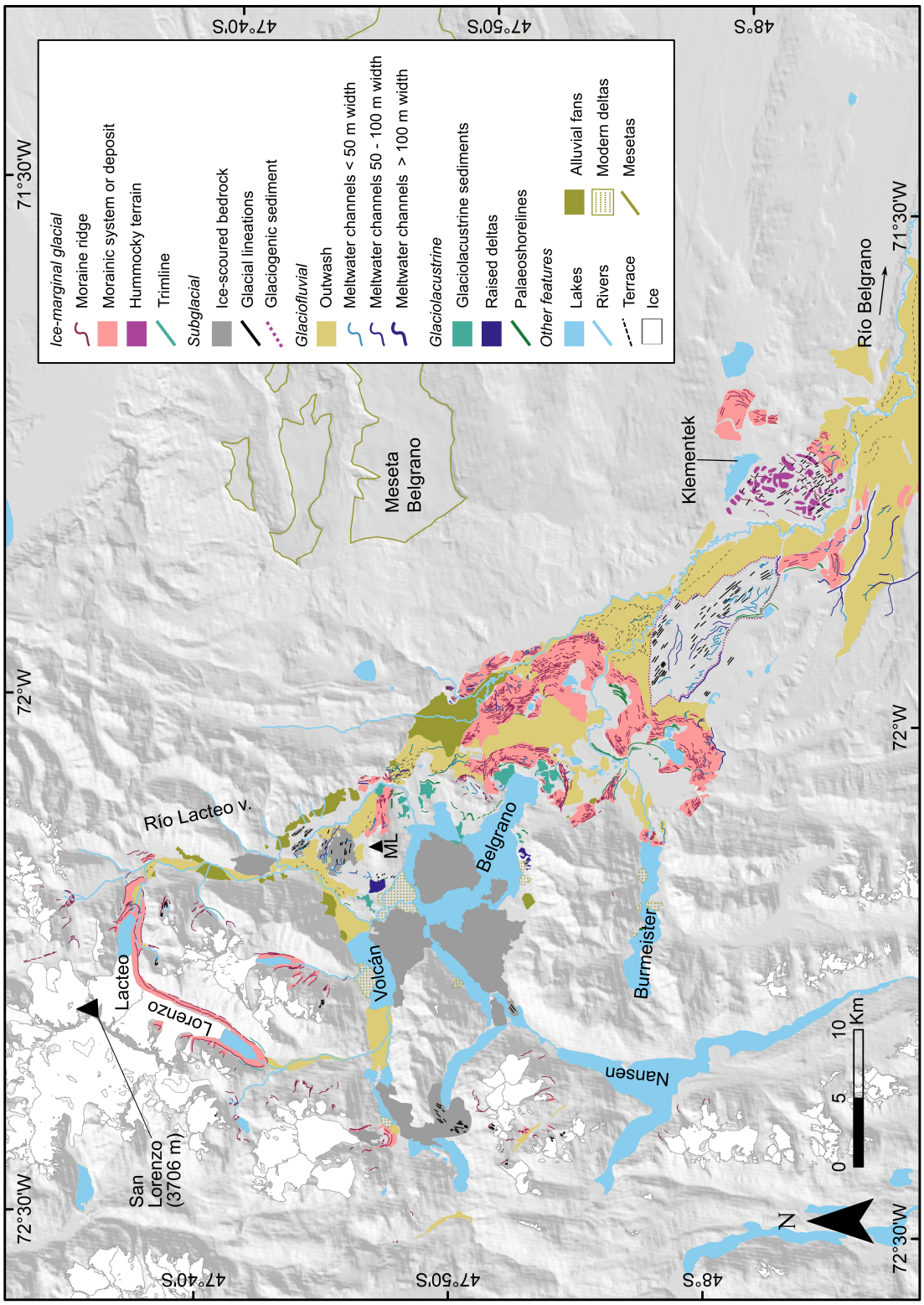

Figure 3.2: The geomorphological map of the Belgrano valley.

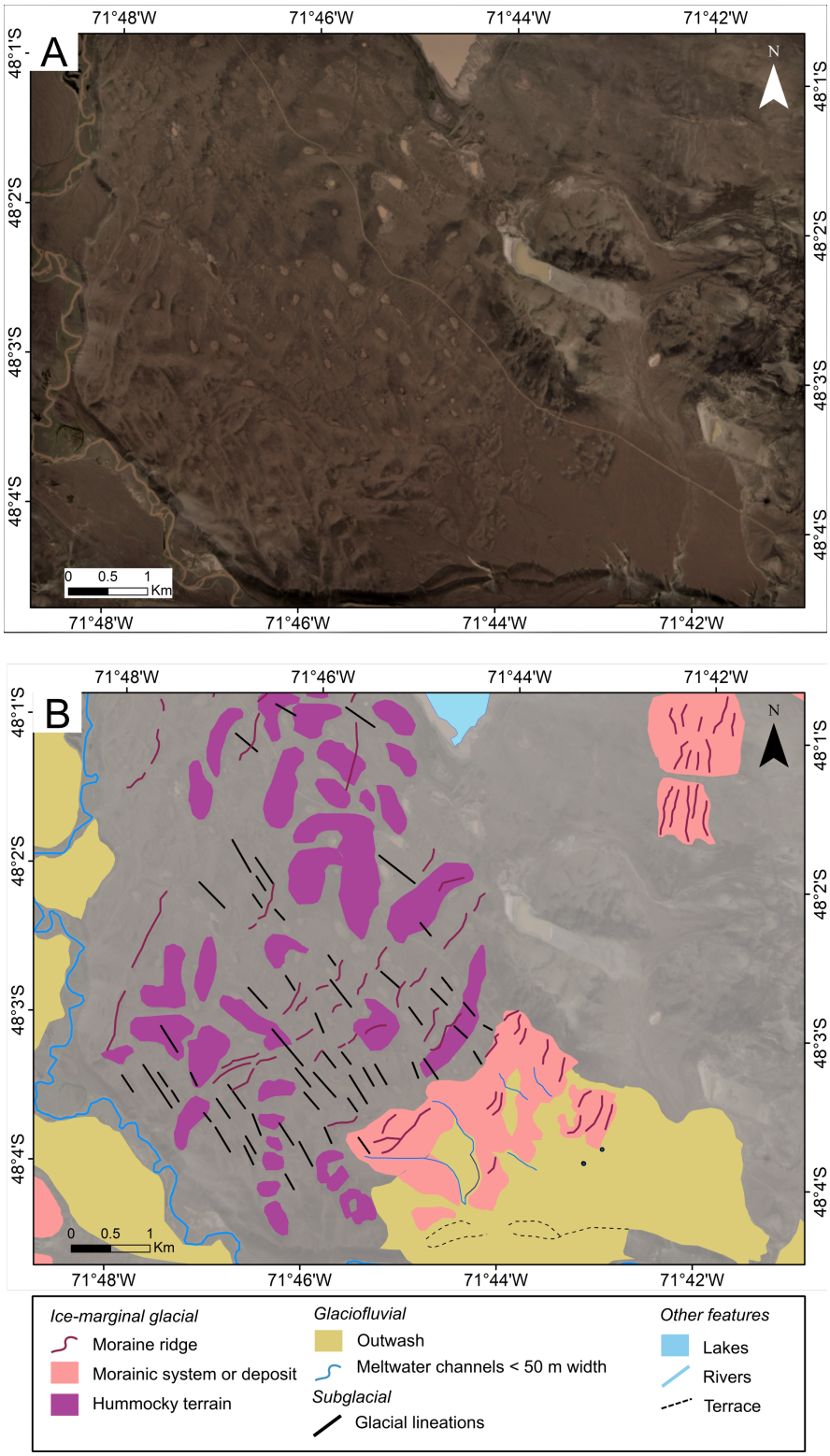

Figure 3.3: A) Satellite image (Sentinel-2) and B) mapped moraine ridges of the Klementek moraine system and the associated hummocky terrain.

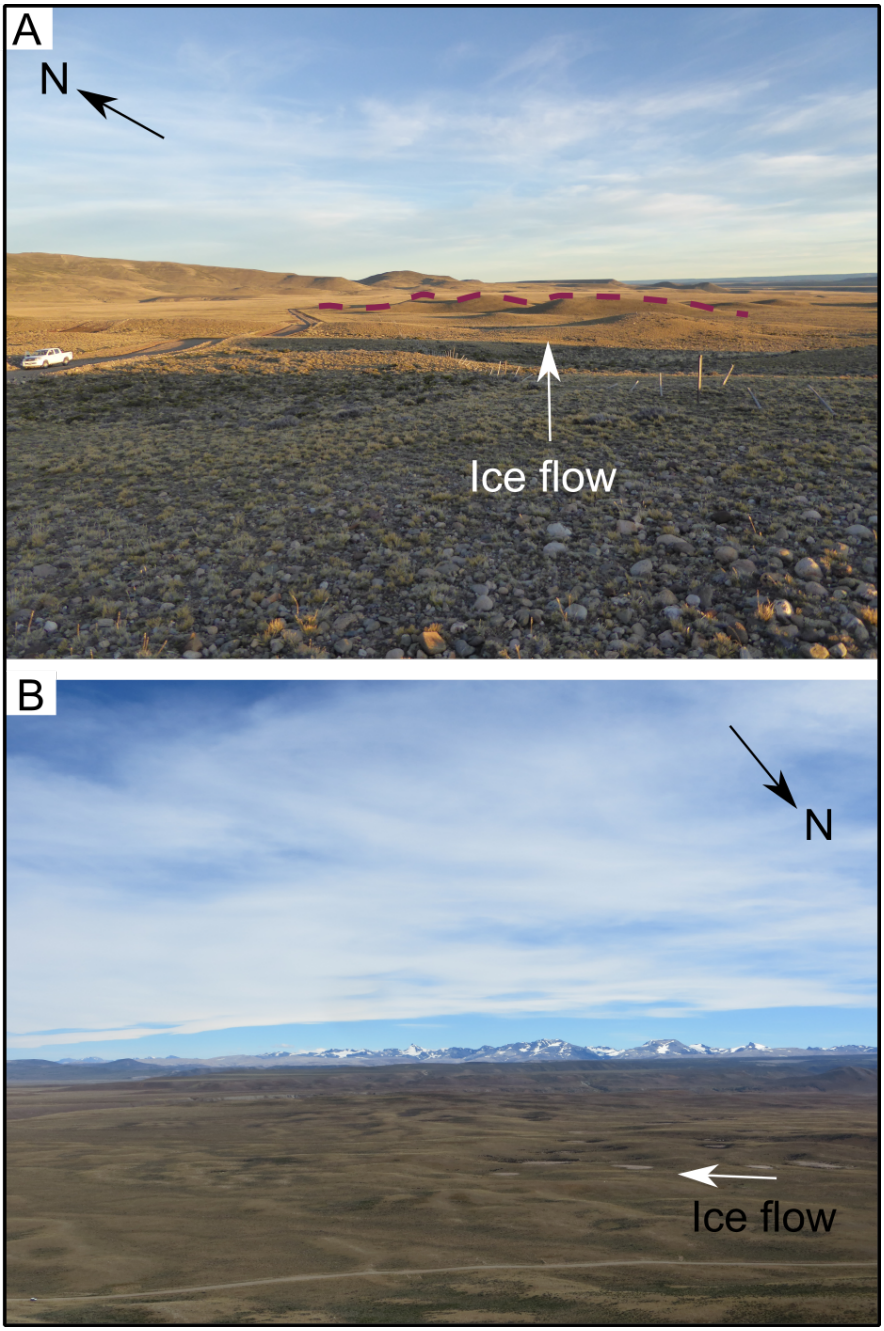

Figure 3.4: A) Photograph showing part of the hummocky terrain, with a vehicle in the bottom left corner for scale. B) Photograph showing the outermost Klementek moraine ridges.

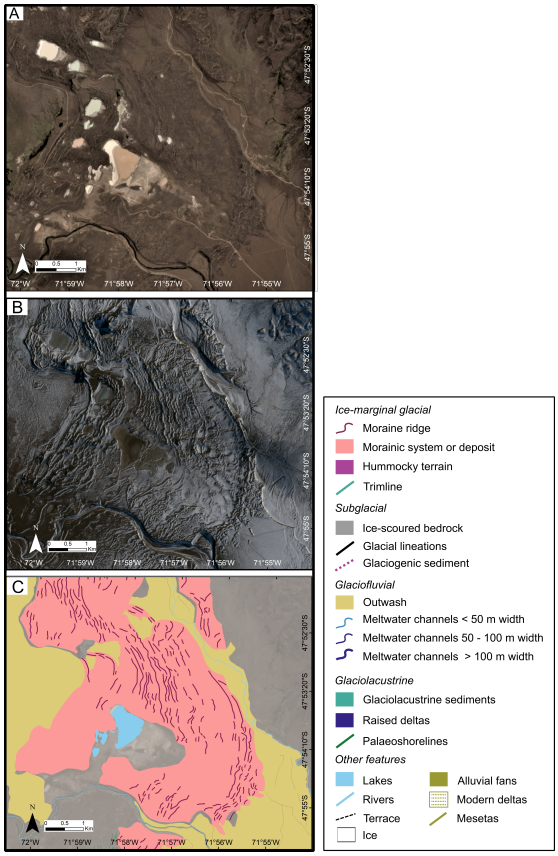

Figure 3.5: Satellite images (Sentinel-2) A) snow-free and B) with snow cover highlighting moraine ridges of the Menelik moraine system and C) a corresponding geomorphological map.

Closer to the present day glacier margins, moraines more often occur as single ridges and form continuous lateral-terminal arcs (Fig. 3.7). Terminal moraines are commonly arcuate or occasionally exhibit a saw-tooth pattern.

3.3.2 Hummocky terrain

The hummocky terrain associated with the Klementek moraines (Fig. 3.3) is characterised by broad less less defined ridges and mounds, which vary in morphology from linear to semi-circular rim-ridges enclosing hollows. Individual ridges and mounds are difficult to delimit, and where possible they were mapped as polygons. The hummocky terrain also exhibits lineations of 200 to 600 m in length and about 60 m in width.

The hummocky terrain with lineations and recessional moraines is likely a palimpsest feature formed by a combination of subglacial (e.g. sedimentation under actively flowing ice and stagnant downwasting ice) and ice-marginal processes during overall ice retreat. The broad and subdued ridges could have been deposited under stagnant downwasting ice during passive ice recession

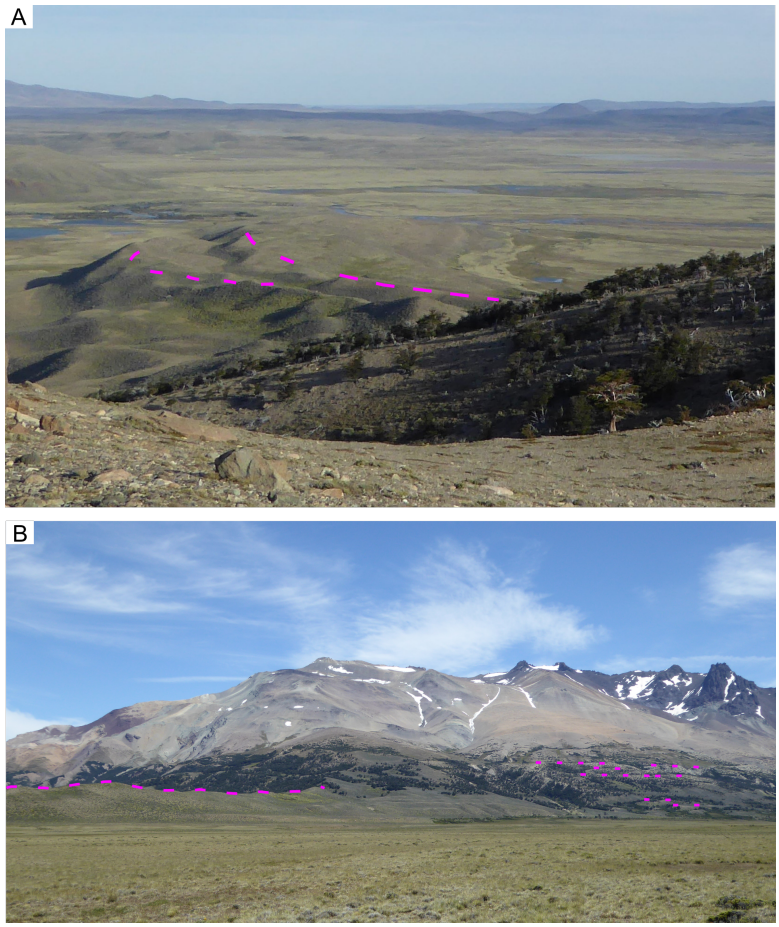

Figure 3.6: A) View of a medial moraine (pink dashed lines) formed by the coalescence of the Belgrano and Burmeister glaciers. B) Photograph showing the lateral moraines on Cerro Mie and the medial moraine.

(Boone and Eyles, 2001) or could be a product of downwasting debris-covered dead ice (Kjær and Krüger, 2001; Spedding and Evans, 2002; Schomacker, 2008). The hummocky terrain could also represent overridden moraines with superimposed recessional moraines similar to fluted overridden moraines observed in Iceland (Evans and Orton, 2015).

3.3.3 Glacigenic sediment

A distinct feature between the Klementek and Menelik moraine systems, raised above the surrounding glacial outwash, and distinguishable by texture and color is interpreted as a glacigenic sediment drift (Fig. 3.8). It is adjacent to fragments of moraine ridges on the southeastern side and exhibits glacial lineations. It is dissected by numerous meltwater channels of varying size, the largest one being over 200 m in width, and contains occasional depressions filled by water. This feature was also described by Wenzens (2005) as a 'ground moraine' of the Klementek terminal moraines. Field inspection was not possible due to access problems.

3.3.4 Glacial lineations

Linear elongate landforms, often occurring in groups, aligned in the direction of former ice flow were mapped as glacial lineations (Fig. 3.8). The term lineation is used here for landforms composed of sediment as well as those carved into bedrock. In the Belgrano valley, sediment lineations occur within the hummocky terrain associated with the Klementek moraines. The lineations here are 250 - 450 m in length and are interspersed with hummocks and hollows. South of the Río Belgrano, within the glacigenic sediment unit, they are up 800 m in length. The sediment lineations in the Belgrano valley are interspersed with other landforms and/or dissected by meltwater channels and do not form well-defined zones. Glacial lineations are common around Patagonia and indicate warm-based ice and fast ice flow (Glasser et al., 2005, 2008). Streamlined glacial landforms, including drumlins, flutes and megaflutes were mapped in the Pueyrredón and Chacabuco valleys (Bendle et al., 2017b), at Lago Argentino (Goyanes and Massabie, 2015), Lago Viedma (Ponce et al., 2019), and around the Strait of Magellan (Clapperton, 1989; Benn and Clapperton, 2000; Lovell et al., 2012; Darvill et al., 2014). Sediment flutes are frequent near present day glacier margins. Bedrock lineations are found in the Lacteo valley where they indicate converging ice flow (Fig. 3.9).

3.3.5 Ice-scoured bedrock

Ice-scoured bedrock occurs commonly along mountain valleys in the study area (Fig. 3.9). It appears on satellite imagery as areas of exposed to lightly vegetated bedrock with rough texture, occasionally containing small ponds and lakes. It

often exhibits glacial lineations and could be partially covered by diamict. Such features indicate areas of glacial erosion under wet-based sliding ice (Sugden and John, 1976). Polished and striated surfaces (Fig. 3.9C & D) were also commonly observed in the study area and indicate subglacial abrasion and plucking.

3.3.6 Meltwater channels

Straight or sinuous channels that begin and terminate abruptly and often lack modern drainage indicate former meltwater pathways. In the study area, they often occur in association with moraine ridges, or they dissect glacigenic sediment (Fig. 3.8). The largest meltwater channels are found in the eastern part of the study area, and are often over 100 m in width.

3.3.7 Glaciofluvial outwash

There are two types of glaciofluvial outwash in the study area: 1) Large flat-topped terraces that grade from terminal moraines and are not active at present (Figs. 3.3 and 4.5). They can be distinguished by surface texture and color, and often exhibit relict braided channels. In places they have been incised by rivers resulting in a series of stepped terraces. These occur in the Belgrano valley and are associated with the terminal moraines systems. Outboard of the Klementek moraine system, outwash terraces extend eastward for 10s of km and exhibit several terrace levels suggesting different stages of outwash deposition. 2) Active glaciofluvial outwash (sandur) that emanates from current pro-glacial areas and often forms narrow valley-parallel tracts with modern drainage (Fig. 3.7). Glaciofluvial outwash terraces are well-developed in valleys on the eastern side of Patagonia and often separate moraine systems (e.g. Caldenius, 1932; Hein et al., 2009, 2011; Glasser et al., 2011; García et al., 2014, 2018; Smedley et al., 2016). Exposure dating of glaciofluvial outwash sediment has also been shown to be a reliable approach for dating glacial advances, in particular predating the gLGM, where outwash terraces can unambiguously be linked to moraine limits (Hein et al., 2009, 2011, 2017; Darvill et al., 2015).

3.3.8 Palaeoshorelines

Horizontal features with no positive relief, which can take a form of terraces or notches cut into bedrock or sediment are interpreted as palaeoshorelines. They are formed by wave erosion and beach deposition by long-lived palaeolakes (Turner et al., 2014). In the Belgrano valley, palaeoshorelines occur on the ice-proximal side of all three moraine limits indicating the presence of proglacial lakes during ice retreat. A prominent shoreline at 885 - 882 m asl was mapped running parallel to the modern shoreline of Lago Belgrano and on the ice-proximal side of the Belgrano moraines indicating former higher level of Lago Belgrano (Fig. 3.10). This palaeolake Belgrano was damned by ice at least 10 km to the west of the

Belgrano moraines and drained to the Atlantic via a spillway through the Belgrano moraines.

3.3.9 Glaciolacustrine deposits

Accumulations of laminated silt and sand sediments were interpreted as glaciolacustrine deposits. They are found in the areas of former lake floor around the modern Lago Belgrano, often in embayments and associated with former shorelines (Fig. 3.10B). These features could be flat-topped or exhibit positive undulating relief. In satellite imagery they appear pale-colored where exposed (Fig. 3.11A), but are often vegetated. Hence, it is difficult to delimit their boundaries and their extent was likely underestimated. Identification of glaciolacutrine sediments is problematic from satellite imagery alone, and we only mapped them where field-checking was possible.

3.3.10 Raised deltas

Gently sloping surfaces occurring along the valleys, raised above the modern valley floor or lake level, often at the foot of small gullies and incised by modern streams, were interpreted as raised deltas. In the study area, examples of raised deltas occur along the southern shore of modern Lago Belgrano (Fig. 3.11). Another feature interpreted as a raised delta is found adjacent to the western side of Monte Leon and above the modern delta of Rio Lacteo. Its elevation corresponds to the 882 - 885 m asl shoreline and it would have been fed by pro-glacial streams of the retreating Lacteo glacier.

3.3.11 Alluvial fan deposits

Fluvial deposits found on valley sides, often exhibiting a fan shape and fed by small streams were mapped as alluvial deposits. In the Lacteo valley, in particular, valley sides are dominated by fluvial activity with fans forming at the base of steep narrow gullies. Similarly, alluvial deposition is evident along the northern side of the Belgrano valley, often overprinting glaciofluvial outwash terraces.

3.4 Interpretation

The mapping reveals three main assemblages of landforms: 1) An assemblage of landforms recording the evolution of the Belgrano glacier found in the the eastern lowland part of the Belgrano valley. This assemblage is dominated by large moraine systems and associated outwash terraces, glacial lineations, as well as meltwater channels, hummocky relief and palaeoshorelines. The moraine systems indicate three major advances of the Belgrano glacier with a land-terminating front as evidenced by extensive outwash terraces grading from

outermost moraines. Pro-glacial lakes formed during ice retreat in the outer part of the Belgrano valley.

2) An assemblage of landforms dominated by palaeoshorelines, raised deltas, and glaciolacustrine sediments, which document a development of a glaciolacustrine environments as the Belgrano glacier retreated to within the trough. The Burmeister glacier had separated and the Belgrano glacier underwent a change from a land-terminating to a freshwater calving front.

3) An assemblage of landforms related to recent mountain glaciation, including younger lateral-terminal moraine arcs, closely spaced recessional moraines, and saw-tooth moraines, which likely developed during the Holocene, trimlines, flutes and active outwash plains.

3.5 Conclusion

This chapter presents a new, comprehensive map of the glacial geomorphology pertaining to the former Belgrano outlet glaciers and its tributaries. The mapping was done from high resolution imagery, supported by field-checking, and includes greater detail, surpassing that of previous studies. The mapped features included moraine ridges and complexes, hummocky relief, glaciofluvial outwash, glacial lineations, meltwater channels, palaeoshorelines, raised deltas and glaciolacustrine sediments. The mapped landforms can be grouped into three assemblages: 1) An assemblage in the outer Belgrano valley dominated by large moraine/outwash complexes. The Klementek, Menelik and Belgrano moraine systems, from the oldest to youngest, mark former limits of the Belgrano glacier. Further moraines were mapped in the Burmeister and Lacteo valleys (Rincon moraines), which were deposited by former tributaries of the Belgrano glacier and occupy the same morphostratigraphic position as the Belgrano moraines. 2) An assemblage documenting the development of glaciolacustrine environment as the Belgrano glacier retreated into the trough. 3) An assemblage of landforms recording recent mountain glaciation. There is potential for more detailed mapping in the mountain valleys, which could not be accessed during the field expeditions and where dense vegetation obscured remote mapping.

The geomorphological mapping guided the sampling strategy for cosmogenic exposure analysis to establish the timing of glacial advances. Moraines were targeted for sampling, and in the case of the two oldest ice limits in the Belgrano valley outwash terraces as well (Chapter 4). Geomorphological mapping was key for linking outwash terraces to specific moraines/glacial events (cf. Hein et al., 2009). A more recent, Holocene moraine deposited by the Lacteo glacier was used in a 3D glacier surface reconstruction and ELA estimates (Chapter 6). Mapping also allowed to establish the relationship between different lake levels and palaeoshorelines. Mapped palaeoshorelines were targeted for cosmogenic surface exposure analysis and glaciolacustrine sediments were sampled for OSL dating to constrain the evolution of a palaeolake Belgrano (Chapter 5). In addition to

underpinning the work presented in Chapters 4, 5 and 6, the geomorphological map may be useful for future detailed studies of ice-dynamics and palaeolake evolution in the area and for the PIS reconstructions using combined empirical and numerical modelling approaches.

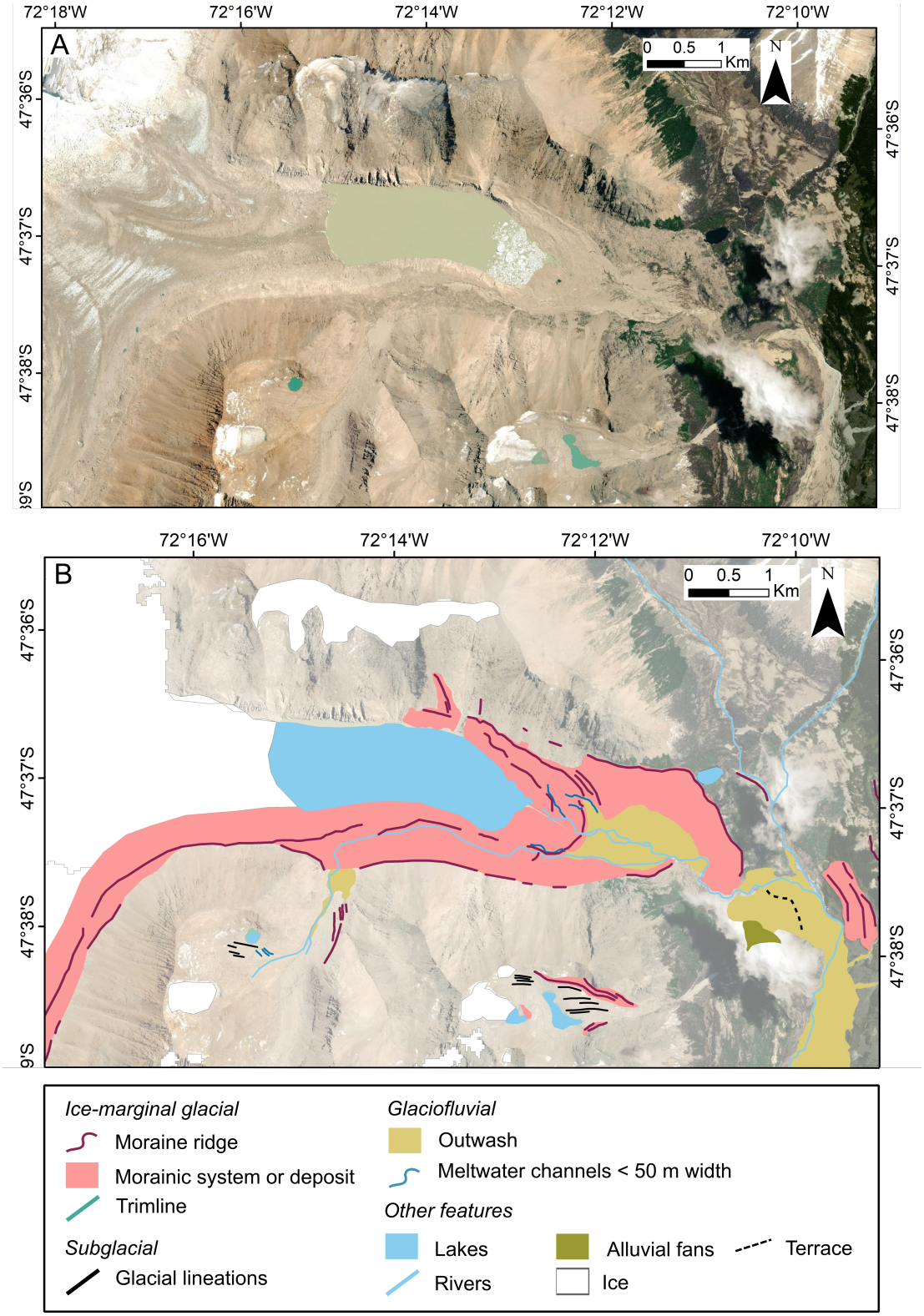

Figure 3.7: A) Satellite image (ESRI World Imagery) and B) mapped landforms near the present day margin of the Lacteo glacier.

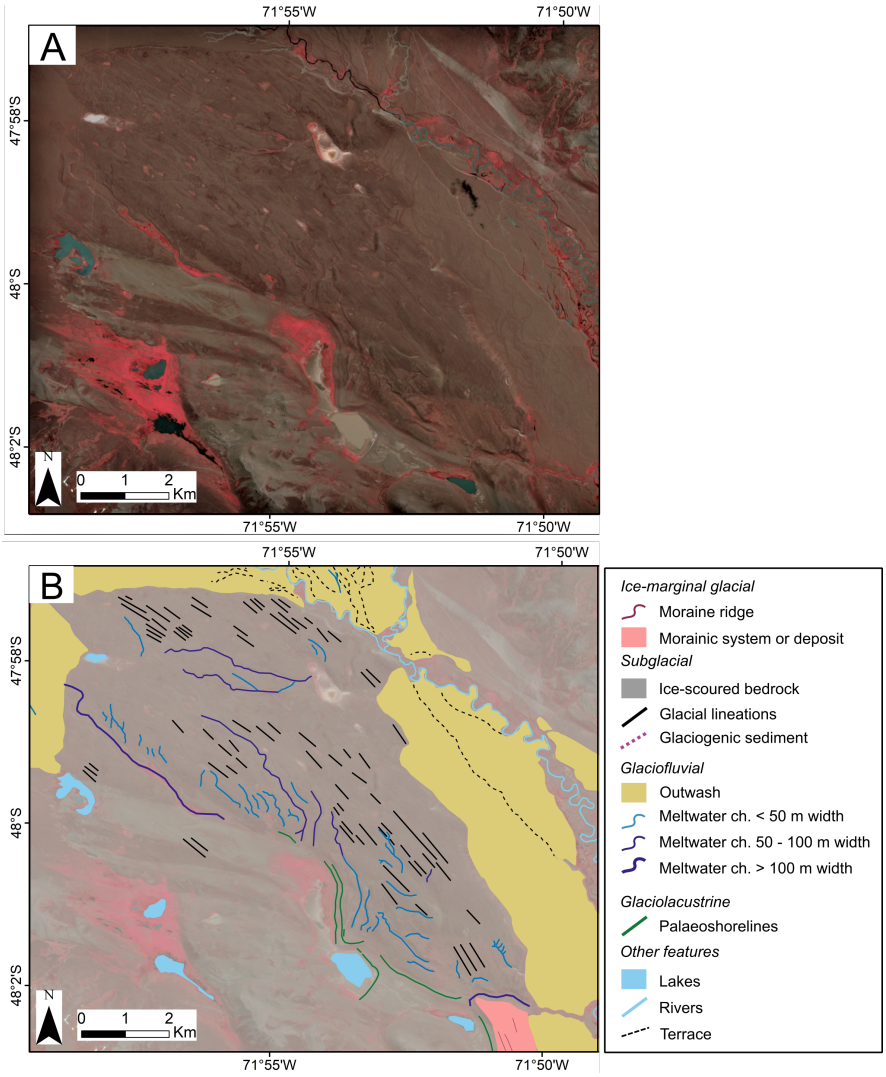

Figure 3.8: A) Satellite image (Sentinel-2) and B) mapped glacial lineations and meltwater channels within the glacigenic sediment.

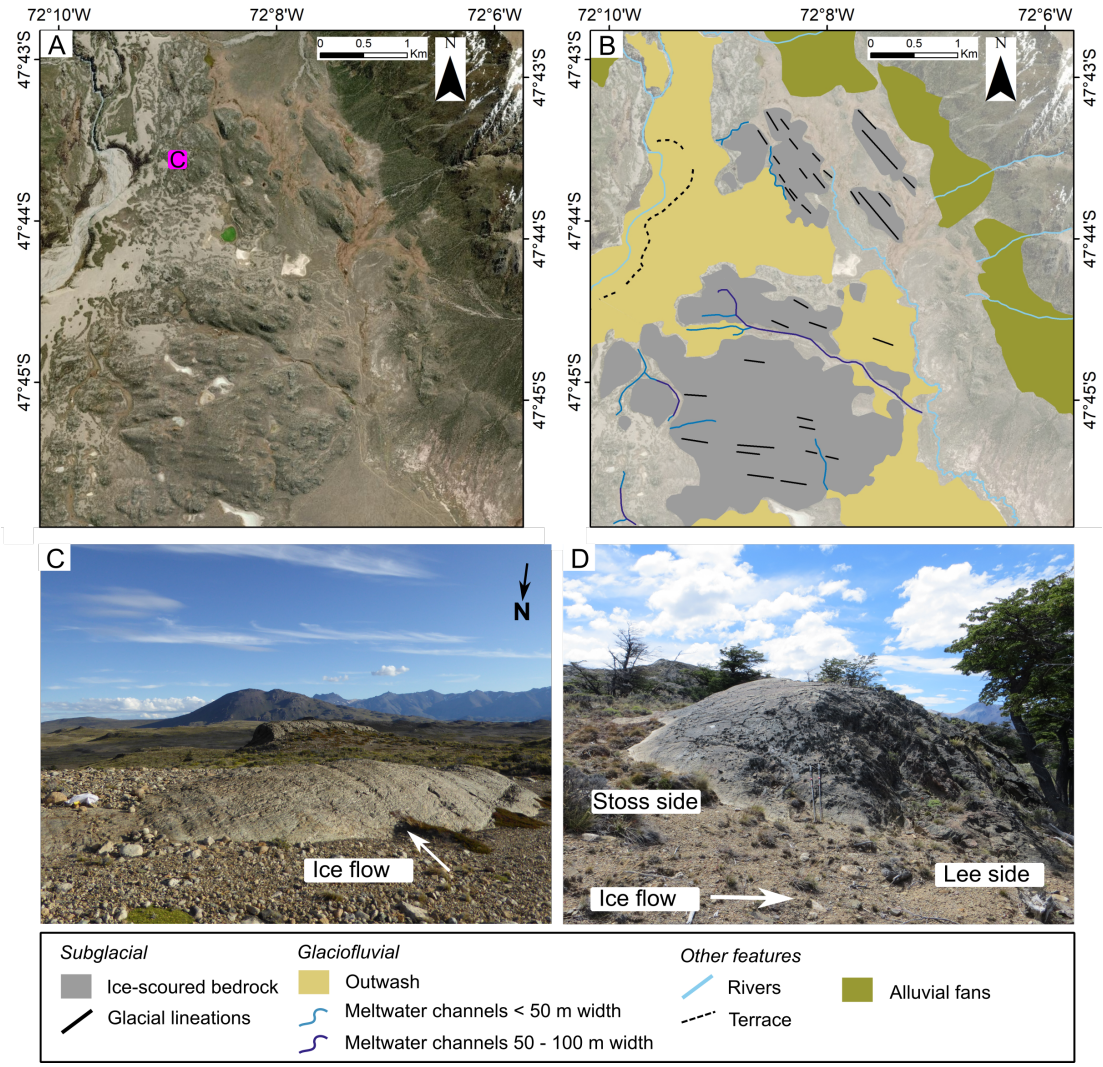

Figure 3.9: A) Satellite images (ESRI World Imagery) and B) mapped ice-scoured bedrock and bedrock lineations in the Lacteo valley. Bedrock is in many place overlain by diamict. C) Striated bedrock in the Lacteo valley, location of the photograph is shown in A). D) Photograph of a roche moutonnée on the Belgrano peninsula.

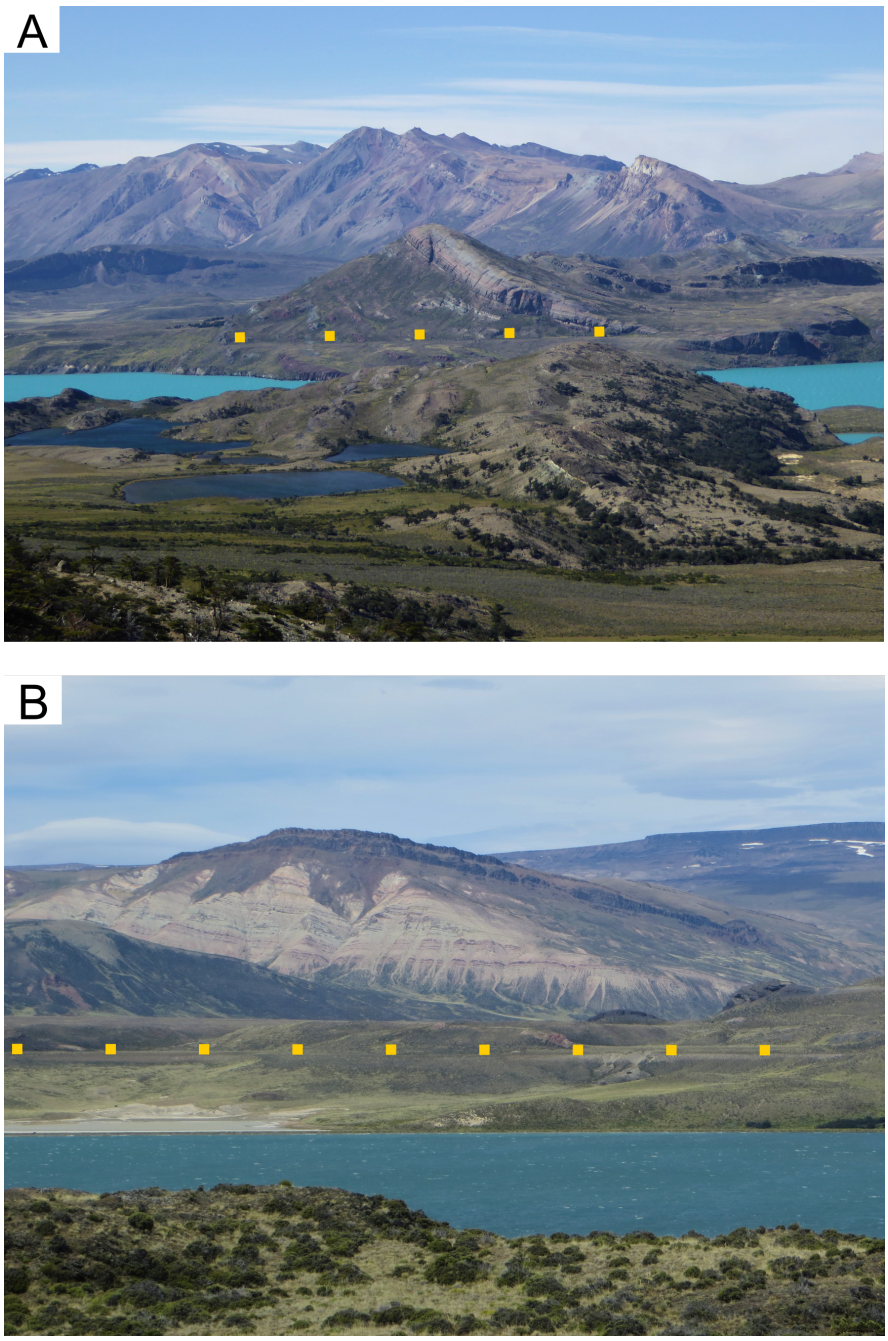

Figure 3.10: A - B) A prominent shoreline (dotted yellow line) at 885 - 882 m asl above the modern Lago Belgrano. Fine pale sediments interpreted as glaciolacustrine deposits are visible in B) below the shoreline.

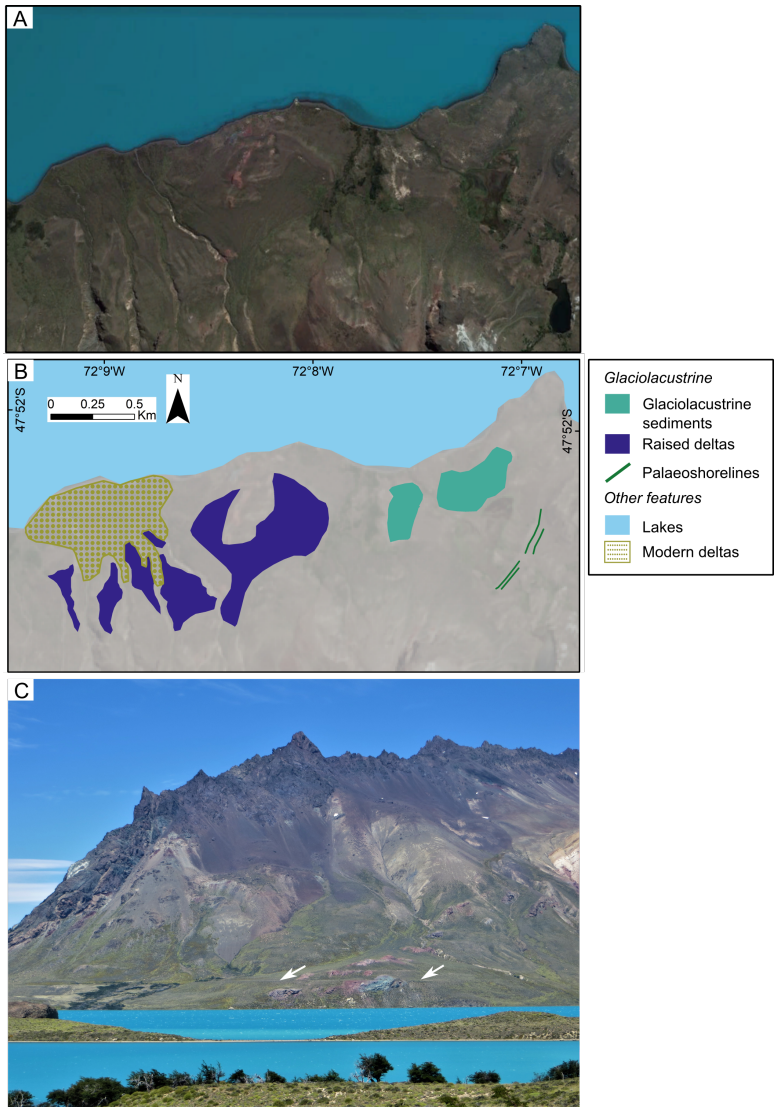

Figure 3.11: A) Satellite image (Google Earth) and B) mapped raised deltas above Lago Belgrano, palaeo shorelines, and glaciolacustrine deposits. C) Photograph of a raised delta.

Chapter 4

Extensive mountain glaciation in central Patagonia during Marine Isotope Stage 5



Abstract The timing and magnitude of glacial advances throughout a glacial cycle can give insight on the underlying drivers of climate change. Our knowledge of glacial activity early in a glacial cycle, however, is limited by incomplete preservation of the geomorphological record. Here, we present a ^{10}Be-dated glacial chronology from early in the last glacial cycle from the Belgrano valley, east of Monte San Lorenzo in central Patagonia. Our chronology reveals the most extensive glacial advance of the last glacial cycle occurred at $\sim$ 75 ka, at the end of Marine Isotope Stage 5. A second, less-extensive advance occurred at $\sim$ 25 ka during the global Last Glacial Maximum. The topographic setting is such that ice growth would have initiated on and around the San Lorenzo massif at the start of the glacial cycle. We suggest reduced southern hemisphere summer insolation at the time played a significant role in driving this early advance. The comparatively smaller glacier extent during the global Last Glacial Maximum is likely a consequence of the build-up of the full Patagonian Ice Sheet, which would have caused ice-divide migration, ice-flow re-routing, and increased aridity on its lee side.

4.1 Introduction

There is a long standing debate on the timing of glaciation in the southern mid-latitudes, its (a-) synchrony with the northern hemisphere and its forcing mechanisms (Mercer, 1984; Denton et al., 1999a; Sugden et al., 2005). Recent studies in the southern mid-latitudes demonstrated numerous substantial glacial advances, in many cases local maxima, prior to the global Last Glacial Maximum (gLGM, ca. 26 - 19 ka, Clark et al., 2009) (e.g. Zech et al., 2011a; Darvill et al., 2015; García et al., 2018; Schaefer et al., 2015; Kelley et al., 2014; Shulmeister et al., 2019; Sutherland et al., 2007). While an early maximum is not uncommon for many mountain glaciers and sectors of large ice sheets (Gillespie and Molnar, 1995; Hughes et al., 2013), it suggests that our understanding of glaciation in the southern mid-latitudes and, in particular its drivers, is incomplete. Orbital parameters, including regional insolation and season duration, latitudinal shifts in southern westerly winds (SWW) and associated oceanic systems, as well as local ice dynamics have been invoked as potential drivers of pre-LGM ice expansion (Doughty et al., 2015; García et al., 2018; Darvill et al., 2015, 2016). Evaluating the drivers of these pre-LGM advances and their role throughout the last glacial cycle is, however, limited by a lack of dated moraines spanning the entire glacial period. Moraine preservation is inherently incomplete due to a range of erosional processes, including the removal of pre-existing moraines by an advancing glacier. As a result, moraine preservation in a landscape is biased toward the most extensive and the more recent glacial advances. Here, we present a ^{10}Be-dated chronology from the Lago Belgrano valley on the eastern side of Monte San Lorenzo (47.6° S, 3706m) in central Patagonia, Argentina, where a

unique topographic setting has allowed preservation of a moraine record from the early stages of glaciation.

4.2 Physical setting

Monte San Lorenzo is an isolated granitoid massif that is situated ∼90 km east of the main spine of the Andes on the border with Chile (Chilean name: Monte Cochrane) (Fig. 4.1). At this latitude, faulting has created a topographic depression that breaks the main chain of the Andes (Lagabrielle et al., 2004) to separate the North Patagonian Icefield (NPI) from the South Patagonian Icefield (SPI), and the San Lorenzo massif from the Pacific coast. The Río Baker and Río Pascua exploit this ∼80 km gap in the mountain chain to drain much of the eastern side of the Andes, including the large cross-border lakes of Lago General Carrera/Buenos Aires (LBA), Lago Cochrane/Pueyrredón (LP), and Lago O'Higgins/San Martín (SM), westward to the Pacific Ocean. The San Lorenzo and southern massifs constitute an area of high topography stepped east of the main Andean chain (Fig. 4.1 C). They are enclosed on their southern, western and northern sides by deep glacial valleys, some of which have been eroded to below sea level (e.g. LP and LBA; Murdie et al., 1998). By comparison, their eastern side is less affected by glacial erosion. Lago Belgrano lies at over 800 m asl. and Lago Burmeister at 900 m asl. The modern drainage divide runs just east of Lago Belgrano (Fig. 4.1 C), with this lake and the eastern outlet glaciers of San Lorenzo draining via a series of interconnected lakes westward into the Pacific Ocean. Lago Burmeister and the eastern part of the Belgrano valley instead drain eastward into the Atlantic Ocean via the Río Belgrano.

The geology of the area comprises Paleozoic basement rocks, intruded and overlain by Jurassic volcanic rocks and sedimentary sequences of Cretaceous and Jurassic age (Ramos et al., 1982; Ramos and Kay, 1992). The eastern part of the Belgrano valley is mainly characterized by Neogene and Paleogene volcanic sequences, the latter is represented by the Meseta Belgrano, which separates the Belgrano and Pueyrredón valleys (Ramos et al., 1982; Ramos and Kay, 1992). Monte San Lorenzo is part of the Patagonian Batholith intrusion, and is the nearest source of granitic boulders.

The climate of Patagonia is dominated by the SWW, which deliver precipitation to the present glaciers and icefields. The SWW are strongest during austral summer with the core situated between $45° - 55°$ S. In winter, they weaken and expand equatorward (Garreaud et al., 2009). The Andes create an orographic barrier to the westerly storms resulting in a strong west-east precipitation gradient. On the Pacific coast, precipitation reaches 5000 - 10 000 mm a^{-1} (Garreaud et al., 2013). East of the mountain divide precipitation decreases sharply to less than 300 mm a^{-1} within tens of kilometres from the mountain front (Garreaud et al., 2013). Air temperatures do not exhibit such a strong west-east gradient, and are pre-dominantly controlled by the SWW (Kilian and Lamy, 2012).

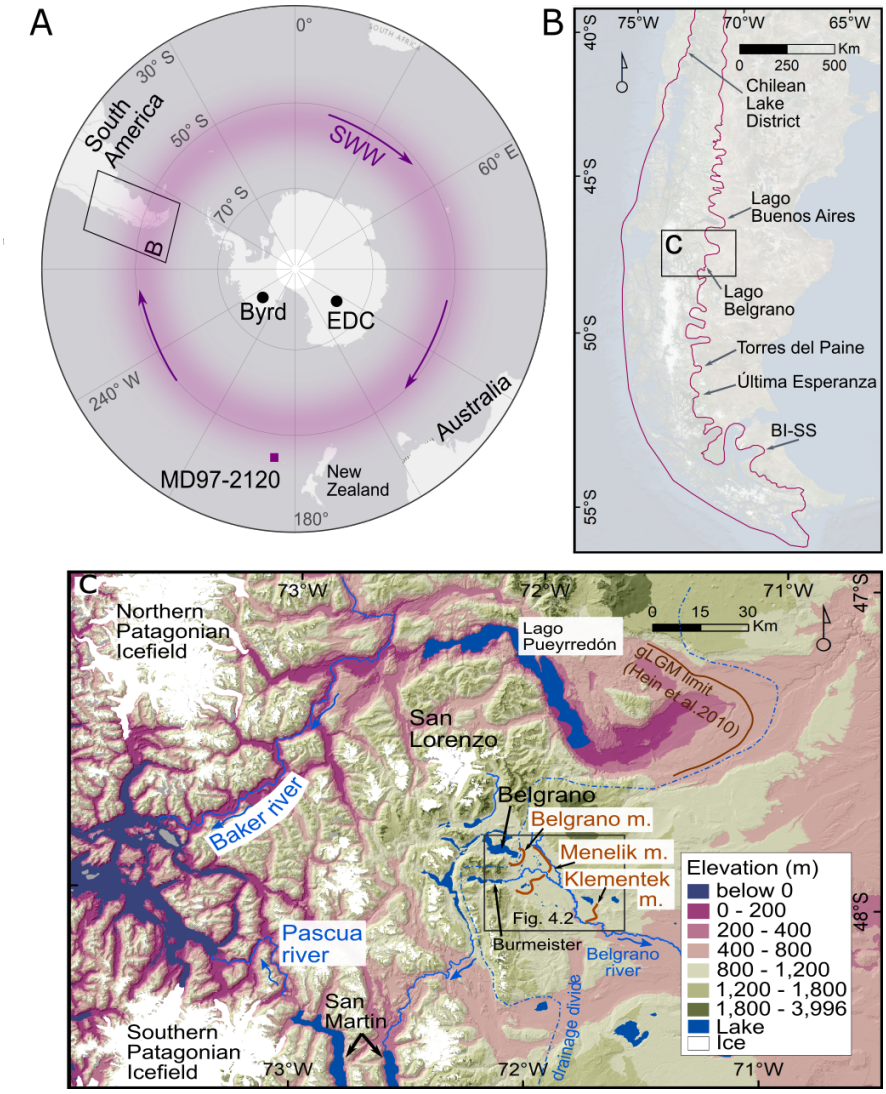

Figure 4.1: A) Location of Patagonia in the southern hemisphere along with Southern Ocean and Antarctic proxies discussed in the text and approximate location of the southern westerlies (SWW). B) Location of our study site in Patagonia and approximate extent of the Patagonian Ice Sheet during the gLGM (Singer et al., 2004). Image: ESRI World Imagery. (LBA: Lago Buenos Aires, TdP: Torres del Paine, UE: Última Esperanza, BI-SS: Bahí Inútil-San Sebastián lobe). C) A map showing the topography of central Patagonia and location of the San Lorenzo massif. Blue arrows depict drainage directions described in the text, blue dotted line represents hydrological drainage divide.The hillshade basemap: (SRTM). Glacier outlines are from the GLIMS database (Falaschi et al., 2017; De Angelis et al., 2015).

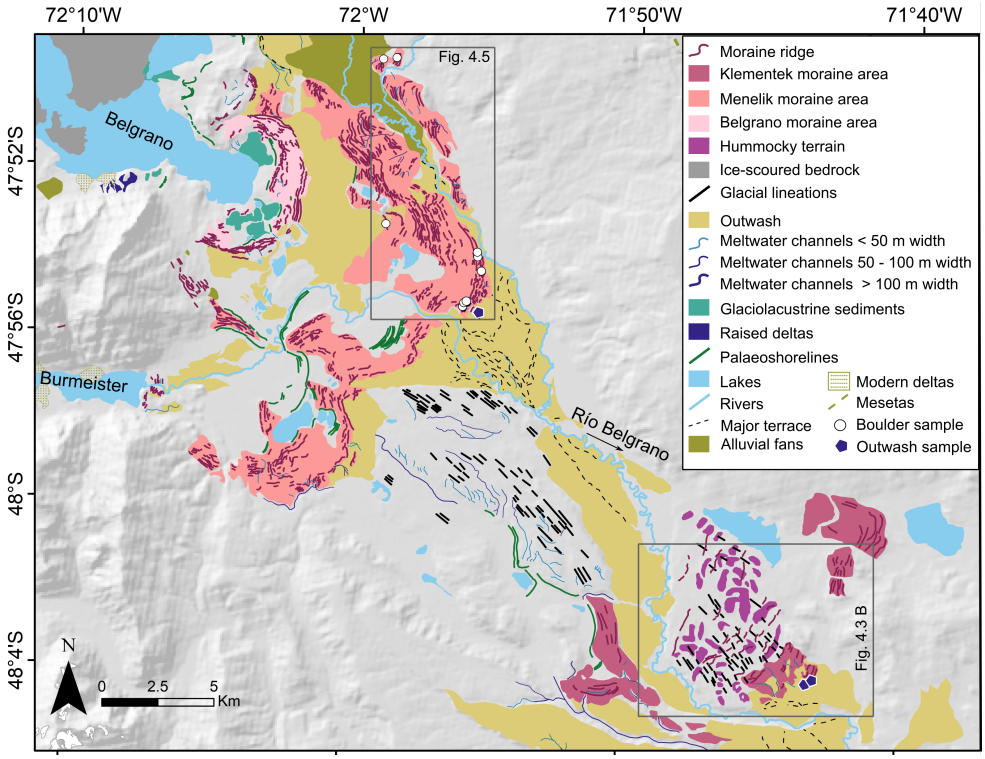

Figure 4.2: Geomorphological map showing the main moraine systems in the Belgrano valley, informally named the Klementek, Menelik and Belgrano moraines from the oldest to youngest. Sample locations are also shown. The hillshade basemap: SRTM.

The San Lorenzo massif, situated about 160 km from the Pacific coast, has a transitional maritime to continental climate (Falaschi et al., 2013). At this latitude, Monte San Lorenzo is the first orographic barrier to the SWW, which sustain this easternmost extensively glaciated area in the region (Falaschi et al., 2013). Glaciers of Monte San Lorenzo and the surrounding mountains cover an area of ∼207 km^2 (Falaschi et al., 2013). The snowline is estimated to be ∼ 1700 m asl on the western side and about 100 m higher on the eastern side of San Lorenzo (Falaschi et al., 2013). Glaciers of central Patagonia can be characterized as warm and wet, and are considered particularly sensitive to temperature changes (Sagredo and Lowell, 2012).

During the last glacial period, several tributary glaciers draining the San Lorenzo and southern massifs coalesced and flowed down the Belgrano valley (here referred to as the Belgrano glacier). By comparison with other outlets glaciers in central Patagonia, the Belgrano glacier was considerably smaller and occupied a relatively high-altitude valley. Three main moraine systems exist in the valley east of Lago Belgrano. Based on local landmarks, we informally name these moraine belts, Klementek, Menelik and Belgrano from the oldest to the youngest (Fig. 4.2). Here, we focus on the Klementek and Menelik moraine systems.

4.3 Glacial history and previous work

4.3.1 Previous work at Lago Belgrano

The glacial history of the Belgrano valley has received little scientific attention and is therefore largely unknown. Even Caldenius (1932), who mapped nearly all of Patagonia in his pioneering work, did not map the Belgrano valley. The area of Lago Belgrano was included in a Patagonia-wide glacial geomorphological map (Glasser et al., 2008), and partly covered by a more detailed geomorphological mapping by Bendle et al. (2017b). The only field-based mapping and chronological work in the Belgrano valley was done by Wenzens (2005) and Horta et al. (2017). Wenzens (2005) documented the glacial geomorphology of the valley and tentatively correlated the outermost moraine belt (the Klementek Moraines) to the LGM. He attributed the Menelik moraine system to the Late Glacial based on a radiocarbon age of 14.85 ± 0.12 ^{14}C ka from a kettle hole (18.0 ± 0.2 cal ka BP [1]). Horta et al. (2017) focused on the palaeolake history and obtained radiocarbon ages from lacustrine sediments inboard of the Menelik moraines. The Late Glacial and Holocene glacier history has been investigated by several workers, mainly on the western and northern flanks of Monte San Lorenzo (Mercer, 1968; Davies et al., 2018; Glasser et al., 2012; Sagredo et al., 2016, 2018; Martin et al., 2019).

4.3.2 Pre- gLGM glacial history of Patagonia

In Patagonia, the evidence for pre-gLGM ice expansion is largely restricted to Marine Isotope Stage (MIS) 3 and earlier glacial cycles. In southern Patagonia (49° − 55° S), several studies indicate MIS 3 advances that were significantly more extensive than the MIS 2 advances. On Tierra del Fuego (53-54° S), Darvill et al. (2015) determined that the Bahía Inútil - San Sebastián ice lobe advanced at 45.6 (+139.9/ − 14.3) ka and 30.1 (+45.6/ − 23.1) ka, and was up to 100 km more extensive than the subsequent gLGM limits (Kaplan et al., 2004; McCulloch et al., 2005b). The Torres del Paine and Última Esperanza outlet glaciers (50° S) reached their maximum at 48.0 ± 1.6 ka with subsequent advances at 39.2 ± 2.0 ka and 34.0 ± 1.3 ka dated by ^{10}Be exposure ages (García et al., 2018; Sagredo et al., 2011). Here, the MIS 2 ice advances (21.5 ± 1.8 ka) were half the extent of the MIS 3 maximum (García et al., 2018). Tentative exposure dates from the San Martin valley (49° S) follow a similar pattern (Glasser et al., 2011).

In northern Patagonia (40° − 44° S), glaciers also advanced during MIS 3 and MIS 2, but in contrast to southern Patagonia, the relative magnitudes were similar. In the CLD, stratigraphic evidence and radiocarbon chronology suggest ice expansion at 33.6 ∼ 0.2 ka, but this was similar in magnitude or smaller than later advances (Denton et al., 1999a; Moreno et al., 2015). Zech et al. (2011a) reported an advance at 39° S on the eastern side of the Andes dated by ^{10}Be at ∼

[1] Recalibrated using the OxCal online calibration program (version 4.3; Bronk Ramsey, 2009) and the SHCal13 calibration curve (Hogg et al., 2013)

39 ka. Much of the glacial deposits on the eastern side of the Andes in northern Patagonia remains undated, which precludes firm conclusions on the magnitude and timing of the maximum ice expansion in the north.

In central Patagonia ($44° - 49°$ S), two chronologies from large former outlet glaciers suggest maximum ice expansion roughly during the gLGM, between $\sim$ 27 - 25 ka at LBA (Kaplan et al., 2004; Douglass and Bockheim, 2006), and $\sim$ 28 ka and perhaps $\sim$ 35 ka at LP (Hein et al., 2010, 2009). In both valleys, moraines outside of the MIS 2 limits pre-date the last glacial cycle (Kaplan et al., 2005; Hein et al., 2017, 2009). Smedley et al. (2016) identified MIS 3 advances at LBA (34.0 ± 6.1, 30.8 ± 5.7 ka) using optically stimulated luminescence (OSL) dating of buried outwash sediment. However, there are no preserved moraines related to this advance, which likely only reached to within the MIS 2 limits.

More widely, robust ^{10}Be chronologies from New Zealand indicate glacial advances at $\sim$ 42 ka (Pukaki valley, Kelley et al., 2014), $\sim$ 35.5 ka (Pukaki valley, Doughty et al., 2015) and $\sim$ 32 ka (Ohau valley, Putnam et al., 2013). Overall, ice expansion during MIS 3 appears to be a regional phenomena (Darvill et al., 2016). Despite this, we are still far from fully establishing the magnitude of the MIS 3 glacial expansion throughout Patagonia and its climatic significance.

Chronostratigrahic evidence for glacial expansion prior to MIS 3 in Patagonia is fragmentary. At the time of publishing, there are no firmly dated glacial advances during MIS 4 or 5. In the Chilean Lake District (CLD), the outermost moraine belts of three outlet lobes have been tentatively assigned to MIS 4 (Denton et al., 1999b; Heusser et al., 1999; Mercer, 1976) but this assignment is not based on firm geochronological data. Palaeoclimate proxies from the southern mid-latitudes (e.g. Kaiser and Lamy, 2010) and Antarctica (Johnsen et al., 1972; EPICA Community Members, 2004) indicate cold conditions comparable to the gLGM during MIS 4. Dust fluxes to Antarctica (Lambert et al., 2008) and the Southern Ocean (Martínez-Garcia et al., 2011), which are considered a proxy for glacial activity in Patagonia (Sugden et al., 2009; Kaiser and Lamy, 2010), suggest expansion of Patagonian glaciers at the time. It is likely that MIS 4 glacial records exist in Patagonia, but they have not yet been firmly dated. By comparison, in New Zealand, full glacial conditions during MIS 4 are well documented (e.g. McCarthy et al., 2008; Shulmeister et al., 2018; Schaefer et al., 2015). The only tentative evidence for ice expansion in Patagonia during MIS 5 comes from two individual ^{10}Be ages (91.4 ± 4.1 ka, 96.8 ± 4.8 ka) from Lago San Martin (49° S; Glasser et al., 2011). As a consequence, little is known about the development of the Patagonian Ice Sheet (PIS) from the onset of the last glaciation towards the gLGM.

4.4 Methods

4.4.1 Geomorphic mapping

Geomorphological mapping was done using high resolution imagery (2.5 m to sub-meter) available through the ESRI^{TM} World Imagery service, along with 10 m Sentinel-2 imagery. An ALOS PALSAR radiometrically terrain-corrected digital elevation model with a resolution of 12.5 m was used to aid landform identification. Geomorphological features were identified and mapped following well established criteria (Glasser et al., 2008; Bendle et al., 2017b; Darvill et al., 2014; Martin et al., 2019). Mapping was supported by ground-truthing during two field campaigns in the austral summers of 2016 and 2018.

4.4.2 Dating approach and sampling

Cosmogenic nuclide surface exposure ages from glacial boulders are commonly used to establish the timing of glacial advances/still-stands in a range of environmental settings (e.g. Heyman et al., 2011). The technique works well in most settings on timescales relevant to the gLGM, but it can break down on older moraine systems due to site specific environmental factors that can affect nuclide concentrations, such as moraine degradation and boulder erosion (Putkonen and Swanson, 2003; Hallet and Putkonen, 1994; Briner et al., 2005; Hein et al., 2009, 2017; Heyman et al., 2011; Gillespie and Molnar, 1995; Applegate et al., 2010). Depending on the environmental conditions, direct dating of glaciofluvial outwash sediments directly linked to a moraine system can circumvent some of these issues to be an effective way of constraining the timing of a glacial advance. This is because outwash terraces are flat, unlike moraine ridges, and less susceptible to gravity-driven surface lowering, which minimises the potential for exhumation of surface clasts. Furthermore, the outwash cobbles rooted in the terraces are subject to less wind erosion, which is a significant source of boulder erosion in Patagonia. The outwash method has proved effective at dating pre-LGM glacial advances as old as one million years in this region (Hein et al., 2009, 2011, 2017; Darvill et al., 2015; Cogez et al., 2018). To develop our chronology, we measured cosmogenic ^{10}Be in both moraine boulders and glacio-fluvial outwash cobbles.

To date the Menelik moraines, we sampled six boulders on the outermost moraine ridges, one boulder on the inner moraine and two samples came from moraines near the northern valley side. In addition, we sampled five cobbles from its associated outwash terrace. To date the Klementek system, we sampled six surface cobbles from two sites on the outwash terrace associated with the outermost moraines. Surface boulders on this moraine system are rare; those we found were significantly eroded and unsuitable for dating. The sample details are presented in Table 4.1. When sampling, we preferentially targeted large (ideally >1 m) stable boulders on moraine crests that showed minimal signs of surface erosion (cf. Heyman et al., 2016; Putkonen and Swanson, 2003). Samples were

collected by hammer and chisel from the centre of the boulder surface (Gosse and Phillips, 2001; Darvill, 2013). Outwash cobbles were collected whole from locations where the outwash terrace could be unambiguously linked to the moraine system, but far enough from the moraine ridges to avoid material transported down its slopes and onto the terrace surface (Hein et al., 2011, 2009).

4.4.3 Preparation

Samples were prepared at two cosmogenic nuclide laboratories: the Natural Environment Research Council's Cosmogenic Isotope Analysis Facility (NERC-CIAF) and the University of Edinburgh's Cosmogenic Nuclide Laboratory. The samples were crushed, milled and then sieved to obtain the 250 μm to 500 μm (CIAF), or 250 μm to 710 μm (Edinburgh) size fraction. Large cobbles (>10 cm) were cut to an appropriate thickness parallel to the surface prior to crushing, while the majority of the cobbles were fist-sized and these were crushed whole. All measurements of ^{10}Be concentrations were done at the Scottish Universities Environmental Research Centre (SUERC) Accelerator Mass Spectrometry (AMS) facility.

NERC-CIAF Preparation

The 250 μm to 500 μm fraction was magnetically separated using a Franz machine and the non-magnetic fractions were recovered. To remove carbonates and soluble oxides, the samples were first treated with a 6:1:1 solution of water, HCl (37%) and HNO_3 (68%, aqua regia), on a hot-plate ($\sim 50°C$) and the supernatant was discarded. The samples were then treated with a 100:1 mixture of water and concentrated (40%) HF on a shaker table for one hour to slightly etch feldspar and mica grain surfaces. Supernatant liquid was discarded. Feldspar and mica minerals were then removed through froth floatation (Herber, 1969): the samples were repeatedly treated with eucalyptus oil, to make the etched grains hydrophobic, and a carbonated surfactant solution. Floating minerals were then discarded and quartz grains that did not float were recovered. The samples were then etched three times in a 1 litre solution of water, HF (40%) and HNO_3 (150:2:1) in a high power ultrasonic tank to isolate the cores of the quartz grains. An aliquot of the final quartz sand was dissolved and its purity was tested for Al, Be, Fe, Ca and Ti by ICP-OES at SUERC. The samples were dissolved in pure HF and each sample and process blanks (n=2) were spiked with $\sim$ 0.2 mg of ^{9}Be carrier. After dissolution, the HF was evaporated and replaced by HCl. The solutions were first passed through anion exchange chromatography columns to remove Fe. The Fe-free fraction was then evaporated and the HCl was replaced by diluted H_2SO_4. The sulphate solutions were then passed through cation exchange chromatography columns to remove Ti and B, and to separate Be and Al fractions. The ^{10}Be fractions were precipitated as hydroxides and oxidised at $\sim 900°C$. Resulting BeO were mixed with Nb (1:6) and pressed into

Table 4.1: Sample details and nuclide concentrations

Sample	Latitude (DD)	Longitude (DD)	Elevation (m)	Boulder height (m)	Thickness (cm)	Shielding correction	Quartz dissolved (g)	^{10}Be atoms g-1	± 1σ atoms g-1	^{10}Be/^{9}Be ratio	± 1σ	AMS ID	Laboratory facility
Menelik moraine boulders													
LB1614	-47.90459	-71.923341	920	1	2.5	0.9999	20.85	2.33E+05	6.69E+03	2.99E-13	8.37E-15	b10569	CIAF
LB1615	-47.89716	-71.926587	925	2	2.5	1.0000	17.60	2.11E+05	5.71E+03	2.29E-13	5.94E-15	b10570	CIAF
LB1616	-47.89831	-71.92643	927	1.3	3.5	0.9998	11.54	2.31E+05	5.74E+03	1.63E-13	3.71E-15	b10543	CIAF
LB1617	-47.91733	-71.931457	913	2	1.5	0.9999	20.39	2.23E+05	5.69E+03	2.77E-13	6.84E-15	b10571	CIAF
LB1618	-47.91796	-71.93321	920	0.5	1.5	0.9998	14.40	1.69E+05	5.37E+03	1.68E-13	4.97E-15	b10545	CIAF
LB1619	-47.91963	-71.934285	910	0.7	2	0.9999	21.84	2.38E+05	6.87E+03	3.18E-13	8.96E-15	b10572	CIAF
LB1612	-47.82028	-71.987082	951	2.0	5	0.9990	21.03	2.10E+05	8.50E+03	2.70E-13	1.05E-14	b10925	Edin
LB1630	-47.88703	-71.982271	913	0.7	1.5	0.9998	24.85	1.54E+05	6.35E+03	2.36E-13	9.26E-15	b10927	Edin
LB1632	-47.81968	-71.978975	980	0.5	3.5	0.9990	23.43	1.73E+05	5.77E+03	2.49E-13	7.90E-15	b10928	Edin
Menelik outwash cobbles													
LB1620	-47.9222	-71.925146	887	-	5*	0.9999	12.33	2.23E+05	5.96E+03	1.86E-13	4.60E-15	b10546	CIAF
LB1621	-47.92219	-71.925114	885	-	6	0.9999	6.26	2.26E+05	8.19E+03	9.74E-14	3.01E-15	b10547	CIAF
LB1622	-47.92222	-71.925088	887	-	5*	0.9999	13.23	2.11E+05	6.41E+03	1.89E-13	5.41E-15	b10548	CIAF
LB1623	-47.92224	-71.925067	885	-	5*	0.9999	12.27	3.21E+05	9.56E+03	2.66E-13	7.67E-15	b10551	CIAF
LB1624	-47.92226	-71.925055	886	-	5*	0.9999	5.87	2.07E+05	7.39E+03	8.43E-14	2.40E-15	b10552	CIAF
Klementek outwash cobbles													
LB1637	-48.06456	-71.71924	824	-	8	0.9999	23.34	5.96E+05	1.47E+04	8.36E-13	2.04E-14	b10929	Edin
LB1638	-48.06455	-71.719243	825	-	8	0.9999	22.42	6.95E+05	1.48E+04	9.38E-13	1.98E-14	b10930	Edin
LB1639	-48.06458	-71.719171	822	-	6	0.9999	25.06	5.52E+05	1.36E+04	8.34E-13	2.03E-14	b10931	Edin
LB1640	-48.06456	-71.719194	822	-	10	0.9999	22.59	6.33E+05	1.56E+04	8.61E-13	2.10E-14	b10934	Edin
LB1641	-48.06459	-71.71918	822	-	6	0.9999	22.96	6.22E+05	1.53E+04	8.60E-13	2.10E-14	b10936	Edin
LB1642	-48.0629	-71.716157	819	-	5.5	0.9999	20.77	5.94E+05	1.47E+04	7.47E-13	1.82E-14	b10937	Edin

Rock density is assumed to be 2.7 g cm^{-3}.

*Samples that were cut prior to crushing, reported thickness is after cutting.

Concentrations were corrected for process blanks; blank corrections ranged between about 1 and 4 % of the sample ^{10}Be/^{9}Be ratios. The uncertainty of the blank correction is included in the stated one-sigma uncertainties.

Measurements were normalised to NIST SRM4325 with nominal ^{10}Be/^{9}Be ratios of 2.79x10^{-11} and half-life of 1.36 Ma (Nishiizumi et al., 2007).

CIAF - Cosmogenic Isotope Analysis Facility, Edin - the University of Edinburgh's Cosmogenic Nuclide Laboratory.

All measurements were made at the AMS facility at SUERC.

copper cathodes for AMS analysis. All measurements were normalized to NIST SRM4325 standard with nominal ratios of 2.79×10^{-11} $^{10}Be/^{9}Be$ (Nishiizumi et al., 2007) and half-life of 1.36 Ma. The blank corrections ranged between 1 and 4% of the sample $^{10}Be/^{9}Be$ ratios.

Edinburgh Preparation

At the University of Edinburgh's Cosmogenic Nuclide Laboratory, quartz was isolated through repeated acid etching following standard procedures (Nishiizumi et al., 2007; Bierman et al., 2002). The samples and the process blanks (n=2) were spiked with $\sim$ 0.25 mg ^{9}Be carrier. The samples were prepared as BeO targets for AMS analysis following procedures detailed by Hein (2009), which are similar to those described above. $^{10}Be/^{9}Be$ measurements were normalized to the standards of Nishiizumi et al. (2007) with nominal ratios of 2.79×10^{-11}. The blank corrections were under 1% of the sample $^{10}Be/^{9}Be$ ratios.

Age Calculations

The ^{10}Be ages were calculated using the online exposure age calculator formerly known as the CRONUS-Earth online calculator (version 3, Balco et al., 2008), with the Patagonia production rate (Kaplan et al., 2011) obtained from the ICE-D online database (`http://calibration.ice-d.org/`). Throughout the paper we report ages calculated using the time-dependent scaling scheme of Lal (1991) modified by Stone (2000). Using the New Zealand ^{10}Be production rate (Putnam et al., 2010b), our ages decrease by less than 1%, and using the global production rate (Borchers et al., 2016) the ages decrease by $\sim$ 6%. Summary statistics for each moraine system are provided in Figure 4.6. We base our discussion on the arithmetic mean and 1 σ standard deviation for each moraine system.

The ages presented here assume zero erosion and are therefore minimum ages. Topographic shielding was measured in the field and is negligible for all samples ($\sim$ 0.99). The ages are not corrected for snow, vegetation or soil shielding. Vegetation is sparse in the area, mostly comprises steppe grasses and is unlikely to introduce significant shielding. Owing to high winds and the semi-arid environment, we expect snow shielding to be minimal. Soils in the field area are thin (normally 0-10 cm) and spatially variable, and a significant lag is expected before soil develops following ice retreat. Quantifying soil shielding over the exposure history is therefore difficult, but we expect the impact on ages to be minimal.

4.5 Results

4.5.1 Moraine Record

The Klementek moraine system comprises of well-defined outermost moraine ridges with 25 m relief and slopes up to 12° deposited in the eastern part of the valley, ∼ 65 km from present day glacier margins (Fig. 4.2). The outermost moraine ridges are discontinuous and up-valley transition into a hummocky terrain, which extends for 10 km on the northern side of the Río Belgrano (Fig. 4.3). Hummocks and hollows are interspersed with streamlined, ice-flow parallel landforms of 250 - 450 m in length. Small narrow ridges of up to one kilometer in length, perpendicular to former ice flow, are superimposed on the hummocky terrain, and are interpreted as recessional moraines. Occasional, significantly eroded boulders with fluting and ventifacts are scattered on the hummocky terrain. A glacio-fluvial outwash terrace emanates from the distal margin of the outermost moraine ridges. Relict braided channels can be traced from the surface of the outwash to the moraines. The outermost moraine ridges are interpreted to mark a former ice margin position of the Belgrano glacier, while the hummocky terrain was likely formed by a combination of subglacial and ice-marginal processes during ice retreat. The morphology of the Klementek moraine system is suggestive of a pre-LGM age.

The Menelik moraines (Fig. 4.4 and 4.5) are 22 km up valley and are separated from the Klementek moraines by a >10 km long broad glacio-fluvial outwash terrace. The double-lobate shape of the Menelik moraines and the presence of a medial moraine indicate the coalescence of the Belgrano and Burmeister glaciers. The outermost Menelik moraines are prominent, cross-valley ridges with broad crests, and 30 m relief and slopes up to 15° (Fig. 4.4 and 4.5). Clusters of exposed gravel and abundant boulders can be found on moraine crests. Inboard, moraines diminish in size and in places are interspersed with numerous ponds and depressions. Numerous small (1-2 m relief) moraine ridges are preserved on higher ground (Fig. 4.4 A). The sequence of smaller moraines extends up valley over a distance of ∼ 10 km, and suggests deposition during ice recession. Palaeoshorelines indicate formation of shallow proglacial lakes as the ice margin retreated (Fig. 4.2). Near the northeast shore of Lago Belgrano, the Menelik moraines are cross-cut by the younger Belgrano moraines (Fig. 4.2). This indicates that the glacier retreated into the Belgrano trough prior to a subsequent re-advance, which also removed part of the inner Menelik moraine system. Glacio-fluvial outwash terraces emanate from the Menelik moraines with preserved relict surface channels. The outwash plain has been incised by two rivers, leaving the area sampled isolated and unaffected by post deposition fluvial processes.

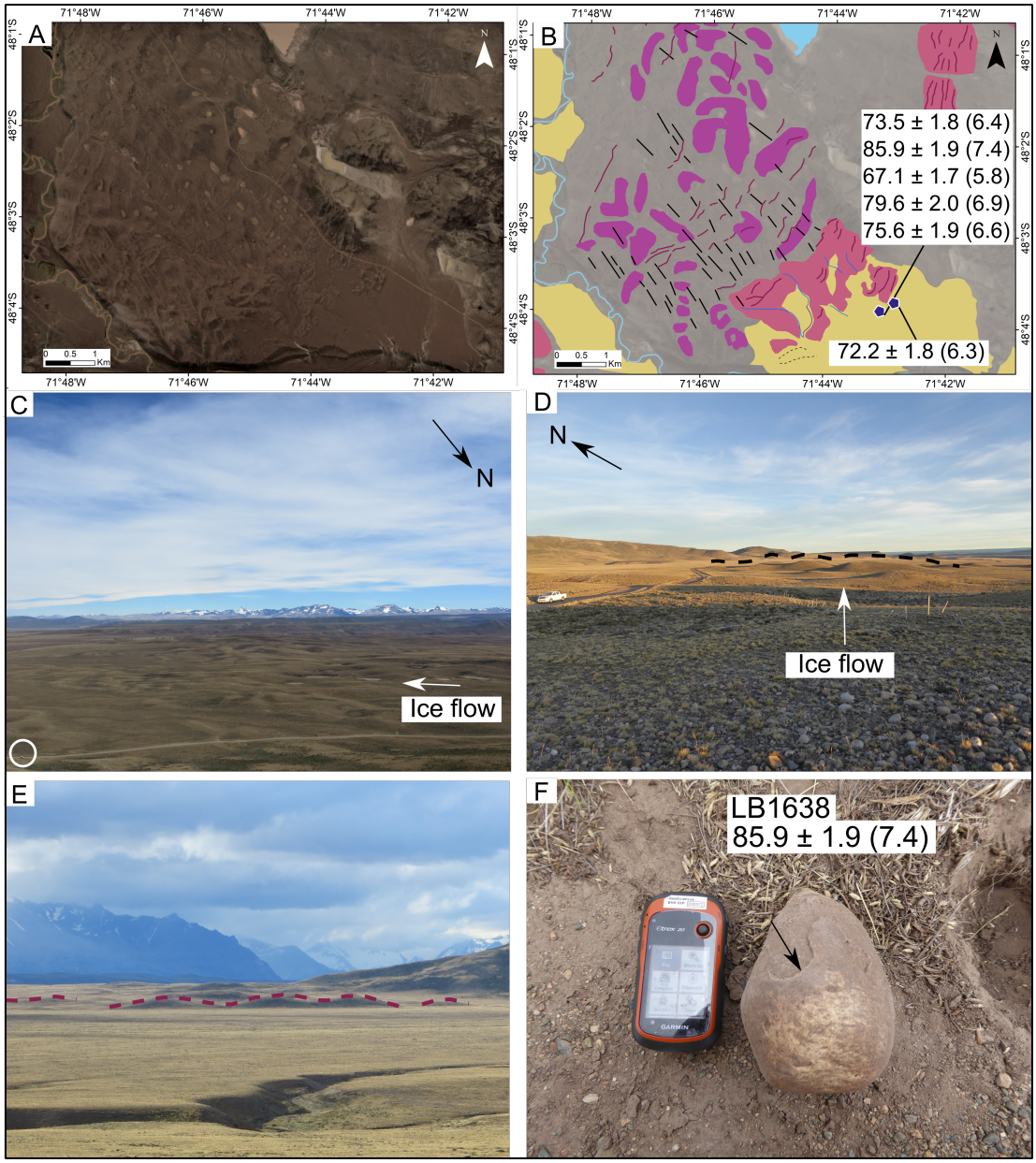

Figure 4.3: A) Satellite image (Sentinel-2) and B) mapped moraine ridges of the Klementek moraine system and the associated hummocky terrain. Sample locations and ^{10}Be exposure ages are also shown. C) Photograph showing part of the hummocky terrain, with a vehicle in the bottom left corner for scale. D) Photograph showing the outermost Klementek moraine ridges. E) Photograph showing the outermost Klementek moraine ridges and the associated outwash in foreground that was sampled for surface exposure analysis. F) An example of an outwash cobble sampled, which still exhibits fluvial shape, but some surface erosion is evident (maximum 3 mm).

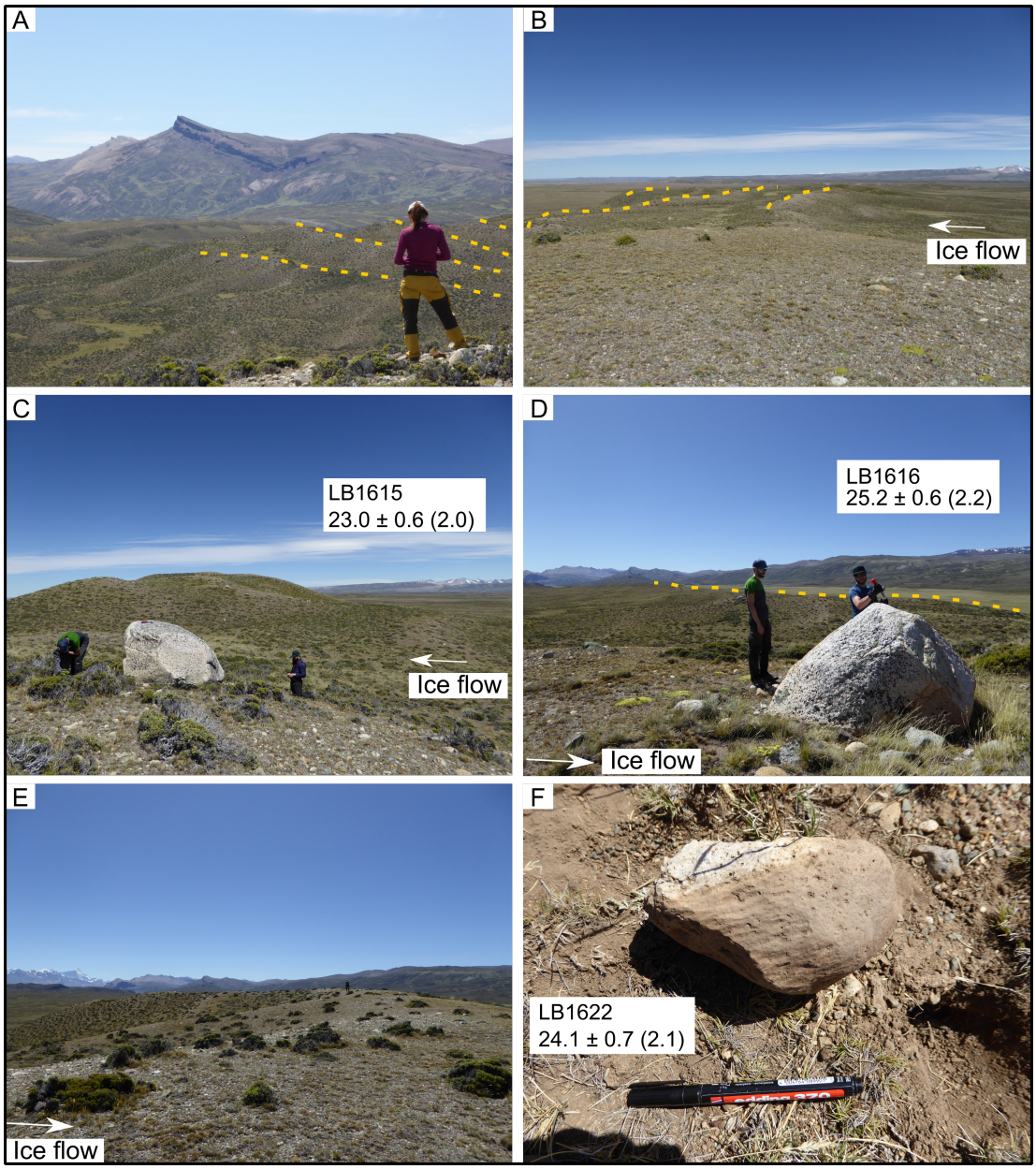

Figure 4.4: A) Photograph showing the Menelik moraines (dashed yellow lines) draped on higher ground. B-E) Photographs showing the outermost Menelik moraines (dashed yellow lines) along with examples of sampled boulders. F) Example of a cobble sampled from the outwash associated with Menelik moraines. Ventifacts on the surface suggest long surface exposure (cf. Hein et al., 2011).

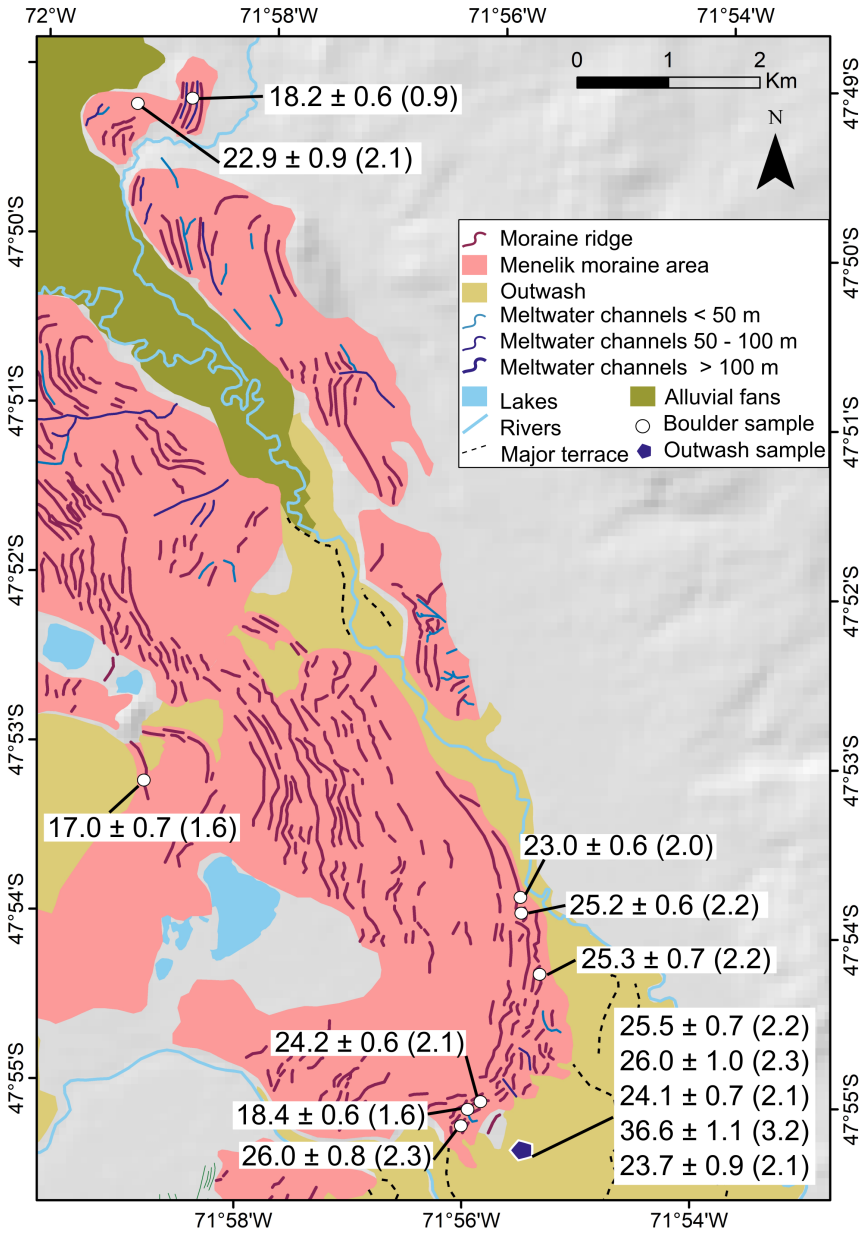

Figure 4.5: Enlarged geomorphological map showing the Menelik moraine system along with sample locations and ^{10}Be exposure ages.

4.5.2 Exposure ages

We present 20 new exposure ages from the Klementek and Menelik moraine systems. The ^{10}Be data are presented in Figures 4.3 B and 4.5, and Tables 4.2. The probability density diagrams ('camelplots') are shown in Figure 4.6. In the following, we report individual ^{10}Be ages with 1 σ internal uncertainties.

The ages from the Klementek outwash range from 67.1 ± 1.7 ka to 85.9 ± 1.9 ka (n = 6; Fig. 4.3 B and 4.6 A). The distribution of ages contains a cluster of four ages, with one younger and one older age. The ages yield a mean of 75.7 ± 5.9 ka (all data), or 75.2 ± 2.8 ka with the outliers excluded.

The boulder ages from the Menelik outermost moraines range from 18.4 ± 0.6 ka to 26.0 ± 0.8 ka (n=6; Fig. 4.5 and 4.6 B). We consider the youngest sample (18.4 ± 0.6 ka) an outlier because it was taken from a short, partly buried boulder and was likely exhumed from the moraine matrix post-deposition. The remaining samples range from 23.0 ± 0.6 ka to 26.0 ± 0.8 ka and yield a mean age of 24.8 ± 1.1 ka. The two boulders from moraines near the Belgrano valley side yielded ages of 22.9 ± 0.9 and 18.3 ± 0.6 ka. The boulder from the inner Menelik moraine gave an age of 17.0 ± 0.7 ka. Cobble ages from the Menelik outwash (Fig. 4.5 and 4.6 C) range from 23.7 ± 0.9 ka to 26.0 ± 1.0 ka, excluding an older age of 36.6 ± 1.1 ka, and yield a mean age of 24.8 ± 0.9 ka.

4.6 Discussion

4.6.1 The age of the Klementek outwash

Geomorphic considerations

The distribution of the Klementek outwash cobble ages suggests that the samples may have been affected by pre- and post-depositional processes. One possibility is that the cobbles are erroneously young because they were exhumed through bio- or cryo-turbation, or as the terrace surface lowered through time. We do not expect bio- or cryo-turbation processes to significantly affect the exposure ages because soils at the site are thin, which should limit this process. Terrace deflation is also expected to be insignificant based on a study in the neighboring Lago Pueyrredón valley to the north. Here, Hein et al. (2009) estimated outwash terrace surface lowering rates at 0.53 mm ka^{-1} using a depth-profile approach. This rate would imply about 45 mm of total terrace surface lowering over the past 86 ka (the age of oldest outwash sample), which would not significantly decrease the apparent exposure ages. Rock surface erosion is another potential source of geological scatter and erroneously young apparent exposure ages. Our ages assume no rock surface erosion, but minor surface erosion is evident on most Klementek cobble samples (Fig. 4.3 F). The erosion depth is variable but less than ∼ 3 mm (Figures 4.3 F). This amount of erosion integrated over ∼ 86 ka

Table 4.2: Exposure ages

Sample	Lm			LSDn			St		
	Age	**Inter**	**Exter**	**Age**	**Inter**	**Exter**	**Age**	**Inter**	**Exte**
		Years			Years			Years	
Klementek	**outwash**								
LB1637	73531	1849	6407	76046	1914	6634	72158	1814	6251
LB1638*	85924	1874	7431	89053	1943	7711	84365	1839	7252
LB1639*	67089	1680	5835	69391	1739	6042	65888	1650	5697
LB1640	79600	2003	6946	82415	2075	7200	78157	1966	6780
LB1641	75642	1904	6594	78264	1971	6831	74281	1869	6438
LB1642	72164	1815	6286	74654	1879	6510	70841	1781	6135
Menelik	**moraines outer**								
LB1614	25318	733	2212	25987	752	2272	24904	721	2164
LB1615	22976	625	1993	23503	639	2040	22625	615	1952
LB1616	25240	631	2174	25905	647	2232	24823	620	2126
LB1617	24230	622	2091	24831	638	2144	23853	612	2047
LB1618*	18427	589	1626	18669	597	1649	18217	582	1600
LB1619	26002	755	2273	26709	776	2336	25574	743	2223
Menelik	**moraines inner**								
LB1612	22908	931	2104	23438	953	2154	22546	916	2061
LB1630	17020	702	1566	17189	709	1582	16849	695	1543
LB1632	18330	614	1628	18568	622	1650	18088	606	1599
Menelik	**outwash**								
LB1620	25449	685	2207	26122	703	2266	25058	674	2161
LB1621	26010	951	2345	26716	977	2411	25605	936	2297
LB1622	24140	738	2121	24733	756	2175	23788	727	2079
LB1623*	36632	1101	3222	37803	1137	3327	35993	1082	3148
LB1624	23728	851	2132	24296	872	2184	23388	839	2091

Scaling schemes: Lm is the time-dependent version of Lal (1991) and Stone (2000), LSDn - time-dependent scheme of Lifton et al. (2014), and St - time-independent version of Lal (1991) and Stone (2000).
*Ages are reported with 1 internal and external uncertainties, the latter includes production rate and scaling uncertainties. Ages assume zero erosion and no correction for shielding by snow and/or vegetation. Elevation flag is std. Grey shading indicates ages reported here. Samples marked with * are outliers.*

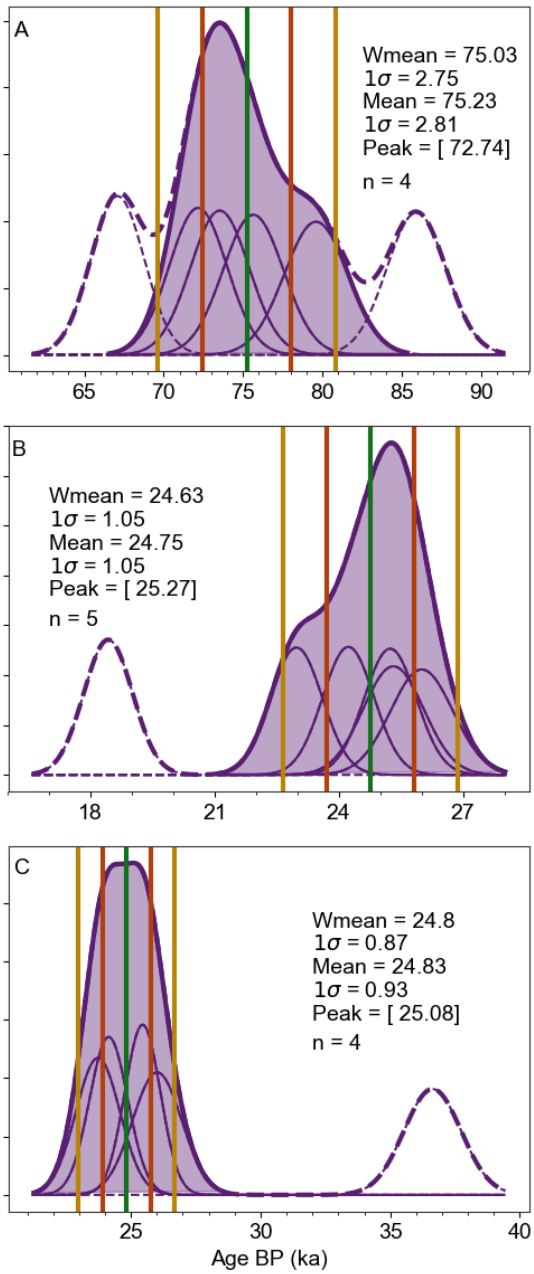

Figure 4.6: Probability density diagrams ('camelplots') for A) the Klementek cobble ages, A) Menelik boulder ages, and C) Menelik cobble ages. Thin purple curves represent Gaussian curves for individual samples. Thick purple curve represent the summed probability distribution for the data, excluding outliers. Outliers are represented by dashed curves. Vertical lines denote an arithmetic mean (dark green, excluding outliers), and 1 and 2 σ (paired brown and yellow lines respectively) confidence intervals of the mean. Wmean: uncertainty-weighted mean.

(age of oldest sample) yields an erosion rate of 0.035 mm ka^{-1}. Applying this erosion rate to the age calculations would increase the ages by less than 1 %, which is within the analytical uncertainty.

Nuclide inheritance is a potential source of geological scatter that would make the ages erroneously old. We assume inheritance is negligible because the outwash sediment was shielded, transported and eroded by warm-based ice before deposition. This assumption is supported by depth-profile measurements in the neighbouring Lago Pueyrredón valley where average inheritance was demonstrated to be negligible (Hein et al., 2009), and by the similarity of outwash cobble and moraine boulder exposure ages. Given the similarity of ages obtained from the Menelik moraine boulders and outwash surface cobbles, we too conclude inheritance is low.

Age interpretation

There are several ways to interpret the outwash exposure ages: 1) If we assume that the oldest sample remained on the surface the longest and the other samples were exhumed later as the outwash terrace deflated, then the oldest age approach (cf. Hein et al., 2009) would provide the closest age for the deposition of the outwash at $\sim$ 86 ka. 2) The youngest and oldest ages were affected by pre- (85.9 $\pm$ 1.9 ka, e.g. inheritance) and post-depositional processes (67.1 $\pm$ 1.7 ka, exhumation). If we exclude them as outliers, we obtain a mean age of 75.2 $\pm$ 2.8 ka (n=4), which would be the best possible age for the deposition of the outwash. 3) All ages are correct and the outwash is of composite age, and was deposited during ice expansion between $\sim$ 86 and 67 ka. Given the clustering of ages and our assessment of the significance of terrace deflation, exhumation and inheritance, we tentatively suggest the mean age of 75.2 $\pm$ 2.8 ka (scenario 2) as the best estimate for the culmination of the ice advance that deposited the outwash. However, since we cannot exclude other scenarios, we acknowledge that the outwash might be as old as 86 ka or it could have been deposited between 86 - 67 ka.

Our mapping suggests the Klementek moraines are age-equivalent to the dated outwash and therefore represent a glacial advance at 75.2 $\pm$ 2.8 ka ka; the morphology of the moraine system is consistent with this age. We acknowledge that the hummocky terrain with superimposed moraine ridges could be a palimpsest feature younger than the dated outwash and could have been deposited during MIS 4 and 3.

4.6.2 The age of Menelik moraines and outwash

The Menelik outermost moraine boulders yield a mean age of 24.8 $\pm$ 1.1 ka, excluding one young outlier. The outwash cobbles yield a mean age of 24.8 $\pm$ 0.9 ka, excluding one older outlier. As with the Klementek outwash, there are several ways to interpret the Menelik outwash ages: 1) the oldest age approach (36.6 $\pm$

1.1 ka, LB1623); 2) the oldest age is an outlier (e.g. contains inherited nuclides or reworked from previous advance) 3) all ages are correct, and the outwash is of composite age. The relative clustering of the boulder and outwash ages indicates that scenario 2) is most likely. Our field observations, however, provide some support for scenario 3, since there is a remnant of a smaller moraine just outboard of the outermost Menelik moraine sampled. It is possible the oldest outwash sample (36.6 ± 1.1 ka) represent this earlier, slightly more extensive advance, and therefore we tentatively suggest an advance at this time. The remaining four samples, which produce a central peak (Fig. 4.6 C), would therefore relate to the major advance that deposited the prominent outermost moraines and (part-) deposited the outwash. Excluding two ages (LB1618 and LB1623), the remaining outwash and moraine boulder exposure ages are indistinguishable and when combined together yield a mean age of 24.8 ± 1.0 ka, which we interpret as the timing of this major advance.

4.6.3 The last glacial cycle at Lago Belgrano

Our ^{10}Be ages suggest the most extensive advance of the Belgrano glacier occurred early in the last glacial cycle at 75.2 ± 2.8 ka ka toward the end of MIS 5. Given the scatter in our exposure ages and the extent of the hummocky terrain with recessional moraines, it is possible the glacier oscillated near its maximum position between 86 - 67 ka. The advance precedes major cooling during MIS 4, when some New Zealand glaciers had reached full glacial conditions (e.g. McCarthy et al., 2008; Shulmeister et al., 2018; Schaefer et al., 2015). Whilst we find no unambiguous evidence for an advance during MIS 4, we recognize the youngest age of 67.1 ± 1.7 ka overlaps in timing. We only dated outwash associated with the outermost moraines, it is therefore possible that some of the recessional moraines were deposited during MIS 4.

We have tentative evidence for an advance during MIS 3 (36.6 ± 1.1 ka), but this requires further chronological constraint. Significant MIS 3 glacial advances have been identified at several locations elsewhere in Patagonia (Darvill et al., 2015; Smedley et al., 2016; García et al., 2018; Denton et al., 1999b). A second major, but considerably smaller, advance of the Belgrano glacier is represented by the Menelik moraines and occurred at 24.8 ± 1.1 ka, coeval with the gLGM.

4.6.4 Evidence for MIS 5 glaciation

The Belgrano glacier reached its maximum extent much earlier than elsewhere in Patagonia, where MIS 3 is the more dominant signal. Our data provide the first robust evidence for MIS 5 glaciation in Patagonia. Elsewhere in the southern mid-latitudes, evidence for MIS 5 glaciation is fragmentary. In southern Patagonia, the maximum expansion of the Lago San Martin outlet glacier may have occurred during late MIS 5 (Glasser et al., 2011). In New Zealand, ^{10}Be ages from the Cascade valley, suggest an advance at ∼ 90 ka (Sutherland et al.,

2007). Shulmeister et al. (2010) reported glacier advances at ∼ 100 - 90 ka and ∼ 80 ka in the Rakaia Valley based on stratigraphic evidence and OSL ages. The advance of Belgrano glacier could correlate with ice expansion evident in New Zealand during MIS 5b-a.

In the northern hemisphere, there is evidence for expansion of mountain glaciers and ice sheets during MIS 5. For example, glaciers in central Asia (Röhringer et al., 2012; Koppes et al., 2008), NE Siberia (Zech et al., 2011b), as well as in NW Washington and in the Pyrenees (Pallàs et al., 2010; Lewis et al., 2009) reached their maximum during MIS 5. Sectors of large northern hemisphere ice sheets expanded to their maximum position early in the last glacial cycle. For example, the Barents-Kara ice sheet reached its maximum extent during MIS 5 (90 - 80 ka), and was less extensive during subsequent glaciations (Svendsen et al., 2004).

These studies demonstrate substantial glaciation of mid-latitude mountain areas globally, as well as the growth of ice sheets, during MIS 5. Our data demonstrates extensive glaciation of the eastern massifs of central Patagonia at this time. We speculate that the onset of glaciation throughout the Patagonian Andes also occurred during MIS 5, but the geomorphic and stratigraphic evidence has largely been destroyed, or remains undiscovered.

4.6.5 gLGM and deglaciation in Patagonia

Our data show that the Belgrano glacier advanced at 24.8 ± 1.0 ka during the gLGM, but this advance was substantially smaller than the MIS 5 advance. The timing of this advance is in good agreement with other glacial records in Patagonia (e.g. Hein et al., 2010; Kaplan et al., 2004, 2008; McCulloch et al., 2005b; Denton et al., 1999b). For example, in central Patagonia, the LP outlet glacier achieved its maximum extent at ∼ 28 ka with a subsequent advance at ∼ 25 ka (Hein et al., 2010). The LBA outlet lobe was at its maximum at ∼ 27 - 25 ka followed by several smaller re-advances/still-stands (Kaplan et al., 2004; Douglass and Bockheim, 2006). Advances during the gLGM in southern Patagonia were substantially less extensive than the MIS 3 advances (García et al., 2018; Darvill et al., 2015; McCulloch et al., 2005b; Kaplan et al., 2008).

The presence of numerous, regularly spaced recessional moraines indicate that deglaciation from the 25 ka limits at Lago Belgrano was, at least initially, gradual. We speculate that the Belgrano glacier occupied the eastern portion of the valley for at least 8 ka, between ∼ 25 ka and ∼ 17 ka, based on the age from the inner Menelik moraine (17.0 ± 0.7 ka), but further work is needed to confirm this. Shallow proglacial lakes formed as the ice margin retreated from the inner Menelik moraines. Once the glacier retreated into the Belgrano trough, it likely experienced a more dynamic retreat associated with calving. We have no evidence to constrain the maximum recession prior to the re-advance that deposited the Belgrano moraines.

Although we cannot firmly constrain the timing and rate of deglaciation, our

youngest age (17.0 ± 0.7 ka) from the inner Menelik moraine broadly matches the onset of deglaciation elsewhere in Patagonia. At LP, deglaciation began as ice withdrew from the youngest Río Blanco moraines dated at ∼ 21 - 19 ka (Hein et al., 2010). Rapid deglaciation of the LP and Chacabuco valleys accompanied by ice thinning is supported by a vertical reconstruction (Boex et al., 2013) and a pollen analysis of a lake core (Henríquez et al., 2017). At LBA, the onset of deglaciation was dated at 18.1 ± 0.2 ka, followed by a short still-stand at 17.7 ± 0.1 ka, which deposited the Menucos moraines (Bendle et al., 2017a; Kaplan et al., 2004; Douglass and Bockheim, 2006). Deglaciation was initially steady, but accelerated after 17.3 ka when the LBA outlet lobe started to calve into a deep lake (Bendle et al., 2017a). Overall, it appears that in central Patagonia deglaciation was underway by 19 - 18 ka (García et al., 2019; Markgraf et al., 2007; Hein et al., 2010; Henríquez et al., 2017; Bendle et al., 2017a), while in southern Patagonia and in the CLD ice retreat initiated about 1 ka later (McCulloch et al., 2005b; García et al., 2014; Kaplan et al., 2008; Sagredo et al., 2011; Denton et al., 1999a; Moreno et al., 2015; Mendelova et al., 2017).

4.6.6 Causes of glaciation

In the following we consider potential mechanisms that could lead to ice expansion during MIS 5 and the pattern of successively smaller ice extent at Lago Belgrano.

Insolation

Earth's orbital parameters exert a primary control on glacial-interglacial cycles and modulate global climate (Hays et al., 1976; Milankovitch, 1941). Insolation in the southern hemisphere is almost completely out-of-phase with the northern hemisphere, and it has been proposed that southern hemisphere insolation modulates regional climates, and therefore controls glacial advances in the southern mid-latitudes (Vandergoes et al., 2005; Sutherland et al., 2007; Darvill et al., 2015, 2016). A minimum in southern hemisphere summer insolation occurred between 85 - 75 ka (Fig. 4.7 B), and this may have promoted ice advance at Lago Belgrano. As noted by Hughes and Gibbard (2018), insolation played a particularly important role in glacial inception, including the insolation minimum at the end of the previous interglacial. The amplitude of southern hemisphere insolation change is greatest during MIS 5, with a minimum of the last glacial cycle between 115 ka and 100 ka. This would have likely created favorable conditions for glaciation of the Patagonian Andes. Glaciers in mid- and high-northern latitudes are thought to have expanded in response to reduced summer insolation early in the last glacial cycle (e.g. Abramowski et al., 2006; Porter and Swanson, 2008; Farquharson et al., 2018).

Reduced southern hemisphere summer, as well as winter, insolation have been invoked to explain glacier expansion in Patagonia and New Zealand during MIS 3 (Darvill et al., 2015, 2016; García et al., 2018). However, Doughty et al.

(2015) and Darvill et al. (2016) noted that southern hemisphere insolation alone cannot explain the timing of glacier advances observed in the southern mid-latitudes. While insolation was important in driving the onset of glaciation, later in the glacial cycle it may have only played a comparatively minor role (Hughes and Gibbard, 2018). Further, variations in insolation would modulate regional climates differently (Gillespie and Molnar, 1995). The timing and extent of ice advances along the Patagonian Andes was then ultimately determined by local-to-regional factors and feedback mechanisms (cf. Darvill et al., 2016; García et al., 2018).

An alternative hypothesis suggests that the precessional cycle might affect the timing of glacial advances in the southern mid-latitudes by controlling southern hemisphere seasonality and the pole-to-equator thermal gradient, which in turn drives westerly circulation (Shulmeister, 1999; Shulmeister et al., 2004). Glacial advances would therefore occur at southern hemisphere precessional maxima, i.e. 23 ka, 48 ka, 72 ka, and 96 ka (Shulmeister et al., 2010). In this model, ice expansion at Lago Belgrano might have been driven by a precessional maximum at 96 ka and at 72 ka. There is evidence for ice advances in Patagonia at $\sim$ 48 ka (García et al., 2018), and in NZ at $\sim$ 42 ka (Kelley et al., 2014) that could be linked to a precessional maximum at 48 ka.

Moisture availability

While the initial growth of the San Lorenzo ice cap was likely driven by reduced southern hemisphere insolation, we suggest the early maximum and successively smaller ice extent at Lago Belgrano was, in part, related to decreasing moisture delivery over the course of the glacial cycle. The San Lorenzo massif is the easternmost glaciated area in Patagonia today, sustained by westerly precipitation. Early in the glacial cycle, expansion of an independent ice cap over San Lorenzo would have been fostered by westerly precipitation that was able to penetrate through the gap in the Andes. Once the full PIS developed to the west, it blocked this gap and created a lee-side effect that led to a reduction in snowfall over San Lorenzo. As a consequence, the Belgrano glacier was substantially smaller during the gLGM.

Availability of moisture and the role of continentality has been highlighted as an important factor contributing to an early local LGM and a pattern of successively smaller extent of mountain glaciers (Hughes and Gibbard, 2018; Gillespie and Molnar, 1995). For example, maximum glaciation of the mountain ranges in central Asia early in the glacial cycle was attributed to higher precipitation related to the strength and advection of the South Asian monsoon and/or westerlies (e.g. Röhringer et al., 2012; Dong et al., 2018; Zech, 2012; Owen et al., 2002; Finkel et al., 2003; Owen et al., 2003; Abramowski et al., 2006). Development of large northern hemisphere ice sheets would have affected atmospheric circulation and created lee side effects and precipitation starvation in other glaciated areas, thus

indirectly contributing to a pattern of successively smaller glaciation elsewhere that was asynchronous with the global ice volume (e.g. Thackray, 2001; Porter and Swanson, 2008; Svendsen et al., 2004; Zech et al., 2011b; Farquharson et al., 2018).

Antarctic stadials

On millennial time-scales, glacial advances in Patagonia and New Zealand have also been attributed to cooling in the southern mid-latitudes during Antarctic stadials (García et al., 2018; Kelley et al., 2014; Schaefer et al., 2015). An Antarctic millennial-scale climate signature across the southern mid-latitudes is likely an expression of antiphased interhemispheric coupling commonly attributed to the bipolar seesaw (Pedro et al., 2018; Stocker and Johnsen, 2003). Meridional oceanic heat transfer causes the Southern Ocean and Antarctica to cool during warm interstadial conditions in the North Atlantic region, and vice versa (Blunier, 2001; EPICA Community Members, 2006). Likely forced from the North Atlantic, the oceanic teleconnections are accompanied by an atmospheric reorganization (Markle et al., 2017; Buizert et al., 2018), which causes equatorward migration of the SWW during Antarctic stadials (Markle et al., 2017; Lamy, 2004; Buizert et al., 2018). Further, the Antarctic Circumpolar Current weakens (Lamy et al., 2015), and cold water masses are advected northward resulting in lower SST off Chile (Kaiser et al., 2005) and New Zealand (Barrows et al., 2007). Together this could promote glacier expansion in Patagonia and New Zealand.

Antarctic millennial-scale climate variations have been correlated across the southern mid-latitudes by a range of marine proxies (e.g. Barrows et al., 2007; Lamy, 2004; Caniupán et al., 2011). Southern high- to- mid latitude millennial-scale cooling evident in Antarctic ice-cores and several marine records might have also facilitated the glacial advance at our site at $\sim$ 75 ka. Cold stadial conditions at this time are evident in Antarctic ice cores following the prolonged A7 warm event (4.7 F; Blunier, 2001; EPICA Community Members, 2006. A Mg/Ca-based SST reconstruction from east of New Zealand indicates a temperature decrease towards $\sim$ 75 ka (45° S, Pahnke et al., 2003; Fig. 4.7 D). Although the resolution of exposure dating and associated geological uncertainties do not allow for precise correlations, it is reasonable to expect that mountain glaciers in the southern mid-latitudes responded to such cooling events.

Build-up of the Patagonian Ice Sheet and ice-divide migration

In the light of the above discussion, we propose a conceptual model of the build-up of the PIS (Fig. 4.8). The San Lorenzo massif and surrounding high topography (and present day NPI and SPI) likely acted as nucleation points for the ice sheet. Ice inception here allowed for the development of an independent ice cap at the time of reduced southern hemisphere insolation and higher moisture availability early in the glacial cycle. Growth of the San Lorenzo ice cap would have been

sustained by westerly precipitation that was able to reach the eastern massif through the gap in the Andes (Fig. 4.8 A). Later in the glacial cycle, the individual ice masses that were building up on high topography, including the San Lorenzo massif, the NPI and the SPI, coalesced to form a continuous ice sheet (Fig. 4.8 B). Approaching peak glacial conditions (Fig. 4.8 C), we expect the ice-divide migrated westward towards the precipitation source, and in the process caused re-organization of ice-drainage routes to focus ice flow into the major outlets of the PIS that surround the San Lorenzo and southern massifs (LP and SM). Furthermore, increasing the ice-sheet elevation and migrating the ice-divide would create an effective barrier to westerly precipitation, causing a reduction in snowfall reaching the San Lorenzo massif (cf. Sugden et al., 2002). The successively smaller glacial extent of the Belgrano glacier can therefore be explained by reduced moisture on the lee side of the PIS and ice-drainage re-organization as a consequence of ice-divide migration. This explains why the Belgrano glacier was relatively small at $\sim$ 25 ka, at a time when the major regional outlets of the PIS (LP and LBA) were at their local maximum (Hein et al., 2010, 2009; Kaplan et al., 2004).

4.7 Conclusion

Our ^{10}Be ages and geomorphological mapping demonstrate that the Belgrano glacier reached its maximum extent of the last glacial cycle at $\sim$ 75 ka towards the end of MIS 5. A second, substantially smaller advance occurred at $\sim$ 25 ka during the gLGM. The topographic setting prevented overprinting of the MIS 5 moraine record by later advances. We suggest that an independent ice cap developed over San Lorenzo early in the last glacial cycle, likely in response to reduced southern hemisphere summer insolation. Fostered by relatively high westerly precipitation, this led to the most extensive advance of the Belgrano glacier early in the last glacial cycle. Successively smaller ice extent at Lago Belgrano can be explained by snow starvation, ice-divide migration and ice-flow re-organization as the full PIS developed to the west of San Lorenzo. Our data provide first robust evidence for glaciation of the Patagonian Andes during MIS 5. However, more work is needed to elucidate the drivers of glaciation in Patagonia, from the onset early in the glacial cycle through to the full glacial conditions.

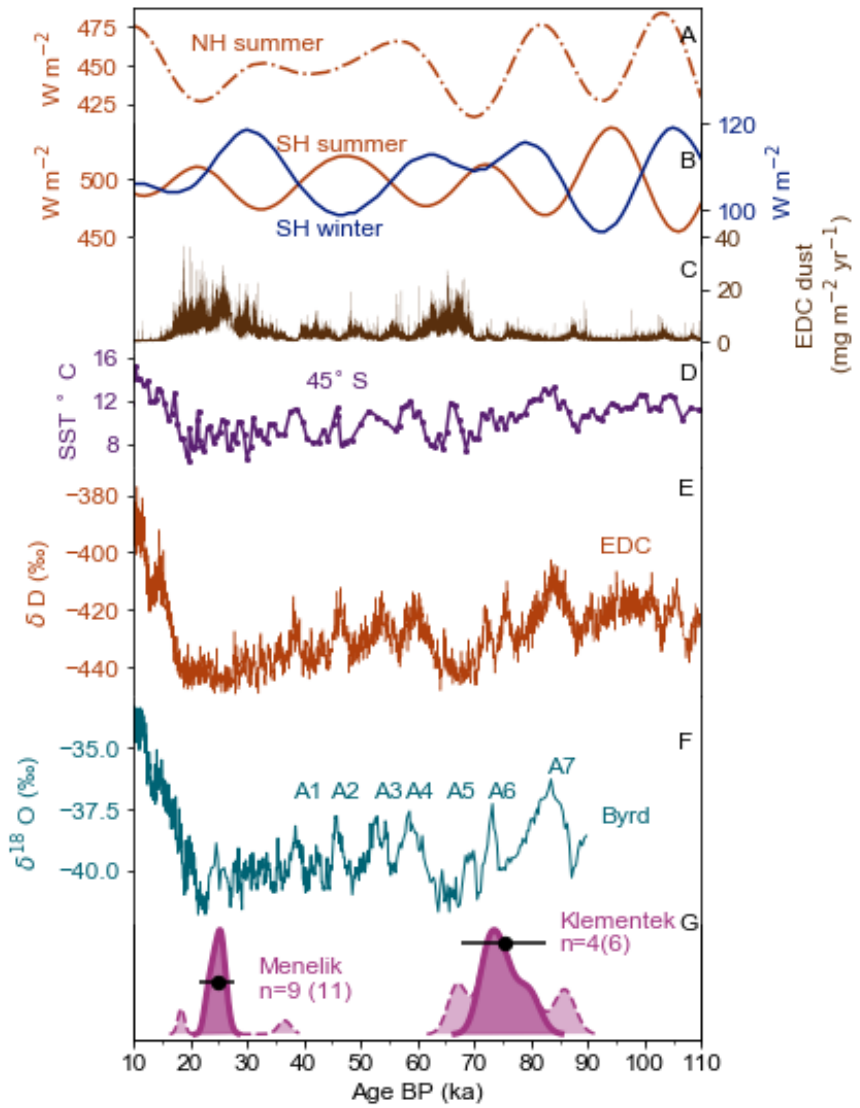

Figure 4.7: Comparison of our ^{10}Be ages and other proxies. A: July insolation intensity for $60°$ N (Berger and Loutre, 1991). B: July (orange) and December (blue) insolation intensity for $50°$ S (Berger and Loutre, 1991). C: EDC dust record (Lambert et al., 2012). D: SST (Mg/CA) record from off New Zealand (MD97-2120) (Pahnke et al., 2003). E: EDC deuterium record (EPICA Community Members, 2004) plotted on AICC2012 timescale (Veres et al., 2013). F: Oxygen isotope record from Byrd ice core (Johnsen et al., 1972) plotted on GISP2 timescale (Blunier, 2001). G: Summed probability density functions ('camelplots') for the Klementek outwash, and the Menelik boulders and outwash cobbles combined (plotted on individual y-axis; dashed curves represent outliers). Circles indicate the arithmetic means of the Klementek and Menelik ages (after outliers have been excluded) and error bars indicate uncertainty of the mean, which includes propagated individual internal uncertainties of the ^{10}Be ages and production rate uncertainty (Kaplan et al., 2011).

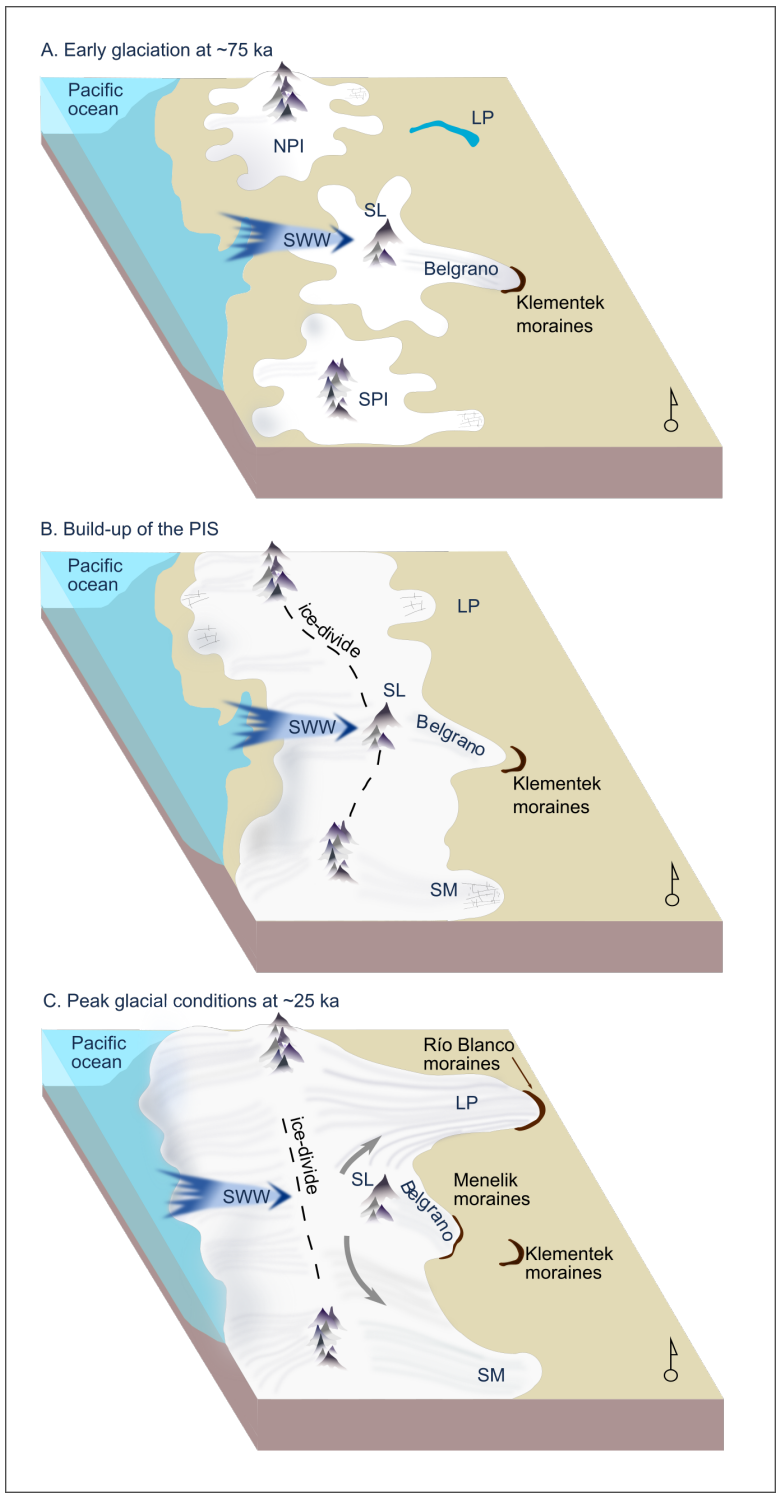
A. Early glaciation at ~75 ka
Pacific ocean
LP
NPI
SL
SWW
Belgrano
Klementek moraines
SPI
B. Build-up of the PIS
Pacific ocean
ice-divide
LP
SL
SWW
Belgrano
Klementek moraines
SM
C. Peak glacial conditions at ~25 ka
Pacific ocean
Río Blanco moraines
LP
ice-divide
SL
SWW
Belgrano
Menelik moraines
Klementek moraines
SM

Figure 4.8

Figure 4.8: A conceptual model of the build-up of the last Patagonian Ice Sheet (PIS). A) The initial inception of the Patagonian Ice Sheet begins with nucleation centres over the present day North and South Patagonian Icefields (NPI, SPI), and the San Lorenzo massif (SL), likely triggered by reduced summer insolation in the southern hemisphere. At this time, the Southern Westerly Winds (SWW) can freely penetrate through the topographic depression between the present icefields to bring snowfall east to the San Lorenzo ice cap. Ice expansion is greatest down the high-elevation eastern Belgrano valley, since glaciers draining to the south, west and north of the massif descended into deep valleys. B) The individual ice masses coalesce, causing reorganization of ice (and fluvial) drainage routes, and reducing ice flux down the Belgrano valley. C) Under peak glacial conditions, the ice-divide increased in elevation, and migrated westward towards the precipitation source. This caused snow starvation to the San Lorenzo massif, and significant re-organization of ice-drainage routes to focus ice flow into the major outlets of the Patagonian Ice Sheet that surround the San Lorenzo massif (LP and SM). These processes limited ice expansion in the Belgrano valley when the major outlet to its north, LP (and also LBA, which is not shown) was near its maximum last glacial extent indicated by the Río Blanco moraines (Hein et al., 2010).

Chapter 5

Glacier advance in central Patagonia during the Antarctic Cold Reversal followed by retreat and stabilisation during the Younger Dryas



Abstract

The spatial-temporal footprint of millennial-scale climate events during the last glacial-interglacial transition can yield insights into the underlying drivers of climate change, but remains poorly resolved in Patagonia. Here, we assess the glacier response to abrupt cold events and palaeolake evolution using geomorphological mapping along with ^{10}Be ages and optically stimulated luminescence ages from near Lago Belgrano (47.9° S) on the eastern side of Monte San Lorenzo. The former Belgrano glacier was sustained by a climatically sensitive ice cap, making the site ideal for investigating the glacier response to abrupt cold reversals. Our data reveal an extensive re-advance at 13.1 ± 0.6 ka, consistent with cooling and increased precipitation during the Antarctic Cold Reversal (ACR). Subsequently, ice retreated by at least 10 km and created an ice-dammed proglacial lake in the Belgrano valley. Rapid recession was punctuated by smaller advances/still-stands sufficient to maintain an ice-dam for the palaeolake and deposit a lateral moraine dated at 12.4 ± 0.3 ka during the Younger Dryas (YD). The final withdrawal of glaciers to the mountains allowed the palaeolake to drain and resulted in an Atlantic/Pacific drainage reversal. This marks the final separation of the Patagonian Ice Sheet into the individual ice fields at the YD-Holocene transition. Our data demonstrate the dominant ACR climate signal in central Patagonia, but also reveals a co-occurrence of the northern hemisphere YD signal, albeit of smaller magnitude. The ACR re-advance was primarily climatically controlled, but its relative magnitude was likely a consequence of ice divide migration and ice flow re-routing during the break-up of the Patagonian Ice Sheet.

5.1 Introduction

The last glacial-interglacial transition (LGIT, 18 - 11 ka) was characterized by the demise of ice-sheets, reorganization of the atmospheric and oceanic systems accompanied by increasing atmospheric CO^2, and millennial-scale warm/cold events (Denton et al., 2010). The interhemispheric phasing of climate change during this period has generated much debate, in particular the occurrence of the Antarctic Cold Reversal (ACR; ∼ 14.6 - 12.8 ka, Lemieux-Dudon et al., 2010) and the northern hemisphere Younger Dryas (YD; ∼ 12.9 - 11.7 ka; Blunier et al., 1998) climate signals in the southern hemisphere (e.g. Denton et al., 1999a; Sugden et al., 2005; McCulloch et al., 2005a; Putnam et al., 2010a; Glasser et al., 2012). The relative magnitude and the spatial-temporal footprint of these abrupt events can yield insights into the processes involved in initiation and propagation of climate change, but remains poorly resolved in Patagonia.

Patagonia is well-situated for studying this as it intersects the Southern Westerly Winds (SWW), which modulate the global carbon cycle, exert a strong influence on Southern Ocean circulation, and which played an important role in

the LGIT by controlling atmospheric CO^2 (Lamy et al., 2007; Toggweiler et al., 2006a; Anderson et al., 2009; Marshall and Speer, 2012). The global climate models predict a poleward shift and strengthening of the SWW in the future, yet also show considerable spatial variability in the magnitude of the strength and position change (Meijers, 2014). Better constraining the timing and magnitude of past glacier fluctuations along latitudinal gradients in the southern mid-latitudes can help to improve our understanding of past climate change, including the role of the SWW, and can help to improve projections of future climate change. Further, examining the consequences of the past rapid climate events on the terrestrial environments, including the cryospheric component, is important for contextualizing present and future climate change in the region.

In Patagonia, the ACR signal is well-documented south of 50° S by both glacier chronologies and palaeovegetation records, which reveal glacier advances and cooling coeval with the ACR (Mansilla et al., 2016; Moreno et al., 2012; Björck et al., 2012; García et al., 2012; Moreno et al., 2009; Fogwill and Kubik, 2005; Strelin et al., 2011; Kaplan et al., 2011; Ackert et al., 2008; Sugden et al., 2005; McCulloch et al., 2005a). Here, subsequent ice retreat and warming was interrupted by stabilisation of glaciers during the YD (Kaplan et al., 2011; Moreno et al., 2009). North of 50° S, the glacier response to climate during the LGIT remains poorly resolved. Glacier advances/still-stands during the ACR (Sagredo et al., 2018; Davies et al., 2018; Nimick et al., 2016) as well as YD (Sagredo et al., 2018; Glasser et al., 2012; Nimick et al., 2016) have been reported east of the Northern Patagonian Icefield and on the north-western flanks of Monte San Lorenzo. Many of these glaciers calved into a large regional palaeolake during most of the LGIT (Davies et al., 2018; Thorndycraft et al., 2019), and this process together with topographic pinning points on the ice bed likely exerted a strong influence on their dynamics and response to cold reversals (Davies et al., 2018). In addition, many exposure ages from moraine boulders previously interpreted as dating YD advances (Glasser et al., 2012), are considered erroneously young as a consequence of their submergence in a palaeolake (Thorndycraft et al., 2019). In some cases, the relationship between the dated moraines (e.g. Nimick et al., 2016) and palaeolakes remains unclear. Where YD moraines have been dated, they are based on a limited number of exposure ages (≤ 2) (Sagredo et al., 2018; Glasser et al., 2012). Thus, firm dating of YD ice limits has not yet been achieved.

Terrestrial palaeovegetation proxies from central Patagonia (49° S - 44° S) either: (i) do not document any clear changes from which an ACR or YD signal can be inferred (Haberle and Bennett, 2004; Bennett et al., 2000; Lumley and Switsur, 1993; Markgraf et al., 2007; de Porras et al., 2014, 2012; Iglesias et al., 2016), or (ii) suggest persistence of cold/cool and wet conditions from about 16 ka to 11.8 ka (Villa-Martínez et al., 2012). Only one terrestrial record so far suggests increased precipitation coeval with the ACR, based on an increase of cold-resistant hygrophilous taxa between 14 ka and 13.5 ka (Henríquez et al., 2017). This is supported by pollen analysis on a marine core recovered from offshore of Chile

(46° S; MD07-3088, Montade et al., 2013). The absence of the ACR and/or YD signal in many records might be masked by high climate variability during the LGIT , combined with the effects of local climate and/or insensitivity of proxies to minor cooling (Markgraf et al., 2007; Villa-Martínez et al., 2012; Mendelova et al., 2017).

The aim of this study is to assess the glacier response to cold reversals during the LGIT in the Belgrano and Lacteo valleys on the eastern side of Monte San Lorenzo. We selected this site because the relatively small San Lorenzo ice cap would have been more sensitive to climate change than the larger Patagonian icefields. At its maximum extent during the LGIT, the former Belgrano glacier had a land-terminating margin rather than a calving margin, and thus glacier fluctuations here are more likely to reflect changes in climate. These characteristics make the site ideal for investigating the regions glacier response to abrupt millennial-scale cooling events during the LGIT. We use geomorphological mapping, cosmogenic ^{10}Be surface exposure dating and optically-stimulated luminescence (OSL) analysis to determine the timing of 1) major glacier re-advances/stillstands during the LGIT, and 2) the formation and evolution of palaeolakes in the valleys. Our mapping and chronology gives insight on the processes involved in the break-up of the former Patagonian Ice Sheet (PIS) and rates of deglaciation.

5.2 Study area and previous work

5.2.1 Physical setting

Monte San Lorenzo (3706 m, Chilean name: Monte Cochrane) is an isolated massif located $\sim$ 80 km east of the main spine of the Patagonian Andes (Figs. 5.1 and 5.2). At this latitude, the main chain of the Andes exhibits a tectonic depression, which separates Monte San Lorenzo massif from the Pacific coast, and the Northern Patagonian Icefield from the Southern Patagonian Icefield. The Lago Belgrano valley is a relatively small, low gradient, high elevation valley at over 850 m asl. This contrasts with the large over-deepened basins to the north and south (e.g. Lago Pueyrredón, 150 m) that have been eroded to below sea level (Murdie et al., 1998). The low gradient Belgrano valley also contrasts with mountain valleys on the northern and western flanks of Monte San Lorenzo, which have steeper elevation profiles as they descend to low elevations ($\sim$ 500 - 200 m asl) within tens of km of the mountain. San Lorenzo is part of the Patagonian Batholith intrusion (Ramos and Kay, 1992; Ramírez de Arellano et al., 2012), and is the main source of granitic erratics that are found in the Belgrano valley.

The precipitation-bearing SWW have a dominant influence on climate and sustain the present day ice-fields and glaciers. Westerly precipitation can reach 5,000 - 10,000 mm a^{-1} on the western side of the Andes and falls to less than 300 mm a^{-1} tens of km downwind of the mountain front (Garreaud et al., 2013).

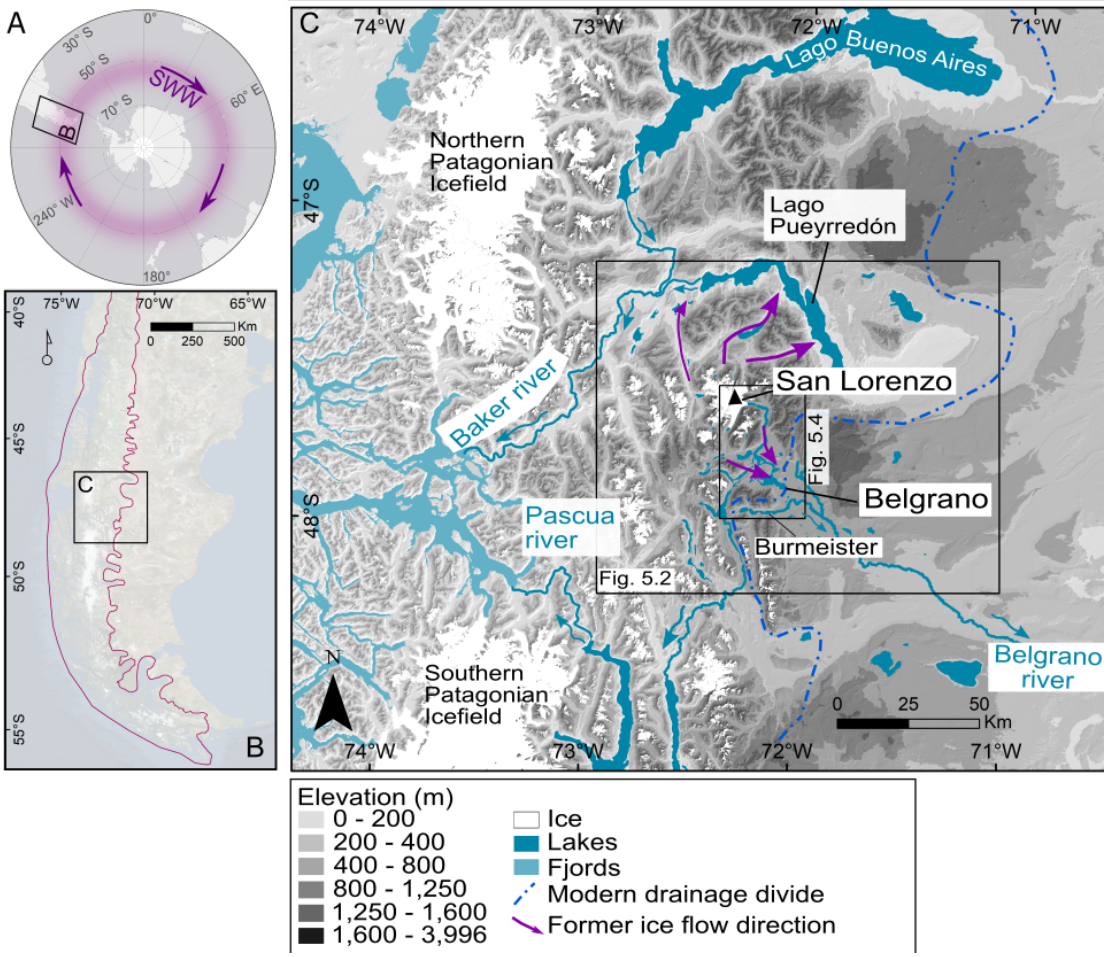

Figure 5.1: A) Location of Patagonia in the southern hemisphere with approximate location of the Southern Westerly Winds. B) Location of the study area in Patagonia, with an approximate extent of the PIS at the global Last Glacial Maximum (pink line). Image: ESRI World Imagery. C) Map of central Patagonia showing contemporary ice fields and ice caps (outlines were downloaded from the GLIMS database (Falaschi et al., 2017; De Angelis et al., 2015)), modern drainage divide and location of Monte San Lorenzo and Lago Belgrano valley. Magenta arrows indicate former ice discharge routes from the San Lorenzo. Basemap: SRTM DEM.

As a consequence of the topographic depression, the Monte San Lorenzo massif is the first orographic barrier to the SWW, and has a transitional maritime to continental climate (Falaschi et al., 2013).

The San Lorenzo massif sustains four valley glaciers and several smaller ice bodies covering a total area of $\sim$ 139 km^2 (Falaschi et al., 2013). The snowline is estimated to be $\sim$ 1700 - 1750 m a.s.l on the western side and about 100 m higher on the eastern side of the massif (Falaschi et al., 2013). All glaciers of the San Lorenzo massif and Lago Belgrano drain westward to the Pacific Ocean via rivers, which exploit the gap in the mountain chain (Fig. 5.2). The drainage divide is located east of Lago Belgrano, and Lago Burmeister ($\sim$ 900 m asl; Fig. 5.2) is over the divide and instead drains eastward to the Atlantic Ocean via the Río Belgrano. During glacial cycles, the build-up of ice along the Andean mountain chain blocked Pacific drainage pathways, causing large-scale drainage reversals. The break-up of the Patagonian Ice Sheet is thus associated with large-scale drainage reversals across many parts of Patagonia (Caldenius, 1932; Turner et al., 2005; Thorndycraft et al., 2019).

5.2.2 Previous work

During full glacial conditions, the San Lorenzo ice cap coalesced with the larger PIS (Caldenius, 1932; Wenzens, 2005; Glasser et al., 2005; Mendelová et al., 2020b). Ice from the San Lorenzo centre discharged northwards to join the Lago Pueyrredón outlet glacier and south-eastwards into the Belgrano valley (Fig. 5.1 C; Wenzens, 2002). The Belgrano glacier had additional ice contribution from accumulation areas on the mountains to the west and south of Lago Belgrano.

Following disintegration of the Lago Pueyrredón lobe, ice on the northern and western flanks of San Lorenzo was largely confined to the mountain valleys (Davies et al., 2018; Martin et al., 2019; Sagredo et al., 2018). Here, advances of the Tranquilo and Calluqueo glaciers were dated at 13.8 $\pm$ 0.5 ka and 13.2 $\pm$ 0.2 ka, respectively, coeval with the ACR (Fig. 5.2; Sagredo et al., 2018; Davies et al., 2018). At this time, the Calluqueo glacier calved into a palaeolake, and part of the moraine was subaqueous (Davies et al., 2018). YD stabilisation is suggested by a couple of exposure ages from inset moraines in both valleys (Fig 5.2; 12.5 $\pm$ 0.4 and 11.6 $\pm$ 0.4 ka in the Tranquilo valley (Sagredo et al., 2018), and 12.9 $\pm$ 0.8 and 12.0 $\pm$ 0.5 in the Salto valley (Glasser et al., 2012)).

The Belgrano glacier reached its full last glacial extent at 75.0 $\pm$ 2.8 ka based on ^{10}Be exposure ages from outwash cobbles (Fig. 5.2; Mendelová et al., 2020b). This early maximum suggests that an independent ice mass developed on San Lorenzo early in the last glacial cycle toward the end of MIS 5. A second major advance deposited the Menelik moraines dated using ^{10}Be ages at 24.7 $\pm$ 1.0 ka (Fig. 5.2; Mendelová et al., 2020b), coeval with the global Last Glacial Maximum (gLGM).

The Late Glacial history at Lago Belgrano is only constrained by two minimum radiocarbon ages of 12.6 $\pm$ 0.06 cal ka BP and 9.5 $\pm$ 0.04 cal ka BP (Wenzens,

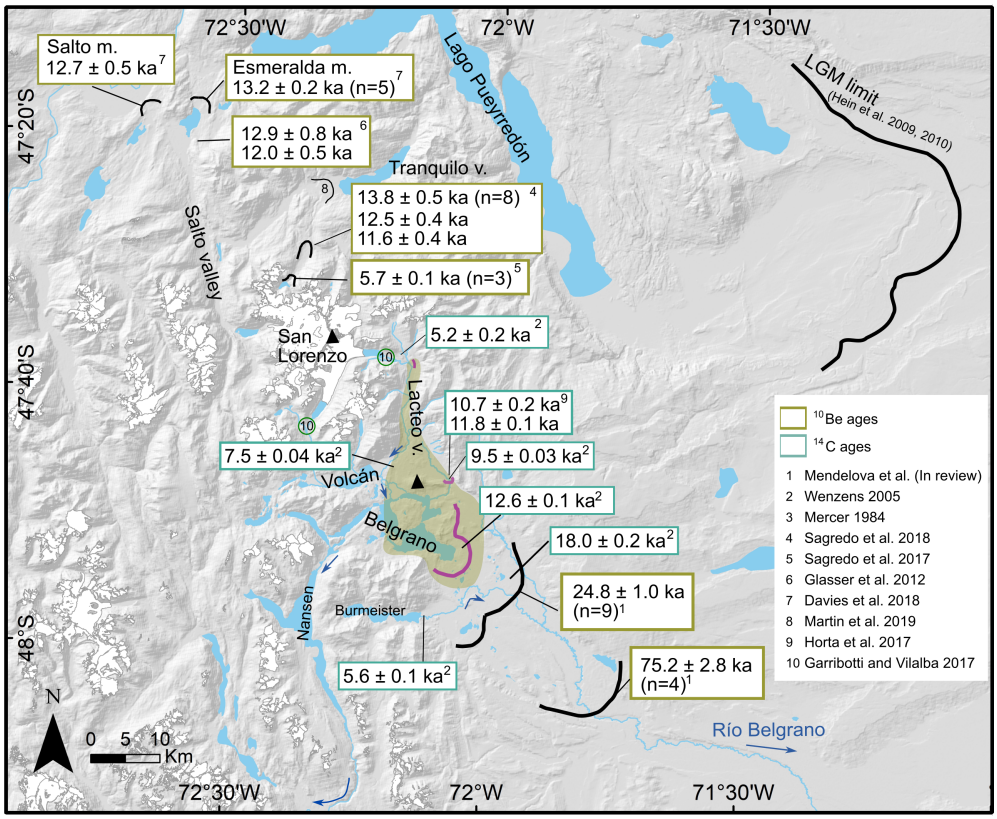

Figure 5.2: Map showing Monte San Lorenzo, Lago Belgrano and Lacteo valleys, along with published chronologies (black curves indicate dated ice margins). Where more than 2 ages exist for a landform, uncertainty-weighted means with 1 σ standard deviation are presented. Otherwise, individual ages are given with 1 σ uncertainty (internal in case of ^{10}Be ages). Green shading indicates our study area, and ice margins dated in this study are highlighted in pink. Glacier outlines were downloaded from the GLIMS database (Falaschi et al., 2017; De Angelis et al., 2015). River drainage directions are indicated with blue arrows.

2005; Fig. 5.2). With the exception of the Tranquilo valley, where Sagredo et al. (2018) dated an advance to 5.7 ka ± 0.1 ka using ^{10}Be, our knowledge of the Holocene dynamics of the San Lorenzo glaciers is limited to minimum radiocarbon ages and lichenometry (Garibotti and Villalba, 2017; Mercer, 1984; Wenzens, 2005). In the Lacteo valley (Fig. 5.2), Wenzens (2005) obtained an age of 7.5 ± 0.04 cal ka BP from a kettle hole, and further up valley, Mercer (1984) obtained a maximum age of 5.2 ± 0.2 cal ka BP from an overridden tree incorporated within a moraine 5 km from the present day margin of the Lacteo glacier. Wenzens (2005) obtained a minimum age of 5.6 ± 0.06 cal ka BP from a kettle hole within the moraines bounding Lago Burmeister (Fig 5.2). Horta et al. (2017) proposed a palaeolake in the Belgrano valley at 900 - 920 m a.s.l. between

11.7 and 10.8 ka on the basis of two radiocarbon ages from lacustrine deposits (Fig 5.2).

Geomorphological mapping of the valleys on the eastern side of Monte San Lorenzo along with a robust chronology will allow us to assess the response of this small ice cap to climate fluctuations during the ACR and YD, and will provide insight on the overall pattern and rate of deglaciation.

5.3 Methods

In this study, we focus on a moraine system that bounds the eastern end of Lago Belgrano, here informally named the Belgrano moraine system, and the area to the north, including the Lacteo valley (Figs. 5.2 and 5.4). The two older moraine systems in the Belgrano valley (Fig. 5.2) and associated chronologies are described by Mendelová et al. (2020b).

Geomorphological mapping was done from high resolution optical satellite imagery (2.5 m to sub-meter) distributed by the ESRI^{TM} World Imagery service, 10 m Sentinel-2 imagery and Google Earth. ALOS PALSAR (12.5 m) and Shuttle Radar Topography Mission (30 m) digital elevation models were used to aid landform identification. Geomorphological features were mapped following established criteria (e.g. Glasser et al., 2008; Darvill et al., 2014; Bendle et al., 2017b; Martin et al., 2019). Mapping was field-checked during two field campaigns in 2016 and 2018. Published ^{10}Be ages from Patagonia described in this paper were recalculated using the protocol outlined in section 4.4.3, and ages are presented as uncertainty (internal) weighted means with 1 σ standard deviation per moraine. Published radiocarbon ages (Table 2.1) were re-calibrated using the OxCal online calibration program (version 4.3; Bronk Ramsey, 2009) and the southern hemisphere calibration curve (SHCal13, Hogg et al., 2013). The calibrated median ages (95.4 % confidence interval) are presented as "cal. ka BP", rounded to the nearest 100 a.

5.3.1 Surface exposure dating

Sampling

For cosmogenic nuclide analysis, we collected samples from the top centre of large boulders embedded in the moraine crests using hammer and chisel (Gosse and Phillips, 2001; Darvill, 2013). We targeted granitic boulders that showed minimal surface erosion, and appeared stable. We sampled four to six boulders per moraine limit (cf. Putkonen and Swanson, 2003). Three samples were collected from boulders and cobbles deposited atop bedrock outcrops along a transect in the Lacteo valley to date deglaciation of the valley. Additionally, we collected two surface samples from beach gravels on former shorelines. The shoreline samples consisted of an amalgamation of 30-40 quartz-rich pebbles (2-4 cm).

Sample locations were recorded with a handheld Garmin GPS with a reported accuracy of 3 - 5 m. Topographic shielding was measured in the field using a compass and clinometer, and shoreline altitudes were cross-checked with a barometric altimeter. Sample details are presented in Table 2 and sample locations are shown in Figure 5.4.

The samples were crushed whole, except sample RV1609, which was cut horizontally to reduce its thickness. Subsequently, the samples were sieved to obtain the sand fraction and then prepared as ^{10}Be AMS targets at two different cosmogenic nuclide laboratories: the Natural Environment Research Council's Cosmogenic Isotope Analysis Facility (NERC-CIAF), and the University of Edinburgh's Cosmogenic Nuclide Laboratory. All Accelerator Mass Spectrometry (AMS) measurements were conducted at the Scottish Universities Environmental Research Centre (SUERC) AMS Facility. Sample preparation for cosmogenic nuclide analysis is described in Mendelová et al. (2020b).

Age calculations

^{10}Be ages were calculated using the online exposure age calculator described by Balco et al. (2008), version 3, with a local ^{10}Be production rate for Patagonia (Kaplan et al., 2011), derived from the ICE-D online database (`http://calibration.ice-d.org/`). Ages presented here (Table 5.3) use the time-dependent Lm scaling scheme of Lal (1991) modified by Stone (2000). The ages decrease by 0.5 % if calculated using the New Zealand production rate of Putnam et al. (2010b) and decrease by 6% with the global production rate of Borchers et al. (2016). Summary statistics for each moraine are given in Table 5.4. We base our discussion on the uncertainty-weighted means and 1 σ standard deviation.

No correction is applied for shielding by vegetation or snow because the moraines are sparsely vegetated by grasses with the exception of some Nothofagus trees scattered on the lateral moraines in the Lacteo valley. Given high winds and low precipitation, we expect the snow cover to be minimal and short-lived in the Belgrano valley. Closer to the mountain front, snow cover would be more persistent, but boulders perched on moraines are likely to sit above the snowpack where they can be blown free of snow. Exposure ages assume zero erosion, although rates of 0.2 mm ka^{-1} have been estimated nearby (Hein et al., 2017; Douglass et al., 2007). Including this rate would increase ages by less than 1%, which is within analytical uncertainties.

The moraine boulder ages are interpreted to date moraine stabilisation following ice withdrawal, and thus the ages provide a minimum age for the ice advance. The cosmogenic nuclide ages are considered minimum ages, given the potential for post-depositional processes (e.g. erosion and exhumation of boulders) that could affect surface exposure. That said, we acknowledge inheritance could interfere with this assumption, and this is discussed explicitly.

The exposure ages from shorelines are interpreted to date the abandonment (stabilisation) of the shoreline, and therefore dropping of the lake level. We

Table 5.1: Sample details and nuclide concentrations

Sample ID	Latitude (DD)	Longitude (DD)	Elevation (m)	Sample type	Boulder height (cm)	Thickness (cm)	Shielding correction	Quartz dissolved (g)	^{10}Be atoms g^{-1}	± 1σ atoms g^{-1}	^{10}Be/^{9}Be ratio	± 1σ	AMS ID	Laboratory facility
Belgrano inner moraines														
LB1601	-47.8735	-72.05325	900	b	140	5	0.99949	16.94	1.18E+05	3.92E+03	1.24E-13	3.74E-15	b10564	CIAF
LB1603	-47.8699	-72.04876	903	b	91	3	0.99974	22.12	1.08E+05	3.33E+03	1.47E-13	4.21E-15	b10565	CIAF
LB1604	-47.8699	-72.04883	898	b	130	2	0.99974	23.47	1.22E+05	3.68E+03	1.76E-13	5.02E-15	b10566	CIAF
LB1605	-47.8748	-72.04993	906	b	163	2.5	0.99970	14.13	1.16E+05	3.63E+03	1.12E-13	3.01E-15	b10539	CIAF
Belgrano outer moraines														
LB1608	-47.8816	-72.0336	902	b	88	2	0.99965	13.24	1.10E+05	3.78E+03	1.01E-13	2.93E-15	b10540	CIAF
LB1609	-47.8803	-72.0336	905	b	50	3	0.99958	19.11	1.20E+05	3.66E+03	1.43E-13	3.99E-15	b10567	CIAF
LB1610	-47.8763	-72.03358	901	b	60	2	0.99989	11.12	1.17E+05	3.97E+03	8.98E-14	2.46E-15	b10541	CIAF
LB1611	-47.8755	-72.03368	902	b	65	1.5	0.99992	15.09	1.11E+05	3.80E+03	1.04E-13	3.12E-15	b10542	CIAF
Rincon moraines														
RV1601	-47.7836	-72.06461	953	b	170	2	0.99618	22.06	1.22E+05	3.22E+03	1.65E-13	4.05E-15	b10575	CIAF
RV1602	-47.7833	-72.06385	969	b	66	3	0.99504	23.35	1.13E+05	3.42E+03	1.62E-13	4.58E-15	b10576	CIAF
RV1603	-47.7816	-72.0677	963	b	160	3	0.99382	10.71	1.47E+05	4.83E+03	1.08E-13	3.04E-15	b10553	CIAF
RV1623	-47.7843	-72.07035	958	b		4.5	0.99817	22.83	1.19E+05	3.57E+03	1.68E-13	4.72E-15	b10587	CIAF
Lacteo lateral moraines														
RV1617	-47.6269	-72.15348	1067	b	66	5	0.99597	9.03	1.39E+05	5.55E+03	8.73E-14	2.93E-15	b10559	CIAF
RV1618	-47.6269	-72.15341	1072	b	18	5	0.99597	15.80	1.17E+05	3.78E+03	1.15E-13	3.32E-15	b10581	CIAF
RV1619	-47.6275	-72.15311	1059	b	35	3.5	0.99368	17.30	1.25E+05	4.00E+03	1.34E-13	3.93E-15	b10582	CIAF
RV1620	-47.6275	-72.15312	1061	b	30	3.5	0.99368	11.35	1.24E+05	6.69E+03	9.74E-14	4.80E-15	b10560	CIAF
RV1621	-47.6281	-72.15319	1053	b	58	3	0.99493	18.14	1.21E+05	3.94E+03	1.36E-13	4.07E-15	b10583	CIAF
RV1622	-47.6285	-72.15322	1075	b	48	2.5	0.99493	19.67	1.47E+05	4.02E+03	1.79E-13	4.58E-15	b10584	CIAF
Bedrock outcrop transect														
RV1606	-47.7266	-72.14829	986	c	-	6.5	0.99730	23.54	9.06E+04	2.77E+03	1.32E-13	3.65E-15	b10577	CIAF
RV1608	-47.7519	-72.12057	954	b	47	4	0.99848	6.08	2.24E+05	7.57E+03	9.40E-14	2.61E-15	b10554	CIAF
RV1609	-47.6877	-72.16423	1014	c	-	4.5	0.99257	5.56	1.09E+05	5.92E+03	4.38E-14	1.49E-15	b10555	CIAF
Shorelines														
BSH181	-47.8143	-72.07198	882	a	-	2.5	0.99802	23.61	1.07E+05	3.32E+03	1.56E-13	4.63E-15	b11143	Edin
BSH183	-47.8326	-72.10655	885	a	-	2.5	0.99963	23.18	9.51E+04	3.04E+03	1.37E-13	4.16E-15	b11144	Edin

Rock density is assumed to be 2.7 g cm^{-3}. Reported thickness of the samples is after cutting, where necessary.
Sample type: b – boulder, c – cobble, a – amalgamated pebbles.
Concentrations were corrected for process blanks; blank corrections ranged between 1 and 7 % of the sample ^{10}Be/^{9}Be ratios. The uncertainty of the blank correction is included in the stated 1σ uncertainties.
Measurements were normalised to NIST SRM4325 with nominal ^{10}Be/^{9}Be ratios of 2.79x10^{-11} and half-life of 1.36 Ma (Nishiizumi et al., 2007).
All measurements were made at the AMS facility at SUERC.

assume that wave action cuts into existing sediment and subjects individual clasts to surface erosion such that inheritance is negligible. This assumption is, however, difficult to test without several samples from each shoreline. Our approach of amalgamating many surface clasts should go some way toward minimising the influence of inheritance on the final ^{10}Be concentration of the sample.

5.3.2 OSL dating

We collected two samples for OSL dating from laminated silt and sand sediments interpreted as glaciolacustrine deposits. OSL dating determines when mineral grains were last exposed to sunlight prior to burial. We interpret the ages to date the deposition of glaciolacustrine sediments, and they should therefore give a minimum age for the development of a palaeolake.

Samples for luminescence dating were collected in opaque tubes and prepared for analysis under subdued lighting conditions. To calculate the environmental dose-rate throughout burial for each sample, U, Th and K concentrations were measured for $\sim$ 80 g of the bulk sediment sample using high-resolution gamma spectrometry. Water contents of 5 $\pm$ 2 % were estimated considering the field water contents, and the environmental history for each sample. Cosmic dose-rates were calculated after Prescott and Hutton (1994). Environmental dose-rates determined for samples RV1801 and LBSH1801 are shown in Table S1. Grains of K-feldspar were used to determine equivalent doses (D_e). Samples were first treated with a 10 % v/v dilution of 37 % HCl and with 20 % v/v of H_2O_2 to remove carbonates and organics, respectively. Dry sieving then isolated the 125 - 180 μm (sample LBSH1801) or 212 - 250 μm (sample RV1801) diameter grains, which were subject to density separation using sodium polytungstate ($<$ 2.58 g cm^{-3} K-feldspar dominated) and then etched using hydrofluoric acid. Finally, grains of K-feldspar were mounted on a 9.8 mm diameter aluminium single-grain disc for analysis, which contained a 10 by 10 grid of 300 μm diameter holes. Note that sample LBSH01-01 was analysed using microhole analysis rather than single grains (i.e. up to four grains in each hole due to a grain size of 125 - 180 μm).

All luminescence measurements were performed using a Risø TL/OSL DA-15 automated single-grain system equipped with a ^{90}Sr/^{90}Y beta source (Bøtter-Jensen et al., 2003) fitted with a blue filter pack (BG39, Coring 7-59) in front of the photomultiplier tube. Single aliquot regenerative dose (SAR) protocols (Murray and Wintle, 2000) were used for the post-IR IRSL analyses performed at 225 $^{\circ}C$ (Thomsen et al., 2008), termed the pIRIR$_{225}$ signal. A preheat temperature of 250 $^{\circ}C$ for 60 s was used prior to stimulations of 2 s using the infra-red laser at 225 $^{\circ}C$. The IRSL signal measured performed at 50 $^{\circ}C$ prior to the pIRIR$_{225}$ measurement and the elevated temperature bleach of 330 $^{\circ}C$ for 200 s at the end of each L_x/T_x cycle were performed using the IR LEDs. The location of the single-grain discs was performed at room temperature, rather than elevated temperatures to prevent thermal annealing of the IRSL signal (after Smedley and Duller, 2013). The first 0.3 s and final 0.6 s of stimulation were summed

to calculate the initial and background IRSL signals, respectively. The grains were accepted after applying the following screening criteria and accounting for the associated uncertainties: (1) whether the test dose response was greater than three sigma above the background, (2) whether the test dose uncertainty was less than 10 %, (3) whether the recycling and OSL-IR depletion ratios were within the range of ratios 0.9 to 1.1, and (4) whether recuperation was less than 5 % of the response from the largest regenerative dose.

Grains from both samples were used for dose-recovery experiments and successfully recovered a given dose within 10 % using the $pIRIR_{225}$ signal. Fading experiments were performed on three multi-grain aliquots per sample and reported g-values of -0.4 ± 0.7 %/decade (RV18-01) and -1.0 ± 0.7 %/decade (LBSH18-01), which suggests that no fading correction was required for the $pIRIR_{225}$ signal. D_e values were calculated from all grains passing all the screening criteria. The minimum age model (MAM; (Galbraith et al., 1999; Galbraith and Laslett, 1993)) was applied to determine an age for the samples as the asymmetrical D_e distributions suggested the samples were partially bleached prior to burial (Fig. 5.3). The scatter in the D_e distribution arising from intrinsic and extrinsic sources were combined in quadrature to determine σb for the MAM (Table 5.2). The overdispersion values arising from intrinsic sources for sample RV1801 (12 %) and LBSH18-01 (13 %) were derived from the dose-recovery experiments, while the over-dispersion arising from variability in the internal dose-rates of K-feldspar grains for both samples was assumed to be 10 % (after Smedley and Pearce, 2016). Additional over-dispersion (20 %) was incorporated for sample RV1801 to account for the variability in single-grain D_e distributions caused by external microdosimetry (after Smedley et al., 2017). The D_e values were then divided by the environmental dose-rates to determine an age for each sample (Table 5.2).

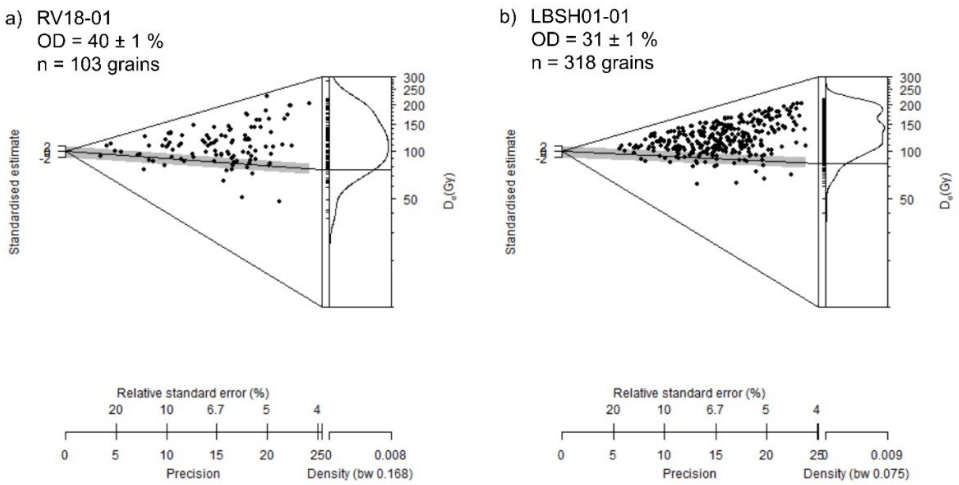

Figure 5.3: Abanico plots of the D_e values determined for OSL dating, where the grey shading shows the MAM D_e for each distribution. Note that sample LBSH0101 was analysed using microhole analysis rather than single grains (i.e. up to four grains in each hole due to a grain size of 125 180 μm) but it is likely that the OSL signal was dominated by one brighter grain.

Table 5.2: Luminescence dating results

Sample	Grain size (m)	U (ppm)	Th (ppm)	K (%)	Internal dose-rate (Gy/ka)	External alpha dose-rate (Gy/ka)	External beta dose-rate (Gy/ka)	External gamma dose-rate (Gy/ka)
RV1801	212-250	5.2 ± 0.4	22.3±0.4	2.6±0.4	0.97±0.15	0.30±0.05	2.84±0.27	2.17±0.11
LBSH1801	125-180	5.3±0.4	20.7±0.4	2.8±0.4	0.70±0.13	0.44±0.09	3.11±0.30	2.16±0.11
Sample	Cosmic dose-rate (Gy/ka)	Total dose-rate (Gy/ka)	g-value (%/dec.)	n/N	OD (%)	MAM De (Gy)	Age (ka)	
RV1801	0.28±0.03	6.59±0.35	-0.4±0.7	103/600	40±0	76.7±6.1	11.6±1.1	
LBSH1801	0.28±0.03	6.68±0.36	-1.0±0.7	318/1000	31±1	85.1±1.8	12.7±0.7	

Environmental dose-rates were determined using high-resolution gamma spectrometry. The dose-rates were calculated using the conversion factors of Guérin et al. (2011) and alpha (Bell, 1980) and beta (Guérin et al., 2012) dose-rate attenuation factors. Water contents (5 ± 2 %) were estimated considering the field and saturated water contents, and the environmental history for each sample; these values are expressed as a percentage of the mass of dry sediment. An internal K-content of 10 ± 2 % (Smedley et al., 2012) and internal U and Th concentrations of 0.3 ± 0.1 ppm and 1.7 ± 0.4 ppm (Smedley and Pearce, 2016) were used to determine the internal dose-rates. An a-value of 0.10 ± 0.02 (Balescu and Lamothe, 1993) was used to calculate the alpha dose-rates. Cosmic dose-rates were determined after Prescott and Hutton (1994). Dose-rates were calculated using the Dose Rate and Age Calculator (DRAC; Durcan et al., 2015. G-values (%/decade) were measured using the $pIRIR_{225}$ signal for three aliquots of K-feldspar for each sample, normalised to 2 days and are presented as weighted means and standard errors. The number of grains that were used to determine a D_e value (n) are shown as a proportion of the total grains measured (N).

5.4 Results

5.4.1 Geomorphology

The Belgrano moraine system (Figs. 5.5 and 5.6) is comprised of up to 10 arcuate moraine ridges with undulating crests. The outermost moraine ridge is subdued at 3 m height and a slope of 5°. The morphology of this moraine ridge may indicate that the glacier occupied this position for a shorter time or the moraine ridge degraded post-deposition. The next two moraine ridges are the most prominent and continuous with about 10 m in height and slopes up to 22°. Inboard of these the moraines appear more hummocky with occasional inter-morainic depressions. The inner moraine ridges are again distinct with 10 m in relief. The moraines are vegetated by grasses and short shrubs with patches of exposed coarse gravel and large cobbles. We sampled four boulders on the innermost moraine ridges, and four boulders on the outermost subdued moraine ridge (Fig. 5.5). A broad glaciofluvial outwash plain grades from the moraines toward the east with preserved braided channels.

The Belgrano moraines cross-cut older recessional moraines (cf. Mendelová et al., 2020b) on the northeastern side of the lake (Figs. 5.6 and 5.7), indicating that the Belgrano moraines were deposited by a re-advance of the Belgrano glacier, rather than a still-stand during overall deglaciation. The location of the older recessional moraines suggest that after the culmination of the gLGM advances/still-stands, the Belgrano glacier withdrew and was largely confined to its trough prior to the re-advance.

To the north of the Belgrano moraines exists a series of latero-terminal moraines (Fig. 5.6), here informally termed the Rincon moraines, which were deposited by the Lacteo glacier. The Rincon moraines occupy the same morphostratigraphic position as the Belgrano moraines. They are situated on the northern slope of Monte Leon and in the gap between Monte Leon and the NE valley side. The terminal moraine ridges (Figs. 5.8 A and B) are discontinuous and have been dissected by several meltwater channels up to 40 m in width. We collected four ^{10}Be samples from the terminal moraine ridges. A glaciofluvial outwash grades from the moraines toward the southeast, extending for about 6 km until it merges with the Belgrano outwash. Immediately outboard of the Rincon moraines, the outwash terrace has been incised by meltwater channels creating a series of stepped terraces.

About 20 km upvalley from the Rincon moraines, and 7 km from the present day margin of the Lacteo glacier, there is a prominent multi-crested lateral moraine perched 45 - 60 m above the valley floor (Fig. 5.9). This lateral moraine spans a width of 100 m with several distinct crests (2-5 m in relief) that are rich in surface boulder (Figs. 5.8 C & D). Given that the lateral moraine is only 45 - 60 m above the valley floor, we interpret the moraine to be morphostratigraphically younger than the Rincon moraines. We collected six ^{10}Be samples from this lateral moraine.

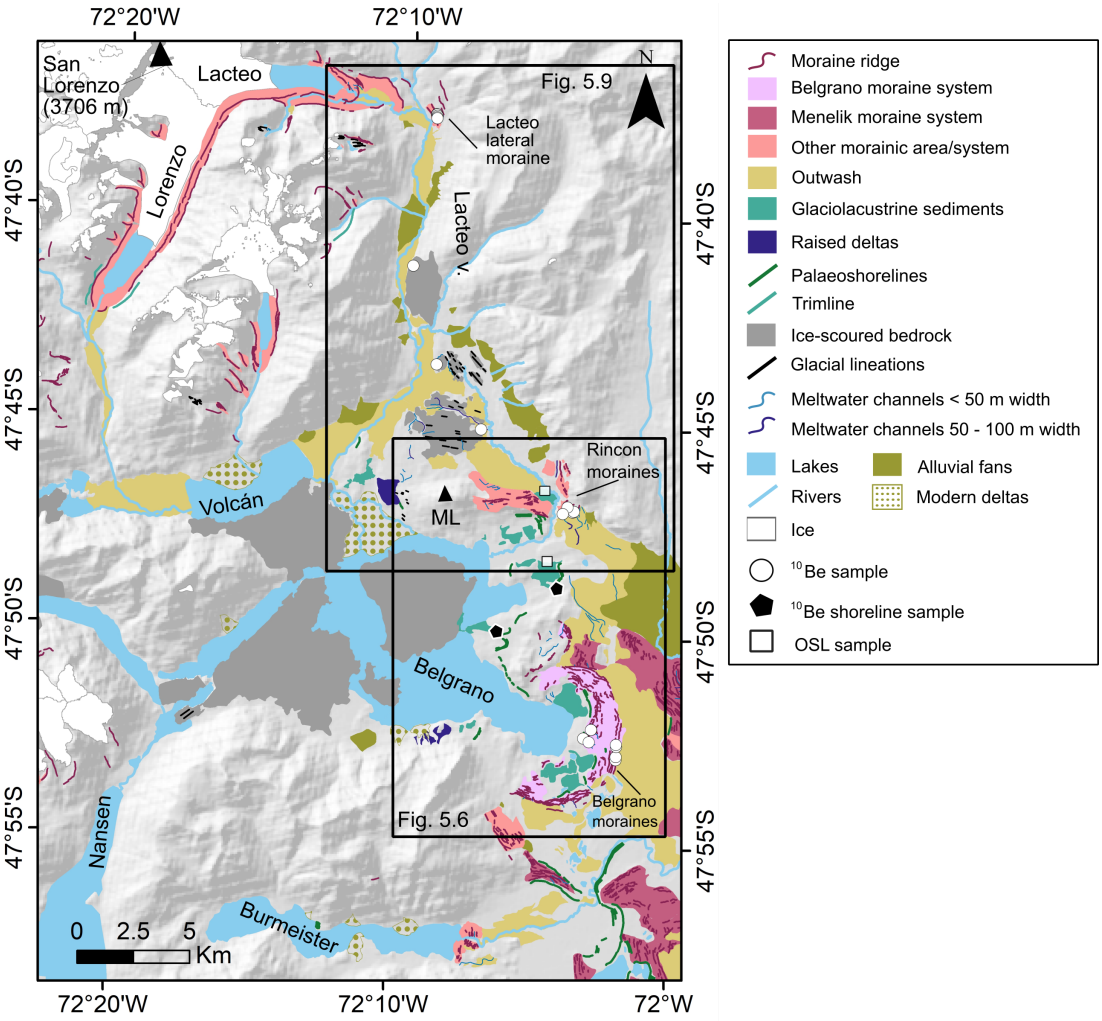

Figure 5.4: The geomorphological map of the Belgrano and Lacteo valleys. Sample locations are also shown (white circles). The hillshade basemap: SRTM DEM.

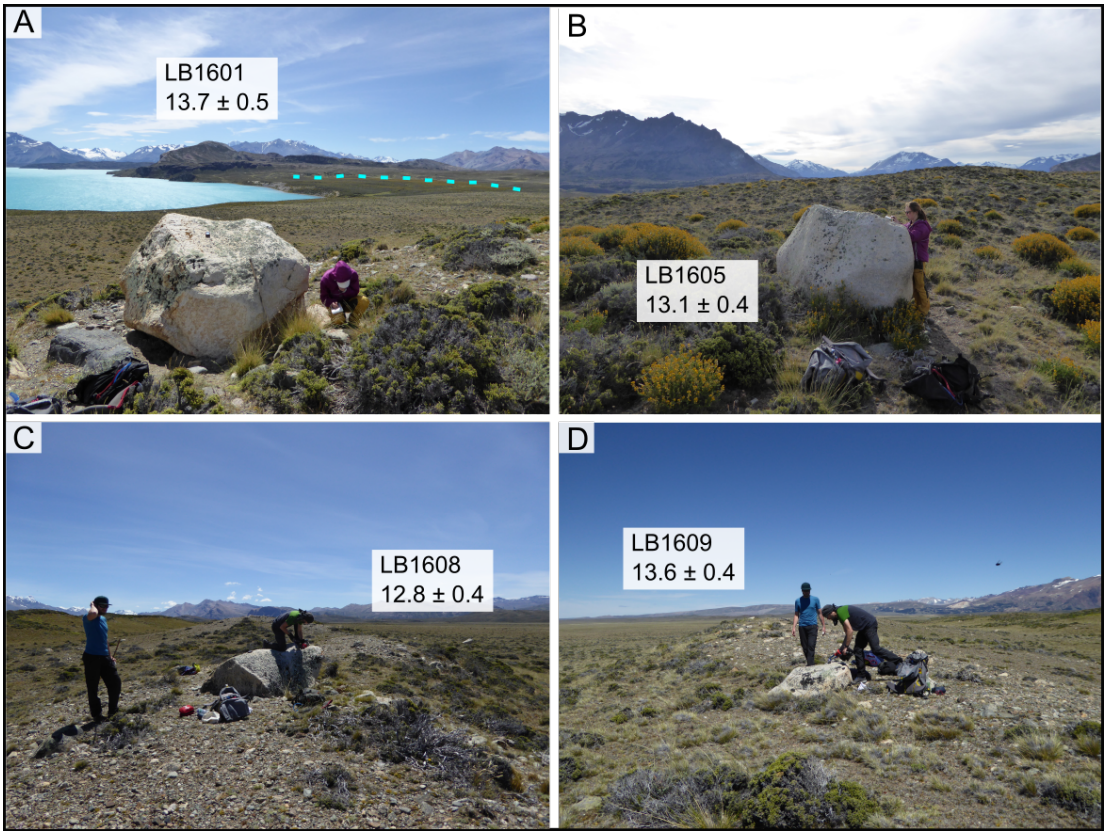

Figure 5.5: Examples of moraine boulders sampled for surface exposure analysis. (A & B) Boulders on the innermost Belgrano moraine, a former shoreline is visible in the background (A, dashed line). (C & D) Boulders on the outermost Belgrano moraine.

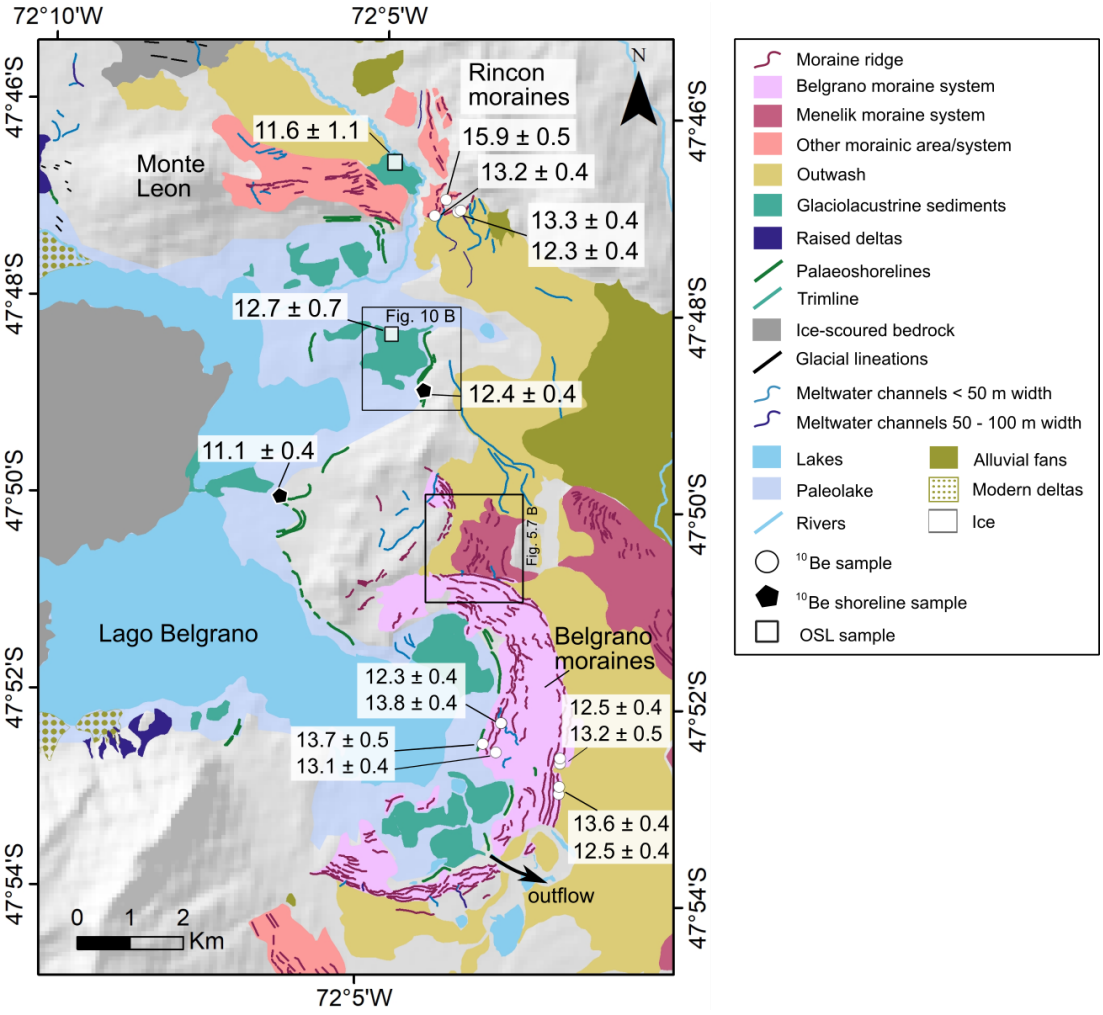

Figure 5.6: Enlarged geomorphology map showing the Belgrano and Rincon moraines. The locations of moraine boulder samples, shoreline samples and OSL samples collected from glaciolacustrine deposits are also shown. The area where the Belgrano moraines cross-cut older recessional moraines is indicated with a box (Fig. 5.7). The ^{10}Be ages presented here are individual ages with 1 σ internal uncertainty. The approximate area of the palaeolake is indicated. This is based on 882 m asl elevation extracted from an SRTM DEM with resolution of 30 m.

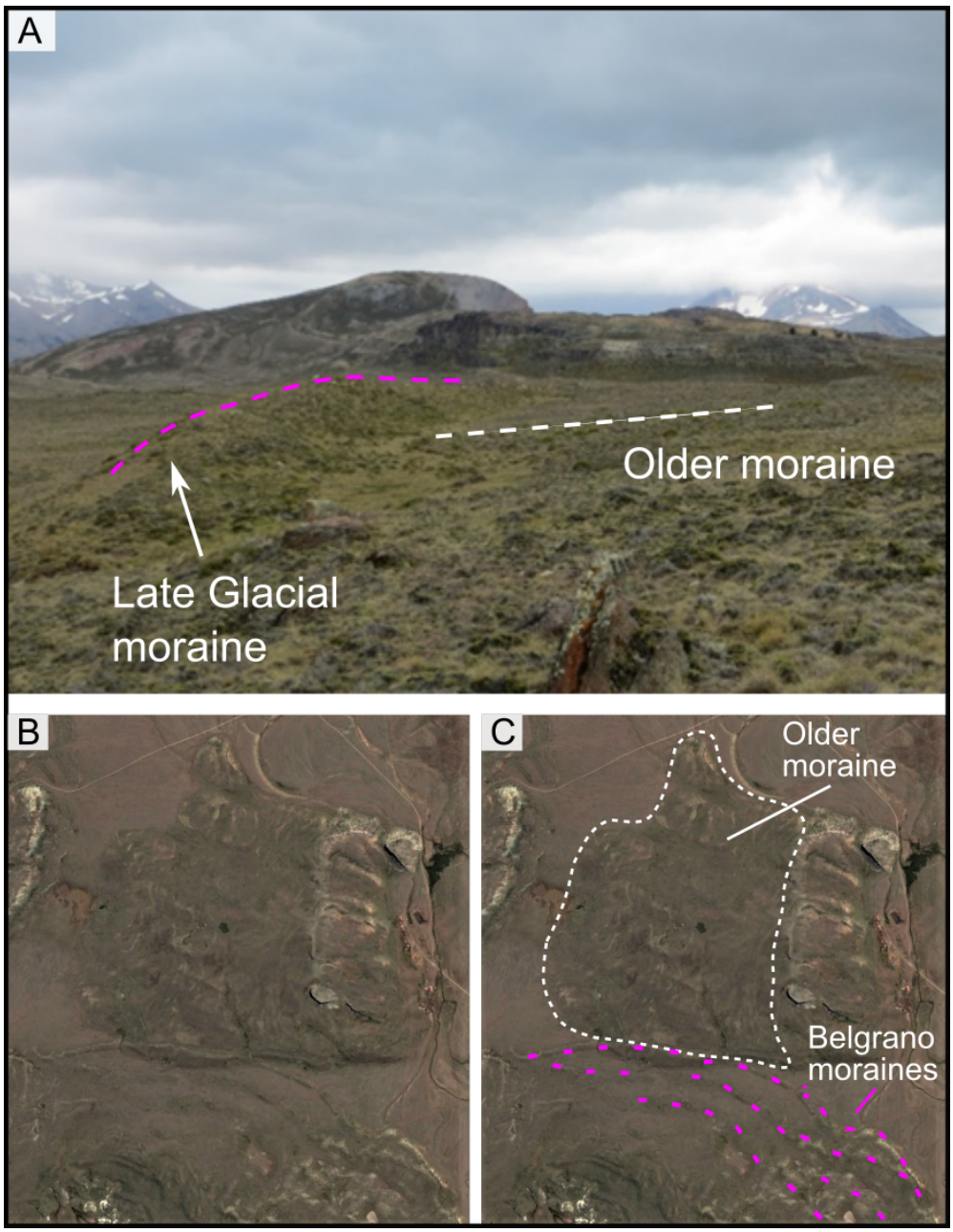

Figure 5.7: (A) Photograph showing the area where the Belgrano moraines cross-cut older moraines. (B & C) Satellite images showing the cross-cutting relationship (Image: Google Earth).

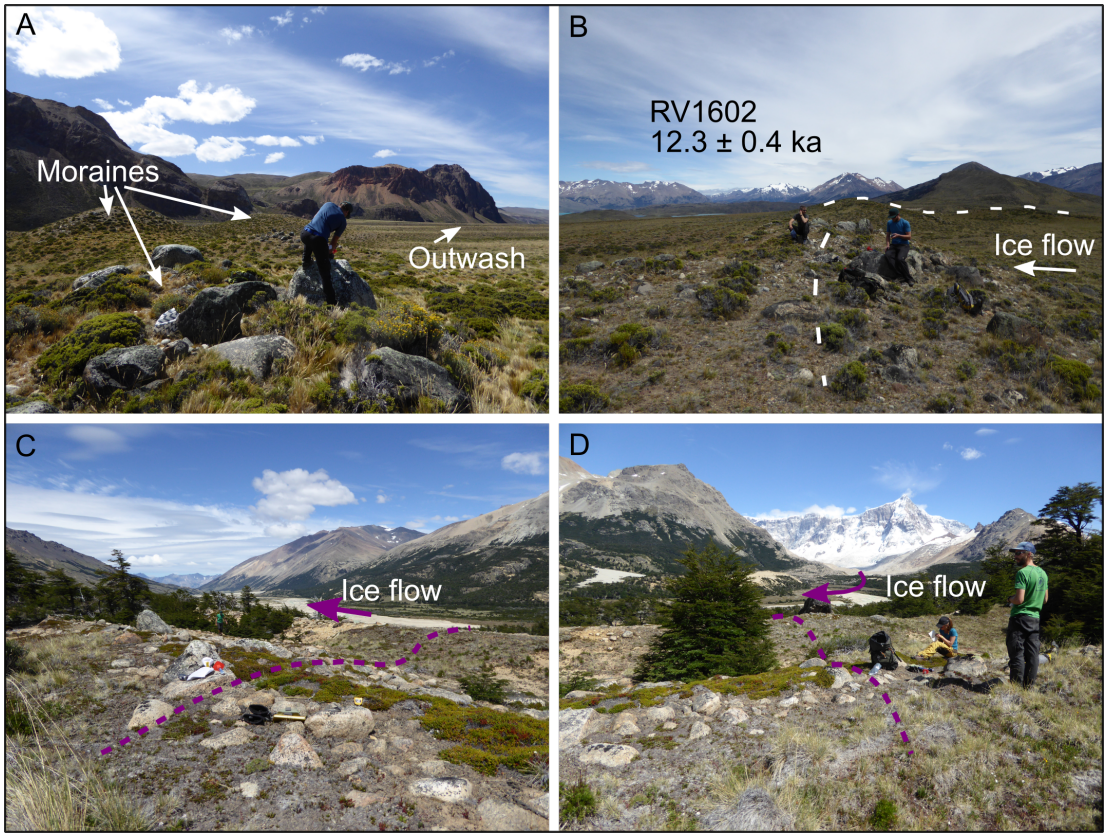

Figure 5.8: (A & B) Photographs showing the Rincon moraines and an outwash plain grading from the moraines to the SE. The outwash terrace was incised by meltwater creating a series of stepped terraces. (C & D) Photographs showing the multi-crested lateral moraine in the Lacteo valley, about 7 km from the present day margin of the Lacteo glacier.

Palaeo shorelines

A major palaeo-shoreline at 882 - 885 m asl can be traced along the southern and northern shores of Lago Belgrano and on the ice-proximal side of the Belgrano moraines (Figs. 5.6 and 5.10). This shoreline is most prominent on the eastern end of the lake where wave action from westerly winds would have been at its greatest. Here, the shoreline is etched into bedrock and sediment, but traces of the shoreline were observed at least 10 km upvalley, and thus the lake covered a substantial area. Higher shorelines can also be found (e.g. at $\sim$ 889 - 892 m asl.), but are spatially restricted, and could indicate a higher palaeolake level or smaller ice-marginal lakes.

The palaeolake drained eastward to the Atlantic via an outflow through the Belgrano moraines at $\sim$ 883 m asl (Fig. 5.6). The palaeolake Belgrano existed when the drainage route through to Lago Nansen (Fig. 5.2) was blocked by ice. The lowering of the lake indicates the loss of this ice dam, and the retreat of ice back into the high mountains. Sediment from this lake, mainly laminated silt to sandy-silts, are preserved at several locations throughout the basin. We collected two ^{10}Be samples from the 882 - 885 m asl shorelines (Figs. 5.6 and 5.10). The shorelines in this area take a form of a flat gravel beach berm up to 30 m wide. On the surface they are composed of medium well-sorted gravel (clasts up to 4 cm) and little to no vegetation.

OSL sample LBSH1801 (850 m; Figs. 5.6 and 5.10) came from a road exposure of silty sediments that infill the valley bottom directly below the the 882 - 885 m asl shoreline. The sediments are laminated sandy silts with water escape features. Numerous boulders and cobbles are visible on the surface of the deposit but less frequently within the exposure. We interpret these sediments as glaciolacustrine sediments, which relate to the 882 - 885 shorelines.

The second OSL sample (RV1801, 893 m; Fig. 5.6) came from a horizontally - laminated silt and sand deposit situated inside of the Rincon moraines in the Lacteo valley. We interpret this deposit as glaciolacustrine sediments from a smaller proglacial lake that formed in the Lacteo valley and was independent to the Belgrano palaeolake.

5.4.2 Chronology

Timing of the readvance

The Belgrano and Rincon moraines are contemporaneous and represent a readvance of the Belgrano and Lacteo glaciers. ^{10}Be ages from the outermost Belgrano moraine ridge range from 12.5 $\pm$ 0.4 ka to 13.6 $\pm$ 0.4 ka, and yield a weighted mean of 13.0 $\pm$ 0.5 ka. The innermost moraines yield ages ranging from 12.3 $\pm$ 0.4 ka to 13.8 $\pm$ 0.4 ka, with a weighted mean of 13.2 $\pm$ 0.6 ka (Table 5.3, Figs. 5.6 and 5.11). The ages from the inner and outer moraine ridges are statistically indistinguishable. Within the dating resolution, we cannot distinguish the indi-

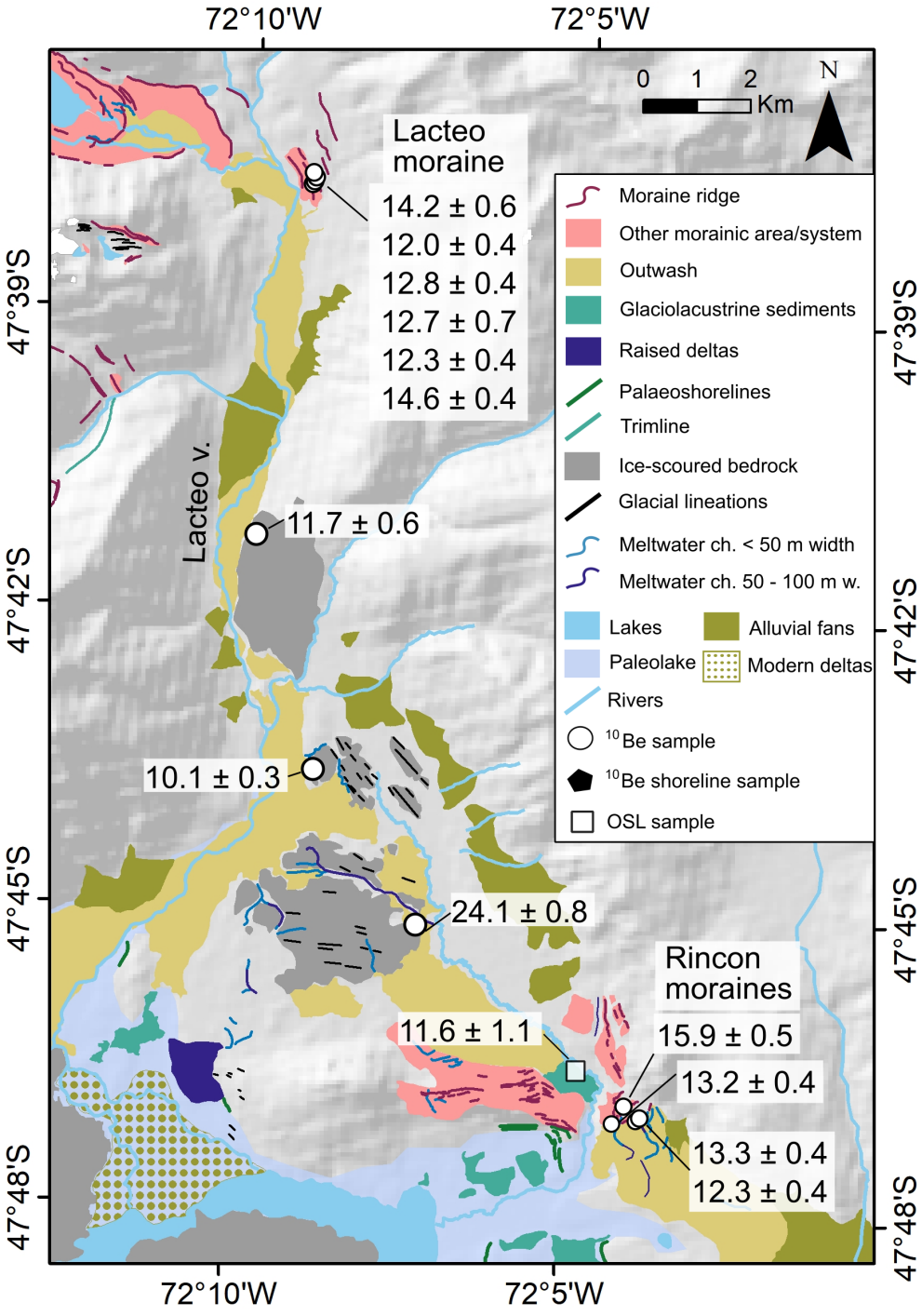

Figure 5.9: Enlarged geomorphology map of the Lacteo valley. Locations of samples collected from the Lacteo lateral moraine and along a transect in the valley are shown. The ^{10}Be ages presented here are individual ages with 1 σ internal uncertainty.

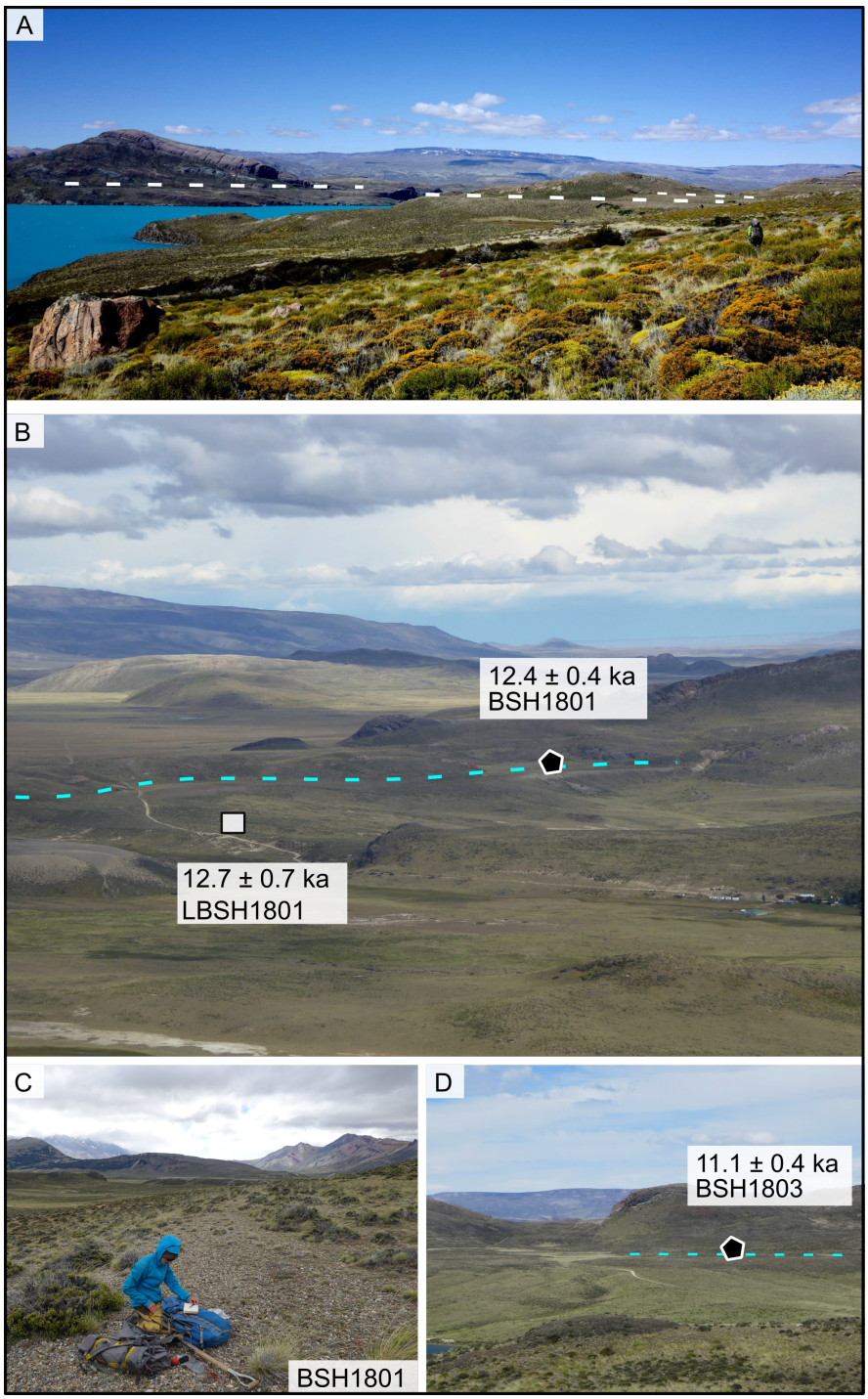

Figure 5.10: (A) Photograph showing raised shorelines above the modern Belgrano lake. (B) Photograph showing a palaeoshoreline with the location of surface exposure (black hexagon) and OSL (square) samples. The valley bottom below the shoreline is infilled with glaciolacutrine sediments. (C) Photograph showing the surface of a shoreline where sample BSH1801 was taken. (D) Photograph of a shoreline where sample BSH1803 was taken.

vidual advances, instead, we group the ages together to date the readvance at 13.1 ± 0.6 ka (weighted mean). The Rincon moraines yielded similar ages of 12.3 ± 0.4, 13.3 ± 0.4, and 13.2 ± 0.4 ka, and a weighted mean age of 12.9 ± 0.4 ka (Figs. 5.6 and 5.11 C). We excluded one sample with an older age of 15.9 ± 0.5 ka as an outlier.

Ice withdrawal and stabilisation

The Lacteo lateral moraine 20 km up valley from the Rincon moraines affords ages in range of 12.0 ± 0.4 ka to 14.6 ± 0.4 ka (Fig. 5.9). The ages display a significant spread and a bi-modal distribution (Fig. 5.11 D). All ages fall within 2 σ of the weighted mean of 13.0 ± 1.0 ka, and thus there is no statistical grounds for excluding any ages. However, the moraines are morphostratigraphically younger than the Rincon moraines (12.9 ± 0.4 ka), and so we exclude the older two ages (14.2 ± 0.6 and 14.6 ± 0.4 ka) as outliers and instead use the weighted mean of the younger ages to date the advance at 12.4 ± 0.3 ka. This interpretation fits with the wider chronology throughout the valley. The two older samples were probably reworked from an earlier advance.

Samples from a transect along the Río Lacteo valley (Fig. 5.9) yielded ages of 24.1 ± 0.8 (RV1608), 10.1 ± 0.3 (RV1606), and 11.7 ± 0.6 ka (RV1609) (in the order of distance from the Rincon moraines). The oldest sample is chronostratigraphically an outlier and likely relates to the gLGM. The remaining two ages likely afford minimum ages for deglaciation of the Lacteo valley. The sample RV1609 came from a cobble on a bedrock outcrop about 30 m higher in elevation than the sample RV1606, which could explain its older age despite being 4.5 km further up the valley.

Palaeolake development

The two ^{10}Be samples from the palaeo-shorelines yield ages of 12.4 ± 0.4 and 11.1 ± 0.4 ka, which is consistent with the slightly older ages for the Belgrano moraines (Table 3 and Fig. 5.6). The age difference between the two beach gravels could result from post-depositional processes or inheritance, and without additional samples it is difficult to resolve. The OSL sample (12.7 ± 0.7 ka) that came from glaciolacustrine sediments associated with the 882 - 885 shoreline is within dating uncertainties consistent with the shoreline ^{10}Be ages. The palaeolake likely formed at or before 12.7 ka and persisted for at least several hundred years, but perhaps over a millennium. The OSL sample from lacustrine sediments inboard of the Rincon moraines (Fig. 5.6), with an age of 11.6 ± 1.1 ka, fits with the slightly older ^{10}Be ages from the bounding Rincon moraines. This proglacial lake formed between the Lacteo glacier and the Rincon moraines, and likely drained into palaeolake Belgrano.

Table 5.3: Exposure ages

Sample	Lm			LSDn			St		
	Age	**Inter**	**Exter**	**Age**	**Inter**	**Exter**	**Age**	**Inter**	**Exter**
		Years			Years			Years	
Belgrano	**inner m.**								
LB1601	13684	455	1213	13612	452	1200	13691	455	1214
LB1603	12297	382	1080	12260	381	1071	12220	379	1074
LB1604	13753	417	1205	13677	415	1192	13762	417	1206
LB1605	13104	412	1153	13044	411	1142	13072	411	1151
Belgrano	**outter m.**								
LB1608	12497	429	1113	12456	428	1104	12426	427	1107
LB1609	13642	416	1196	13566	414	1183	13644	416	1197
LB1610	13197	450	1174	13135	448	1163	13172	450	1173
LB1611	12547	430	1117	12505	429	1108	12478	428	1111
Rincon	**moraines**								
RV1601	13254	352	1145	13169	350	1131	13229	351	1143
RV1602	12320	374	1079	12256	372	1068	12238	371	1072
RV1603*	15852	524	1405	15686	519	1383	15972	528	1416
RV1623	13170	395	1152	13089	393	1139	13140	395	1150
Lacteo	**lateral m.**								
RV1617*	14185	566	1296	14017	560	1275	14215	568	1299
RV1618	11958	388	1056	11859	385	1042	11859	385	1048
RV1619	12795	410	1128	12687	406	1113	12728	408	1123
RV1620	12673	684	1246	12568	678	1230	12598	680	1239
RV1621	12333	404	1091	12236	401	1076	12242	401	1083
RV1622*	14586	399	1264	14401	394	1241	14631	400	1268
Transect									
RV1606	10099	310	885	10073	309	878	9941	305	872
RV1608	24135	821	2151	23751	808	2106	24754	842	2208
RV1609	11674	635	1150	11610	632	1139	11572	630	1141
Raised	**shorelines**								
BSH181	12414	386	1091	12389	385	1083	12342	384	1085
BSH183	11067	355	976	11072	355	971	10929	351	964

Scaling schemes: Lm is the time-dependent version of Lal (1991) and Stone (2000), LSDn - time-dependent scheme of Lifton et al. (2014), and St - time-independent version of Lal (1991) and Stone (2000).
*Ages are reported with 1 internal and external uncertainties, the latter includes production rate and scaling uncertainties. Ages assume zero erosion and no correction for shielding by snow and/or vegetation. Elevation flag is std. Grey shading indicates ages reported here. Samples marked with * are outliers.*

Table 5.4: Summary statistics for moraine ages

	Age	**Std**	**Inter**	**Inter + PR**
Belgrano inner				
Mean (n=4)	13.21	0.58	0.83	1.37
Weighted mean (n=4)	13.15	0.60		
Peak	13.56			
Belgrano outer				
Mean (n=4)	12.97	0.48	0.86	1.37
Weighted mean (n=4)	12.98	0.48		
Peak	12.68			
Belgrano combined				
Mean (n=8)	13.09	0.55	1.20	1.61
Weighted mean (n=4)	13.07	0.56		
Rincon				
Mean (n=4)	13.65	1.32	0.82	1.39
Mean (n=3)	12.91	0.42	0.65	1.24
Weighted mean (n=4)	12.92	0.42		
Peak	13.56			
Lacteo				
Mean (n=6)	13.09	0.96	1.20	1.88
Mean (n=4)	12.44	0.33	0.97	1.41
Weighted mean (n=4)	12.38	0.34		
Peak	12.36			

Std - 1σ standard deviation, Inter - propagated internal uncertainty, Inter + PR- propagated internal uncertainty + production rate uncertainty.

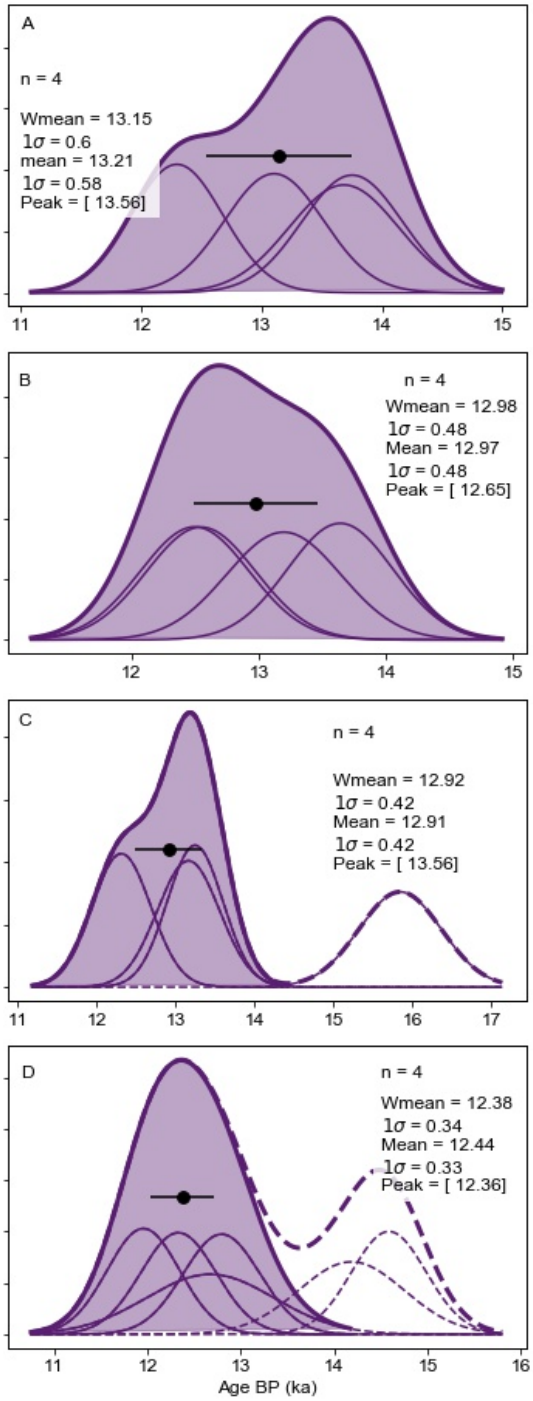

Figure 5.11: Normal kernel density diagrams for exposure ages from moraines: (A) the Belgrano inner moraines,(B) the Belgrano outer moraines, (C) the Rincon, and (D) the Lacteo lateral moraine. Thin purple curves represent Gaussian curves for each age and thick purple curves the summed probabilities. Outliers are represented by dashed lines. Circles represent uncertainties-weighted mean of ages after excluding the outliers and 1σ standard deviations.

5.5 Discussion

5.5.1 LGIT at Lago Belgrano

Our ^{10}Be chronology indicates that a major re-advance of the Belgrano and Lacteo glaciers culminated at $\sim$ 13 ka toward the end of the ACR. At this time, the Belgrano glacier advanced to within 8 km of its gLGM limit (24.7 $\pm$ 1.0 ka, Mendelová et al., 2020b). Our mapping reveals up to 10 advances/still-stands during the ACR, but the dating resolution is insufficient to distinguish between them. The reconstructed extent of the Belgrano and Lacteo glaciers during the ACR is shown in Figure 5.12.

Following the culmination of these advances/still-stands, the ice margin retreated and abandoned the Belgrano moraines. In the process, a palaeolake formed at 882 - 885 m asl, which was dammed by ice at least 10 km west of the Belgrano moraines. The OSL age (12.7 $\pm$ 0.7 ka) from glaciolacustrine sediments and the ^{10}Be ages from lake shorelines (12.4 $\pm$ 0.4 and 11.1 $\pm$ 0.4 ka) suggest that this lake formed at $\sim$12.7 ka and likely existed throughout the YD period. A minimum radiocarbon age of 12.6 $\pm$ 0.06 cal ka BP (Wenzens, 2005; Fig. 5.2) for ice retreat from the Belgrano moraines is consistent with this interpretation. Based on the above ages and the extent of mapped shorelines, we infer a retreat of at least 10 km within several hundred years, which was probably facilitated by calving in the proglacial lake. Although glacial retreat had initiated, the ice remained extensive enough to maintain an ice dam capable of blocking the southward drainage route through Lago Nansen.

The extent of mapped shorelines suggests that by this time, the Lacteo glacier had separated from the Belgrano glacier, and retreated at least 5 km from the Rincon moraines (Fig. 5.12). A proglacial lake formed inboard of the Rincon moraines. The OSL age from the glaciolacustrine sediments here (11.6 $\pm$ 1.1 ka) suggest that this lake existed at roughly the same time as the paleaolake Belgrano. The lateral moraines further up the Lacteo valley, with an age of 12.4 $\pm$ 0.3 ka, indicates the glacier margin then stabilised during the YD. Two ages from bedrock outcrops in the Lacteo valley (10.1 $\pm$ 0.3 and 11.7 $\pm$ 0.6 ka) indicate that the lower part of the valley deglaciated by the end of YD.

The moraines bounding Lago Burmeister occupy the same morphostratigraphic position as the Belgrano moraines, suggesting that they represent an ACR advance of the Burmeister glacier. A minimum radiocarbon age from a kettle within these moraines (Wenzens, 2005), however suggests that they are mid-Holocene in age. Further chronological control would be needed to confirm this.

5.5.2 Deglaciation of the central sector of the PIS

The PIS had retreated and thinned significantly during the first phase of deglaciation after 18-19 ka (Boex et al., 2013; Hein et al., 2010; Henríquez et al.,

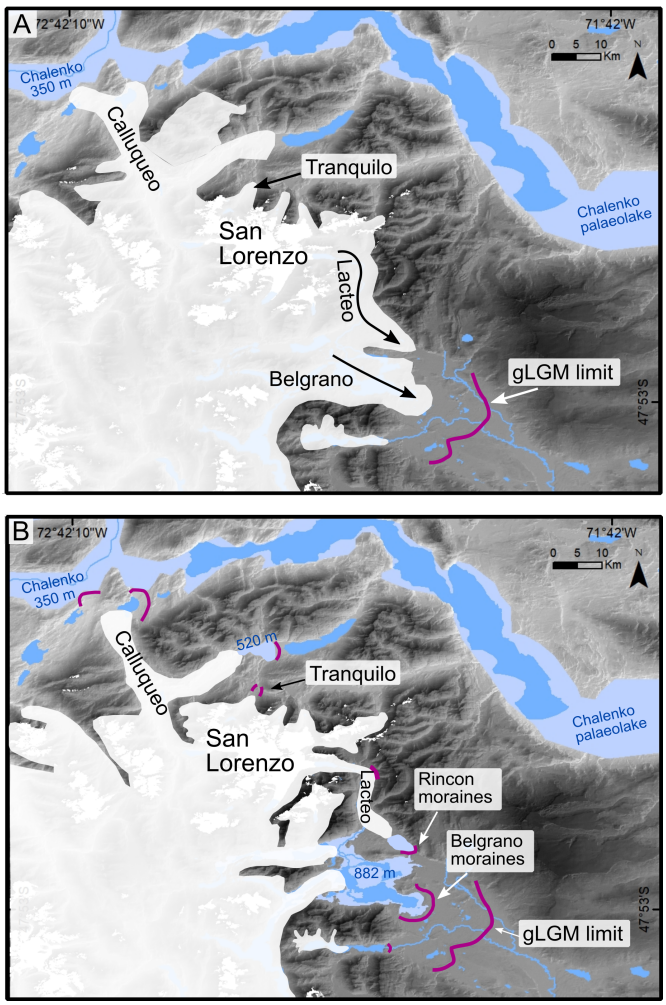

Figure 5.12: Model of ice and palaeolake evolution (A) during the ACR and (B) during the YD. The extent of the Belgrano and Lacteo glaciers during the ACR, and the extent of the palaeolake Belgrano during the YD are based on our geomorphological mapping and chronology. The extent of the Calluqueo and Tranquilo glaciers, and palaeolakes (pale blue) on the northern flanks of the San Lorenzo is based on published work (Davies et al., 2018; Sagredo et al., 2018; Glasser et al., 2012; Martin et al., 2019; Thorndycraft et al., 2019). Moraines delineating the extent of these glaciers are highlighted in pink. Elevation of the palaeolakes is also indicated in m asl. Darker blue colour indicates modern lakes.

2017), and had started to separate into the Northern Patagonian Icefield and the San Lorenzo ice cap by $\sim$ 15 ka (Davies et al., 2018; Thorndycraft et al., 2019). The major basins of Lago Pueyrredón and Lago Buenos Aires had deglaciated by about 16 ka (Hein et al., 2010; Turner et al., 2005; Bendle et al., 2017b; Boex et al., 2013). By the time of the ACR, ice margins of the Northern Patagonian Icefield were within a few tens of km of the modern glacier margins (75-100 km upstream of the LGM limits; Davies et al., 2018; Thorndycraft et al., 2019; Nimick et al., 2016). Northern and western outlet glaciers of the San Lorenzo ice cap were no longer interacting with the PIS, as evidenced by the ACR moraines deposited by the Tranquilo and Calluqueo glaciers (Davies et al., 2018; Sagredo et al., 2018).

Our chronology from the Belgrano valley provides robust evidence for glacier expansion in central Patagonia during the ACR. Cross-cutting of the older Menelik moraines by the ACR Belgrano moraines demonstrates that this was a re-advance, in the case of the Belgrano glacier, rather than a still-stand during overall deglaciation. Together with the data from the Salto and Tranquilo valleys (Davies et al., 2018; Sagredo et al., 2018), this indicates a uniform response of the San Lorenzo glaciers to the ACR climate signal. To maintain an outlet glacier in the Belgrano valley, the ice cap likely also covered mountains to the south of the San Lorenzo massif, but the wider geomorphology suggest it was largely independent of the shrinking ice-sheet by this time.

Glacier advances/still-stands in central Patagonia during the ACR were a response to colder and wetter conditions reconstructed from pollen data. The Lago Edita record (47° S, Henríquez et al., 2017) revealed an increase in cold-resistant taxa between 14 ka - 13.5 ka. A northward expansion of the Magellanic moorland between 14.5 - 12.8 ka was documented by a marine pollen record off the Chilean coast (46° S, Montade et al., 2013; Fig. 5.13). These palaeovegetation changes were interpreted to indicate increased precipitation due to enhanced influence of the SWW at this latitude, and a pause in deglacial warming in the area (Henríquez et al., 2017; Montade et al., 2013).

Following the ACR advances, ice in the Belgrano valley retreated by at least 10 km before stabilising again. This is evidenced by the palaeolake Belgrano, which formed once ice abandoned the Belgrano moraines and existed during the YD period, as well as by the lateral moraines in the Lacteo valley (12.4 $\pm$ 0.3 ka). The initial ice recession was likely a response to a regional warming trend as indicated by the retreat of the Magellanic moorland after 12.8 ka (Montade et al., 2013; Fig. 5.13), and palaeovegetation changes in the Lago Edita record (Henríquez et al., 2017). The YD ice margin stabilisation in central Patagonia is supported by provisional ^{10}Be ages from moraines inboard of the ACR limits in the Tranquilo and Salto valleys (Fig. 5.2; Glasser et al., 2012; Sagredo et al., 2018), and by ^{10}Be ages from the eastern side of the Northern Patagonian Icefield (Nimick et al., 2016; Glasser et al., 2012). Minor advances or still stands during the YD may reflect the continued influence of the SWW in central Patagonia. Pollen assemblages from the Lago Augusta core (47° S) were interpreted to indicate

a highly variable precipitation regime under cool/wet climate between 13.8 and 11.8 ka (Villa-Martínez et al., 2012), while palaeovegetation changes in the Lago Edita record were interpreted to reflect the declining but continued influence of the SWW under warmer conditions until 11 ka (Henríquez et al., 2017).

Our data provide support for the final break-up and a complete separation of the PIS into the Northern Patagonian Icefield, the San Lorenzo and the Southern Patagonian Icefield by the end of the YD, when the ice-dammed palaeolake Belgrano drained. Our exposure ages from the palaeoshorelines (12.4 ± 0.4, 11.1 ± 0.4 ka) indicate that the Belgrano palaeolake likely drained at a similar time as the palaeolake Chalenko (Fig. 5.12 with a Bayesian modelled age of 12 - 11 ka (Thorndycraft et al., 2019). By this time ice masses in central Patagonia were likely close to their present day configuration.

5.5.3 Factors controlling the relative magnitude of glacier advances

The ACR re-advance of the Belgrano glacier reached to within 8 km of its gLGM extent. This is in contrast with the ACR ice margins east of the Northern Patagonian Icefield and on the northern flank of San Lorenzo, which are ∼ 100 - 120 km upvalley from the gLGM limits. While the Belgrano ACR advance was primarily climatically controlled, the relative magnitude of the ACR and gLGM advances at Lago Belgrano can, at least in part, be explained by ice divide migration, catchment size and ice flow re-routing.

During the gLGM, the ice divide of the PIS was located west of San Lorenzo, along the main chain of the Andes. This potentially reduced the catchment size of the Belgrano glacier due to ice flow re-routing, while ice from the northern side of San Lorenzo was confluent with ice from the Northern Patagonian icefield and focused ice flow into the Lago Pueyrredón valley. This allowed a glacier in the Lago Pueyrredón valley to advance further east, while the Belgrano glacier was relatively small at the gLGM. The full elevation of the PIS also blocked westerly moisture penetration (Mendelová et al., 2020b) and reduced snow fall over San Lorenzo during the gLGM further restricting the Belgrano glacier.

During deglaciation, the ice divide would have migrated eastward as the PIS thinned and broke down along its major basins, leading to ice flow reorganization and eventual ice divide break-up prior to the ACR. Glacier in the Lago Pueyrredón valley would have largely disintegrated by this time leaving ice margins of the former tributaries 100 - 120 km upstream of the gLGM limit (Hein et al., 2010; Turner et al., 2005; Boex et al., 2013; Henríquez et al., 2017). The thinning PIS would have also allowed for increased penetration of westerly precipitation to the San Lorenzo massif, relative to the gLGM, and enabled the Belgrano glacier to advance close to its gLGM limit. This process also explains why the Belgrano glacier was considerably smaller during the gLGM compared to its maximum extent of the last glacial cycle at ∼ 75 ka (Mendelová et al., 2020b). Thus, the

real anomaly in the Belgrano valley is the comparatively small gLGM ice extent, rather than an exceptionally large ACR.

The catchment size and hypsometry also played a role in determining relative extents of the San Lorenzo glaciers during the ACR. The small extent of the Tranquilo glacier during the ACR, compared to the Belgrano and Calluqueo glaciers can be explained by their catchment size. While the former had a single smaller accumulation area on San Lorenzo (Sagredo et al., 2018), the latter two had additional ice contribution from the surrounding mountains. The difference in hypsometry will have played a role. The northern and western flanks of San Lorenzo have greater relief and a steeper elevation profile, and thus glaciers here would reach the ablation zone in a shorter distance when compared to ice discharging into the high elevation Belgrano valley to the east. A somewhat lower ELA on the western side of San Lorenzo (Falaschi et al., 2013), would have, to some extent, compensated for the lower altitude of the Salto valley and thereby allow the Calluqueo glacier to advance to the lower elevation of ∼300 m asl Davies et al., 2018).

5.5.4 Regional view

Our data reveals a structure of the LGIT advances/still-stands at Lago Belgrano that is similar to southern Patagonia (51° S - 50° S; García et al., 2012; Moreno et al., 2009; Fogwill and Kubik, 2005; Ackert et al., 2008; Strelin et al., 2011; Kaplan et al., 2011) and New Zealand (Putnam et al., 2010a; Kaplan et al., 2010, 2013). Glaciers were most extensive during the ACR and then underwent recession punctuated by smaller advances/still-stands during the YD.

The ACR cooling is recorded in pollen records from NW Patagonia (41° - 43° S; Moreno and Videla, 2016; Pesce and Moreno, 2014), and a pause in deglacial warming coeval with the ACR is reflected in sea surface temperature records along the Chilean coast as far north as 41° S (Fig. 5.13; Kaiser et al., 2005; Haddam et al., 2018; Caniupán et al., 2011). At the moment, there are no glacial chronologies spanning the LGIT in northern Patagonia to evaluate the glacier response to cold reversals here. In southernmost Patagonia (54° S - 55° S), contradictory interpretations of the ACR extent of the Cordillera Darwin ice field warrant further work (McCulloch et al., 2005a; Hall et al., 2013, 2017). East of the Cordillera Darwin, glaciers were confined to cirques during the ACR (Menounos et al., 2013). Colder climatic conditions during the ACR in Tierra del Fuego (53° S) are, however, indicated by palaeovegetation proxies (Mansilla et al., 2016).

Our data supports a widespread atmospheric and oceanic cooling throughout the southern mid-latitudes contemporaneous with cooling identified in the Antarctic ice cores (Fig. 5.13). Latitudinal displacement of the SWW belt and associated oceanic fronts could facilitate the propagation of the climate signals (Pesce and Moreno, 2014; Moreno et al., 2012; Lamy, 2004). A northward shift of the coupled system during the ACR would have caused cooling and increased pre-

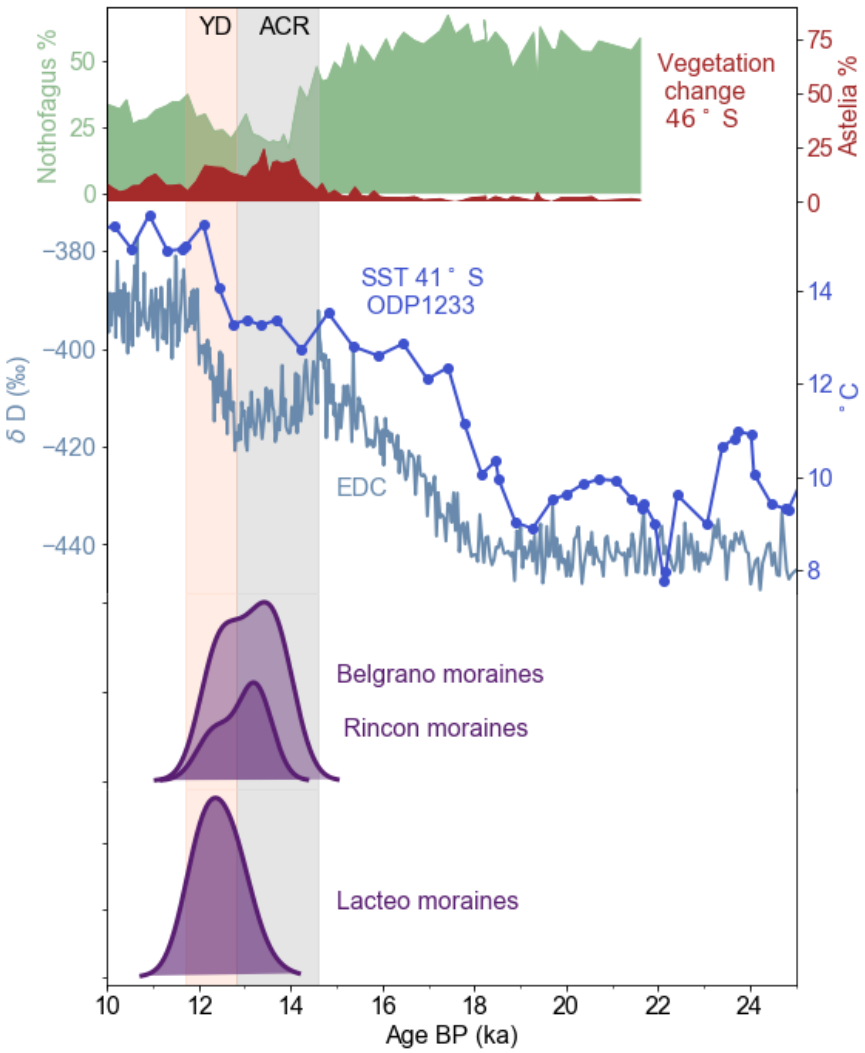

Figure 5.13: Comparison of our exposure ages to other proxies: *Nothofagus dombeyi* type and *Astelia pumila* pollen record from core MD07-3088 off the Chilean coast (46° S, Montade et al., 2013) plotted on on a scale from Montade et al. (2019), sea surface temperature reconstruction from core ODP 1233 off the Chilean coast (Kaiser et al., 2005) and the δ D record from EDC, east Antarctica (EPICA Community Members, 2004) plotted on AICC2012 timescale (Veres et al., 2013). The exposure ages are plotted after outliers have been removed. *Astelia* is a plant typical of the Magellanic moorland that at present grows south of 48° S.

cipitation, promoting glacier expansion in Patagonia and New Zealand (García et al., 2012; Sagredo et al., 2018; Putnam et al., 2010b). Such a shift in the coupled system was likely driven by interhemispheric oceanic teleconnections and associated atmospheric reorganization commonly attributed to the bipolar see-saw (Pedro et al., 2018; Stocker and Johnsen, 2003; Buizert et al., 2018).

5.6 Conclusions

Our geomorphological mapping along with ^{10}Be and OSL ages document a major re-advance of the Belgrano glacier at 13.1 ± 0.6 ka, and a re-advance/still-stand of the Lacteo glacier at 12.9 ± 0.4 ka, coeval with the ACR. The San Lorenzo ice cap covered an extensive area at this time, but was largely independent of at least the Northern Patagonian Icefield. Following the culmination of the ACR advances/still-stands, ice in the Belgrano valley retreated by at least 10 km and an ice-dammed proglacial lake formed at 882 - 885 m asl. The ^{10}Be ages from the palaeoshorelines and an OSL age from glaciolacustrine sediments suggest that the lake likely existed between ∼12.7 and ∼11.1 ka, implying stabilisation of ice margins during the YD. The ^{10}Be ages from a lateral moraine in the Lacteo valley (12.4 ± 0.3 ka) indicate a smaller advance/still-stand during the YD. We suggest that the final break-up of the PIS occurred at the end of the YD, when glaciers retreated back to the mountains and the palaeolake Belgrano drained. Our data from the Belgrano valley supports the dominant ACR climate signal in the southern mid-latitudes, but also suggest a co-occurrence of the northern hemisphere YD signal, albeit of smaller magnitude. Glacier expansion in the southern mid-latitudes during the ACR is in line with the northward migration of the coupled oceanic-atmospheric system.

Chapter 6

Holocene glacial dynamics



Abstract

The Holocene period provides a test ground for improving our understanding of hemispheric to regional controls on glacier activity and their sensitivity to climate. In Patagonia, detailed chronologies documenting Holocene glacier change are still too few in many areas. Here, new ^{10}Be ages, 3D glacier reconstruction and ELA estimates for the Lacteo glacier are presented. The Lacteo glacier advanced/ stabilised at 2.8 $\pm$ 0.2 ka and was less extensive since. The glacier reconstruction indicates that an ELA lowering of 221 - 271 m relative to the present was required to match the 2.8 ka extent. This implies temperatures lower by $\sim$ 1.3 - 1.6 ° Celsius assuming an adiabatic lapse rate of 0.6 °C / 100 m and no change in precipitation. In line with other records, the results indicate that glaciers in Patagonia achieved larger Holocene extent prior to the last millennium. The advance coincided with a climatic deterioration recorded by a number of proxies and may have been caused by reduced solar activity at the time.

6.1 Introduction

Glaciers in the mid- and high latitudes of the Northern Hemisphere were generally smaller than today during the early to mid-Holocene and then expanded with advances culminating during the Little Ice Age (LIA) between 1500 - 1800 (e.g. Solomina et al., 2015). This long-term trend broadly followed decreasing NH summer insolation (Solomina et al., 2015). In contrast, glaciers in New Zealand were progressively smaller over the course of the Holocene (Schaefer et al., 2009; Putnam et al., 2012; Kaplan et al., 2013), a trend attributed to insolation driven changes to atmospheric circulation. This trend is, however, not replicated throughout Patagonia, and more detailed chronologies spanning the Holocene are still too few and restricted to the southern part, hindering our understanding of controls on glacier activity.

In the Cordillera Darwin, southernmost Patagonia, glaciers retreated to near their present day configuration in the early Holocene (Bertrand et al., 2017; Boyd et al., 2008; Hall et al., 2013, 2019). Advances then occurred multiple times from mid-Holocene with largest advances over the last 1.3 ka (Bertrand et al., 2017; Hall et al., 2019). Some glaciers of the SPI also retreated to near their modern limits in the early Holocene followed by maximum Holocene expansion between 6.1 and 4.8 ka, with a second phase of smaller advances/stillstands after 2 ka (Kaplan et al., 2016; Strelin et al., 2014, 2011). This mid- and late Holocene glacier expansion has been linked to the dominance of negative Southern Annual Mode (SAM) causing wetter and colder conditions over Patagonia (Moreno et al., 2014; Kaplan et al., 2016; Moreno et al., 2018; Reynhout et al., 2019). Some glaciers advanced in the early Holocene (Douglass et al., 2005; Harrison et al., 2012; Reynhout et al., 2019),

despite warm and dry conditions documented by palaeoenvironmental proxies throughout Patagonia (e.g. de Porras et al., 2012, 2014; Markgraf et al., 2007; Montade et al., 2013; Massaferro and Brooks, 2002). An advance of the Torre glacier (SPI) in the early Holocene and its subsequent decreasing extent have been explained by increasing SH insolation over the Holocene (Reynhout et al., 2019). In central Patagonia, the culmination of LIA advances by AD 1870 -1890 is well documented (e.g. Winchester and Harrison, 1996; Harrison and Winchester, 2000; Winchester et al., 2001; Harrison et al., 2007; Glasser et al., 2002, 2004), but well-dated records of glacial activity prior to the LIA are few (e.g. Nimick et al., 2016; Sagredo et al., 2016). Seeking to fill some of the spatial and temporal gaps, this chapter presents new ^{10}Be ages constraining a Holocene advance/stillstand of the Lacteo glacier, reconstruction of the Equilibrium Line Altitudes (ELA) and discusses its Holocene dynamics.

6.2 Study site and previous work

The Lacteo and San Lorenzo glaciers are small valley glaciers ($\sim$ 5 and 8 km in length, respectively) located on the eastern side of Monte San Lorenzo. They have lake terminating margins, low-gradient debris-covered tongues and are bounded by a near vertical headwall of Monte San Lorenzo (Fig. 6.1). Over the 2000 - 2012 period, the Lacteo glacier thinned at a rate of 1.95 m a^{-1} and the San Lorenzo glacier at 1.8 m a^{-1}, with no positive elevation changes observed (Falaschi et al., 2017). The modern ELA was estimated to be $\sim$1800 m asl on the eastern side of San Lorenzo and about 100 m lower on the western side of the massif, which receives higher precipitation (Falaschi et al., 2013). These estimates are based on mapped snowlines using satellite imagery from 2005 - 2008, with standard deviations up to 42 m (Falaschi et al., 2013). Falaschi et al. (2017) suggested that the ELA now likely lies above the maximum surface elevation of the two glaciers.

The Holocene moraines deposited by the Lacteo glacier have previously been mapped by Mercer (1968) and Garibotti and Villalba (2017). Garibotti and Villalba (2017) also mapped moraines in the San Lorenzo valley (Fig. 6.2). For ease of comparison, the moraines are here referred to as M1-M5 in the Lacteo valley and M1 - M6 in the San Lorenzo valley from the oldest to the youngest, following Garibotti and Villalba (2017). These moraines are constrained by a combination of historical photographs and lichenometric ages in both valleys (Garibotti and Villalba, 2017) and a single radiocarbon age from the Lacteo valley (Mercer, 1968) (Fig. 6.2). In the Lacteo valley, the M1 moraine has a maximum radiocarbon age of 5.2 $\pm$ 0.2 ka (Fig. 6.2; Mercer, 1968). This age comes from a rooted tree stump found within a section on the edge of a lagoon impounded by the M1 moraine (Mercer, 1968). The lichenometric ages are shown in Fig. 6.2.

Historical aerial photographs from 1958 show that both Lacteo and San Lorenzo glaciers had started to retreat from their youngest moraines (M5 and M6 respectively) (Garibotti and Villalba, 2017). A photograph taken by de Agostini

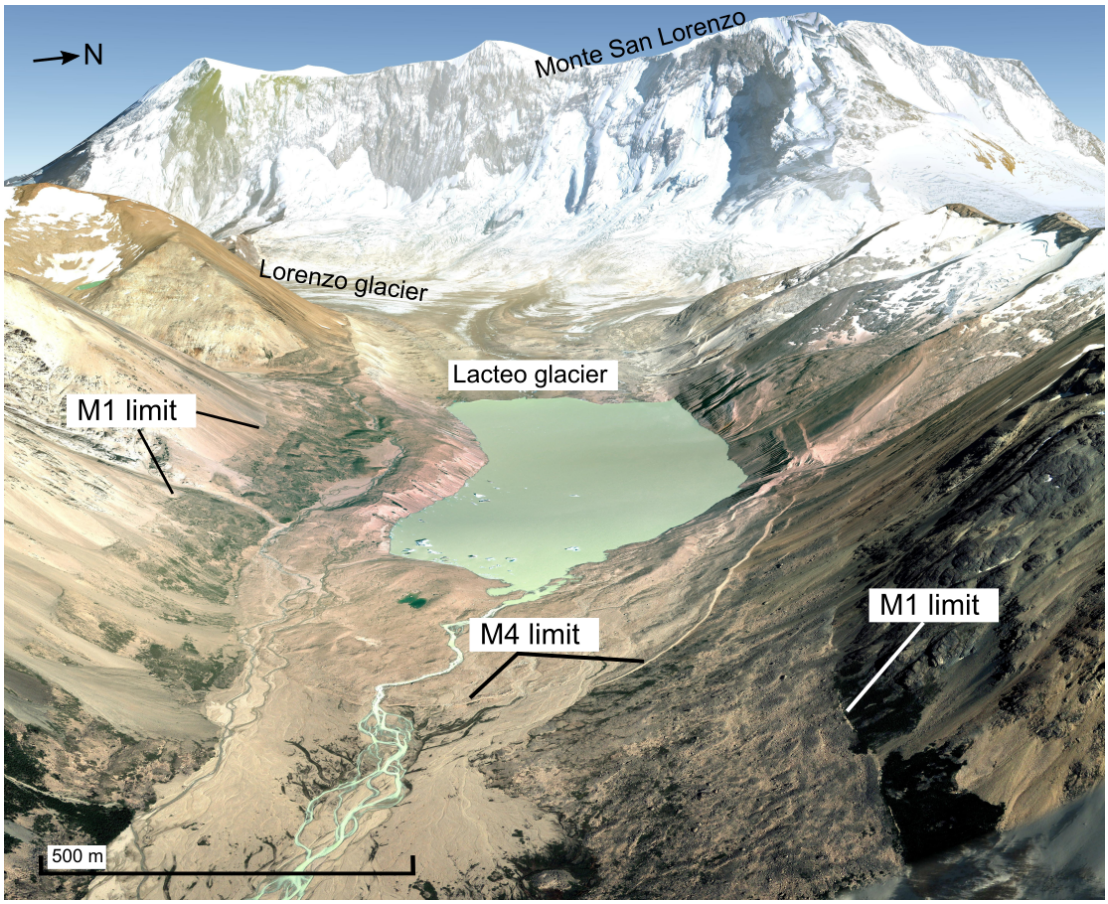

Figure 6.1: A 3D view of Monte San Lorenzo and the Lacteo glacier. Source: Google Earth.

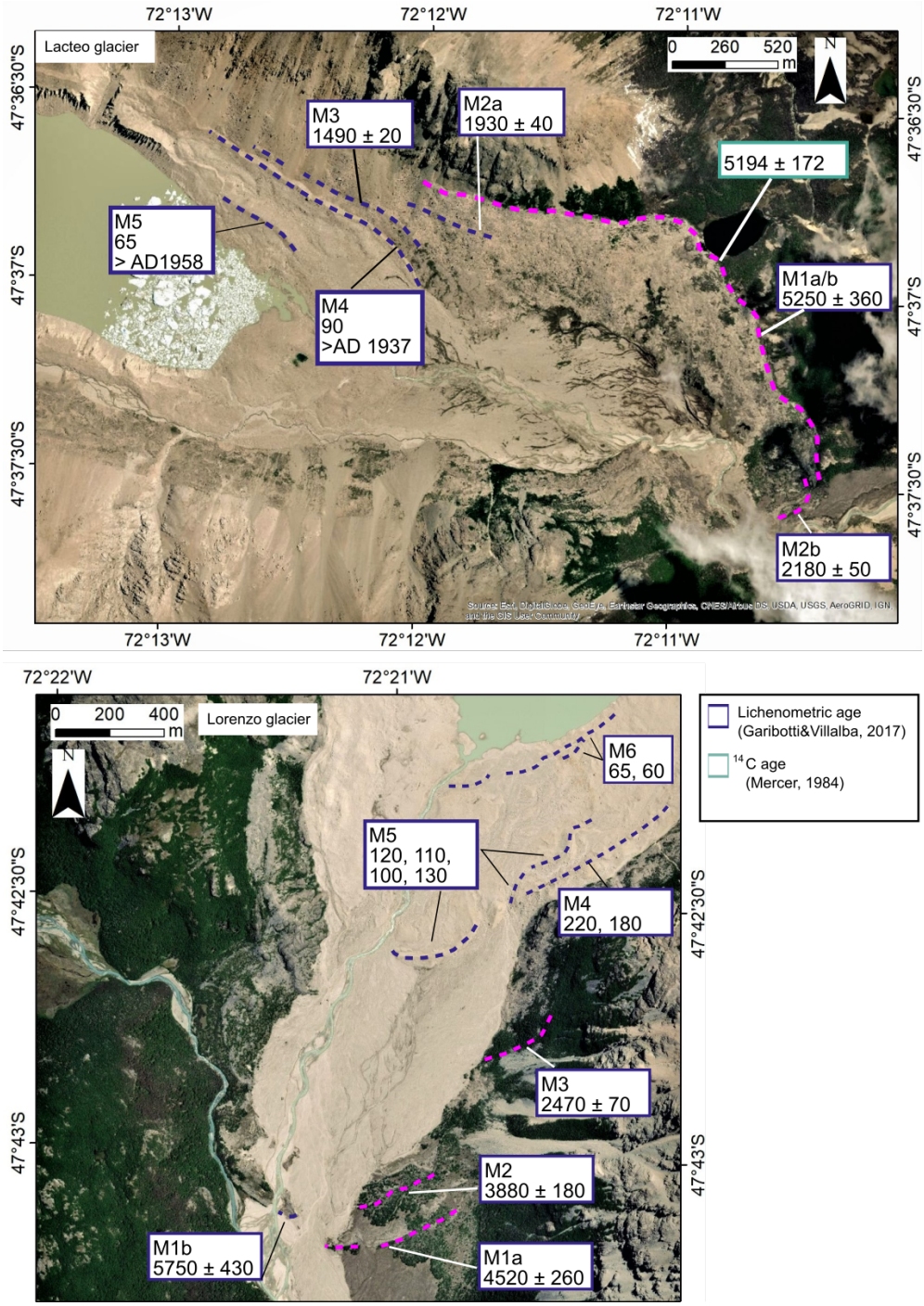

Figure 6.2: Lichenometric ages for the moraines deposited by the Lacteo and Lorenzo glacier (Garibotti and Villalba, 2017) and a maximum radiocarbon age for a moraine of the Lacteo glacier (Mercer, 1984). Moraines are shown with dashed lines as mapped and labelled by Garibotti and Villalba (2017).

(1937) shows the terminus of the Lacteo glacier in 1937 inside of the M4 moraine (Garibotti and Villalba, 2017). These photographs provide minimum ages for the youngest moraines in both valleys. Together with lichen data from other sites, they were used as control ages for the lichen growth curve presented by Garibotti and Villalba (2017). Beyond 450 a BP, their lichen growth rate curve is based on the moraine dated by Mercer (1968) with only a maximum ^{14}C age, thus the lichenometric ages older than 450 a BP should be interpreted with caution. Thus the exact timing of advances in both valleys prior to the early 20th is uncertain.

6.2.1 The moraine sequence

Aiming to improve the Holocene chronology of the Lacteo glacier, the M1 terminal moraine is dated here using exposure analysis on moraine boulders. The glacier surface and the ELA is then reconstructed for this limit.

The M1 moraine in the Lacteo valley is a prominent lateral-terminal moraine, partly deposited against a bedrock outcrop about 2 km up-valley from the Late Glacial lateral moraine described and dated in Chapter 5. The M1 terminal moraine ridge is composed of clast-supported angular to sub-angular boulders, the largest one being up to 4 m in length. It is sparsely vegetated by mosses and occasional patches of short shrubs. Dense Nothofagus forest has developed outside of the moraine, while inside of the moraine vegetation is sparse. Sediment cover associated with this moraine, which can be clearly distinguished in satellite imagery, extends from the lateral margins down to the valley floor. Two less defined ridges can be seen within it, mapped by Garibotti and Villalba (2017) as M2a and M3 moraines. The composition of the M1 moraines (Fig. 6.3) is in sharp contrast to the Late Glacial lateral moraine in the valley, which is composed of sandy, matrix-supported diamicton with rounded boulders embedded in the crests. The next prominent lateral moraine (M4) is found about 2 km up-valley, it is fresh in appearance and has no vegetation.

6.3 Methods

6.3.1 Exposure dating

Four samples were collected from moraine boulders on the M1 terminal moraine in the Lacteo valley. Large boulders with flat top surfaces, showing no sign of surface erosion and resting in a stable position on the moraine crest were sampled. The samples were collected from the center of the top boulder surfaces using a hammer and chisel. The sample details are presented in Table 6.1 and the sample locations are shown in Fig. 6.4. Sample processing details are described in detail in Chapter 4 Section 4.4.3.

The ^{10}Be ages were calculated using the version 3 of the online CRONUS calculator (Balco et al., 2008) and the Patagonian production rate (Kaplan et al.,

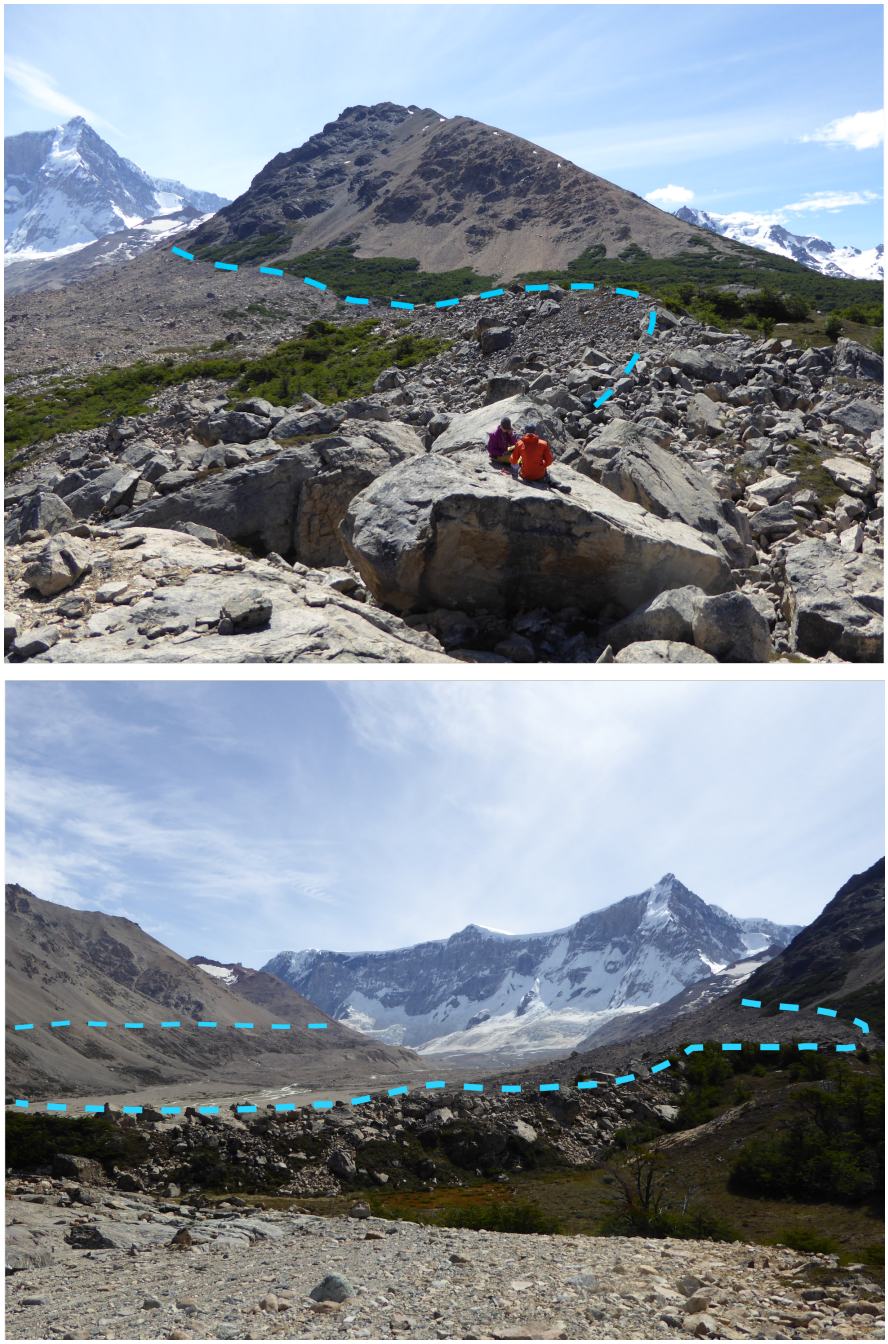

Figure 6.3: Photographs showing the M1 lateral-terminal moraine in the Lacteo valley, from which moraine boulder samples were collected.

2011) derived from the ICE-D database. The ages were corrected for topographic shielding, which was measured in the field using compass and clinometer (~ 0.995 for all samples). The ages are presented with zero erosion and should thus be considered minimum ages. Applying erosion rate of 0.2 mm ka^{-1}, derived in the LP valley (Hein et al., 2017; Douglass et al., 2007), increases the ages by 0.03 % (

$\sim$ 1 year), which is within analytical uncertainty. Although, erosion rate may be slightly higher within the mountains, over such a short time scale it is likely to have negligible effect on the exposure ages. Boulders showing no sign of surface erosion were sampled. Persistent deep snow would shield surfaces and reduce production of cosmogenic nuclides, thus reducing the exposure age. Shielding from snow within the mountains is more likely than lower down in the Belgrano valley. However, strong winds would tend to remove snow from moraine crests and boulder tops, limiting snow depth and persistence in winter months. Sampling taller boulders should also reduce the likelihood of long-term burial. For these reason correction for snow cover is not applied.

The ^{10}Be ages are reported as exposure ages before present (2016, year of sampling). Radiocarbon age is reported as calibrated years BP (before 1950). This results in age discrepancy of 66 years, which is within analytical uncertainties and does not change any interpretations.

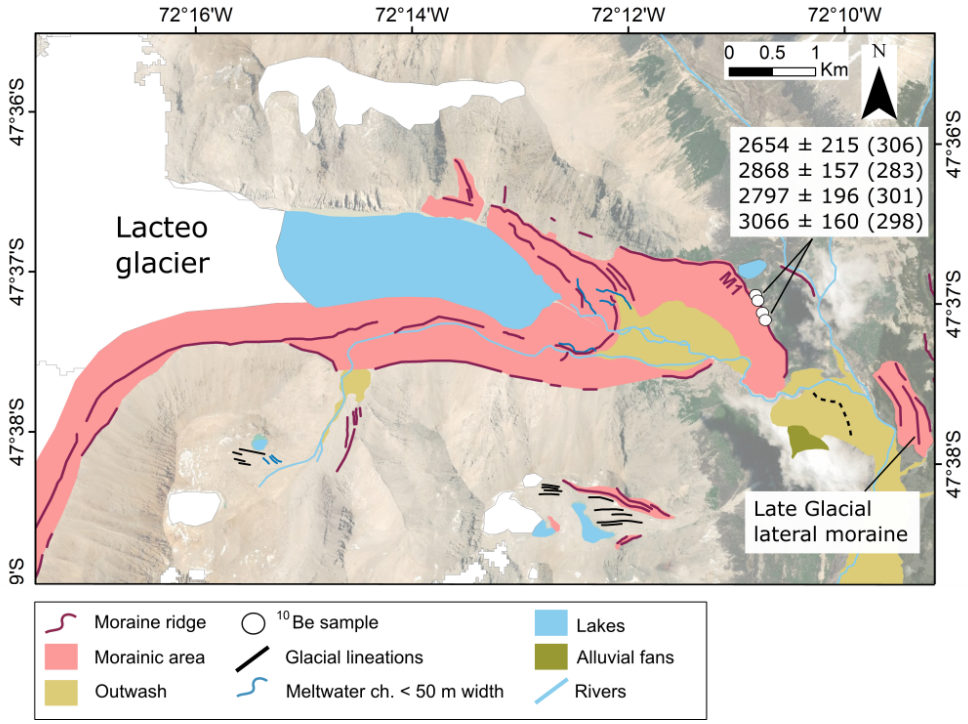

Figure 6.4: Geomorphological map showing the Holocene moraine sequence in the foreground of the Lacteo glacier. Sample locations and exposure ages are also shown. Shaded relief base map was made using the SRTM DEM (30m).

Table 6.1: Sample details and nuclide concentration

Sample	**Latitude** (DD)	**Longitude** (DD)	**Elev** (m asl)	**Bldr. h** (cm)	**Thickn.** (cm)	**Quartz** (g)	^{10}**Be** atoms g^{-1}	$\pm$**1**σ atoms g^{-1}	^{10}**Be**/^{9}**Be** ratio	$\pm$ **1**σ	**Blank** corr. (%)
RV1610	-47.617086	-72.178903	1148	150	3	15.65	2.70E+04	2.19E+03	2.85E-14	1.46E-15	10.23
RV1611	-47.617124	-72.178809	1147	200	5	22.10	2.87E+04	1.57E+03	4.10E-14	1.50E-15	7.06
RV1612	-47.617628	-72.178557	1146	120	3	15.77	2.84E+04	1.99E+03	2.99E-14	1.19E-15	9.71
RV1613	-47.617624	-72.178371	1143	140	2	22.42	3.14E+04	1.64E+03	4.58E-14	1.68E-15	6.41

Rock density is assumed to be 2.7 g cm^{-3}.
Topographic shielding was negligible (0.99523) for all samples.
Concentrations were corrected for process blanks. Blank corrections shown as % of the sample $^{10}Be/^{9}Be$ ratios. The uncertainty of the blank correction is included in the stated 1 σ uncertainties.
Measurements were normalised to NIST SRM4325 with nominal $^{10}Be/^{9}Be$ ratios of 2.79x10^{-11} and half-life of 1.36 Ma (Nishiizumi et al., 2007). All measurements were made at the AMS facility at SUERC.
**Boulder height. .*

6.3.2 Glacier reconstruction

DEM

An Advanced Spaceborne Thermal Emission and Reflection Radiometer Global Digital Elevation Model (ASTER GDEM) Version 3 distributed by the NASA Land Processes Distributed Active Archive Center was used for glacier reconstruction. ASTER GDEM V3 has a spatial resolution of 30 m (1 arc sec) and vertical accuracy of 12.7 m for mountainous areas (Tachikawa et al., 2011). The DEM was georeferenced to the Universal Transverse Mercator (UTM) WGS 1984 Zone 18S projection.

Glacier geometry

The geometry of the Lacteo glacier and the ELAs were reconstructed for the M1 terminal positions. The glacier geometry was reconstructed using the Glare Arc GIS package (Pellitero et al., 2016), briefly described below. All the calculations were done at 30 m interval considering the spatial resolution of the DEM.

The Glare package (Pellitero et al., 2016) implements iterative numerical approach of Benn and Hulton (2010) to derive an ice surface profile along the central flow-line. The model assumes perfect plasticity rheology, not accounting for basal sliding, and is based on the equation of Schilling and Hollin (1981):

$$h_{i+1} = h_i + \frac{\tau_{av}}{F_i \rho g} \frac{\Delta x}{H_i} \tag{6.1}$$

where, h is ice surface elevation, τ_{av} is basal shear stress (in Pa), F is a shape factor, ρ is ice density (900 kg m^{-3}), g is the acceleration due to gravity (9.81 ms^{-2}), Δx is step length (metres), H is ice thickness, and i refers to the iteration step number.

The equation 6.1, however, does not have a solution at the snout of the glacier, and was modified by Van der Veen. In his approach the basal shear stress and ice thickness are calculated at a mid-point of a step $(i + 1/2)$, giving:

$$h_{i+1}^2 - h_{i+1}(b_i + b_{i+1}) + h_i(b_{i+1} - H_i) - \frac{2\Delta x \overline{\tau}_{av}}{Fg} \tag{6.2}$$

where b is the bed elevation and the overbar shows that the stress is an average for the interval (Pellitero et al., 2016). The generated ice thickness flow-line data points are then interpolated to compute a 3D glacier surface.

Bed topography There are no empirical measurements of ice thickness for the modern Lacteo glacier. Bed topography under the extant glacier was thus calculated along the central flow-line from modern ice elevation data using an inversion of Benn and Hulton (2010) approach as implemented in the Glare toolbox (Pellitero et al., 2016). Modern ice elevation data were extracted from the ASTER DEM. The extant (present day) glacier outline was obtained from the GLIMS database and modified to match the glacier extent captured by the

DEM (Fig. 6.5). The proglacial lake at the time of the data capture for the DEM is is < 500 m in length (Fig. 6.5). Since its depth is unknown, it was not removed from the DEM. The reconstruction presented here should be regarded as a first-order approximation given uncertainties related to the bed topography under the extant glacier and proglacial lake bathymetry.

Central flow-lines and tributaries

Central flow-lines were mapped from terminal moraine positions to the headwall, parallel to, and at a mid-point between lateral glacier margins/valley sides (Fig. 6.5). Geomorphological evidence indicating possible tributaries is not clear. It is assumed that the glacier received contribution from three cirques to the north, and tributary flow-lines are digitised to reconstruct ice profiles here.

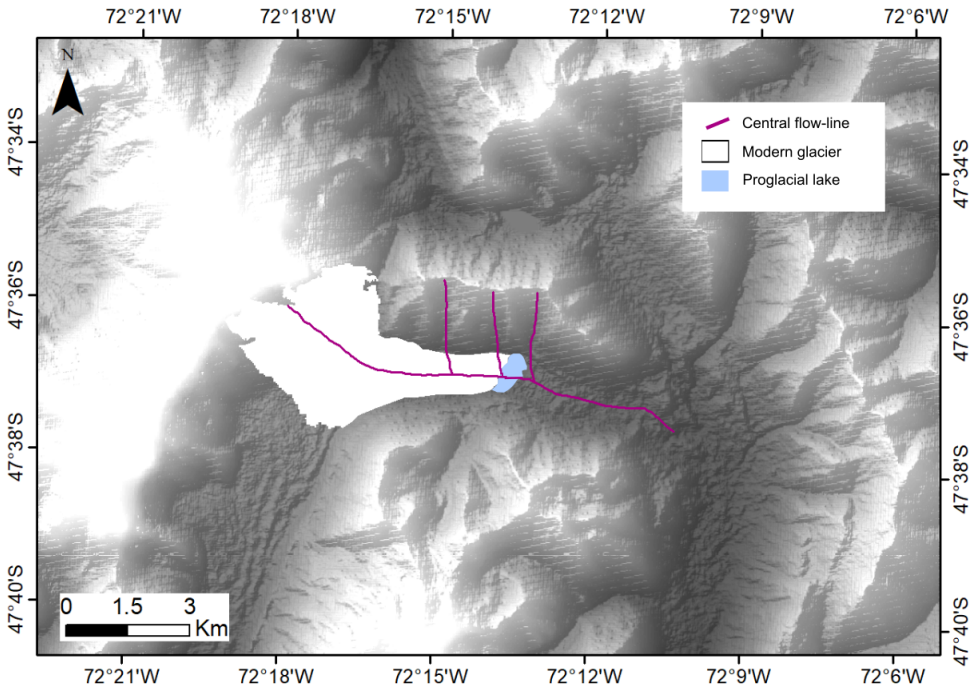

Figure 6.5: Map showing the central flow-line used in the glacier reconstruction and the extent of the Lacteo glacier and the proglacial lake as captured by the ASTER DEM, which was used as the basis for the glacier reconstruction. This glacier outline was used to calculate bed topography under the extant glacier using the inversion method of Benn and Hulton (2010).

Basal shear stress

Basal shear stress (τ_{av}) is a key parameter in Equation 6.1, which affects the reconstructed glacier thickness. τ_{av} normally lies between 50 and 150 kPa for valley glaciers (Paterson, 1994), but would vary between individual glaciers because of ice viscosity, basal water pressure, basal sliding and subglacial sediment deformation (Cuffy and Paterson, 2010). A constant τ_{av} value is used along the central flow-line because it has be shown to adequately reproduce ice thickness

values (Li et al., 2012). Ice thickness was initially calculated with the default basal shear stress of 100 kPa and then adjusted to fit the geomorphological evidence on the vertical ice extent. For the M1 terminal position, τ_{av} of 70 kPa was found to best fit the lateral moraines. Although, the perfect plasticity model assumes internal deformation only, for wet-based glaciers, basal sliding may contribute to motion and affect basal shear stress. Choosing τ_{av} value to fit the geomorphological evidence, rather than a reference value (e.g. Rea and Evans, 2007), should go some way to account for basal sliding (James et al., 2019).

Shape factor

The effect of lateral drag on ice flow in topographically constrained glaciers is accounted for by incorporating a shape factor (F) into the perfect plasticity model (Schilling and Hollin, 1981; Benn and Hulton, 2010). In the Glare model (Pellitero et al., 2016), this is defined as:

$$F = A/Hp \tag{6.3}$$

where, A is the cross-sectional area, H is the ice thickness and p is the length of the cross section ice-bed contact. The shape factor is calculated automatically at chosen valley cross-sections, representative of different parts of the valley, and propagated up-glacier.

ELA calculation

ELA is the altitude on a glacier where annual accumulation and annual ablation equal zero. Several methods for estimating past ELA have been developed. Here, two methods are used, the median glacier elevation (Hmed) and the accumulation-area ratio method (AAR). Both have been commonly used for calculating the ELA, including in Patagonia (e.g. Carrivick et al., 2016; Sagredo et al., 2016, 2018). The AAR assumes the accumulation area occupies a fixed proportion of a total area of a glacier in a steady state. Unlike the more complex Area-Altitude Balance Ratio method (AABR), the AAR method does not account for hypsometry or mass balance gradients (Osmaston, 1975; Furbish and Andrews, 1984). The AABR method is, however, unsuitable for debris covered glaciers and glaciers, which may receive snow avalanche input (Benn and Lehmkuhl, 2000). The Lacteo glacier may have been fed by avalanches or wind-blown snow and for this reason, the AABR method is not used here. Modern ELA at 1800 m asl, estimated by Falaschi et al. (2013) is used as a baseline for comparing the reconstructed ELAs. The ELA is calculated based on the reconstructed 3D glacier surface using an ArcGIS package written by Pellitero et al. (2015). A systematic error of ±30 m is considered given the spatial resolution of the DEM.

Table 6.2: Exposure ages

Sample	Lm Age	Lm Inter	Lm Exter	LSDn Age	LSDn Inter	LSDn Exter	St Age	St Inter	St Exter
		Years			Years			Years	
RV1610	2654	215	306	2639	214	303	2531	205	292
RV1611	2869	157	283	2850	156	280	2734	150	270
RV1612	2797	196	301	2776	194	298	2667	187	287
RV1613	3066	160	298	3050	159	295	2932	153	285
Stats:	*Mean=*	*2846*	*std= 171*	*Int =*	*373*	*Int+PR=*	*440*		

Scaling schemes: Lm - the time-dependent version of Lal (1991) and Stone (2000) LSDn - time-dependent scheme of Lifton et al. (2014)
St - time-independent version of Lal (1991) and Stone (2000).
Ages are reported with 1 internal and external uncertainties, the latter includes production rate and scaling uncertainties. Ages assume zero erosion and no correction for shielding by snow and/or vegetation. Elevation flag is std.
Grey shading indicates ages reported here.
Std - 1σ standard deviation, Int - propagated internal uncertainty, Int + PR - propagated internal uncertainty + production rate uncertainty.

6.4 Results and discussion

6.4.1 ^{10}Be chronology

The ^{10}Be ages for the M1 moraine are presented in Table 6.2 and probability distributions ('camelplots') are shown in Fig. 6.6. The ^{10}Be ages are internally consistent and yield a mean age of 2.8 ± 0.2 (1 σ std) ka. Post-depositional processes such as exhumation of boulders from the moraine matrix may complicate interpretation of landform ages. In a high mountain setting with a short sediment transport distance, inheritance is also likely to affect the exposure ages. The angular shape of boulders on the moraine may indicate supraglacial transport, and the possibility of a rockfall-derived material cannot be excluded. However, inheritance would be unique to each sample as it is very unlikely that all the sampled boulders would have been deposited with a pre-exposed surface up. The internal consistency of the ages indicates neither inheritance nor exhumation affected the ages. The mean moraine age of 2.8 ± 0.2 ka is thus considered a close minimum age for the deposition.

6.4.2 Glacier reconstruction and ELAs

The model reproduces the glacier surface profile at 2.8 ka well by applying basal shear stress of 70 kPa (Fig. 6.7), which was used for the ELA calculations. The AAR ratios between 0.55 and 0.65 are commonly used for mid-latitude glaciers

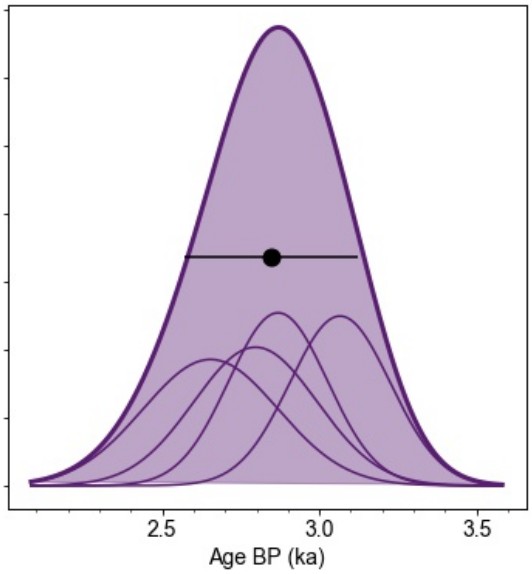

Figure 6.6: Probability distributions of the exposure ages from the M1 moraine deposited by the Lacteo glacier. Black circle shows the mean and error bar shows 1σ standard deviation.

(Porter, 1975; Sagredo et al., 2016; Kaplan et al., 2010; Putnam et al., 2012), and these yield an ELA in range of 1529 - 1479 m (Table 6.3). The Hmed method gives an ELA of 1579 m. The actual ELA may have been higher than the reconstructed ELAs for two reasons: 1) Input of snow from avalanching or wind-blown would affect the mass balance gradients. The Lacteo glacier may have received part of its accumulation from collapsed cornices developed on the headwall cliff of San Lorenzo. 2) Surface debris cover would also affect mass balance gradient. Thick debris cover would insulate the glacier surface and may expand the ablation area relative to the accumulation area, i.e. lower the AAR ratios, inhibiting glacier retreat (Clark et al., 1994; Benn and Lehmkuhl, 2000; Mills et al., 2012). Mills et al. (2012) proposed lowering the AAR values to 0.45 for valley glaciers with surface debris. Kulkarni (1992) suggested AAR of 0.44 for debris-covered glaciers in the Himalayas based on mass balance records. The angularity of boulders on the M1 moraine indicate that the Lacteo glacier may have had some supraglacial debris at this time. Applying the AAR of 0.45 would give slightly higher ELA of 1579 m. Potential presence of surface debris poses a challenge for palaeo-glacier reconstructions. The AAR values would likely be glacier-specific and would depend on the extent and thickness of surface debris cover and the local topography. To account for potential effects of external snow input and surface debris, a conservative ELA in a range of 1579 (AAR 0.45) - 1529 (AAR 0.55) m is proposed. This would imply a change of 221 - 271 m relative to present day. Using an adiabatic lapse rate of 0.6 °C/ 100 m (e.g. Sagredo et al., 2018; Kaplan et al., 2013; Wolff et al., 2013) and no change in precipitation, this

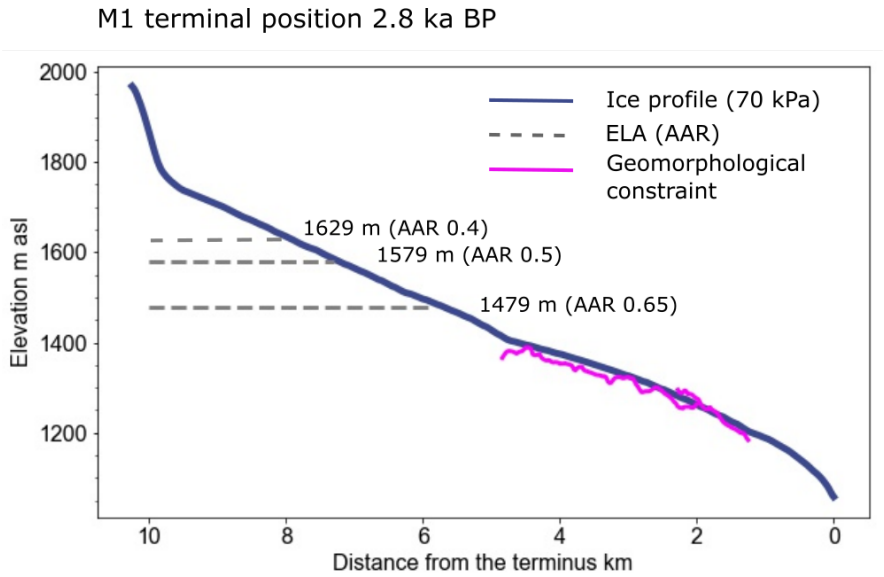

Figure 6.7: Modelled ice surface profile for the Lacteo glacier at the M1 terminal position. The modelled glacier surface profile matches the geomorphological constraints well with imposed basal shear stress of 70 kPa.

Table 6.3: Palaeo-ELAs (m asl) for the M1 (2.8 ka) terminal position of the Lacteo glacier calculated using different AARs and the median glacier elevation method.

AAR	0.4	0.45	0.5	0.55	0.6	0.65
ELA (m asl)	1629	1579	1579	1529	1529	1479
Hmed (m asl)	1579					

would imply a temperature lowering of $\sim$ 1.3 - 1.6 °C. Using a 'wet' lapse rate of 0.55 °C/100 m (cf. Putnam et al., 2012), gives a cooling of 1.2 - 1.5 °C.

6.4.3 Regional comparison

The ^{10}Be ages demonstrate that Lacteo glacier advanced/stabilised at 2.8 $\pm$ 0.2. The neighbouring San Lorenzo glacier likely advanced at a similar time as suggested by the morphostratigraphically equivalent moraine in the San Lorenzo valley. Both glaciers likely responded to the same climatic signal but further dating in the San Lorenzo valley is needed to confirm this. The next well-defined moraine in the Lacteo valley (M4) was abandoned by the Lacteo glacier prior to 1937 as shown by a historical photograph (Agostini, 1937 in Garibotti and Villalba, 2017). This advance likely correlates to the late 19th century advances identified around the NPI (e.g. Winchester and Harrison, 1996; Harrison and Winchester, 2000; Winchester et al., 2001; Harrison et al., 2007; Glasser et al., 2002, 2004). Historical aerial photographs from 1958 show the Lacteo and Lorenzo

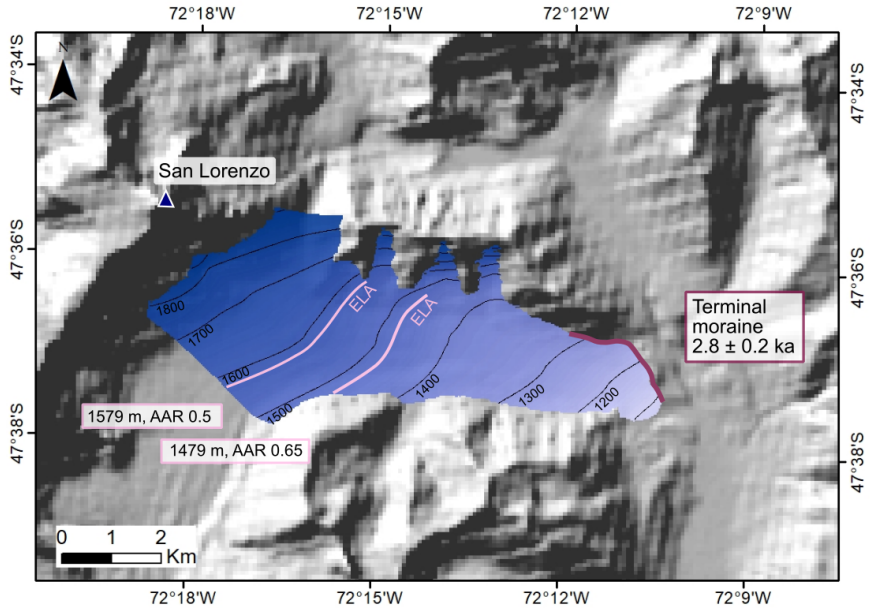

Figure 6.8: Reconstructed ice surface of the Lacteo glacier at 2.8 ka (basal shear stress of 70 kPa) and the ELA estimated using the AAR method with 0.5 and 0.65 ratios. Shaded relief base map was made using the SRTM DEM (30m).

glaciers with land-terminating margins retreating from the youngest moraines in the respective valleys (Garibotti and Villalba, 2017).

There are limited data on glacier activity in central Patagonia during the late Holocene, prior to the 19th century. Glacier advances between 3 and 2.2 ka were inferred from an offshore terrigenous sediment record recovered off the Chilean coast at 46° S (Siani et al., 2010) (Fig. 6.9). The Leones glacier (the NPI) deposited a terminal moraine before 2.5 ka as shown by OSL ages (Harrison et al., 2008). ^{10}Be ages from the same moraine are considerably younger (1.2 - 0.7 ka) and the authors suggest that the glacier may have occupied the same position for a longer time (Harrison et al., 2008). These advances may correlate with the advance of the Lacteo glacier at 2.8 ka. On the eastern side of the SPI, late Holocene advances occurred slightly later, from 2.3 - 2.0 ka (Kaplan et al., 2016) (Fig. 6.9). Glacier activity here has been linked to the persistence of the negative SAM (Moreno et al., 2014; Kaplan et al., 2016; Moreno et al., 2018; Reynhout et al., 2019). Based on a non-arboreal pollen record from southern Patagonia, Moreno et al. (2018) reconstructed phases of prolonged cold & wet and warm & dry events, which they attributed to the SAM (Fig. 6.9). The cold & wet phase between 2.7 and 0.2 ka, associated with the negative SAM (Moreno et al., 2018), coincided with expansion of the SPI glaciers (Kaplan et al., 2016; Reynhout et al., 2019). The advance of the Lacteo glacier occurred prior to this cold & wet phase (Moreno et al., 2018) and preceded by about 500 years the late Holocene advances of the SPI (Kaplan et al., 2016) (Fig. 6.9). In the Cordillera Darwin, the Marinelli

glacier also advanced earlier (3.8 - 2.4 ka, Hall et al., 2019), towards the end of a dry & warm phase observed in the non-arboreal pollen record (Moreno et al., 2018). Larger advances though, occurred after 1.3 ka (Hall et al., 2019). It is unclear if these differences are related to local climates, glacier specific factors (e.g. hypsometry, glacial dynamics) or preservation of moraines.

Cold and/or wet conditions between $\sim$ 3.5 and 2.5 ka were detected in a number of proxy records in southernmost (Kilian and Lamy, 2012; van Geel et al., 2000; Chambers et al., 2007) and northwestern Patagonia (Bertrand et al., 2008; Lamy et al., 2001). A high-resolution iron content record from the Chilean continental shelf (41° S), interpreted to reflect rainfall variability linked to the latitudinal position of the SWW, indicates a humid peak between 3.4 and 2.5 ka (Lamy et al., 2001). More widely, a climatic cooling at this time was documented in proxy records around the world, in particular in the North Atlantic (e.g. Van Geel et al., 1996; Bakke et al., 2010; Nesje et al., 2001; Renssen et al., 2006; Bond et al., 2001). A climatic perturbation during this time interval has been linked to reduced solar activity (e.g. van Geel et al., 2000; Bond et al., 2001; Chambers et al., 2007; Bertrand et al., 2008; Solomina et al., 2015), with two pronounced drops observed in the total solar irradiance record (Wu et al., 2018) (Fig. 6.9). Varma et al. (2011) demonstrated a significant correlation between the iron content record from Chile (Lamy et al., 2001) and solar activity over the last 3 ka. Through transient climate simulations they demonstrated a northwards displacement of the SWW at times of reduced solar activity (Varma et al., 2011). Coupled climate model demonstrated a global cooling at 2.7 ka in response to solar forcing, amplified by oceanic feedback in the North Atlantic (Renssen et al., 2006). Lara et al. (2020) also noted a persistent influence of total solar irradiance on the centennial temperature variability over the last $\sim$ 5.7 ka reconstructed using a composite tree-ring record from northern Patagonia. Variations in solar activity are generally considered to have played a role in the Holocene climate variability. However, disentangling forcing mechanisms is often problematic as is the case for the solar and volcanic forcings during the LIA (PAGES 2k Consortium, 2013). The advance of the Lacteo glacier at 2.8 ka may be a response to reduced solar activity and/or changes to the position/intensity of the SWW induced by solar irradiance.

The advance/still-stand of the Lacteo glacier at 2.8 ka required an estimated ELA lowering of 221 - 271 m relative to the present. This implies a potential cooling of $\sim$ 1.3 - 1.6 °C relative to present day, assuming an adiabatic lapse rate of 0.6 °C/ 100 m and no change in precipitation. Few other ELA estimates or quantitative temperature reconstructions for this time period exist to allow for comparison. Sagredo et al. (2016) estimated an ELA lowering of 130 - 170 m relative the present (the AAR of 0.55 - 0.66) to match a limit of the Tranquilo glacier on the northern flank of San Lorenzo assumed to date to the last millennium. This would require temperature lowering of 0.7 - 1.0 °C

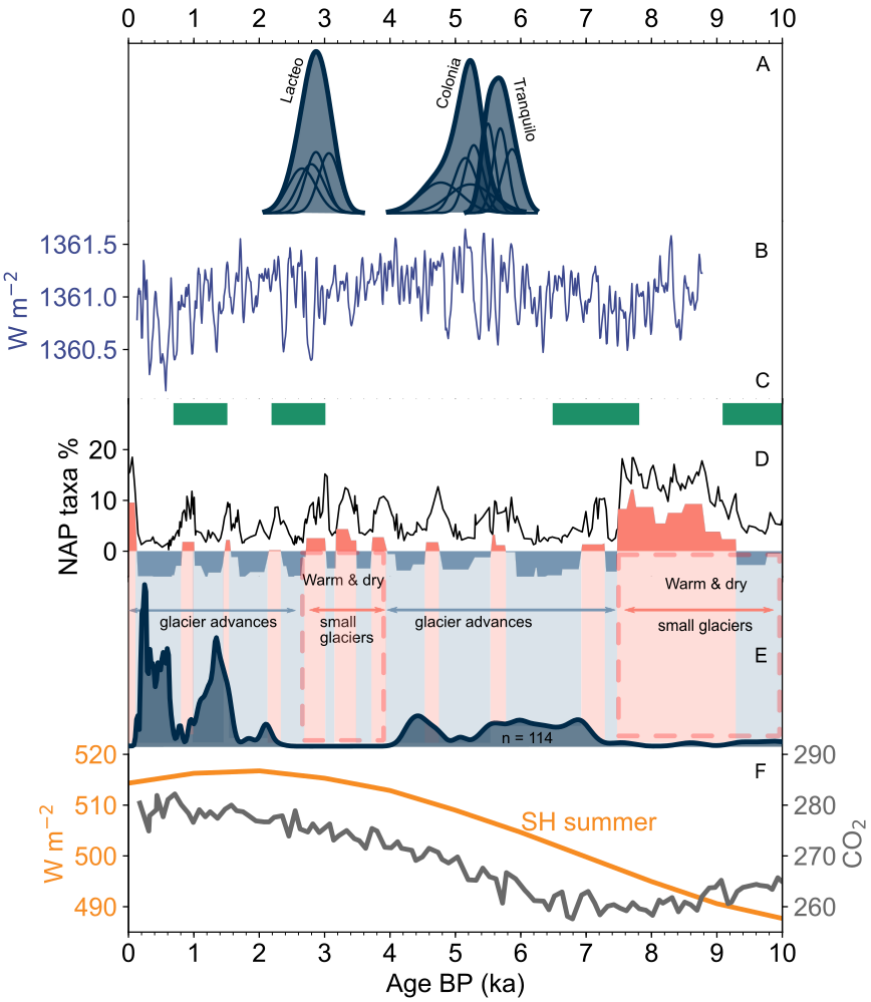

Figure 6.9: Comparison of the exposure ages from the Lacteo valley with other proxy records. A) Kernel probability density diagrams for exposure ages from the Lacteo glacier (this study), Tranquilo glacier (Sagredo et al., 2016) and Colonia glacier (Nimick et al., 2016). Each thin curve represents a Gaussian probability distribution of an individual exposure age, while the thick curves represent summed probabilities for a moraine. B) Reconstructed total solar irradiance (Wu et al., 2018) C) The timing of glacier advances inferred from the terrigenous sediment record off the Chilean coast at 46° S (Siani et al., 2010). D) Non-arboreal pollen taxa record from southern Patagonia (Moreno et al., 2018) and a regime shift analysis showing alternating warm/dry (light pink) and cold/wet events (light blue), linked to the SAM. E) Summed probability distribution of the exposure ages from outlet glaciers of the Southern Patagonian Icefield (Kaplan et al., 2016; Reynhout et al., 2019). F) Summer insolation intensity at 50° S (Berger and Loutre, 1991), and atmospheric CO_2 concentrations from the Dome C Antarctic ice core (Monnin et al., 2001).

relative to the present assuming the same adiabatic lapse rate and no precipitation change (Sagredo et al., 2016). A tree-ring based temperature reconstruction from northern Chilean Patagonia (41° S - 42° S) showed temperatures ∼ 0.5 - 1 °C lower than present between ∼ 3 - 2.7 ka (Lara et al., 2020). The estimated temperature lowering of ∼ 1.3 - 1.6 °C based on the ELA reconstruction presented here is plausible. However, these are maximum values given no change in precipitation was taken into account.

Additional insight into the earlier Holocene glacial history of the Lacteo glacier is afforded by a radiocarbon-dated tree stump from the distal edge of the M1 moraine (Mercer, 1968). Although the ^{10}Be ages showed that the M1 moraine is younger than the maximum bracketing ^{14}C age (5.2 ± 0.2 ka, Mercer, 1968), the latter may date an earlier advance. The radiocarbon-dated tree may have been killed by an advancing glacier, implying likely expansion of the Lacteo glacier at ∼ 5.2 ka. About 0.5 km down-valley from the M1 moraine, there is a ridge composed of diamicton, perched on a cliff edge, which may have been deposited during this earlier advance/still-stand. This is similar in timing to the advances of the Tranquillo glacier on the northern side of San Lorenzo at 5.7 ± 0.1 ka (Sagredo et al., 2016) and the Colonia glacier at 5.0 ± 0.2 ka (the NPI) (Nimick et al., 2016) (Fig. 6.9). Outlet glaciers of the SPI reached their maximum Holocene extent between 6.1 and 4.5 ka after recession in the early Holocene (Strelin et al., 2014, 2011; Kaplan et al., 2016). Further, Mercer (1968) described multiple rooted tree stumps in the section at the distal edge of the M1 moraine. This suggests that the trees were growing *in situ*, and the Lacteo glacier likely withdrew behind this moraine prior to 5.2 ka to allow colonization by trees. This is plausible given the warm and dry conditions in the early Holocene (∼ 10.5 - 7.5 ka) documented throughout Patagonia (e.g. Haberle and Bennett, 2004; Montade et al., 2013; Massaferro and Brooks, 2002; de Porras et al., 2012, 2014; Markgraf et al., 2007). Glacier recession in the early Holocene to near modern margins was also documented for glaciers of the SPI as well as in the Cordillera Darwin (Strelin et al., 2014, 2011; Kaplan et al., 2016; Hall et al., 2019).

The results presented in this chapter together with earlier work from the Lacteo valley (Mercer, 1968; Garibotti and Villalba, 2017) indicate a similar broad pattern of Holocene glacier change as observed elsewhere in Patagonia, i.e. recession in the early Holocene followed by advances during the mid- and late Holocene. This differs to a trend of decreasing glacier extent over the course of the Holocene observed in New Zealand (Schaefer et al., 2009; Putnam et al., 2012; Kaplan et al., 2013). In agreement with other studies (e.g. Kaplan et al., 2016; Harrison et al., 2008; Hall et al., 2019), results from the Lacteo valley also demonstrate that during the Holocene, glaciers in central Patagonia were greater in extent prior to the last millennium or the LIA. More work is needed to refine glacial chronologies, in particular in central and northern Patagonia, and to determine the causes of regional differences in the exact timing of glacial advances.

6.5 Conclusion

The ^{10}Be ages presented in this chapter demonstrate an advance/still-stand of the Lacteo glacier at 2.8 ± 0.2 ka. The reconstructed ELA at this time was between 221 - 271 m lower than the modern ELA. This implies a temperature lowering of ∼ 1.3 - 1.6 °C relative to the present assuming an adiabatic lapse rate of 0.6 °C/ 100 m and no change in precipitation. The San Lorenzo glacier likely advanced/stabilised at the same time based on morphostratigraphy but further dating is required to confirm this. These results demonstrate a greater Holocene glacier extent prior to the last millennium, a trend observed elsewhere in Patagonia. The advance at 2.8 ka broadly coincided with cooling observed in a number of proxy records regionally and worldwide and reduced solar activity.

Chapter 7

Conclusions



7.1 Synthesis of findings

The aim of this thesis was to reconstruct the glacial history of the climatically sensitive San Lorenzo ice cap and the Belgrano outlet glacier. In particular this thesis aimed to gain insights into 1) pre-gLGM glacial history, 2) glacier response to millennial-scale climate events during the LGIT, and 3) glacier change over the Holocene. To do so I undertook detailed geomorphological mapping to identify main limits (Ch 4), developed a chronology using cosmogenic surface exposure analysis to determine the timing of glacial advances and palaeolake drainage (Ch 5 - 7), and derived ELAs for the late Holocene ice limit (Ch 7). The principal conclusions from this work are as follows:

7.1.1 Geomorphological map

Chapter 4 presented a detailed map of the glacial geomorphology on the eastern side of San Lorenzo and the Belgrano valley based on mapping from high-resolution satellite imagery and DEMs, supported by field checking. The map provides higher detail than previous mapping efforts (e.g. Glasser et al., 2008; Wenzens, 2005) and the spatial coverage necessary for reconstructing the fluctuations of the Belgrano glacier and its tributaries.

The new mapping reveals a complex assemblage of landforms associated with the Klementek moraine limit, unrecognized by previous geomorphological mapping (Wenzens, 2005), and suggests that it may be a palimpsest feature deposited over multiple advances or by a combination of ice marginal and subglacial processes. Sedimentological work may clarify the genesis of these landforms and depositional processes and provide insights into ice dynamics.

Mapping of raised shorelines also clarified the relationship between palaeolakes and the glacial limits in the Belgrano valley. Proglacial lakes formed inside the Klementek and Menelik moraines as ice retreated and higher palaeolake levels exist above the modern Belgrano lake inside the Belgrano moraines. The mapped raised shorelines do not support a large palaeolake in the valley, which would have flooded the Menelik and Belgrano moraine systems as suggested by Horta et al. (2017).

There are areas which presented a major challenge for mapping due to difficult access and dense vegetation, in particular the western end of Lago Belgrano and the basins near the mountain front, as well as areas in the Belgrano valley south of the Río Belgrano, and these would benefit from further investigation.

7.1.2 Early glaciation and the gLGM

In Chapter 5, I dated the outermost, Klementek moraine system at 75.2 ± 2.8 ka using cosmogenic nuclide exposure dating of glaciofluvial cobbles from the associated outwash terrace. This is the first robustly dated glacial limit related to late MIS 5 in Patagonia. The second, considerably smaller advance occurred

at 24.8 ± 1.0 ka coeval with the gLGM dated by internally consistent moraine boulder and outwash cobble ages from the Menelik moraine system.

The main implications of these findings are twofold. First, it indicates that glaciation of the Patagonian Andes began early in the last glacial cycle during MIS 5. Although the precise timing may have varied, this is similar to the onset of mountain glaciation in the Himalayas and sectors of ice sheets in the NH. The San Lorenzo, the surrounding massifs and high mountain valleys acted as an ice nucleation centre, which developed into an independent ice cap. This work thus provides a significant insight into the inception of the PIS, previously only investigated through numerical modelling at regional scale (Sugden et al., 2002). Second, the topography and reduced snowfall on the lee-side of the growing PIS restricted ice extent in the Belgrano valley during later stages of the glacial cycle.

I suggested that build-up of the San Lorenzo Ice Cap and the advance of the Belgrano glacier towards the end of MIS 5 were driven by decreases in SH insolation as a first-order control, but this hypothesis requires further testing. Evidence for advances during late MIS 5 from the San Martín valley (Glasser et al., 2011) and New Zealand (Sutherland et al., 2007; Shulmeister et al., 2010) gives support to a common regional driver. The wide distribution of ages obtained from the Klementek outwash makes comparison to other palaeorecords and the assessment of possible triggers for glacier expansion problematic. As discussed in Chapter 5, the Klementek moraine/outwash system may be as old as 86 ka or it may have been deposited over 86 - 67 ka period. Obtaining additional ages or developing an outwash profile, should suitable sites be found, may increase the dating accuracy. The area south of the Río Belgrano, where the continuation of the Klementek moraines and outwash terraces is found, would be a candidate for further chronological work.

The advance at ∼ 25 ka occurred at a similar time to other glaciers in Patagonia and New Zealand (e.g. Denton et al., 1999b; Moreno et al., 2015; Darvill et al., 2016). Deglaciation from the 25 ka limit was characterised by gradual retreat and thinning as suggested by numerous small moraines within the moraine system. Initial ages suggest that the glacier margin may have remained outside of the trough until about 16 ka, but the deglaciation chronology requires further refinement.

7.1.3 Glacier response to millennial-scale cold reversals and palaeolake evolution.

In Chapter 6, I constrained the timing of Late Glacial advances/stillstands and reconstructed the evolution of palaeolake Belgrano. Cross-cutting moraine relationship and ^{10}Be ages reveal an extensive re-advance of the Belgrano glacier at 13.1 ± 0.6 ka to within 8 km of its 25 ka limit. Subsequently, rapid retreat of at least 10 km is inferred accompanied by a proglacial lake development. OSL ages from glaciolacustrine sediments and ^{10}Be from raised shorelines indicate that

the ice-dammed palaeolake formed at ∼ 12.7 ka and likely persisted for several hundred years, possibly up to a millennia. Together with a lateral moraine dated at 12.4 ± 0.3 ka, this indicates ice margin stabilisation at the time of the NH YD.

This work clarifies the response of glaciers in central Patagonia to millennial-scale climate events. It provides a strong evidence for a dominant Antarctic climate signal at these latitudes and also a co-occurrence of the NH YD signal. The San Lorenzo glaciers responded to the ACR signal near synchronously (within dating uncertainties) as supported by studies from the northern flank of San Lorenzo (Sagredo et al., 2018; Davies et al., 2018). Numerical simulation of deglaciation in this sector of Patagonia (Hubbard et al., 2005) matches well the geomorphological evidence on the extent of the San Lorenzo Ice Cap at ∼ 14 - 13 ka (Ch 6, Sagredo et al., 2018; Davies et al., 2018).

There are several aspects of the glacial and palaeolake history that would benefit from further refinement. For example, the rate of deglaciation after the culmination of the ACR advances/stillstands is only inferred based on the extent of mapped palaeoshorelines and the initial ages for the formation and duration of the palaeolake. The geomorphological mapping (Ch 3) did not reveal any younger moraines in the Belgrano valley, and any geomorphological evidence is likely submerged in the lake, or remains undiscovered in the less accessible and densely-vegetated western part of the valley. The lateral moraine in the Lacteo valley support stabilisation at 12 ka, but terminal moraines are not preserved. Based on the ^{10}Be ages from palaeoshorelines, I inferred that by the Late Glacial/Holocene transition, glaciers had likely withdrawn back to the mountains to allow the lake drainage. The drainage of the ice-dammed palaeolake Chalenko (12.4 - 11.8 ka, Thorndycraft et al., 2019) further supports this. Glacier configuration similar to the present by ∼ 11.5 ka was also shown by the numerical simulation by Hubbard et al. (2005).

These findings demonstrated a rapid landscape change, which may have implications for the human occupation of the valley. Evidence for human presence, such as cave paintings, is found immediately outside of the ACR ice margins and above the palaeolake Belgrano.

7.1.4 Holocene dynamics

In Chapter 6, I dated an advance/stillstand of the Lacteo glacier at 2.8 ± 0.2 ka. This required a lowering of the ELA by 221 - 271 m relative to the present. Assuming an adiabatic lapse rate of 0.6 °C/ 100 m and no change in precipitation, this translates to a temperature lowering of ∼ 1.3 - 1.6 °C. This is plausible as an upper limit, given no precipitation change is taken into account, but more ELA reconstructions and quantitative temperature records are needed to allow for comparison. The San Lorenzo glacier likely advanced/stabilised at a similar time as indicated by the morphostratigraphy and both glaciers thus likely responded to the same climatic signal. In both, Lacteo and San Lorenzo valleys, younger, well-defined moraines mark advances/stillstands (Garibotti and Villalba, 2017) that

may correlate to the late 19th century advances identified throughout the region (e.g. Winchester and Harrison, 1996; Harrison and Winchester, 2000; Winchester et al., 2001; Harrison et al., 2007; Glasser et al., 2002, 2004). The Holocene extent of these glaciers prior to 2.8 ka remains uncertain. The radiocarbon age and section described by Mercer (1968) indicate an earlier advance at 5.2 ± 0.2 ka and a likely recession to behind the 2.8 ka moraine during the early Holocene. During the Late Glacial at ∼ 13 ka, the Lacteo glacier terminated ∼ 20 km down valley from the 2.8 ka moraine and the San Lorenzo glacier contributed ice to the former Belgrano glacier (Ch 5). The results presented in this chapter together with earlier work from the Lacteo valley (Mercer, 1968; Garibotti and Villalba, 2017) demonstrate a trend of Holocene glacier change similar to elsewhere in Patagonia (e.g. Strelin et al., 2014, 2011; Kaplan et al., 2016; Hall et al., 2019), i.e. retreat in the early Holocene followed by advances/still-stands during the mid- and late Holocene and culminating in smaller advances/still-stands during the LIA. This differs to a trend of progressively smaller glaciers over the Holocene documented in New Zealand (Schaefer et al., 2009; Putnam et al., 2012; Kaplan et al., 2013). More work is needed to refine Holocene glacial chronologies in Patagonia and to determine factors responsible for regional differences. Finally, the advance at 2.8 ka identified in this chapter broadly coincided with a cooling documented by proxy records regionally (e.g. Kilian and Lamy, 2012; van Geel et al., 2000; Chambers et al., 2007; Lamy et al., 2001) and worldwide (e.g. Van Geel et al., 1996; Bakke et al., 2010; Nesje et al., 2001; Renssen et al., 2006; Bond et al., 2001) and may have been triggered by reduced solar activity (van Geel et al., 2000; Bond et al., 2001; Chambers et al., 2007; Bertrand et al., 2008; Solomina et al., 2015, cf.[]).

7.2 Implications

7.2.1 The role of topography, catchment size and ice-divides

One of the key implications of this work is that the topography, the shifting ice divides and catchment size played a key role in determining the magnitude of glacier advances between different valleys and influenced the build-up and break-up of the PIS in this sector. This is reflected in the magnitude of advances and the pattern of preserved limits in the Belgrano valley (75, 25 and 13 ka) compared to the neighbouring valleys. The Belgrano glacier reached its maximum extent early in the glacial cycle when it was fed by the independent San Lorenzo ice cap (Ch 5). Later the individual ice fields coalesced and the San Lorenzo was incorporated into the growing PIS. The ice-divide migrated west and accumulation was increasingly concentrated on the west, up-wind side of the PIS (cf. Sugden et al., 2002). San Lorenzo may have served as an independent ice dome, but it became starved of precipitation. In addition, ice flow re-routing may have reduced the catchment size of the Belgrano glacier. This resulted in a smaller extent of the Belgrano

glacier at 25 ka. A similar pattern of successively smaller ice limits is found in the Lago San Martín valley (Glasser et al., 2011), which may be a result of a similar interplay between the topography, precipitation availability, the shifting ice divide and ice-flow re-routing. In contrast, in the large basins of LBA and LP, the maximum limits of the last glacial cycle date to $\sim$ 35 - 27 ka (Hein et al., 2009, 2010; Kaplan et al., 2004, 2005; Douglass et al., 2006). Older limits from the last glacial cycle were either less extensive (and thus obliterated), removed by other process (e.g. meltwater) or remain to be discovered and dated. I speculate that these ice lobes only reached their maximum extent once they were able to acquire a maximum catchment size.

Conversely, during deglaciation, as the PIS was breaking up and thinning, the LBA and LP ice lobes lost large parts of their catchment area. Flowing at low elevations and calving into deep proglacial lakes, they disintegrated and by the ACR the margins were 100 - 120 km upstream of the LGM limits (Turner et al., 2005; Boex et al., 2013; Thorndycraft et al., 2019; Davies et al., 2018). San Lorenzo, emerging from the rainshadow of the PIS, was likely able to sustain an outlet glacier in the Belgrano valley for longer. However, this hypothesis requires further testing as there is limited data on the timing and extent of deglaciation prior to the ACR advance/still-stand. Thus a combination of reduced rainshadow effect relative to the gLGM, and the regional cooling during the ACR enabled the Belgrano glacier to advance close to its 25 ka limits.

Overall, this is important for two reasons: 1) It highlights the benefit of chronologies from multiple valleys 2) Non-climatic factors played a role in determining the magnitude of glacial advances and should be considered carefully before making inferences about regional climate.

7.2.2 How extensive was the mountain glaciation during MIS 5?

In Chapter 5 I suggested that a substantially large ice cap developed over San Lorenzo, which fed the Belgrano glacier and enabled it to advance 80 km from the mountain divide. As discussed above, preliminary results from the Lago San Martín valley also indicate the maximum ice extent during MIS 5 (Glasser et al., 2011). This raises a question about the extent of this early mountain glaciation. The area between the NPI and the SPI is characterised by high, currently glaciated massifs, including San Lorenzo and Sierra de Sangra, $\sim$ 100 km to the south of San Lorenzo. It is thus conceivable that this area would have supported ice development early in the glacial cycle, similar to San Lorenzo. The numerical simulation of the inception of PIS (Sugden et al., 2002) does not capture the development of an extensive ice cap over San Lorenzo and the area between the NPI and SPI is only glaciated once ice from the NPI and SPI ice centres coalesce. This seems to contrast with what the data presented in this thesis suggests. This

necessitates an updated modelling of the inception of the PIS to explore the ice dynamics and climatic forcing during the onset of glaciation.

7.3 Future research directions

- **The Klementek moraine system - sedimentological work and improved glacial chronology.** The geomorphological mapping (Ch 3) revealed a complex assemblage of landforms associated with the Klementek moraine system. Sedimentological work could clarify the depositional processes and provide insights into the ice dynamics. The age constraints on the Klementek limit can also be improved by: 1) Obtaining additional ages and/or developing an outwash profile from the Klementek moraine/outwash system (e.g. Hein et al., 2009; Darvill et al., 2015) 2) Stratigraphic investigation coupled with OSL dating in the area inside of the Klementek moraines on the southern side of the Río Belgrano (e.g. Smedley et al., 2016; Shulmeister et al., 2010, 2018). 3) Dating of palaeoshorelines inboard of the Klementek system can reveal the timing of deglaciation from this limit. Overall this can refine the chronology and provide additional insights into the glacial history (e.g. post-MIS 5).

- **The extent of MIS 5 glaciation.** Dating the limits of the Sierra de Sangra outlet glacier, immediately south of the Lago Belgrano valley, and further developing the chronology in the San Martín valley may provide further insights into the development of central sector of the PIS. Both of these glaciers drained ice from the sector between the NPI and SPI. Initial ages from the San Martín valley indicate that limits here were deposited over the last $\sim$ 100 ka (Glasser et al., 2011). New age constraints may help to establish the extent of this early glaciation and strengthen interpretations on the drivers of southern hemisphere glaciation. Together with the data presented in this thesis, it would provide empirical constraints for numerical simulation of the inception of the PIS.

- **MIS 4 and 3 in Patagonia.** The research in this thesis did not identify any limits dating to MIS 4 or MIS 3, even though the evidence reviewed in Chapter 2 suggest that conditions should have been favorable for ice expansion. Palaeoclimate proxies from the Southern Hemisphere indicate that MIS 4 was as cold as, or colder than MIS 2 (e.g. Kaiser et al., 2005; Johnsen et al., 1972; EPICA Community Members, 2004). Therefore it remains an open question whether the lack of evidence for MIS 4 ice advances in Patagonia is due to a lack of discovery, preservation potential or most glaciers were smaller than at later times. Targeting pre-gLGM moraines for dating, in particular further north ($< 46^\circ$ S) in Patagonia, where chronologies are sparse can help to resolve this question. For example, in the Chilean Lake District glacial advances during MIS 4 are suspected

but not dated (Heusser et al., 1999; Denton et al., 1999b). This may also help to reveal if extensive mid-MIS 3 advances (48 - 45 ka, Darvill et al., 2015; García et al., 2018) were confined to the southernmost Patagonia and thus may relate to a more southward position of the SWW during this time (cf. Darvill et al., 2015)?

- **Numerical modelling** The work presented in this thesis suggest the development of an independent ice cap/ice dome not captured by previous modelling experiment of the inception of the PIS (cf. Sugden et al., 2002). Thus there is a need for new numerical modelling to explore the ice dynamics during the build-up of the PIS and to test for climatic conditions necessary for ice expansion early in the last glacial cycle as revealed in this thesis. Further, chronological studies over the last decade have generated new empirical data (e.g. Hein et al., 2010; García et al., 2018; Darvill et al., 2015) that can be used to produce new modelled-based reconstructions of the PIS and explore different climate forcing.

- **Further geomorphological mapping and palaeolake evolution.** Detailed geomorphological mapping in the western, vegetated part of the Belgrano valley could identify post-ACR ice marginal positions, clarify the extent of the palaeolake Belgrano and identify potential cols. The evolution of the palaeolake Belgrano can be refined by obtaining additional exposure ages from palaeoshorelines, OSL ages from raised deltas and glaciolacutrine sediments, better shoreline elevation data (e.g. using a combination of LiDar and differential GPS) and accounting for isostatic rebound (cf. Thorndycraft et al., 2019). Glaciolacustrine sediments were mapped in the Belgrano valley (Ch 3) and these can be investigated for the potential of developing a varve chronology as has been done in the LBA valley (Bendle et al., 2017b). This has a potential to provide an annually-resolved chronology for deglaciation and can be compared to other proxies to elucidate climatic controls (cf. Bendle et al., 2017b, 2019).

- **Dating of raised shorelines**. I demonstrated that using cosmogenic nuclide exposure analysis on amalgamated pebbles from palaeoshorelines could be an effective tool for directly dating these features and the lowering/drainage of palaeolakes (Ch 5). Further work is required to constrain potential inheritance in such sediments, which can be achieved by obtaining multiple samples from the same shoreline, ideally combined with an independent chronometer, for example OSL. This approach can then be applied in similar environments elsewhere.

- **Holocene glacier dynamics.** This thesis only scratched the surface when it comes to understanding the Holocene glacier dynamics in the region. Developments in cosmogenic nuclide dating technique have enabled

increasingly younger surfaces to be dated (e.g. Kaplan et al., 2016; Reynhout et al., 2019) and this can be combined with other approaches to develop detailed chronologies. In addition to radiocarbon dating, measuring *in situ* $^{14}C/^{10}Be$ in proglacial bedrock can reveal when glaciers were smaller/larger than today (Goehring et al., 2011). Developing more detailed glacier chronologies would help to improve our understanding of glacier sensitivities to different climate signals in the region.

References

Abramowski, U., Bergau, A., Seebach, D., Zech, R., Glaser, B., Sosin, P., Kubik, P.W., Zech, W., 2006. Pleistocene glaciations of Central Asia: results from 10Be surface exposure ages of erratic boulders from the Pamir (Tajikistan), and the Alay-Turkestan range (Kyrgyzstan). Quaternary Science Reviews 25, 1080–1096.

Ackert, R., Becker, R.A., Singer, B.S., Kurz, M.D., Caffee, M.W., Mickelson, D.M., 2008. Patgonian Glacier Response during the Late Glacial Holocene Transition. Science 321, 392–396.

Anderson, R.F., Ali, S., Bradtmiller, L.I., Nielsen, S.H.H., Fleisher, M.Q., Anderson, B.E., Burckle, L.H., 2009. Wind-Driven Upwelling in the Southern Ocean and the Deglacial Rise in Atmospheric CO2. Science 323, 1443–1448.

Anderson, R.S., Dühnforth, M., Colgan, W., Anderson, L., 2012. Far-flung moraines: Exploring the feedback of glacial erosion on the evolution of glacier length. Geomorphology 179, 269–285.

Aniya, M., 1995. Holocene Glacial Chronology in Patagonia: Tyndall and Upsala Glaciers. Arctic and Alpine Research 27, 311.

Aniya, M., 1996. Holocene variations of Ameghino Glacier, southern Patagonia. Holocene 6, 247–252.

Aniya, M., Naruse, R., 1999. Late-Holocene glacial advances at Glaciar Soler, Hielo Patagonico Norte, South America. Transactions Japanese Geomorphological Union 20, 69–83.

Applegate, P.J., Urban, N.M., Laabs, B.J., Keller, K., Alley, R.B., 2010. Modeling the statistical distributions of cosmogenic exposure dates from moraines. Geoscientific Model Development 3, 293–307.

Aravena, J.C., Luckman, B.H., 2009. Spatio-temporal rainfall patterns in Southern South America. International Journal of Climatology 29, 2106–2120.

Ramírez de Arellano, C., Putlitz, B., Müntener, O., Ovtcharova, M., 2012. High precision U/Pb zircon dating of the Chaltén Plutonic Complex (Cerro Fitz Roy,

Patagonia) and its relationship to arc migration in the southernmost Andes. Tectonics 31, TC4009.

Bakke, J., Dahl, S.O., Paasche, Ø., Riis Simonsen, J., Kvisvik, B., Bakke, K., Nesje, A., 2010. A complete record of Holocene glacier variability at Austre Okstindbreen, northern Norway: an integrated approach. Quaternary Science Reviews 29, 1246–1262.

Balco, G., Stone, J.O., Lifton, N.A., Dunai, T.J., 2008. A complete and easily accessible means of calculating surface exposure ages or erosion rates from 10Be and 26Al measurements. Quaternary Geochronology 3, 174–195.

Balescu, S., Lamothe, M., 1993. Thermoluminescence dating of the holsteinian marine formation of Herzeele, northern France. Journal of Quaternary Science 8, 117–124.

Bamonte, F.P., Mancini, M.V., 2011. Palaeoenvironmental changes since Pleistocene-Holocene transition: Pollen analysis from a wetland in southwestern Patagonia (Argentina). Review of Palaeobotany and Palynology 165, 103–110.

Barrows, T.T., Juggins, S., De Deckker, P., Calvo, E., Pelejero, C., 2007. Long-term sea surface temperature and climate change in the Australian-New Zealand region. Paleoceanography 22, 1–17.

Bell, C.M., 2008. Punctuated drainage of an ice-damned Quaternary lake in Southern South America. Geografiska Annaler 90A, 1–17.

Bell, W.T., 1980. Alpha dose attenuation in quartz grains for thermoluminescence dating. Ancient TL 12, 4–8.

Bendle, J.M., Palmer, A.P., Thorndycraft, V.R., Matthews, I.P., 2017a. High-resolution chronology for deglaciation of the Patagonian Ice Sheet at Lago Buenos Aires (46.5°S) revealed through varve chronology and Bayesian age modelling. Quaternary Science Reviews 177, 314–339.

Bendle, J.M., Palmer, A.P., Thorndycraft, V.R., Matthews, I.P., 2019. Phased Patagonian Ice Sheet response to Southern Hemisphere atmospheric and oceanic warming between 18 and 17 ka. Scientific Reports 9, 4133.

Bendle, J.M., Thorndycraft, V.R., Palmer, A.P., 2017b. The glacial geomorphology of the Lago Buenos Aires and Lago Pueyrredón ice lobes of central Patagonia. Journal of Maps 13, 654–673.

Benn, D.I., Clapperton, C.M., 2000. Pleistocene glacitectonic landforms and sediments around central Magellan Strait, southernmost Chile: evidence for fast outlet glaciers with cold-based margins. Quaternary Science Reviews 19, 591–612.

Benn, D.I., Hulton, N.R.J., 2010. An Excel spreadsheet program for reconstructing the surface profile of former mountain glaciers and ice caps. Computers and Geosciences 36, 605–610.

Benn, D.I., Lehmkuhl, F., 2000. Mass balance and equilibrium-line altitudes of glaciers in high-mountain environments, in: Quaternary International, pp. 15–29.

Benn, D.I., Warren, C.R., Mottram, R.H., 2007. Calving processes and the dynamics of calving glaciers. Earth-Science Reviews 82, 143–179.

Bennett, K.D., Haberle, S.G., Lumley, S., 2000. The Last Glacial-Holocene Transition in Southern Chile. Science 290, 325–328.

Berger, A., Loutre, M.F., 1991. Insolation values for the climate of the last 10 million years. Quaternary Science Reviews 10, 297–317.

Bertrand, S., Charlet, F., Charlier, B., Renson, V., Fagel, N., 2008. Climate variability of southern Chile since the Last Glacial Maximum: A continuous sedimentological record from Lago Puyehue (40°S). Journal of Paleolimnology 39, 179–195.

Bertrand, S., Lange, C.B., Pantoja, S., Hughen, K., Van Tornhout, E., Wellner, J.S., 2017. Postglacial fluctuations of Cordillera Darwin glaciers (southernmost Patagonia) reconstructed from Almirantazgo fjord sediments. Quaternary Science Reviews 177, 265–275.

Bierman, P.R., Caffee, M.W., Davis, P.T., Marsella, K., Pavich, M., Colgan, P., Mickelson, D., Larsen, J., 2002. Rates and Timing of Earth Surface Processes From In Situ-Produced Cosmogenic Be-10. Reviews in Mineralogy and Geochemistry 50, 147–205.

Björck, S., Rundgren, M., Ljung, K., Unkel, I., Wallin, A., 2012. Multi-proxy analyses of a peat bog on Isla de los Estados, easternmost Tierra del Fuego: A unique record of the variable Southern Hemisphere Westerlies since the last deglaciation. Quaternary Science Reviews 42, 1–14.

Blunier, T., 2001. Timing of Millennial-Scale Climate Change in Antarctica and Greenland During the Last Glacial Period. Science 291, 109–112.

Blunier, T., Chappellaz, J., Schwander, J., Dällenbach, A., Stauffer, B., Stocker, T.F., Raynaud, D., Jouzel, J., Clausen, H.B., Hammer, C.U., Johnsen, S.J., 1998. Asynchrony of Antarctic and Greenland climate change during the last glacial period. Nature 394, 739–743.

Blunier, T., Schwander, J., Stauffer, B., Stocker, T., Dällenbach, A., Indermühle, A., Tschumi, J., Chappellaz, J., Raynaud, D., Barnola, J.M., 1997. Timing of

the Antarctic Cold Reversal and the atmospheric CO2 increase with respect to the Younger Dryas event. Geophysical Research Letters 24, 2683–2686.

Boex, J., Fogwill, C., Harrison, S., Glasser, N.F., Hein, A., Schnabel, C., Xu, S., 2013. Rapid thinning of the late Pleistocene Patagonian Ice Sheet followed migration of the Southern Westerlies. Scientific Reports 3, 2118.

Bond, G., Kromer, B., Beer, J., Muscheler, R., Evans, M.N., Showers, W., Hoffmann, S., Lotti-Bond, R., Hajdas, I., Bonani, G., 2001. Persistent solar influence on north atlantic climate during the Holocene. Science 294, 2130–2136.

Boone, S.J., Eyles, N., 2001. Geotechnical model for great plains hummocky moraine formed by till deformation below stagnant ice. Geomorphology 38, 109–124.

Borchers, B., Marrero, S., Balco, G., Caffee, M., Goehring, B., Lifton, N., Nishiizumi, K., Phillips, F., Schaefer, J., Stone, J., 2016. Geological calibration of spallation production rates in the CRONUS-Earth project. Quaternary Geochronology 31, 188–198.

Bøtter-Jensen, L., Andersen, C., Duller, G., Murray, A., 2003. Developments in radiation, stimulation and observation facilities in luminescence measurements. Radiation Measurements 37, 535–541.

Bourgois, J., Cisternas, M.E., Braucher, R., Bourlès, D., Frutos, J., 2016. Geomorphic Records along the General Carrera (Chile)Buenos Aires (Argentina) Glacial Lake (46° - 48°S), Climate Inferences, and Glacial Rebound for the Past 79 ka. The Journal of Geology 124, 27–53.

Boyce, E.S., Motyka, R.J., Truffer, M., 2007. Flotation and retreat of a lake-calving terminus, Mendenhall Glacier, southeast Alaska, USA. Journal of Glaciology 53, 211–224.

Boyd, B.L., Anderson, J.B., Wellner, J.S., Fernández, R.A., 2008. The sedimentary record of glacial retreat, Marinelli Fjord, Patagonia: Regional correlations and climate ties. Marine Geology 255, 165–178.

Bracegirdle, T.J., Shuckburgh, E., Sallee, J.B., Wang, Z., Meijers, A.J., Bruneau, N., Phillips, T., Wilcox, L.J., 2013. Assessment of surface winds over the atlantic, indian, and pacific ocean sectors of the southern ocean in cmip5 models: Historical bias, forcing response, and state dependence. Journal of Geophysical Research Atmospheres 118, 547–562.

Briner, J.P., Kaufman, D.S., Manley, W.F., Finkel, R.C., Caffee, M.W., 2005. Cosmogenic exposure dating of late Pleistocene moraine stabilization in Alaska. Bulletin of the Geological Society of America 117, 1108–1120.

Bronk Ramsey, C., 2009. Bayesian Analysis of Radiocarbon Dates. Radiocarbon 51, 337–360.

Buizert, C., Sigl, M., Severi, M., Markle, B.R., Wettstein, J.J., McConnell, J.R., Pedro, J.B., Sodemann, H., Goto-Azuma, K., Kawamura, K., Fujita, S., Motoyama, H., Hirabayashi, M., Uemura, R., Stenni, B., Parrenin, F., He, F., Fudge, T.J., Steig, E.J., 2018. Abrupt ice-age shifts in southern westerly winds and Antarctic climate forced from the north. Nature 563, 681–685.

Caldenius, C., 1932. Las glaciaciones cuaternarias en la Patagonia y Tierra del Fuego. Geografiska Annaler 14, 1–164.

Caniupán, M., Lamy, F., Lange, C.B., Kaiser, J., Arz, H., Kilian, R., Baeza Urrea, O., Aracena, C., Hebbeln, D., Kissel, C., Laj, C., Mollenhauer, G., Tiedemann, R., 2011. Millennial-scale sea surface temperature and Patagonian Ice Sheet changes off southernmost Chile (53°S) over the past 60 kyr. Paleoceanography 26, PA3221.

Caniupán, M., Lamy, F., Lange, C.B., Kaiser, J., Kilian, R., Arz, H.W., Leon, T., Mollenhauer, G., Sandoval, S., De Pol-Holz, R., Pantoja, S., Wellner, J., Tiedemann, R., 2014. Holocene sea-surface temperature variability in the Chilean fjord region. Quaternary Research (United States) 82, 342–53.

Carrivick, J.L., Davies, B.J., James, W.H.M., Quincey, D.J., Glasser, N.F., 2016. Distributed ice thickness and glacier volume in southern South America. Global and Planetary Change 146, 122–132.

Chambers, F.M., Mauquoy, D., Brain, S.A., Blaauw, M., Daniell, J.R., 2007. Globally synchronous climate change 2800 years ago: Proxy data from peat in South America. Earth and Planetary Science Letters 253, 439–444.

Chandler, B.M., Lovell, H., Boston, C.M., Lukas, S., Barr, I.D., Benediktsson, I.Ø., Benn, D.I., Clark, C.D., Darvill, C.M., Evans, D.J., Ewertowski, M.W., Loibl, D., Margold, M., Otto, J.C., Roberts, D.H., Stokes, C.R., Storrar, R.D., Stroeven, A.P., 2018. Glacial geomorphological mapping: A review of approaches and frameworks for best practice. Earth-Science Reviews 185, 806–846.

Clague, J.J., Barendregt, R.W., Menounos, B., Roberts, N.J., Rabassa, J., Martinez, O., Ercolano, B., Corbella, H., Hemming, S.R., 2020. Pliocene and Early Pleistocene glaciation and landscape evolution on the Patagonian Steppe, Santa Cruz province, Argentina. Quaternary Science Reviews 227.

Clapperton, C.M., 1989. Asymmetrical drumlins in Patagonia, Chile. Sedimentary Geology 62, 387–398.

Clapperton, C.M., 1993. Nature of environmental changes in South America at the Last Glacial Maximum. Palaeogeography, Palaeoclimatology, Palaeoecology 101, 189–208.

Clark, D.H., Clark, M.M., Gillespie, A.R., 1994. Debris-covered glaciers in the sierra nevada, california, and their implications for snowline reconstructions. Quaternary Research 41, 139–153.

Clark, P.U., Dyke, A.S., Shakun, J.D., Carlson, A.E., Clark, J., Wohlfarth, B., Mitrovica, J.X., Hostetler, S.W., McCabe, A.M., 2009. The Last Glacial Maximum. Science 325, 710–714.

Cogez, A., Herman, F., Pelt, E., Reuschlé, T., Morvan, G., Darvill, C.M., Norton, K.P., Christl, M., Märki, L., Chabaux, F., 2018. U-Th and 10Be constraints on sediment recycling in proglacial settings, Lago Buenos Aires, Patagonia. Earth Surface Dynamics 6, 121–140.

Cuffy, K., Paterson, W.S.B., 2010. The Physics of Glaciers. Butterworth-Heinemann/Elsevier, Burlington, MA. 4th ed. edition.

Darvill, C.M., 2013. Cosmogenic nuclide analysis. Geomophological techniques 10, 1–25.

Darvill, C.M., Bentley, M.J., Stokes, C.R., Hein, A.S., Rodés, À., 2015. Extensive MIS 3 glaciation in southernmost Patagonia revealed by cosmogenic nuclide dating of outwash sediments. Earth and Planetary Science Letters 429, 157–169.

Darvill, C.M., Bentley, M.J., Stokes, C.R., Shulmeister, J., 2016. The timing and cause of glacial advances in the southern midlatitudes during the last glacial cycle based on a synthesis of exposure ages from Patagonia and New Zealand. Quaternary Science Reviews 149, 200–214.

Darvill, C.M., Stokes, C.R., Bentley, M.J., Evans, D.J., Lovell, H., 2017. Dynamics of former ice lobes of the southernmost Patagonian Ice Sheet based on a glacial landsystems approach. Journal of Quaternary Science 32, 857–876.

Darvill, C.M., Stokes, C.R., Bentley, M.J., Lovell, H., 2014. A glacial geomorphological map of the southernmost ice lobes of Patagonia: the Bahía Inútil San Sebastián, Magellan, Otway, Skyring and Río Gallegos lobes. Journal of Maps 10, 500–520.

Darwin, C., 1842. On the distribution of erratic boulders and on the contemporaneous unstratified deposits of South America. Transactions Geological Society London Second Ser, 415–431.

Davies, B., Thorndycraft, V., Fabel, D., Martin, J., 2018. Asynchronous glacier dynamics during the Antarctic Cold Reversal in central Patagonia. Quaternary Science Reviews 200, 287–312.

Davies, B.J., Darvill, C.M., Lovell, H., Bendle, J.M., Dowdeswell, J.A., Fabel, D., García, J.L., Geiger, A., Glasser, N.F., Gheorghiu, D.M., Harrison, S., Hein, A.S., Kaplan, M.R., Martin, J.R., Mendelova, M., Palmer, A., Pelto, M., Rodés, ., Sagredo, E.A., Smedley, R., Smellie, J.L., Thorndycraft, V.R., 2020. The evolution of the Patagonian Ice Sheet from 35 ka to the present day (PATICE). Earth-Science Reviews , 103152.

Davies, B.J., Glasser, N.F., 2012. Accelerating shrinkage of Patagonian glaciers from the Little Ice Age (AD 1870) to 2011. Journal of Glaciology 58, 1063–1084.

De Angelis, H., Miles, E., Moelg, N., Paul, F., Sharp, M., Wyatt, F., 2015. GLIMS Glacier Database.

Denton, G., Heusser, C.J., Lowel, T., Moreno, P., Andersen, B., Heusser, L.E., Schluhter, C., Marchant, D., 1999a. Interhemispheric Linkage of Paleoclimate During the Last Glaciation. Geografiska Annaler, Series A: Physical Geography 81, 107–153.

Denton, G.H., Anderson, R.F., Toggweiler, J.R., Edwards, R.L., Schaefer, J.M., Putnam, a.E., 2010. The Last Glacial Termination. Science 328, 1652–1656.

Denton, G.H., Lowell, T.V., Heusser, C.J., Schluchter, C., Andersen, B.G., Heusser, L.E., Moreno, P.I., Marchant, D.R., 1999b. Geomorphology, stratigraphy, and radiocarbon chronology of Llanquihue Drift in the area of the Southern Lake District, Seno Reloncavi, and Isla Grande de Chiloe, Chile. Geografiska Annaler Series A Physical Geography 81 A, 167–229.

Dong, G., Zhou, W., Yi, C., Fu, Y., Zhang, L., Li, M., 2018. The timing and cause of glacial activity during the last glacial in central Tibet based on 10Be surface exposure dating east of Mount Jaggang, the Xainza range. Quaternary Science Reviews 186, 284–297.

Doughty, A.M., Schaefer, J.M., Putnam, A.E., Denton, G.H., Kaplan, M.R., Barrell, D.J.A., Andersen, B.G., Kelley, S.E., Finkel, R.C., Schwartz, R., 2015. Mismatch of glacier extent and summer insolation in Southern Hemisphere mid-latitudes. Geology 43, 407–410.

Douglass, D., Singer, B., Kaplan, M., Mickelson, D., Caffee, M., 2006. Cosmogenic nuclide surface exposure dating of boulders on last-glacial and late-glacial moraines, Lago Buenos Aires, Argentina: Interpretive strategies and paleoclimate implications. Quaternary Geochronology 1, 43–58.

Douglass, D.C., Bockheim, J.G., 2006. Soil-forming rates and processes on Quaternary moraines near Lago Buenos Aires, Argentina. Quaternary Research 65, 293–307.

Douglass, D.C., Singer, B.S., Ackert, R.P., Kaplan, M.R., Caffee, M.W., 2007. Constraining Boulder Erosion Rates and Ages of Mid-Pleistocene Moraines. Lago Buenos Aires, Argentina. GSA Abstracts and Programs Northeastern Section, 42nd Annual Meeting .

Douglass, D.C., Singer, B.S., Kaplan, M.R., Ackert, R.P., Mickelson, D.M., Caffee, M.W., 2005. Evidence of early Holocene glacial advances in southern South America from cosmogenic surface-exposure dating. Geology 33, 237–240.

Durcan, J.A., King, G.E., Duller, G.A., 2015. DRAC: Dose Rate and Age Calculator for trapped charge dating. Quaternary Geochronology 28, 54–61.

EPICA Community Members, 2004. Eight glacial cycles from an Antarctic ice core. Nature 429, 623–628.

EPICA Community Members, 2006. One-to-one coupling of glacial climate variability in Greenland and Antarctica. Nature 444, 195–198.

Evans, D.J., Orton, C., 2015. Heinabergsjökull and Skalafellsjökull, Iceland: active temperate piedmont lobe and outwash head glacial landsystem. Journal of Maps 11, 415–431.

Falaschi, D., Bolch, T., Rastner, P., Lenzano, M.G., Lenzano, L., Lo Vecchio, A., Moragues, S., 2017. Mass changes of alpine glaciers at the eastern margin of the Northern and Southern Patagonian Icefields between 2000 and 2012. Journal of Glaciology 63, 258–272.

Falaschi, D., Bravo, C., Masiokas, M., Villalba, R., Rivera, A., 2013. First Glacier Inventory and Recent Changes in Glacier Area in the Monte San Lorenzo Region (47°S), Southern Patagonian Andes, South America. Arctic, Antarctic, and Alpine Research 45, 19–28.

Falaschi, D., Huber, J., 2017. GLIMS Glacier Database.

Farquharson, L., Mann, D., Rittenour, T., Groves, P., Grosse, G., Jones, B., 2018. Alaskan marine transgressions record out-of-phase Arctic Ocean glaciation during the last interglacial. Geology 46, 783–786.

Feruglio, E., 1944. Estudios geológicos y glaciológicos en la región del Lago Argentino (Patagonia).

Finkel, R.C., Owen, L.A., Barnard, P.L., Caffee, M.W., 2003. Beryllium-10 dating of Mount Everest moraines indicates a strong monsoon influence and glacial synchroneity throughout the Himalaya. Geology 31, 561.

Fletcher, M.S., Moreno, P.I., 2012. Have the Southern Westerlies changed in a zonally symmetric manner over the last 14,000 years? A hemisphere-wide take on a controversial problem. Quaternary International 253, 32–46.

Fogwill, C.J., Kubik, P.W., 2005. A glacial stage spanning the Antarctic Cold Reversal in Torres del Paine (51°S), Chile, based on preliminary cosmogenic exposure ages. Geografiska Annaler, Series A: Physical Geography 87, 403–408.

Foresta, L., Gourmelen, N., Weissgerber, F., Nienow, P., Williams, J.J., Shepherd, A., Drinkwater, M.R., Plummer, S., 2018. Heterogeneous and rapid ice loss over the Patagonian Ice Fields revealed by CryoSat-2 swath radar altimetry. Remote Sensing of Environment 211, 441–455.

Furbish, D.J., Andrews, J.T., 1984. The use of hypsometry to indicate long-term stability and response of valley glaciers to changes in mass transfer. Journal of Glaciology 30, 199–211.

Galbraith, R., Laslett, G., 1993. Statistical models for mixed fission track ages. Nuclear Tracks and Radiation Measurements 21, 459–470.

Galbraith, R.F., Roberts, R.G., Laslett, G.M., Yoshida, H., Olley, J.M., 1999. Optical dating of single and multiple grains of quartz from Jinmium rock shelter, northern Australia: Part I, experimental design and statistical models. Archaeometry 41, 339–364.

García, J.L., Hall, B.L., Kaplan, M.R., Vega, R.M., Strelin, J.A., 2014. Glacial geomorphology of the Torres del Paine region (southern Patagonia): Implications for glaciation, deglaciation and paleolake history. Geomorphology 204, 599–616.

García, J.L., Hein, A.S., Binnie, S.A., Gómez, G.A., González, M.A., Dunai, T.J., 2018. The MIS 3 maximum of the Torres del Paine and Última Esperanza ice lobes in Patagonia and the pacing of southern mountain glaciation. Quaternary Science Reviews 185, 9–26.

García, J.L., Kaplan, M.R., Hall, B.L., Schaefer, J.M., Vega, R.M., Schwartz, R., Finkel, R., 2012. Glacier expansion in southern Patagonia throughout the Antarctic cold reversal. Geology 40, 859–862.

García, J.L., Maldonado, A., De Porras, M.E., Delaunay, A.N., Reyes, O., Ebensperger, C.A., Binnie, S.A., Lüthgens, C., Méndez, C., 2019. Early deglaciation and paleolake history of Río Cisnes Glacier, Patagonian Ice Sheet (44°S). Quaternary Research (United States) 91, 194–217.

Garibotti, I.A., Villalba, R., 2017. Colonization of mid- and late-Holocene moraines by lichens and trees in the Magellanic sub-Antarctic province. Polar Biology 40, 1739–1753.

Garreaud, R., Lopez, P., Minvielle, M., Rojas, M., 2013. Large-scale control on the Patagonian climate. Journal of Climate 26, 215–230.

Garreaud, R.D., Vuille, M., Compagnucci, R., Marengo, J., 2009. Present-day South American climate. Palaeogeography, Palaeoclimatology, Palaeoecology 281, 180–195.

van Geel, B., Heusser, C., Renssen, H., Schuurmans, C., 2000. Climatic change in Chile at around 2700 BP and global evidence for solar forcing: a hypothesis. The Holocene 10, 659–664.

Gillespie, A., Molnar, P., 1995. Asynchronous maximum advances of mountain and continental glaciers. Reviews of Geophysics 33, 311–364.

Gilli, A., Anselmetti, F.S., Ariztegui, D., Beres, M., McKenzie, J.A., Markgraf, V., 2005. Seismic stratigraphy, buried beach ridges and contourite drifts: The Late Quaternary history of the closed Lago Cardiel basin, Argentina (49°S). Sedimentology 52, 1–23.

Gilli, A., Anselmetti, F.S., Ariztegui, D., Bradbury, J.P., Kelts, K.R., Markgraf, V., McKenzie, J.A., 2001. Tracking abrupt climate change in the Southern Hemisphere: a seismic stratigraphic study of Lago Cardiel, Argentina (49°S). Terra Nova 13, 443–448.

Glasser, N.F., Ghiglione, M.C., 2009. Structural, tectonic and glaciological controls on the evolution of fjord landscapes. Geomorphology 105, 291–302.

Glasser, N.F., Hambrey, M.J., Aniya, M., 2002. An advance of Soler Glacier, North Patagonian Icefield, at c. AD 1222-1342. The Holocene 12, 113–120.

Glasser, N.F., Harrison, S., Ivy-Ochs, S., Duller, G.A.T., Kubik, P.W., 2006. Evidence from the Rio Bayo valley on the extent of the North Patagonian Icefield during the Late Pleistocene-Holocene transition. Quaternary Research 65, 70–77.

Glasser, N.F., Harrison, S., Schnabel, C., Fabel, D., Jansson, K.N., 2012. Younger Dryas and early Holocene age glacier advances in Patagonia. Quaternary Science Reviews 58, 7–17.

Glasser, N.F., Harrison, S., Winchester, V., Aniya, M., 2004. Late Pleistocene and Holocene palaeoclimate and glacier fluctuations in Patagonia. Global and Planetary Change 43, 79–101.

Glasser, N.F., Holt, T.O., Evans, Z.D., Davies, B.J., Pelto, M., Harrison, S., 2016. Recent spatial and temporal variations in debris cover on Patagonian glaciers. Geomorphology 273, 202–216.

Glasser, N.F., Jansson, K.N., 2005. Fast-flowing outlet glaciers of the Last Glacial Maximum Patagonian Icefield. Quaternary Research 63, 206–211.

Glasser, N.F., Jansson, K.N., Goodfellow, B.W., de Angelis, H., Rodnight, H., Rood, D.H., 2011. Cosmogenic nuclide exposure ages for moraines in the Lago San Martin Valley, Argentina. Quaternary Research 75, 636–646.

Glasser, N.F., Jansson, K.N., Harrison, S., Kleman, J., 2008. The glacial geomorphology and Pleistocene history of South America between 38°S and 56°S. Quaternary Science Reviews 27, 365–390.

Glasser, N.F., Jansson, K.N., Harrison, S., Rivera, A., 2005. Geomorphological evidence for variations of the North Patagonian Icefield during the Holocene. Geomorphology 71, 263–277.

Goehring, B.M., Schaefer, J.M., Schluechter, C., Lifton, N.A., Finkel, R.C., Jull, A.J., Akçar, N., Alley, R.B., 2011. The Rhone Glacier was smaller than today for most of the Holocene. Geology 39, 679–682.

Gosse, J.C., Phillips, F.M., 2001. Terrestrial in situ cosmogenic nuclides: Theory and application. Quaternary Science Reviews 20, 1475–1560.

Goyanes, G., Massabie, A., 2015. Push moraines in the upper valley of Santa Cruz river , southwest Argentina . Structural analysis and relationship with Late Pleistocene paleoclimate. Journal of South American Earth Sciences 57, 1–11.

Guérin, G., Mercier, N., Adamiec, G., 2011. Dose-rate conversion factors: update. Ancient TL 29, 5–8.

Guérin, G., Mercier, N., Nathan, R., Adamiec, G., Lefrais, Y., 2012. On the use of the infinite matrix assumption and associated concepts: A critical review. Radiation Measurements 47, 778–785.

Gutiérrez, F., Gioncada, A., González Ferran, O., Lahsen, A., Mazzuoli, R., 2005. The Hudson Volcano and surrounding monogenetic centres (Chilean Patagonia): An example of volcanism associated with ridge-Trench collision environment. Journal of Volcanology and Geothermal Research 145, 207–233.

Haberle, S.G., Bennett, K.D., 2004. Postglacial formation and dynamics of North Patagonian Rainforest in the Chonos Archipelago, Southern Chile. Quaternary Science Reviews 23, 2433–2452.

Haddam, N.A., Siani, G., Michel, E., Kaiser, J., Lamy, F., Duchamp-Alphonse, S., Hefter, J., Braconnot, P., Dewilde, F., Isgüder, G., Tisnerat-Laborde, N., Thil, F., Durand, N., Kissel, C., 2018. Changes in latitudinal sea surface temperature gradients along the Southern Chilean margin since the last glacial. Quaternary Science Reviews 194, 62–76.

Hall, B., Lowell, T., Bromley, G., Denton, G., Putnam, A., 2019. Holocene glacier fluctuations on the northern flank of Cordillera Darwin, southernmost South America. Quaternary Science Reviews 222, 105904.

Hall, B.L., Denton, G., Lowell, T., Bromley, G.R.M., Putnam, A.E., 2017. Retreat of the Cordillera Darwin icefield during Termination I. Cuadernos de Investigación Geográfica 43, 751.

Hall, B.L., Porter, C.T., Denton, G.H., Lowell, T.V., Bromley, G.R.M., 2013. Extensive recession of Cordillera Darwin glaciers in southernmost South America during Heinrich Stadial 1. Quaternary Science Reviews 62, 49–55.

Hallet, B., Putkonen, J., 1994. Surface dating of dynamic landforms: Young boulders on aging moraines. Science 265, 937–940.

Harrison, S., Glasser, N., Winchester, V., Haresign, E., Warren, C., Duller, G.a.T., Bailey, R., Ivy-Ochs, S., Jansson, K., Kubik, P., 2008. Glaciar León, Chilean Patagonia: late-Holocene chronology and geomorphology. The Holocene 18, 643–652.

Harrison, S., Glasser, N.F., 2011. The Pleistocene Glaciations of Chile. Developments in Quaternary Science 15, 739–756.

Harrison, S., Glasser, N.F., Duller, G.A.T., Jansson, K.N., 2012. Early and mid-Holocene age for the Tempanos moraines, Laguna San Rafael, Patagonian Chile. Quaternary Science Reviews 31, 82–92.

Harrison, S., Winchester, V., 2000. Nineteenth- and Twentieth-Century Glacier Fluctuations and Climatic Implications in the Arco and Colonia Valleys, Hielo Patagónico Norte, Chile. Arctic, Antarctic, and Alpine Research 32, 55–63.

Harrison, S., Winchester, V., Glasser, N., 2007. The timing and nature of recession of outlet glaciers of Hielo Patagónico Norte, Chile, from their Neoglacial IV (Little Ice Age) maximum positions. Global and Planetary Change 59, 67–78.

Hays, J.D., Imbrie, J., Shackleton, N.J., 1976. Variations in the Earth's Orbit: Pacemaker of the Ice Ages. Science 194, 1121–1132.

Hein, A.S., 2009. Quaternary Glaciations in the Lago Pueyrredon Valley, Argentina. Ph.D. thesis. The University of Edinburgh.

Hein, A.S., Cogez, A., Darvill, C.M., Mendelova, M., Kaplan, M.R., Herman, F., Dunai, T.J., Norton, K., Xu, S., Christl, M., Rodés, À., 2017. Regional mid-Pleistocene glaciation in central Patagonia. Quaternary Science Reviews 164, 77–94.

Hein, A.S., Dunai, T.J., Hulton, N.R.J., Xu, S., 2011. Exposure dating outwash gravels to determine the age of the greatest Patagonian glaciations. Geology 39, 103–106.

Hein, A.S., Hulton, N.R., Dunai, T.J., Schnabel, C., Kaplan, M.R., Naylor, M., Xu, S., 2009. Middle Pleistocene glaciation in Patagonia dated by cosmogenic-nuclide measurements on outwash gravels. Earth and Planetary Science Letters 286, 184–197.

Hein, A.S., Hulton, N.R., Dunai, T.J., Sugden, D.E., Kaplan, M.R., Xu, S., 2010. The chronology of the Last Glacial Maximum and deglacial events in central Argentine Patagonia. Quaternary Science Reviews 29, 1212–1227.

Henríquez, W.I., Villa-Martínez, R., Vilanova, I., De Pol-Holz, R., Moreno, P., 2016. The Last Glacial Termination on the eastern flank of the central Patagonian Andes (47°S). Climate of the Past Discussions , 1–36.

Henríquez, W.I., Villa-Martínez, R., Vilanova, I., De Pol-Holz, R., Moreno, P.I., 2017. The last glacial termination on the eastern flank of the central Patagonian Andes (47 ° S). Climate of the Past 13, 879–895.

Herber, L., 1969. Separation of feldspar from quartz by flotation. The American Mineralogist 54, 1212–1215.

Heusser, L., Heusser, C., Kleczkowski, A., Crowhurst, S., 1999. A 50,000-yr Pollen Record from Chile of South American Millennial-Scale Climate Instability during the Last Glaciation. Quaternary Research 52, 154–158.

Heyman, J., Applegate, P.J., Blomdin, R., Gribenski, N., Harbor, J.M., Stroeven, A.P., 2016. Boulder height exposure age relationships from a global glacial 10Be compilation. Quaternary G 34, 1–11.

Heyman, J., Stroeven, A.P., Harbor, J.M., Caffee, M.W., 2011. Too young or too old: Evaluating cosmogenic exposure dating based on an analysis of compiled boulder exposure ages. Earth and Planetary Science Letters 302, 71–80.

Hogg, A.G., Hua, Q., Blackwell, P.G., Niu, M., Buck, C.E., Guilderson, T.P., Heaton, T.J., Palmer, J.G., Reimer, P.J., Reimer, R.W., Turney, C.S.M., Zimmerman, S.R.H., 2013. SHCal13 Southern Hemisphere Calibration, 0-50,000 Years cal BP. Radiocarbon 55, 1889–1903.

Horta, L.R., Georgieff, S.M., Aschero, C.A., Goñi, R.A., 2017. Paleolacustrine records from Late Pleistocene Holocene in the Perito Moreno National Park, Argentinian Patagonian Andes. Quaternary International 436, 8–15.

Hubbard, A., Hein, A.S., Kaplan, M., Hulton, N., Glasser, N., 2005. A Modelling Reconstruction Of The Last Glacial Maximum Ice Sheet And Its Deglaciation In

The Vicinity Of The Northern Patagonian Icefield, South America. Geografiska Annaler, Series A: Physical Geography 87, 375–391.

Hughes, P.D., Gibbard, P.L., 2018. Global glacier dynamics during 100 ka Pleistocene glacial cycles. Quaternary Research 90, 222–243.

Hughes, P.D., Gibbard, P.L., Ehlers, J.J., 2013. Timing of glaciation during the last glacial cycle: Evaluating the concept of a global 'Last Glacial Maximum' (LGM). Earth-Science Reviews 125, 171–198.

Hulton, N., Purves, R., McCulloch, R., Sugden, D., Bentley, M., 2002. The Last Glacial Maximum and deglaciation in southern South America. Quaternary Science Reviews 21, 233–241.

Iglesias, V., Markgraf, V., Whitlock, C., 2016. 17,000 years of vegetation, fire and climate change in the eastern foothills of the Andes (lat. 44°S). Palaeogeography, Palaeoclimatology, Palaeoecology 457, 195–208.

Izagirre, E., Darvill, C.M., Rada, C., Aravena, J.C., 2018. Glacial geomorphology of the Marinelli and Pigafetta glaciers, Cordillera Darwin Icefield, southernmost Chile. Journal of Maps 14, 269–281.

James, W.H., Carrivick, J.L., Quincey, D.J., Glasser, N.F., 2019. A geomorphology based reconstruction of ice volume distribution at the Last Glacial Maximum across the Southern Alps of New Zealand. Quaternary Science Reviews 219, 20–35.

Johnsen, S.J., Dansgaard, W., Clausen, H.B., Langway, C.C., 1972. Oxygen isotope profiles through the antarctic and greenland ice sheets. Nature 235, 429–434.

Kaiser, J., Lamy, F., 2010. Links between Patagonian Ice Sheet fluctuations and Antarctic dust variability during the last glacial period (MIS 4-2). Quaternary Science Reviews 29, 1464–1471.

Kaiser, J., Lamy, F., Arz, H., Hebbeln, D., 2007. Dynamics of the millennial-scale sea surface temperature and Patagonian Ice Sheet fluctuations in southern Chile during the last 70kyr (ODP Site 1233). Quaternary International 161, 77–89.

Kaiser, J., Lamy, F., Hebbeln, D., 2005. A 70-kyr sea surface temperature record off southern Chile (Ocean Drilling Program Site 1233). Paleoceanography 20, PA4009.

Kaplan, M., Moreno, P., Rojas, M., 2008. Glacial dynamics in southernmost South America during Marine Isotope Stage 5e to the Younger Dryas chron: a brief review with a focus on cosmogenic nuclide measurements. Journal of Quaternary Science 23, 649–658.

Kaplan, M.R., Ackert, R.P., Singer, B.S., Douglass, D.C., Kurz, M.D., 2004. Cosmogenic nuclide chronology of millennial-scale glacial advances during O-isotope stage 2 in Patagonia. Bulletin of the Geological Society of America 116, 308–321.

Kaplan, M.R., Douglass, D.C., Singer, B.S., Ackert, R.P., Caffee, M.W., 2005. Cosmogenic nuclide chronology of pre-last glacial maximum moraines at Lago Buenos Aires, 46°S, Argentina. Quaternary Research 63, 301–315.

Kaplan, M.R., Hein, A.S., Hubbard, A., Lax, S.M., 2009. Can glacial erosion limit the extent of glaciation? Geomorphology 103, 172–179.

Kaplan, M.R., Schaefer, J.M., Denton, G.H., Barrell, D.J.A., Chinn, T.J.H., Putnam, A.E., Andersen, B.G., Finkel, R.C., Schwartz, R., Doughty, A.M., 2010. Glacier retreat in New Zealand during the Younger Dryas stadial. Nature 467, 194–197.

Kaplan, M.R., Schaefer, J.M., Denton, G.H., Doughty, A.M., Barrell, D.J.A., Chinn, T.J.H., Putnam, A.E., Andersen, B.G., Mackintosh, A., Finkel, R.C., Schwartz, R., Anderson, B., 2013. The anatomy of long-term warming since 15 ka in New Zealand based on net glacier snowline rise. Geology 41, 887–890.

Kaplan, M.R., Schaefer, J.M., Strelin, J.A., Denton, G.H., Anderson, R.F., Vandergoes, M.J., Finkel, R.C., Schwartz, R., Travis, S.G., Garcia, J.L., Martini, M.A., Nielsen, S.H.H., 2016. Patagonian and southern South Atlantic view of Holocene climate. Quaternary Science Reviews 141, 112–125.

Kaplan, M.R., Strelin, J.A., Schaefer, J.M., Denton, G.H., Finkel, R.C., Schwartz, R., Putnam, A.E., Vandergoes, M.J., Goehring, B.M., Travis, S.G., 2011. In-situ cosmogenic 10Be production rate at Lago Argentino, Patagonia: Implications for late-glacial climate chronology. Earth and Planetary Science Letters 309, 21–32.

Kelley, S.E., Kaplan, M.R., Schaefer, J.M., Andersen, B.G., Barrell, D.J.A., Putnam, A.E., Denton, G.H., Schwartz, R., Finkel, R.C., Doughty, A.M., 2014. High-precision 10 Be chronology of moraines in the Southern Alps indicates synchronous cooling in Antarctica and New Zealand 42,000 years ago. Earth and Planetary Science Letters 405, 194–206.

Kilian, R., Lamy, F., 2012. A review of Glacial and Holocene paleoclimate records from southernmost Patagonia (49-55°S). Quaternary Science Reviews 53, 1–23.

Kjær, K.H., Krüger, J., 2001. The final phase of dead-ice moraine development: processes Kötlujökull, Iceland. Sedimentology 48, 935–952.

Koppes, M., Gillespie, A.R., Burke, R.M., Thompson, S.C., Stone, J., 2008. Late Quaternary glaciation in the Kyrgyz Tien Shan. Quaternary Science Reviews 27, 846–866.

Kulkarni, A.V., 1992. Mass balance of Himalayan glaciers using AAR and ELA methods. Journal of Glaciology 38, 101–104.

Lagabrielle, Y., Suárez, M., Rossello, E.A., Hérail, G., Martinod, J., Régnier, M., de la Cruz, R., 2004. Neogene to Quaternary tectonic evolution of the Patagonian Andes at the latitude of the Chile Triple Junction. Tectonophysics 385, 211–241.

Lal, D., 1991. Cosmic ray labeling of erosion surfaces: in situ nuclide production rates and erosion models. Earth and Planetary Science Letters 104, 424–439.

Lambert, F., Bigler, M., Steffensen, J.P., Hutterli, M.A., Fischer, H., 2012. EDC dust flux 800 kyr (full resolution).

Lambert, F., Delmonte, B., Petit, J.R., Bigler, M., Kaufmann, P.R., Hutterli, M.A., Stocker, T.F., Ruth, U., Steffensen, J.P., Maggi, V., 2008. Dust-climate couplings over the past 800,000 years from the EPICA Dome C ice core. Nature 452, 616–619.

Lamy, F., 2004. Antarctic Timing of Surface Water Changes off Chile and Patagonian Ice Sheet Response. Science 304, 1959–1962.

Lamy, F., Arz, H.W., Kilian, R., Lange, C.B., Lembke-Jene, L., Wengler, M., Kaiser, J., Baeza-Urrea, O., Hall, I.R., Harada, N., Tiedemann, R., 2015. Glacial reduction and millennial-scale variations in Drake Passage throughflow. Proceedings of the National Academy of Sciences 112, 13496–13501.

Lamy, F., Hebbeln, D., Röhl, U., Wefer, G., 2001. Holocene rainfall variability in southern Chile: a marine record of latitudinal shifts of the Southern Westerlies. Earth and Planetary Science Letters 185, 369–382.

Lamy, F., Kaiser, J., Arz, H.W., Hebbeln, D., Ninnemann, U., Timm, O., Timmermann, A., Toggweiler, J., 2007. Modulation of the bipolar seesaw in the Southeast Pacific during Termination 1. Earth and Planetary Science Letters 259, 400–413.

Lamy, F., Kilian, R., Arz, H.W., Francois, J.P., Kaiser, J., Prange, M., Steinke, T., 2010. Holocene changes in the position and intensity of the southern westerly wind belt. Nature Geoscience 3, 695–699.

Landais, A., Masson-delmotte, V., Stenni, B., Selmo, E., Roche, D.M., Jouzel, J., 2015. Invited review A review of the bipolar see e saw from synchronized and high resolution ice core water stable isotope records from Greenland and. Quaternary Science Reviews 114, 18–32.

Lara, A., Villalba, R., Urrutia-Jalabert, R., González-Reyes, A., Aravena, J.C., Luckman, B.H., Cuq, E., Rodríguez, C., Wolodarsky-Franke, A., 2020. +A

5680-year tree-ring temperature record for southern South America. Quaternary Science Reviews 228, 106087.

Le Quere, C., Rodenbeck, C., Buitenhuis, E.T., Conway, T.J., Langenfelds, R., Gomez, A., Labuschagne, C., Ramonet, M., Nakazawa, T., Metzl, N., Gillett, N., Heimann, M., 2007. Saturation of the Southern Ocean CO2 Sink Due to Recent Climate Change. Science 316, 1735–1738.

Lemieux-Dudon, B., Blayo, E., Petit, J.R., Waelbroeck, C., Svensson, A., Ritz, C., Barnola, J.M., Narcisi, B.M., Parrenin, F., 2010. Consistent dating for Antarctic and Greenland ice cores. Quaternary Science Reviews 29, 8–20.

Lewis, C.J., McDonald, E.V., Sancho, C., Peña, J.L., Rhodes, E.J., 2009. Climatic implications of correlated Upper Pleistocene glacial and fluvial deposits on the Cinca and Gállego Rivers (NE Spain) based on OSL dating and soil stratigraphy. Global and Planetary Change 67, 141–152.

Li, H., Ng, F., Li, Z., Qin, D., Cheng, G., 2012. An extended perfect-plasticity method for estimating ice thickness along the flow line of mountain glaciers. Journal of Geophysical Research: Earth Surface 117, n/a–n/a.

Lifton, N., Sato, T., Dunai, T.J., 2014. Scaling in situ cosmogenic nuclide production rates using analytical approximations to atmospheric cosmic-ray fluxes. Earth and Planetary Science Letters 386, 149–160.

Lovell, H., Stokes, C.R., Bentley, M.J., Benn, D.I., 2012. Evidence for rapid ice flow and proglacial lake evolution around the central Strait of Magellan region, southernmost Patagonia. Journal of Quaternary Science 27, 625–638.

Lovenduski, N.S., Gruber, N., Doney, S.C., 2008. Toward a mechanistic understanding of the decadal trends in the Southern Ocean carbon sink. Global Biogeochemical Cycles 22, 1–9.

Lumley, S., Switsur, R., 1993. Late Quaternary Chronology of the Taitao peninsula, southern Chile. Journal of Quaternary Science 8, 161–165.

MacGregor, K.R., Anderson, R.S., Anderson, S.P., Waddington, E.D., 2000. Numerical simulations of glacial-valley longitudinal profile evolution. Geology 28, 1031–1034.

Mansilla, C.A., McCulloch, R.D., Morello, F., 2016. Palaeoenvironmental change in Southern Patagonia during the Lateglacial and Holocene: Implications for forest refugia and climate reconstructions. Palaeogeography, Palaeoclimatology, Palaeoecology 447, 1–11.

Markgraf, V., Bradbury, J.P., Schwalb, A., Burns, S.J., Stern, C., Ariztegui, D., Gilli, A., Anselmetti, F.S., Stine, S., Maidana, N., Markgraf, V., Bradbury,

J.P., Schwalb, A., Burns, S.J., Stern, C., Ariztegui, D., Anselmetti, F.S., Stine, S., Maidana, N., 2003. Holocene palaeoclimates of southern Patagonia: limnological and environmental history of Lago Cardiel, Argentina. The Holocene 13, 581–591.

Markgraf, V., Whitlock, C., Haberle, S., 2007. Vegetation and fire history during the last 18,000 cal yr B.P. in Southern Patagonia: Mallín Pollux, Coyhaique, Province Aisén (45°4130 S, 71°5030 W, 640 m elevation). Palaeogeography, Palaeoclimatology, Palaeoecology 254, 492–507.

Markle, B.R., Steig, E.J., Buizert, C., Schoenemann, S.W., Bitz, C.M., Fudge, T.J., Pedro, J.B., Ding, Q., Jones, T.R., White, J.W., Sowers, T., 2017. Global atmospheric teleconnections during Dansgaard-Oeschger events. Nature Geoscience 10, 36–40.

Marshall, G.J., 2003. Trends in the Southern Annular Mode from Observations and Reanalyses. Journal of Climate 16, 4134–4143.

Marshall, J., Speer, K., 2012. Closure of the meridional overturning circulation through Southern Ocean upwelling. Nature Geoscience 5, 171–180.

Martin, J.R., Davies, B.J., Thorndycraft, V.R., 2019. Glacier dynamics during a phase of Late Quaternary warming in Patagonia reconstructed from sediment-landform associations. Geomorphology 337, 111–133.

Martínez-Garcia, A., Rosell-Melé, A., Jaccard, S.L., Geibert, W., Sigman, D.M., Haug, G.H., 2011. Southern Ocean dust-climate coupling over the past four million years. Nature 476, 312–315.

Massaferro, J., Brooks, S.J., 2002. Response of chironomids to late quaternary environmental change in the Taitao Peninsula, Southern Chile. Journal of Quaternary Science 17, 101–111.

McCarthy, A., Mackintosh, A., Rieser, U., Fink, D., 2008. Mountain Glacier Chronology from Boulder Lake, New Zealand, Indicates MIS 4 and MIS 2 Ice Advances of Similar Extent. Arctic, Antarctic, and Alpine Research 40, 695–708.

McCulloch, R., Bentley, M., Tipping, R., Clapperton, C., 2005a. Evidence for LateGlacial Ice Dammed Lakes In The Central Strait Of Magellan And Bahía Inútil, Southernmost South America. Geografiska Annaler, Series A: Physical Geography 87, 335–362.

McCulloch, R.D., Bentley, M.J., Purves, R.S., Hulton, N.R.J., Sugden, D.E., Clapperton, C.M., 2000. Climatic inferences from glacial and palaeoecological evidence at the last glacial termination, southern South America. Journal of Quaternary Science 15, 409–417.

McCulloch, R.D., Davies, S.J., 2001. Late-glacial and Holocene palaeoenvironmental change in the central Strait of Magellan, southern Patagonia. Palaeogeography, Palaeoclimatology, Palaeoecology 173, 143–173.

McCulloch, R.D., Fogwill, C.J., Sugden, D.E., Bentley, M.J., Kubik, P.W., 2005b. Chronology of the Last Glaciation in Central Strait of Magellan and Bahía Inútil, Southernmost South America. Geografiska Annaler, Series A: Physical Geography 87, 289–312.

Meijers, A.J., 2014. The Southern Ocean in the Coupled Model Intercomparison Project phase 5. Philosophical Transactions of the Royal Society A: Mathematical, Physical and Engineering Sciences 372.

Mendelova, M., Hein, A., McCulloch, R., Davies, B., 2017. The Last Glacial Maximum and deglaciation in central Patagonia, 44°S - 49°S. Cuadernos de Investigación Geográfica 43, 719 – 750.

Mendelová, M., Hein, A.S., Rodés, À., Smedley, R.K., Xu, S., 2020a. Glacier expansion in central Patagonia during the Antarctic Cold Reversal followed by retreat and stabilisation during the Younger Dryas. Quaternary Science Reviews 227.

Mendelová, M., Hein, A.S., Rodés, À., Xu, S., 2020b. Extensive mountain glaciation in central Patagonia during Marine Isotope Stage 5. Quaternary Science Reviews 227.

Menounos, B., Clague, J.J., Osborn, G., Davis, P.T., Ponce, F., Goehring, B.M., Maurer, M., Rabassa, J.O., Coronato, A., Marr, R., 2013. Latest Pleistocene and Holocene glacier fluctuations in southernmost Tierra del Fuego, Argentina. Quaternary Science Reviews 77, 70–79.

Mercer, J.H., 1968. Variations of some Patagonian glaciers since the Late-Glacial. American Journal of Science 266, 91–109.

Mercer, J.H., 1970. Variations of some Patagonian glaciers since the Late-Glacial; II.

Mercer, J.H., 1976. Glacial history of southernmost South America. Quaternary Research 6, 125–166.

Mercer, J.H., 1982. Holocene glacier variations in southern South America. Striae 18, 35 – 40.

Mercer, J.H., 1983. Cenozoic Glaciation in Hemisphere. Annual Review Earth Planetary Sciences , 99–132.

Mercer, J.H., 1984. Simultaneous climatic change in both hemispheres and similar bipolar interglacial warming: Evidence and implications, in: Hansen, J.E., Takahashi, T. (Eds.), Climate Processes and Climate Sensitivity. American Geophysical Union, Washington, D. C.. volume 29 of *Geophysical Monograph Series*, pp. 307–313.

Meredith, M.P., Naveira Garabato, A.C., Hogg, A.M., Farneti, R., 2012. Sensitivity of the overturning circulation in the Southern Ocean to decadal changes in wind forcing. Journal of Climate 25, 99–110.

Milankovitch, M., 1941. Kanon der Erdbestrahlung und Seine Andwendung auf das Eiszeitenproblem. Belgrade.

Mills, S.C., Grab, S.W., Rea, B.R., Carr, S.J., Farrow, A., 2012. Shifting westerlies and precipitation patterns during the Late Pleistocene in southern Africa determined using glacier reconstruction and mass balance modelling. Quaternary Science Reviews 55, 145–159.

Monnin, E., Indermühle, A., Dällenbach, A., Flückiger, J., Stauffer, B., Stocker, T.F., Raynaud, D., Barnola, J.M., 2001. Atmospheric CO2 concentrations over the last glacial termination. Science 291, 112–114.

Montade, V., Combourieu Nebout, N., Kissel, C., Haberle, S.G., Siani, G., Michel, E., 2013. Vegetation and climate changes during the last 22,000yr from a marine core near Taitao Peninsula, southern Chile. Palaeogeography, Palaeoclimatology, Palaeoecology 369, 335–348.

Montade, V., Peyron, O., Favier, C., Francois, J.P., Haberle, S.G., 2019. A pollen-climate calibration from western Patagonia for palaeoclimatic reconstructions. Journal of Quaternary Science 34, 76–86.

Moreno, P.I., 2004. Millennial-scale climate variability in northwest Patagonia over the last 15 000 yr. Journal of Quaternary Science 19, 35–47.

Moreno, P.I., Denton, G.H., Moreno, H., Lowell, T.V., Putnam, A.E., Kaplan, M.R., 2015. Radiocarbon chronology of the last glacial maximum and its termination in northwestern Patagonia. Quaternary Science Reviews 122, 233–249.

Moreno, P.I., Francois, J.P., Moy, C.M., Villa-Martínez, R., 2010. Covariability of the Southern Westerlies and atmospheric CO2 during the Holocene. Geology 38, 727–730.

Moreno, P.I., Jacobson, G.L., Lowell, T.V., Denton, G.H., 2001. Interhemispheric climate links revealed by a late-glacial cooling episode in southern Chile. Nature 409, 804–808.

Moreno, P.I., Kaplan, M.R., François, J.P., Villa-Martínez, R., Moy, C.M., Stern, C.R., Kubik, P.W., 2009. Renewed glacial activity during the Antarctic cold reversal and persistence of cold conditions until 11.5 ka in southwestern Patagonia. Geology 37, 375–378.

Moreno, P.I., León, A.L., 2003. Abrupt vegetation changes during the last glacial to Holocene transition in mid-latitude South America. Journal of Quaternary Science 18, 787–800.

Moreno, P.I., Videla, J., 2016. Centennial and millennial-scale hydroclimate changes in northwestern Patagonia since 16,000 yr BP. Quaternary Science Reviews 149, 326–337.

Moreno, P.I., Vilanova, I., Villa-Martínez, R., Dunbar, R.B., Mucciarone, D.A., Kaplan, M.R., Garreaud, R.D., Rojas, M., Moy, C.M., De Pol-Holz, R., Lambert, F., 2018. Onset and Evolution of Southern Annular Mode-Like Changes at Centennial Timescale. Scientific Reports 8.

Moreno, P.I., Vilanova, I., Villa-Martínez, R., Garreaud, R.D., Rojas, M., De Pol-Holz, R., 2014. Southern Annular Mode-like changes in southwestern Patagonia at centennial timescales over the last three millennia. Nature Communications 5, 4375.

Moreno, P.I., Villa-Martínez, R., Cárdenas, M.L., Sagredo, E.A., 2012. Deglacial changes of the southern margin of the southern westerly winds revealed by terrestrial records from SW Patagonia (52°S). Quaternary Science Reviews 41, 1–21.

Murdie, R.E., Pugh, D.T., Styles, P., 1998. A lightweight, portable, digital probe for measuring the thermal gradient in shallow water sediments, with examples from Patagonia. Geo-Marine Letters 18, 315–320.

Murray, A., Wintle, A., 2000. Luminescence dating of quartz using an improved single-aliquot regenerative-dose protocol. Radiation Measurements 32, 57–73.

Nesje, A., Matthews, J.A., Dahl, S.O., Berrisford, M.S., Andersson, C., 2001. Holocene glacier fluctuations of Flatebreen and winter-precipitation changes in the Jostedalsbreen region, western Norway, based on glaciolacustrine sediment records. Holocene 11, 267–280.

Nimick, D.A., McGrath, D., Mahan, S.A., Friesen, B.A., Leidich, J., 2016. Latest Pleistocene and Holocene glacial events in the Colonia valley, Northern Patagonia Icefield, southern Chile. Journal of Quaternary Science 31, 551–564.

Nishiizumi, K., Imamura, M., Caffee, M.W., Southon, J.R., Finkel, R.C., McAninch, J., 2007. Absolute calibration of 10Be AMS standards. Nuclear Instruments and Methods in Physics Research, Section B: Beam Interactions with Materials and Atoms 258, 403–413.

Nordenskjöld, O., 1899. Geologie, geographie und anthropologie. Schwedischen expedition nach den magellansländern, 1895 - 1897. Norstedt and Söner, Stockholm.

Orsi, A.H., Whitworth, T., Nowlin, W.D., 1995. On the meridional extent and fronts of the Antarctic Circumpolar Current. Deep-Sea Research Part I 42, 641–673.

Osmaston, H., 1975. Models for the estimation of firnlines of present and Pleistocene Glaciers, in: Peel, R., Chisholm, M., Haggett, P. (Eds.), Processes in Physical and Human Geography, Bristol Essays. Heinemann, London, pp. 218–245.

Owen, L.A., Finkel, R.C., Caffee, M.W., 2002. A note on the extent of glaciation throughout the Himalaya during the global Last Glacial Maximum. Quaternary Science Reviews 21, 147–157.

Owen, L.A., Finkel, R.C., Haizhou, M., Spencer, J.Q., Derbyshire, E., Barnard, P.L., Caffee, M.W., 2003. Timing and style of Late Quaternary glaciation in northeastern Tibet. Bulletin of the Geological Society of America 115, 1356–1364.

PAGES 2k Consortium, 2013. Continental-scale temperature variability during the past two millennia. Nature Geoscience 6, 339–346.

Pahnke, K., Zahn, R., Elderfield, H., Schulz, M., 2003. 340,000-Year Centennial-Scale Marine Record of Southern Hemisphere Climatic Oscillation. Science 301, 948–952.

Pallàs, R., Rodés, À., Braucher, R., Bourlès, D., Delmas, M., Calvet, M., Gunnell, Y., 2010. Small, isolated glacial catchments as priority targets for cosmogenic surface exposure dating of Pleistocene climate fluctuations, southeastern Pyrenees. Geology 38, 891–894.

Paterson, W.S.B., 1994. The physics of glaciers. Pergamon, Oxford. third edit edition.

Pedro, J.B., Jochum, M., Buizert, C., He, F., Barker, S., Rasmussen, S.O., 2018. Beyond the bipolar seesaw: Toward a process understanding of interhemispheric coupling. Quaternary Science Reviews 192, 27–46.

Pedro, J.B., Van Ommen, T.D., Rasmussen, S.O., Morgan, V.I., Chappellaz, J., Moy, A.D., Masson-Delmotte, V., Delmotte, M., 2011. The last deglaciation: Timing the bipolar seesaw. Climate of the Past 7, 671–683.

Pellitero, R., Rea, B.R., Spagnolo, M., Bakke, J., Hughes, P., Ivy-Ochs, S., Lukas, S., Ribolini, A., 2015. A GIS tool for automatic calculation of glacier equilibrium-line altitudes. Computers and Geosciences 82, 55–62.

Pellitero, R., Rea, B.R., Spagnolo, M., Bakke, J., Ivy-Ochs, S., Frew, C.R., Hughes, P., Ribolini, A., Lukas, S., Renssen, H., 2016. GlaRe, a GIS tool to reconstruct the 3D surface of palaeoglaciers. Computers and Geosciences 94, 77–85.

Pesce, O.H., Moreno, P.I., 2014. Vegetation, fire and climate change in central-east Isla Grande de Chiloé (43°S) since the Last Glacial Maximum, northwestern Patagonia. Quaternary Science Reviews 90, 143–157.

Ponce, J.F., González Guillot, M., Díaz Balocchi, L., Martínez, O., 2019. Geomorphological evidences of paleosurge activity in Lake Viedma Lobe, Patagonia, Argentina. Geomorphology 327, 511–522.

de Porras, M.E., Maldonado, A., Abarzúa, A.M., Cárdenas, M.L., Francois, J.P., Martel-Cea, A., Stern, C.R., Méndez, C., Reyes, O., 2012. Postglacial vegetation, fire and climate dynamics at Central Chilean Patagonia (Lake Shaman, 44°S). Quaternary Science Reviews 50, 71–85.

de Porras, M.E., Maldonado, A., Quintana, F.A., Martel-Cea, A., Reyes, O., Méndez, C., 2014. Environmental and climatic changes in central Chilean Patagonia since the Late Glacial (Mallín El Embudo, 44°S). Climate of the Past 10, 1063–1078.

Porter, S.C., 1975. Equilibrium-line altitudes of late Quaternary glaciers in the Southern Alps, New Zealand. Quaternary Research 5, 27–47.

Porter, S.C., Swanson, T.W., 2008. 36Cl dating of the classic pleistocene glacial record in the northeastern Cascade Range, Washington. American Journal of Science 308, 130–166.

Power, M.J., Marlon, J., Ortiz, N., Bartlein, P.J., Harrison, S.P., Mayle, F.E., Ballouche, A., Bradshaw, R.H., Carcaillet, C., Cordova, C., Mooney, S., Moreno, P.I., Prentice, I.C., Thonicke, K., Tinner, W., Whitlock, C., Zhang, Y., Zhao, Y., Ali, A.A., Anderson, R.S., Beer, R., Behling, H., Briles, C., Brown, K.J., Brunelle, A., Bush, M., Camill, P., Chu, G.Q., Clark, J., Colombaroli, D., Connor, S., Daniau, A.L., Daniels, M., Dodson, J., Doughty, E., Edwards, M.E., Finsinger, W., Foster, D., Frechette, J., Gaillard, M.J., Gavin, D.G., Gobet, E., Haberle, S., Hallett, D.J., Higuera, P., Hope, G., Horn, S., Inoue, J., Kaltenrieder, P., Kennedy, L., Kong, Z.C., Larsen, C., Long, C.J., Lynch, J., Lynch, E.A., McGlone, M., Meeks, S., Mensing, S., Meyer, G., Minckley, T., Mohr, J., Nelson, D.M., New, J., Newnham, R., Noti, R., Oswald, W., Pierce, J., Richard, P.J., Rowe, C., Sanchez Goñi, M.F., Shuman, B.N., Takahara, H., Toney, J., Turney, C., Urrego-Sanchez, D.H., Umbanhowar, C., Vandergoes, M., Vanniere, B., Vescovi, E., Walsh, M., Wang, X., Williams, N., Wilmshurst, J., Zhang, J.H., 2008. Changes in fire regimes since the last glacial maximum: An

assessment based on a global synthesis and analysis of charcoal data. Climate Dynamics 30, 887–907.

Prescott, J.R., Hutton, J.T., 1994. Cosmic ray contributions to dose rates for luminescence and ESR dating: Large depths and long-term time variations. Radiation Measurements 23, 497–500.

Purich, A., Cai, W., England, M.H., Cowan, T., 2016. Evidence for link between modelled trends in Antarctic sea ice and underestimated westerly wind changes. Nature Communications 7, 1–9.

Putkonen, J., Swanson, T., 2003. Accuracy of cosmogenic ages for moraines. Quaternary Research 59, 255–261.

Putnam, A.E., Denton, G.H., Schaefer, J.M., Barrell, D.J.A., Andersen, B.G., Finkel, R.C., Schwartz, R., Doughty, A.M., Kaplan, M.R., Schlüchter, C., 2010a. Glacier advance in southern middle-latitudes during the Antarctic Cold Reversal. Nature Geoscience 3, 700–704.

Putnam, A.E., Schaefer, J.M., Barrell, D.J.A., Vandergoes, M., Denton, G.H., Kaplan, M.R., Finkel, R.C., Schwartz, R., Goehring, B.M., Kelley, S.E., 2010b. In situ cosmogenic 10Be production-rate calibration from the Southern Alps, New Zealand. Quaternary Geochronology 5, 392–409.

Putnam, A.E., Schaefer, J.M., Denton, G.H., Barrell, D.J., Birkel, S.D., Andersen, B.G., Kaplan, M.R., Finkel, R.C., Schwartz, R., Doughty, A.M., 2013. The Last Glacial Maximum at 44°S documented by a 10Be moraine chronology at Lake Ohau, Southern Alps of New Zealand. Quaternary Science Reviews 62, 114–141.

Putnam, A.E., Schaefer, J.M., Denton, G.H., Barrell, D.J.A., Finkel, R.C., Andersen, B.G., Schwartz, R., Chinn, T.J.H., Doughty, A.M., 2012. Regional climate control of glaciers in NewZealand and Europe during the pre-industrial Holocene. Nature Geoscience 5, 627–630.

Rabassa, J., 2008. Late Cenozoic glaciations in Patagonia and Tierra del Fuego: an update review. Developments in Quaternary Sciences 11, 151–204.

Rabassa, J., Clapperton, C.M., 1990. Quaternary Glaciations of the Southern Andes. Quaternary Science Reviews 9, 153–174.

Rabassa, J., Coronato, A., 2009. Glaciations in Patagonia and Tierra del Fuego during the Ensenadan Stage/Age (Early Pleistocene - earliest Middle Pleistocene). Quaternary International 210, 18–36.

Rabassa, J., Coronato, A., Bujalesky, G., Salemme, M., Roig, C., Meglioli, A., Heusser, C., Gordillo, S., Roig, F., Borromei, A., Quattrocchio, M., 2000.

Quaternary of Tierra del Fuego, Southernmost South America: an updated review. Quaternary International 68-71, 217–240.

Ramos, V.A., Kay, S.M., 1992. Southern Patagonian plateau basalts and deformation: Backarc testimony of ridge collisions. Tectonophysics 205, 261–282.

Ramos, V.A., Niemeyer, H., Skarmeta, J., Muñoz, J., 1982. Magmatic evolution of the Austral Patagonian Andes. Earth Science Reviews 18, 411–443.

Rea, B.R., Evans, D.J., 2007. Quantifying climate and glacier mass balance in north Norway during the Younger Dryas. Palaeogeography, Palaeoclimatology, Palaeoecology 246, 307–330.

Renssen, H., Goosse, H., Muscheler, R., 2006. Coupled climate model simulation of Holocene cooling events: oceanic feedback amplifies solar forcing. Climate of the Past 2, 79–90.

Reynhout, S.A., Sagredo, E.A., Kaplan, M.R., Aravena, J.C., Martini, M.A., Moreno, P.I., Rojas, M., Schwartz, R., Schaefer, J.M., 2019. Holocene glacier fluctuations in Patagonia are modulated by summer insolation intensity and paced by Southern Annular Mode-like variability. Quaternary Science Reviews 220, 178–187.

Rignot, E., Rivera, A., Casassa, G., 2003. Contribution of the Patagonia Icefields of South America to Sea Level Rise. Science 302, 434–437.

Rivera, A., Benham, T., Casassa, G., Bamber, J., Dowdeswell, J.A., 2007. Ice elevation and areal changes of glaciers from the Northern Patagonia Icefield, Chile. Global and Planetary Change 59, 126–137.

Rodbell, D.T., Smith, J.A., Mark, B.G., 2009. Glaciation in the Andes during the Lateglacial and Holocene. Quaternary Science Reviews 28, 2165–2212.

Röhringer, I., Zech, R., Abramowski, U., Sosin, P., Aldahan, A., Kubik, P.W., Zöller, L., Zech, W., 2012. The late Pleistocene glaciation in the Bogchigir Valleys (Pamir, Tajikistan) based on 10 Be surface exposure dating. Quaternary Research 78, 590–597.

Sagredo, E., Lowell, T., 2012. Climatology of Andean glaciers: A framework to understand glacier response to climate change. Global and Planetary Change 86-87, 101–109.

Sagredo, E., Moreno, P., Villa-Martínez, R., Kaplan, M., Kubik, P., Stern, C., 2011. Fluctuations of the Última Esperanza ice lobe (52°S), Chilean Patagonia, during the last glacial maximum and termination 1. Geomorphology 125, 92–108.

Sagredo, E.A., Kaplan, M.R., Araya, P.S., Lowell, T.V., Aravena, J.C., Moreno, P.I., Kelly, M.A., Schaefer, J.M., 2018. Trans-pacific glacial response to the Antarctic Cold Reversal in the southern mid-latitudes. Quaternary Science Reviews 188, 160–166.

Sagredo, E.A., Lowell, T.V., Kelly, M.A., Rupper, S., Aravena, J.C., Ward, D.J., Malone, A.G., 2016. Equilibrium line altitudes along the Andes during the Last millennium: Paleoclimatic implications. The Holocene 27, 1019–1033.

Sakakibara, D., Sugiyama, S., 2014. Ice-front variations and speed changes of calving glaciers in the Southern Patagonia Icefield from 1984 to 2011. Journal of Geophysical Research: Earth Surface 119, 2541–2554.

Saunders, K.M., Roberts, S.J., Perren, B., Butz, C., Sime, L., Davies, S., Van Nieuwenhuyze, W., Grosjean, M., Hodgson, D.A., 2018. Holocene dynamics of the Southern Hemisphere westerly winds and possible links to CO2 outgassing. Nature Geoscience 11, 650–655.

Schaefer, J.M., Denton, G.H., Kaplan, M., Putnam, A., Finkel, R.C., Barrell, D.J.A., Andersen, B.G., Schwartz, R., Mackintosh, A., Chinn, T., Schluchter, C., 2009. High-Frequency Holocene Glacier Fluctuations in New Zealand Differ from the Northern Signature. Science 324, 622–625.

Schaefer, J.M., Putnam, A.E., Denton, G.H., Kaplan, M.R., Birkel, S., Doughty, A.M., Kelley, S., Barrell, D.J.A., Finkel, R.C., Winckler, G., Anderson, R.F., Ninneman, U.S., Barker, S., Schwartz, R., Andersen, B.G., Schluechter, C., 2015. The Southern Glacial Maximum 65,000 years ago and its Unfinished Termination. Quaternary Science Reviews 114, 52–60.

Schilling, D., Hollin, J., 1981. Numerical reconstructions of valley glaciers and small ice caps, in: Denton, G., Hughes, T.J. (Eds.), The Last Great Ice Sheets. Wiley, New York, pp. 207–220.

Schneider, C., Glaser, M., Kilian, R., Santana, A., Casassa, G., 2003. Weather observations across the southern andes at 53°S. Physical Geography 24, 97–119.

Schomacker, A., 2008. What controls dead-ice melting under different climate conditions? A discussion. Earth-Science Reviews 90, 103–113.

Shulmeister, J., 1999. Australasian evidence for mid-Holocene climate change implies precessional control of Walker Circulation in the Pacific. Quaternary International 57-58, 81–91.

Shulmeister, J., Goodwin, I., Renwick, J., Harle, K., Armand, L., McGlone, M., Cook, E., Dodson, J., Hesse, P., Mayewski, P., Curran, M., 2004. The Southern Hemisphere westerlies in the Australasian sector over the last glacial cycle: a synthesis. Quaternary International 118-119, 23–53.

Shulmeister, J., Thackray, G.D., Rieser, U., Hyatt, O.M., Rother, H., Smart, C.C., Evans, D.J., 2010. The stratigraphy, timing and climatic implications of glaciolacustrine deposits in the middle Rakaia Valley, South Island, New Zealand. Quaternary Science Reviews 29, 2362–2381.

Shulmeister, J., Thackray, G.D., Rittenour, T.M., Fink, D., Patton, N.R., 2019. The timing and nature of the last glacial cycle in New Zealand. Quaternary Science Reviews 206, 1–20.

Shulmeister, J., Thackray, G.D., Rittenour, T.M., Hyatt, O.M., 2018. Multiple glacial advances in the Rangitata Valley, South Island, New Zealand, imply roles for Southern Hemisphere westerlies and summer insolation in MIS 3 glacial advances. Quaternary Research 89, 375–393.

Siani, G., Colin, C., Michel, E., Carel, M., Richter, T., Kissel, C., Dewilde, F., 2010. Late Glacial to Holocene terrigenous sediment record in the Northern Patagonian margin: Paleoclimate implications. Palaeogeography, Palaeoclimatology, Palaeoecology 297, 26–36.

Singer, B.S., Ackert, R.P., Guillou, H., 2004. 40Ar/39Ar and K-Ar chronology of Pleistocene glaciations in Patagonia. Geological Society of America Bulletin 116, 434.

Smedley, R., Duller, G., Pearce, N., Roberts, H., 2012. Determining the K-content of single-grains of feldspar for luminescence dating. Radiation Measurements 47, 790–796.

Smedley, R.K., Chiverrell, R.C., Ballantyne, C.K., Burke, M.J., Clark, C.D., Duller, G.A., Fabel, D., McCarroll, D., Scourse, J.D., Small, D., Thomas, G.S., 2017. Internal dynamics condition centennial-scale oscillations in marinebased ice-stream retreat. Geology 45, 787–790.

Smedley, R.K., Duller, G., 2013. Optimising the reproducibility of measurements of the post-IR IRSL signal from single-grains of K-feldspar for dating. Ancient TL 31, 49–58.

Smedley, R.K., Glasser, N.F., Duller, G.A.T., 2016. Luminescence dating of glacial advances at Lago Buenos Aires (˜46°S), Patagonia. Quaternary Science Reviews 134, 59–73.

Smedley, R.K., Pearce, N.J., 2016. Internal U, Th and Rb concentrations of alkali-feldspar grains: Implications for luminescence dating. Quaternary Geochronology 35, 16–25.

Solomina, O.N., Bradley, R.S., Hodgson, D.A., Ivy-Ochs, S., Jomelli, V., Mackintosh, A.N., Nesje, A., Owen, L.A., Wanner, H., Wiles, G.C., Young, N.E., 2015. Holocene glacier fluctuations. Quaternary Science Reviews 111, 9–34.

Spedding, N., Evans, D.J.A., 2002. Sediments and landforms at Kv\'i\'arjökull, southeast Iceland: a reappraisal of the glaciated valley landsystem. Sedimentary Geology 149, 21–42.

Stern, C.R., 2004. Active Andean volcanism: its geologic and tectonic setting. Revista geológica de Chile 31, 1–51.

Stine, S., Stine, M., 1990. A record from Lake Cardiel of climate change in southern South America. Nature 345, 705–708.

Stocker, T.F., Johnsen, S.J., 2003. A minimum thermodynamic model for the bipolar seesaw. Paleoceanography 18, 1–9.

Stone, J.O., 2000. Air pressure and cosmogenic isotope production. Journal of Geophysical Research: Solid Earth 105, 23753–23759.

Strelin, J.A., Denton, G.H., Vandergoes, M.J., Ninnemann, U.S., Putnam, A.E., 2011. Radiocarbon chronology of the late-glacial Puerto Bandera moraines, Southern Patagonian Icefield, Argentina. Quaternary Science Reviews 30, 2551–2569.

Strelin, J.A., Kaplan, M.R., Vandergoes, M.J., Denton, G.H., Schaefer, J.M., 2014. Holocene glacier history of the Lago Argentino basin, Southern Patagonian Icefield. Quaternary Science Reviews 101, 124–145.

Sugden, D., Bentley, M., Fogwill, C., Hulton, N., Mcculloch, R., Purves, R., 2005. Lateglacial glacier events in southernmost south america: a blend of northern and 'southern hemispheric climatic signals? Geografiska Annaler: Series A, Physical Geography 87, 273–288.

Sugden, D.E., Hulton, N.R.J., Purves, R.S., 2002. Modelling the inception of the Patagonian icesheet. Quaternary International 95-96, 55–64.

Sugden, D.E., McCulloch, R.D., Bory, A.J.M., Hein, A.S., 2009. Influence of Patagonian glaciers on Antarctic dust deposition during the last glacial period. Nature Geoscience 2, 281–285.

Sutherland, R., Kim, K., Zondervan, A., McSaveney, M., 2007. Orbital forcing of mid-latitude Southern Hemisphere glaciation since 100 ka inferred from cosmogenic nuclide ages of moraine boulders from the Cascade Plateau, southwest New Zealand. Bulletin of the Geological Society of America 119, 443–451.

Svendsen, J.I., Alexanderson, H., Astakhov, V.I., Demidov, I., Dowdeswell, J.A., Funder, S., Gataullin, V., Henriksen, M., Hjort, C., Houmark-Nielsen, M., Hubberten, H.W., Ingólfsson, ., Jakobsson, M., Kjær, K.H., Larsen, E., Lokrantz, H., Lunkka, J.P., Lysså, A., Mangerud, J., Matiouchkov, A., Murray, A., Möller, P., Niessen, F., Nikolskaya, O., Polyak, L., Saarnisto, M., Siegert,

C., Siegert, M.J., Spielhagen, R.F., Stein, R., 2004. Late Quaternary ice sheet history of northern Eurasia. Quaternary Science Reviews 23, 1229–1271.

Swart, N.C., Fyfe, J.C., 2012. Observed and simulated changes in the Southern Hemisphere surface westerly wind-stress. Geophysical Research Letters 39, 6–11.

Swart, N.C., Fyfe, J.C., Gillett, N., Marshall, G.J., 2015. Comparing trends in the southern annular mode and surface westerly jet. Journal of Climate 28, 8840–8859.

Tachikawa, T., Kaku, M., Iwasaki, A., Gesch, D., Oimoen, M., Zhang, Z., Danielson, J., Krieger, T., Curtis, B., Haase, J., Carabajal, C., 2011. ASTER Global Digital Elevation Model Version 2 - summary of validation results. Technical Report. NASA.

Thackray, G.D., 2001. Extensive early and middle Wisconsin Glaciation on the western Olympic Peninsula, Washington, and the variability of Pacific moisture delivery to the northwestern United States. Quaternary Research 55, 257–270.

Thomsen, K.J., Murray, A.S., Jain, M., Bøtter-Jensen, L., 2008. Laboratory fading rates of various luminescence signals from feldspar-rich sediment extracts. Radiation Measurements 43, 1474–1486.

Thorndycraft, V.R., Bendle, J.M., Benito, G., Davies, B.J., Sancho, C., Palmer, A.P., Fabel, D., Medialdea, A., Martin, J.R., 2019. Glacial lake evolution and Atlantic-Pacific drainage reversals during deglaciation of the Patagonian Ice Sheet. Quaternary Science Reviews 203, 102–127.

Toggweiler, J.R., Russell, J., 2008. Ocean circulation in a warming climate. Nature 451, 286–288.

Toggweiler, J.R., Russell, J.L., Carson, S.R., 2006a. Midlatitude westerlies, atmospheric CO 2 , and climate change during the ice ages. Paleoceanography 21, PA2005.

Toggweiler, J.R., Russell, J.L., Carson, S.R., 2006b. Midlatitude westerlies, atmospheric CO ¡sub¿2¡/sub¿ , and climate change during the ice ages. Paleoceanography 21, PA2005.

Toggweiler, J.R., Samuels, B., 1995. Effect of drake passage on the global thermohaline circulation. Deep-Sea Research Part I 42, 477–500.

Turner, A.J., Woodward, J., Stokes, C.R., Ó Cofaigh, C., Dunning, S., 2014. Glacial geomorphology of the Great Glen Region of Scotland. Journal of Maps 10, 159–178.

Turner, K.J., Fogwill, C.J., McCulloch, R.D., Sugden, D.E., 2005. Deglaciation of The Eastern Flank Of The North Patagonian Icefield And Associated Continental-Scale Lake Diversions. Geografiska Annaler, Series A: Physical Geography 87, 363–374.

Van Geel, B., Buurman, J., Waterbolk, H.T., 1996. Archaeological and palaeoecological indications of an abrupt climate change in the Netherlands, and evidence for climatological teleconnections around 2650 BP. Journal of Quaternary Science 11, 451–460.

Vandekerkhove, E., Bertrand, S., Reid, B., Bartels, A., Charlier, B., 2016. Sources of dissolved silica to the fjords of northern Patagonia (44-48°S): the importance of volcanic ash soil distribution and weathering. Earth Surface Processes and Landforms 41, 499–512.

Vandergoes, M.J., Dieffenbacher-Krall, A.C., Newnham, R.M., Denton, G.H., Blaauw, M., 2008. Cooling and changing seasonality in the Southern Alps, New Zealand during the Antarctic Cold Reversal. Quaternary Science Reviews 27, 589–601.

Vandergoes, M.J., Newnham, R.M., Preusser, F., Hendy, C.H., Lowell, T.V., Fitzsimons, S.J., Hogg, A.G., Kasper, H.U., Schlüchter, C., 2005. Regional insolation forcing of late Quaternary climate change in the Southern Hemisphere. Nature 436, 242–245.

Varma, V., Prange, M., Lamy, F., Merkel, U., Schulz, M., 2011. Solar-forced shifts of the Southern Hemisphere Westerlies during the Holocene. Climate of the Past 7, 339–347.

Veres, D., Bazin, L., Landais, A., Toyé Mahamadou Kele, H., Lemieux-Dudon, B., Parrenin, F., Martinerie, P., Blayo, E., Blunier, T., Capron, E., Chappellaz, J., Rasmussen, S.O., Severi, M., Svensson, A., Vinther, B., Wolff, E.W., 2013. The Antarctic ice core chronology (AICC2012): An optimized multi-parameter and multi-site dating approach for the last 120 thousand years. Climate of the Past 9, 1733–1748.

Villa-Martínez, R., Moreno, P.I., 2007. Pollen evidence for variations in the southern margin of the westerly winds in SW Patagonia over the last 12,600 years. Quaternary Research 68, 400–409.

Villa-Martínez, R., Moreno, P.I., Valenzuela, M.A., 2012. Deglacial and postglacial vegetation changes on the eastern slopes of the central Patagonian Andes (47°S). Quaternary Science Reviews 32, 86–99.

WAIS Divide Project Members, 2015. Precise interpolar phasing of abrupt climate change during the last ice age. Nature 520, 661–665.

Warren, C., Aniya, M., 1999. The calving glaciers of southern South America. Global and Planetary Change 22, 59–77.

Warren, C.R., Sugden, D.E., 1993. The Patagonian Icefields: A Glaciological Review. Arctic and Alpine Research 25, 316 – 331.

Wenzens, G., 2002. The influence of tectonically derived relief and climate on the extent of the last Glaciation east of the Patagonian ive fields (Argentina, Chile). Tectonophysics 345, 329–344.

Wenzens, G., 2005. Glacier advances east of the Southern Andes between the Last Glacial Maximum and 5,000 BP compared with lake terraces of the endorrheic Lago Cardiel (49 degrees S, Patagonia, Argentina). Zeitschrift Fur Geomorphologie 49, 433–454.

Whitlock, C., Moreno, P.I., Bartlein, P., 2007. Climatic controls of Holocene fire patterns in southern South America. Quaternary Research 68, 28–36.

Winchester, V., Harrison, S., 1996. Recent oscillations of the San Quintin and San Rafael Glaciers, Patagonian Chile. Geografiska Annaler, Series A: Physical Geography 78, 35–49.

Winchester, V., Harrison, S., Warren, C.R., 2001. Recent retreat Glaciar Nef, Chilean Patagonia, dated by lichenometry and dendrochronology. Arctic, Antarctic, and Alpine Research 33, 266–273.

Wolff, I.W., Glasser, N.F., Hubbard, A., 2013. The reconstruction and climatic implication of an independent palaeo ice cap within the Andean rain shadow east of the former Patagonian ice sheet, Santa Cruz Province, Argentina. Geomorphology 185, 1–15.

Wu, C.J., Krivova, N.A., Solanki, S.K., Usoskin, I.G., 2018. Solar total and spectral irradiance reconstruction over the last 9000 years. Astronomy and Astrophysics 620.

Zech, R., 2012. A late pleistocene glacial chronology from the Kitschi-Kurumdu Valley, Tien Shan (Kyrgyzstan), based on 10Be surface exposure dating. Quaternary Research 77, 281–288.

Zech, R., Zech, J., Kull, C., Kubik, P.W., Veit, H., 2011a. Early last glacial maximum in the southern Central Andes reveals northward shift of the westerlies at ˜39 ka. Climate of the Past 7, 41–46.

Zech, W., Zech, R., Zech, M., Leiber, K., Dippold, M., Frechen, M., Bussert, R., Andreev, A., 2011b. Obliquity forcing of Quaternary glaciation and environmental changes in NE Siberia. Quaternary International 234, 133–145.

Zemp, M., Huss, M., Thibert, E., Eckert, N., McNabb, R., Huber, J., Barandun, M., Machguth, H., Nussbaumer, S.U., Gärtner-Roer, I., Thomson, L., Paul, F., Maussion, F., Kutuzov, S., Cogley, J.G., 2019. Global glacier mass changes and their contributions to sea-level rise from 1961 to 2016. Nature 568, 382–386.

Zolitschka, B., Anselmetti, F., Ariztegui, D., Corbella, H., Francus, P., Lücke, A., Maidana, N.I., Ohlendorf, C., Schäbitz, F., Wastegård, S., 2013. Environment and climate of the last 51,000years - new insights from the Potrok Aike maar lake Sediment Archive Drilling prOject (PASADO). Quaternary Science Reviews 71, 1–12.

Appendix: Mendelová et al., 2017

Cuadernos de Investigación Geográfica *Geographical Research Letters*	2017	Nº 43 (2)	pp. 719-750	ISSN 0211-6820 eISSN 1697-9540

DOI: http://doi.org/10.18172/cig.3263
© Universidad de La Rioja

THE LAST GLACIAL MAXIMUM AND DEGLACIATION IN CENTRAL PATAGONIA, 44° S-49° S

M. MENDELOVA[1*], A.S. HEIN[1], R. McCULLOCH[2], B. DAVIES[3]

[1]School of GeoSciences, University of Edinburgh, Drummond Street, Edinburgh, EH8 9XP, United Kingdom.
[2]Biological and Environmental Sciences, University of Stirling, Stirling, FK9 4LA, United Kingdom.
[3]Centre for Quaternary Research, Department for Geography, Royal Holloway University of London, Egham, Surrey TW20 0EX, United Kingdom.

ABSTRACT. *This paper reviews published geochronological data on glacier fluctuations and environmental changes in central Patagonia (44° S-49° S) from the Last Glacial Maximum (LGM) through to the Holocene. Well-dated glacial chronologies from the southern mid-latitudes can inform on the synchronicity of glacial advances worldwide and provide insight on the drivers of southern hemisphere glaciations. In central Patagonia, two large outlet lobes of the former Patagonian Ice Sheet advanced in broad synchrony with the global LGM. In contrast to other parts of Patagonia, there is no convincing evidence for a more extensive local LGM advance during Marine Isotope Stage 3. Deglaciation initiated at ca. 19 ka, earlier than in other parts of Patagonia and regionally in the Southern Hemisphere, and rapid deglaciation saw ice margins retreat in places by at least 80-120 km within a few millennia. The Lateglacial glacier margins are poorly constrained, but an ice mass substantial enough to maintain a large regional proglacial lake must have persisted at this time. The timing of lake drainage and opening of the Río Baker drainage route to the Pacific Ocean is debated; the only directly dated shoreline suggests this occurred at the end of the Antarctic Cold Reversal at 12.7 ka. Palaeoecological evidence for cooling during the Antarctic Cold Reversal or Younger Dryas remains equivocal, which may reflect both the eurythermic nature of Patagonian vegetation and shifting Southern Westerly Winds. Eastern outlet glaciers appear to have advanced or stabilised at the Lateglacial/Holocene transition when palaeoenvironmental records indicate warmer and drier conditions, but the reason for this is unclear. Our review reveals both spatial and temporal gaps in available data that provide avenues for future research.*

El Último Máximo Glaciar y la deglaciación en Patagonia central, 44º S-49º S

RESUMEN. *Este artículo revisa los datos geocronológicos publicados sobre las fluctuaciones de los glaciares y los cambios ambientales en la Patagonia central (44° S-49° S) desde el Último Máximo Glaciar (LGM) hasta el Holoceno. Las cronologías glaciales bien datadas de las latitudes medias del sur pueden informar sobre la sincronicidad de los avances glaciares en todo el mundo y proporcionar una visión de los factores de las glaciaciones del hemisferio sur. En el centro de Patagonia, dos grandes lóbulos de salida del antiguo Campo de Hielo Patagónico avanzaron en una amplia sincronía con el LGM global. En contraste con otras partes de Patagonia, no hay evidencia convincente de un avance local más extenso que la que tuvo lugar durante el LGM durante la Etapa 3 de Isótopos Marinos. La deglaciación se inició hacia aprox. 19 ka, antes que en otras partes de la Patagonia y regionalmente en el hemisferio sur, y la rápida deglaciación vio los márgenes de hielo retroceder en algunos lugares por lo menos 80-120 km en pocos milenios. Los márgenes de los glaciares del Tardiglaciar están mal delimitados, aunque una masa de hielo sustancialmente suficiente para mantener un gran lago proglaciar regional tuvo que persistir en ese momento. Se discute cuándo ocurrió el drenaje del lago y la apertura de la ruta de drenaje de Río Baker hacia el Océano Pacífico. La única costa directamente datada sugiere que esto ocurrió al final de la Reversión Fría Antártica en 12.7 ka. La evidencia paleoecológica del enfriamiento durante la Reversión Fría Antártica o Younger Dryas sigue siendo equívoca, lo que puede reflejar tanto la naturaleza eutérmica de la vegetación patagónica como los vientos del oeste meridionales cambiantes. Los glaciares de salida oriental parecen haber avanzado o estabilizarse en la transición Tardiglaciar/Holoceno cuando los registros palaeoambientales indican condiciones más cálidas y más secas, pero la razón de esto no está clara. Nuestra revisión revela vacíos espaciales y temporales en los datos disponibles que proporcionan vías para la investigación futura.*

Keywords: Last Glacial Maximum, deglaciation, Holocene, Patagonia, glacial chronology.

Palabras clave: Último Máximo Glaciar, deglaciación, Holoceno, Patagonia, cronología glacial.

Received: 24 February 2017
Accepted: 23 March 2017

*Corresponding author: Monika Mendelova, School of GeoSciences, University of Edinburgh, Drummond Street, Edinburgh, EH8 9XP, United Kingdom. E-mail address: M.Mendelova@sms.ed.ac.uk

1. Introduction

The former Patagonian Ice Sheet (PIS) extended 2000 km along the southernmost Andes, between 38° S and 55° S during the Last Glacial Maximum (LGM; Fig. 1). The ice sheet left a rich glacial geomorphological record of ice limits (e.g. Glasser *et al*., 2008) that are particularly well preserved east of the mountain front, and which offer the opportunity to constrain the history of ice fluctuations throughout the last glacial cycle. The location in the mid-latitudes of the southern hemisphere, distant from the influence of northern hemisphere ice sheets, makes the site suitable to investigate, for example, the geographic extent of the global LGM and its termination, the interhemispheric linkages of climate variability and the forcing behind southern mountain glaciation.

There is a long history of research on Quaternary glaciations in Patagonia that began in the 19th century leading to the pioneering work of Caldenius (1932), who established the first comprehensive mapping of glacier moraine limits throughout Patagonia. The establishment of glacial chronologies that utilised modern radiometric dating techniques, including radiocarbon (^{14}C) and potassium-argon (K-Ar), began in the 1960's through

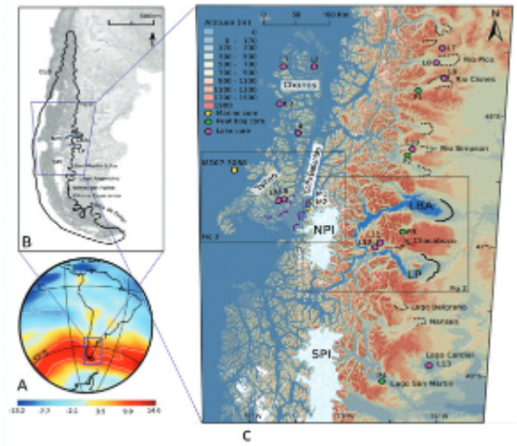

Figure 1. (A) Location of Patagonia, South America, with mean monthly zonal wind strength (m s $^{-1}$) at 850 hPa based on NCEP/NCAR re-analysis data (modified from Vanneste et al.*, 2015). (B) Estimated extent of the PIS at the LGM showing sites mentioned in the text; CLD- Chilean Lake District. (C) Map of Central Patagonia showing locations of palaeoenvironmental proxies, which are summarised in Table 1 and ice limits: black - chronologically constrained ice limits, black dashed– assumed LGM limits, purple – undated moraines on the Taitao Peninsula discussed in the text and moraines of the Gualas/Reicher, Rafael, and San Quintín Glaciers (Image: SRTM).*

the work of John Mercer (e.g. Mercer, 1968, 1976, 1982, 1983). Subsequent efforts to develop the glacial history of the PIS have used a wide range of geochronological techniques and are well summarised by several review papers on Quaternary (McCulloch *et al*., 2000; Rabassa and Clapperton, 1990; Rabassa and Coronato, 2009; Kaplan *et al*., 2008a; Glasser *et al*., 2004; Rodbell *et al*., 2009; Clapperton, 1993; Harrison and Glasser, 2011; Rabassa *et al*., 2000) and pre-Quaternary (Rabassa *et al*., 2011) glaciations.

This paper aims to synthesize existing geochronological data on ice limits and environmental changes during the LGM and subsequent deglaciation, in the central part of the former PIS. We review available dating of glacial moraine sequences as well as palaeoenvironmental proxies; the latter are more geographically dispersed in the region and provide insight into postglacial landscape development and climate. We focus on the area surrounding the present day North Patagonian Icefield (NPI), between latitudes 44° S and 49° S (Fig. 1c), but draw comparisons to other parts of Patagonia. This area has been considered a transitional zone influenced by both Antarctic and Northern Hemisphere climate (Sugden *et al*., 2005), and is an area where climate models suggest a 'discontinuity' in several climatic components (e.g. wind speed, precipitation) (Rojas *et al*., 2009). Our review reveals that glacial advances synchronous with the global LGM (gLGM; 26-19 ka; Clark *et al*., 2009) are constrained at two sites in central Patagonia. Numerous moraines, likely correlative to the local LGM, are found in almost every previously glaciated basin, but have so far received little attention. Tentative evidence suggests pre-LGM advances during the last glacial cycle but further work is needed to constrain these. Deglaciation initiated at about 19 ka, somewhat earlier than in southern Patagonia. Ice marginal positions during the Lateglacial are largely unknown, and the occurrence of cooling coeval with the Antarctic Cold Reversal (ACR; 14.5-12.9 ka) or Younger Dryas (YD; 12.9-11.7 ka) is equivocal.

2. Regional Setting

The regional geology of the southern Andes is characterized by intrusions of the Patagonian batholith within the Andean Cordillera, Mesozoic and Cenozoic volcanics, Mesozoic marine sediments, and a Paleozoic metamorphic complex (Vandekerkhove *et al*., 2016; Lagabrielle *et al*., 2004). The Taitao Peninsula and Chonos Archipelago are formed of Triassic metamorphic rocks and mid-Cenozoic volcanic and sedimentary deposits, with the Patagonian batholith constraining the eastern edges. Basins to the east of the Andes are filled with Pliocene-Quaternary glacial and glaciofluvial sediments (Vandekerkhove *et al*., 2016; Lagabrielle *et al*., 2004). A gap in the active volcanic arc between the Southern Andean Volcanic Zone and Austral Andean Volcanic Zone exists in central Patagonia (46.5° S-49° S), near the Chile Triple Junction, where the Nazca, South American and Antarctic tectonic plates meet (Gutiérrez *et al*., 2005; Stern, 2004).

The region contains the highest mountain in the Patagonian Andes, Mt. San Valentin at 4058 m, which is situated on the northern flank of the NPI. The otherwise topographically continuous chain of the Andes exhibits a break in central Patagonia between latitudes 47° S and 48° S. This gap is occupied by the Río Baker, which drains the eastern outlet glaciers of the NPI, including the large cross-border lakes of Lago Buenos Aires/Lago

General Carrera (LBA) and Lago Pueyrredón/Lago Cochrane (LP) westwards into the Pacific Ocean (Fig. 1c). Therefore, the water divide is unusually located 170 km to the east of the mountain chain. The landscape east of the Andes is characterized by west-east trending over-deepened valleys separated by volcanic plateaus. To the west of the Andes, the landscape is dominated by an extended fjord and island system. The ice flow during successive glaciations exploited pre-existing structural faults, and over-deepened and widened the fjords and valleys through selective erosion (Glasser and Ghiglione, 2009).

The Patagonian Andes of southern South America are situated in the mid-latitudes of the Southern Hemisphere, where the landmass intersects important global atmospheric and oceanic systems. These include the Southern Hemisphere Westerly Winds (SWWs) (Fig.1a), which play a role in modulating global climate through their influence on ocean currents and ventilation of the deep Southern Ocean (Toggweiler *et al*., 2006; Garreaud *et al*., 2013). The SWWs bring precipitation that feeds the largest temperate ice fields in the Southern Hemisphere, the NPI and the South Patagonian Icefield (SPI) (Warren and Sugden, 1993). In addition to these icefields, two smaller icefields, the Cordillera Darwin and Gran Campo Nevado, along with numerous smaller glaciers are all that remain of the former PIS. The present day NPI covers an area of 3976 km^2 (Davies and Glasser, 2012), contains 1234.6 km^3 of ice (3.10 mm sea-level equivalent) (Carrivick *et al*., 2016) and has a mean ice thickness of 305 m. The equilibrium line altitude ranges from ~900 m in the west to ~1300 m in the east (Rivera *et al*., 2007).

The strong circulation at the core of the SWWs (49° S-53° S) is due to limited land at these latitudes, resulting in low friction and a strong pressure gradient between the cold Antarctic and warm subtropics (Aravena and Luckman, 2009; Garreaud *et al*., 2009). The Patagonian Andes act as the only significant barrier to the SWWs, causing a strong orographic effect, as a result forming an extreme climate divide. Precipitation in the west exceeds 3000 mm yr^{-1}, reaching 6000 mm yr^{-1} (in places up to 10,000 mm yr^{-1}) on the mountain tops, and dropping to less than 100-200 mm yr^{-1} within 100 km east of the Andean foothills (Garreaud, 2009). The precipitation gradient creates distinct vegetation zones. In central Patagonia, the North Patagonian rainforest dominates humid western islands and mountain slopes, along with moorland covering some islands. On the leeward mountain side, subantarctic deciduous forest transitions through shrubland to the Patagonian steppe in the semi-arid zone. Subantarctic rainforest fills the gap between the NPI and SPI.

3. Methods

For the purpose of this review we have re-calculated all geochronological data from central Patagonia. Radiocarbon ages were recalculated using the OxCal 4.3 online calibration tool (Bronk Ramsey, 2009) and the ShCal13 Southern Hemisphere calibration curve (Hogg *et al*., 2013), and are presented in the text as median cal ka BP. For cosmogenic ^{10}Be surface exposure ages, we used the online exposure age calculator formerly known as the CRONUS-Earth online calculator (v. 2.2; constants v.2.2.1; Balco *et al*., 2008) and the local ^{10}Be production rate for southern Patagonia (Kaplan *et al*., 2011). Cosmogenic ^{36}Cl ages have been re-calculated using the CRONUScalc web calculator (Marrero *et al*., 2016a) and production rates presented by Marrero *et al*. (2016b). Ages for moraines

Table 1. Palaeoenvironmental proxies discussed in the text.

Site ID*	Core	Site	Lat (DD)	Long (DD)	Elev. (m)	Core length (m)	Stratigraphic range (ka)	Age control	References
Lake cores									
L9	LS0604A	Lake Shaman	46.43	71.18	919	6.13	19 - 0	14C	de Porras *et al.*, 2012
L7	composite	Lago Los Ninos	44.01	71.29	1015	8.12	17 - 0.1	14C	Iglesias *et al.*, 2016
L8	LP09B	Laguna La Pava	44.28	71.31	731	4.8	13.2 - 0.5	14C	Iglesias *et al.*, 2016
L10	CAST01	Lago Castrol	45.6	71.8	699	15.4	41 - 0	14C, floating varve, tephra	Van Daele *et al.*, 2016
L11	composite	Lago Augusta	47	72.38	440	11.53	16 - 0.65	14C, tephra	Villa-Martinez *et al.*, 2012
L12	composite	Lago Edita	47.13	72.42	570	17.26	19 - 9.0	14C, tephra	Henríquez *et al.* (in review)
L1	-	Laguna Facil	44.33	74.28	10	7.63	15.8 - 0	14C	Haberle and Bennet, 2004
L2	-	Laguna Oprasa	44.35	73.66	50	7.26	16.3 - 0	14C	Haberle and Bennet, 2004
L4	-	Laguna Lincoln	45.35	74	< 50	-	-	14C	Bennett *et al.*, 2000
L3	-	Laguna Lofel	44.88	74.41	< 50	-	-	14C	Bennett *et al.*, 2000
L6	-	Laguna Six Minutes	46.42	74.34	< 50	-	-	14C	Bennett *et al.*, 2000
L5	-	Laguna Stibnite	46.45	74.42	< 50	-	-	14C	Bennett *et al.*, 2000
L5	-	Laguna Stibnite			20	4.75	17.4 - 0	14C	Lumley and Switsur, 1993
Peat cores									
P1	composite	Mallín El Embudo	44.66	71.7	686	8.44	13 - 0	14C	De Porras *et al.*, 2014
P2	-	Mallín Pollux	45.69	71.84	640	14.07	18 - 0	14C	Markgraf *et al.*, 2007
P3	-	La Frontera	46.87	71.88	997	3	8.2 - 0.35	14C, tephra	McCulloch *et al.*, 2016
P4	-	La Tercera	49.18	72.36	-	2.19	11.3 - 0	14C	Bamonte and Mancini 2011
Marine cores									
MD07-3088	MD07-3088	-	-	-	-	18.9	22 - 0	δ18O, 14C, tephra	Siani *et al.*, 2010; Montade *et al.*, 2013
M1	JPC14	Golfo Elefantes	-	-	-	-	~ 11.3 - 0	14C	Fernandez *et al.*, 2012
M2	JPC12	Golfo Elefantes	-	-	-	-	~ 11.3 - 0	14C	Fernandez *et al.*, 2012

*refers to site ID in Fig. 1

based on multiple cosmogenic nuclide analyses were derived from camel plots and are presented as the probabilistic peaks. The outliers identified in the original publications were removed from the camel plots. All exposure ages assume zero rock surface erosion and no shielding (snow, soil, loess, vegetation) and thus are minimum ages. However, inclusion of an erosion rate of 0.2 m Ma^{-1} derived in the LBA valley on the basis of paired $^{36}Cl/^{10}Be$ concentrations (Douglass *et al*., 2007), increases an LGM age by less than 1%, and thus is well within the reported internal uncertainties. Individual exposure ages are presented with 1σ external uncertainties to allow comparison to radiocarbon ages. The data used to calculate the exposure ages are presented in Supplementary Table 1 (Available at: http:publicaciones.unirioja.es/revistas/cig2017/Mendelova_TableS1.xlsx). The original publications should be consulted for the original data and further information.

4. Glacial History

Mapping and dating of glacial limits has been done primarily along the eastern flank of the Patagonian Andes. The geomorphological record here is exceptionally well preserved due in part to the arid climate on the eastern side of Andes. Here, moraine systems can be found in nearly every valley between 38° S and 56° S, and often are associated with, or confine large lakes. In the past decade the application of cosmogenic nuclide surface exposure dating and optically stimulated luminescence (OSL) has led to an increase in the concentration and geographic range of glacial chronologies. Numerous well-dated chronologies have been developed in southern Patagonia and Tierra del Fuego (e.g. Darvill *et al*., 2015; Kaplan, *et al*., 2008b; McCulloch *et al*., 2005b). With the exception of two well-dated chronologies from LBA and LP, glacial chronologies remain sparse in central Patagonia, and at the time of writing there are no published chronologies for NE Patagonia. To the west of the Andes, the PIS terminated in the ocean during the LGM and most geomorphological evidence is therefore submarine, with the exception of north-western Patagonia including the Chilean Lake District, where glaciers terminated on land and their advances over the last glacial cycle have been well documented (Denton *et al*., 1999).

Regional distribution of palaeoenvironmental records largely depends on the availability of suitable natural archives (e.g. peat bogs, lakes). However, the location of study sites is also biased towards the east in part due to the limited accessibility of the Chilean fjords, with the exception of Isle Grande Chiloé in north-western Patagonia, and the Chonos Archipelago and Taitao Peninsula in central-western Patagonia. Swath bathymetry can reveal submarine geomorphological evidence and it has been applied in the southern Chilean fjords (e.g. Dowdeswell *et al*., 2016; Dowdeswell and Vásquez, 2013). Less is known about the bathymetry of the fjords between 44° S and 46° S (Völker *et al*., 2013).

Between latitudes 44° S and 49° S, the former PIS drained eastwards by ten topographically controlled outlet glaciers and ice lobes, which extended onto the Andean plains during the LGM (Glasser and Jansson, 2005; Glasser *et al*., 2008). Each of these outlet glaciers left behind a series of moraine limits (Fig. 2). To date, however, most research efforts have focused on just two of these formerly glaciated basins: LBA and LP. Here, argon-argon ($^{40}Ar/^{39}Ar$) dating of basaltic lava flows interbedded with the glacial deposits,

cosmogenic nuclide surface exposure dating, soil formation rates and OSL dating have been used to date glacial advances spanning from the Greatest Patagonian Glaciation (ca. 1.1 Ma) through to the last glacial cycle (e.g. Singer *et al*., 2004; Douglass and Bockheim, 2006; Kaplan *et al*., 2004; Smedley *et al*., 2016; Hein *et al*., 2010). Moraine systems in the other basins, which probably relate to the last glacial cycle, or older, have received little attention. Younger, likely Lateglacial to Holocene moraines are found within the Andean valleys closer to the NPI and present day mountain glaciers. On the western side of the Andes, terrestrial geomorphological evidence is confined to the Taitao Peninsula (Fig. 1c).

The locations of environmental proxies discussed in the paper are shown in Figure 1c and are listed in Table 1. On the western side of the Andes, several peat bog and lake cores have been obtained from the Taitao Peninsula and the Chonos Archipelago, which cover the Lateglacial and Holocene period. A marine core (MD07-3088) recovered off the Taitao Peninsula (46° S) provides a high-resolution pollen, clay mineralogy and major geochemistry record covering the last 22 ka (Siani *et al*., 2010; Montade *et al*., 2013). Multiple peat bog and lake cores have been sampled from valleys along the eastern flank of the Andes and provide a record covering the Lateglacial and Holocene. Minimum radiocarbon ages for deglaciation are listed in Table 2. In the following, we describe the data that constrain the LGM and the onset of deglaciation, the Lateglacial and the Holocene from the western and eastern side of the Andes.

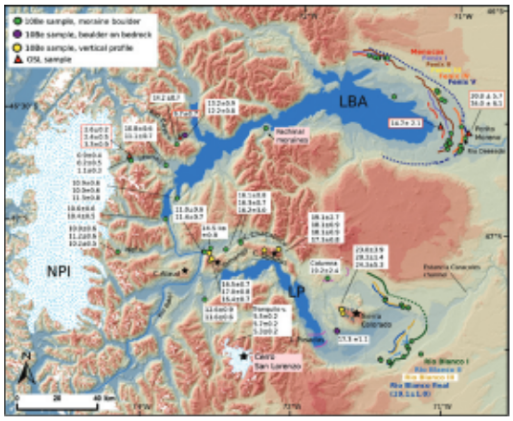

Figure 2. North Patagonian Ice Field (NPI), Lago Buenos Aires/Lago General Carrera (LBA) and Lago Pueyrredón/Lago Cochrane (LP)showing geochronological data (in ka) and delineated moriane limits, Fenix and Río Blanco, corresponding to the global Last Glacial Maximum, Columna and Lago Posadas moraines (pink), and lateral moraines on Sierra Colorado. Camel plots showing age distribution for Fenix, Rio Blanco limits, and Fachinal moraines are presented in Figs. 4 - 6, respectively.

Table 2. Minimum radiocarbon ages for deglaciation.

References	Site	Site ID*	Lat (DD)	Long (DD)	Elev. (m)	^{14}C Age	cal BP (median ± σ)	cal range BP (99.7 %)	Archive	Material	Notes
de Porras *et al.*, 2012	Lake Shaman	L9	46.43	71.18	919	15740 ± 50	18934 ± 72	19187 - 18745	welland core	macrofossils	
Van Daele *et al.*, 2016	Lago Castrol	L10	45.6	71.8	699	36 600 ± 250	41204 ± 272	41905 - 40332	lake core	bulk	below hiatus
Villa-Martinez *et al.*, 2012	Lago Augusta	L11	47.01	72.38	440	16445 ± 45	19792 ± 105	20070 - 19530	lake core	bulk	outlier
						12 785 ± 35	15183 ± 75	15452 - 14862	lake core	bulk	
Henríquez *et al.* (in review)	Lago Edita	L12	47.13	72.41	570	16250 ± 90	19565 ± 142	20001 - 19172	lake core	bulk	
						16020 ± 50	19282 ± 106	19572 - 18989	lake core	bulk	
Turner *et al.*, 2005	Cerro Ataud	-	47.28	72.65	-	13550 ± 95	16267 ± 157	16795 - 15820	kettle hole	peat	
	Cerro Ataud	-	47.28	72.65	-	13107 ± 81	15651 ± 158	16069 - 15231	kettle hole	macrofossils	
Haberle and Bennet, 2004	Laguna Facil	L1	44.32	74.28	10	13230 ± 140	15832 ± 221	16453 - 15187	lake core	bulk	
	Laguna Oprasi	L2	44.35	73.65	50	13560 ± 125	16287 ± 197	16928 - 15751	lake core	bulk	
Lumley and Switsur, 1993	Laguna Sibnite	L5	46.44	74.41	20	14335 ± 145	17401 ± 209	17980 - 16731	lake core	bulk	

*Site ID refers to locations in Fig.1.

**Radiocarbon ages were recalculated using the OxCal 4.3 online tool (Bronk Ramsey, 2009) and the ShCal13 curve (Hogg *et al.*, 2013).

4.1. Last Glacial Maximum

4.1.1. Western Andes

At the LGM, the PIS is thought to have extended over the western islands and terminated in the ocean near the continental shelf edge (Hubbard *et al*., 2005). As a consequence, there is no direct field evidence on the extent and timing of glacier advances during the LGM. However, a terrigenous sediment record recovered from immediately offshore of the Taitao Peninsula (Fig. 1c) was used to infer glacial advances at 21.6-20.9 ka, 20.2-20 ka, 19.6-19.1 ka and 18.5-18 ka, based on rapid short-term fluctuations of smectite/(illite + chlorite) and titanium/potassium (Siani *et al*., 2010). The record indicates increased erosion of the Coastal Range of Chile due to glacier dynamics until ca. 18 ka. An increase in the sediment input from the Andean Cordillera after 18 ka suggests the withdrawal of the ice margin from the western island zone by this time (Siani *et al*., 2010). Minimum radiocarbon ages from Laguna Stibnite suggest that the Taitao Peninsula was ice free by 17.4 ± 0.2 cal ka BP (Lumley and Switsur, 1993), and the northern parts of the Chonos Archipelago by 16.3 ± 0.2 cal ka BP (Haberle and Bennett, 2004).

On the Taitao Peninsula, a series of arcuate terminal moraines indicate that valley glaciers flowing east and south from the centre of the peninsula drained an independent ice cap (Fig. 3) (Heusser, 2002; Glasser *et al*., 2008). In one locality (Laguna Elena), at least twelve distinct moraines indicate multiple re-advances or still-stands (Heusser, 2002). The age of these moraines is unknown, but on the basis of a minimum radiocarbon age for deglaciation of the peninsula (17.4 ± 0.2 cal ka BP) (Lumley and Switsur, 1993),

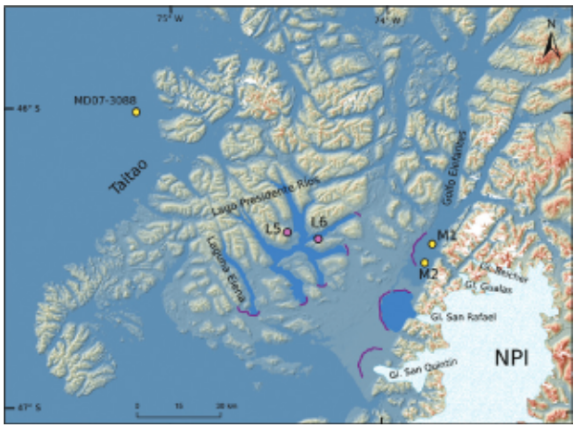

Figure 3. The Taitao Peninsula and adjacent Cordillera showing the locations of undated moraines (purple) discussed in the text, and offshore and lake sediment cores.

it has been suggested that they might date to the LGM (Heusser, 2002). If correct, this would imply either the limited expansion of the PIS to the west at the LGM, or that the deep Golfo Elefantes prevented the ice sheet from overrunning the Taitao Peninsula (Glasser *et al*., 2008). In the former case, the climatological conditions that would allow for growth of an ice cap on the low-lying peninsula, but not support ice expansion from the Cordillera are unclear (Glasser *et al*., 2008), and the scenario is difficult to reconcile with LGM ice expansion further north in the Chilean Lake District (Denton *et al*., 1999). The latter case also seems improbable given that there is morainic evidence to show that the NPI outlet glaciers (Gualas/Reicher Glaciers) advanced over Golfo Elefantes (Heusser, 2002). An alternative is that the moraines on the Taitao Peninsula were deposited during late LGM still-stands, shortly after the separation of the Taitao ice cap from the PIS, and prior to rapid deglaciation on the peninsula.

4.1.2. Eastern Andes

Ten outlet glaciers drained the former PIS between 44° S and 49° S (Glasser *et al*., 2008). Several moraine systems can be found at the eastern end of these formerly glaciated basins. While predominantly undated, the innermost moraines have been tentatively correlated to the LGM (Fig. 1c) (Glasser *et al*., 2008). Rabassa *et al*. (2011) provided a summary of earlier studies that described the drifts and moraines in these basins. In the absence of direct dating of the moraines, radiocarbon ages from lake and peat bog cores provide a minimum deglaciation age (Table 2). In the Río Cisnes valley (44.7° S; Fig. 1), a minimum radiocarbon age from an intermorainic lake (Lago Shaman) indicates that ice abandoned the innermost moraine system before 18.9 ± 0.1 cal ka BP (de Porras *et al*., 2012). Further upstream, a core from Mallín El Embudo, suggests that the middle part of the Río Cisnes valley was occupied by a proglacial lake until ca. 13 cal ka BP (de Porras *et al*., 2014). Further south in the Río Simpson basin (45.6° S), a minimum radiocarbon age of 41.2 ± 0.3 cal ka BP was obtained from Lago Castor. However, a hiatus in the stratigraphy suggests that a later readvance over the site might have occurred (Van Daele *et al*., 2016).

Cosmogenic ^{10}Be ages from moraine boulders revealed that the LBA outlet lobe (46.5° S) reached its maximum extent sometime between 27-25 ka as marked by the Fenix V moraine (Figs. 2, 4). Four subsequent readvances or still-stands are indicated by the Fenix IV-I moraines, with the final advance at ca. 19.3 ka (^{10}Be peak age, Fenix I) (Douglass *et al*., 2006; Kaplan *et al*., 2004). Cosmogenic ^{10}Be ages from moraine boulders on the Río Blanco moraine system showed that the LP ice lobe (47.5° S) reached its maximum extent at ca. 28.0 ka (^{10}Be peak, Río Blanco I), a little earlier than the LBA outlet (Hein *et al*., 2010; Hein *et al*., 2009). Three subsequent re-advances or still-stands are evident by the Río Blanco II-III moraines, with a final advance dated at ca. 21.6 ka (^{10}Be peak; Fig. 5) (Hein *et al*., 2009, 2010). ^{10}Be ages from boulders and bedrock along a mountain transect separating the LP and Chacabuco valleys were used to reconstruct ice surface profiles (Boex *et al*., 2013). Lateral moraines on Sierra Colorado (~1170 m a.s.l.) (Fig. 2) yielded ^{10}Be ages of 23.8 ± 3.9, 28.3 ± 1.4 and 24.3 ± 5.3 ka, thus corresponding to the Río Blanco terminal limits as indicated by

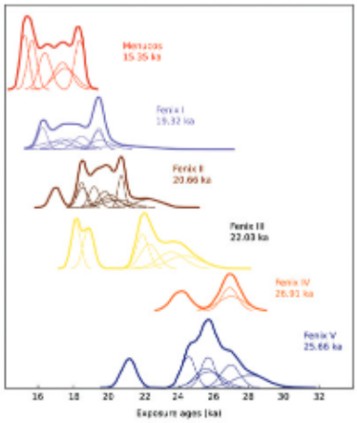

Figure 4. Camel plots summarising distribution of ^{10}Be ages for each of the Fenix moraine limits and Menucos limit, outliers identified in the original publications were removed. Thin lines represent individual Gaussian probability distributions for ^{10}Be ages with 1σ internal error; thick line represents the sum of the individual probability distributions.

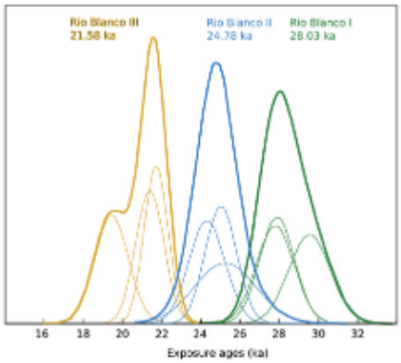

Figure 5. Camel plots summarising distribution of ^{10}Be ages for each of the Río Blanco moraine limits, outliers identified in the original publications were removed. Thin lines represent individual Gaussian probability distributions for ^{10}Be ages with 1σ internal error; thick line represents the sum of the individual probability distributions.

geomorphological mapping. The profiles revealed that the LP lobe had a low surface gradient and a maximum thickness of ~1100 m at this location, a result consistent with previous modelling (Hubbard *et al*., 2005).

Recently, Smedley *et al*. (2016) reported OSL ages of 30.8 ± 5.7 ka and 34.0 ± 6.1 ka from glacial outwash related to the Fenix moraines (LBA). They concluded that an earlier ice advance occurred and deposited the outwash, but the corresponding moraine was not preserved. It is likely the moraine was overrun by a subsequent ice advance or removed by meltwater. These results suggest the local LGM may have occurred earlier than indicated based on the preserved moraine record. Supporting evidence for an earlier advance comes from a single ^{10}Be age from a boulder on a small moraine crest just outside of the outermost Río Blanco limit in the LP valley that gave an age of 35.1 ± 1.2 ka (Hein *et al*., 2010). The retreat of the ice margin initiated at approximately the same time in both the LBA and LP valleys at ca. 19 ka, and coincided with the onset of ice surface lowering revealed by the vertical reconstruction of the ice sheet surface in the LP/Chacabuco valleys (Boex *et al*., 2013). The initial deglaciation in both valleys was interrupted by subsequent re-advances. The LBA outlet lobe initially retreated to an unknown distance, leading to the formation of a proglacial lake. A subsequent re-advance then deposited the Menucos moraine above varved lake sediment (Douglass *et al*., 2006; Kaplan *et al*., 2004; Turner *et al*., 2005). Cosmogenic ^{10}Be ages from moraine boulders on the Menucos moraine yielded range between 18.3 ka and 15.2 ka (Douglass *et al*., 2006). Given that most geological processes act to reduce apparent exposure ages, the older ages of 18.3 ka are probably more representative of the true age of the moraine. Cemented-carbonate concretions in the stratigraphically older varved sediments gave three radiocarbon ages of 15.3 ± 0.3, 15.3 ± 0.2, and 17 ± 0.5 cal ka BP (Kaplan *et al*., 2004; Sylwan, 1989). However, these ages should be interpreted with caution as the origin of carbonate concretions is uncertain (Hein *et al*., 2010). Smedley *et al*. (2016) reported an OSL age of 14.7 ± 2.1 ka from glaciofluvial sediment stratigraphically older than Menucos moraine, and thus there remains an element of uncertainty on the age of the Menucos moraines. After their deposition, the glacier most likely retreated permanently back into the LBA basin.

A re-advance or still-stand also occurred in the LP and Chacabuco valleys depositing the Lago Posadas and Lago Columna moraines (Hein *et al*., 2010). There are limited data to constrain the age of these moraines. A boulder on the Columna moraine yielded a ^{10}Be age of 19.2 ± 2.4 ka (Boex *et al*., 2013), and a boulder on bedrock in the LP valley, which provided a minimum age for the readvance, had a ^{10}Be age of 17.3 ± 1.1 ka (Hein *et al*., 2010). The latter age, which came from an erratic that was submerged in a pro-glacial lake, was also used to infer ice retreat of more than 80 km and draining of the lake by this time. Rapid thinning initiated at ca. 18 ka, as revealed by ^{10}Be ages constraining the ice surface elevation, which lowered to expose both Cerro Oportus and Cerro Tamango completely in approximately 1000 years, equivalent to about 1000 m of ice-surface lowering (Boex *et al*., 2013). The Lago Augusta (440 m) and Lago Edita (570 m) lake records indicate that the Chacabuco Valley was ice free and no longer inundated by a proglacial lake by 15.2 ± 0.1 cal ka BP

(Villa-Martínez *et al*., 2012), or as early as 19.6 ± 0.1 cal ka BP (Henríquez *et al*., 2017). Two radiocarbon ages obtained from a kettle hole near Cerro Ataud, interpreted as minimum deglaciation ages, indicate that the ice had receded close to the Andean foothills by ca. 16 cal ka BP (Turner *et al*., 2005). Cosmogenic ^{10}Be ages for the Río Blanco moraines (Hein *et al*., 2010), Columna moraine, vertical ice surface profiles, minimum radiocarbon deglaciation ages and the Lago Augusta stratigraphy all appear consistent, within uncertainties, suggesting rapid deglaciation of more than 100 km occurred between ca. 19 ka and 16 ka.

There is growing evidence to suggest that in north-western and southern Patagonia, the local LGM occurred during Marine Isotope Stage (MIS) 3, earlier than in central Patagonia. On Tierra del Fuego, the Bahía Inútil-San Sebastián ice lobe (53-54° S) advanced about 100 km beyond the global LGM limit at 45.6 ka and 30.1 ka (Darvill *et al*., 2015). Sagredo *et al*. (2011) dated the local maxima of the Última Esperanza lobe (51-52° S) to ca. 39 ka, and found no limits corresponding to the global LGM. Two exposure dates from a moraine in the Lago San Martin valley (49° S) tentatively indicate an advance at about 34-37 ka (Glasser *et al*., 2011). In north-western Patagonia, the radiocarbon chronology from the Chilean Lake District revealed advances at 33.6 cal ka BP and 30.8 cal ka BP (Denton *et al*., 1999). Pre-LGM advances have been documented elsewhere in the Southern Hemisphere as well; in New Zealand, the Ohau Glacier (44° S) advanced at ~32 ka (Putnam *et al*., 2013), the Pukaki Glacier (44° S) advanced at ~65 ka (Schaefer *et al*., 2015) and again at ~42 ka (Kelley *et al*., 2014), and the Mt. Field glaciers in Tasmania advanced at 44-41 ka (Mackintosh *et al*., 2006).

Deglaciation of the LBA, LP and Chacabuco valleys preceded the onset of warming (18 ka) identified in a marine core off Taitao peninsula (Montade *et al*., 2013; Siani *et al*., 2010) and field evidence suggests that deglaciation occurred earlier and more rapidly than predicted by modelling experiments (Hubbard *et al*., 2005). Deglaciation in central Patagonia appears to have initiated about 1000 years earlier than in southern Patagonia or the Chilean Lake District. Recession of the Última Esperanza ice lobe started after 17.5 ka (Sagredo *et al*., 2011), deglaciation in Torres del Paine was underway by ca. 17.4 ka (García *et al*., 2014), the Strait of Magellan and Bahía Inútil were underway by ca. 17 ka (Kaplan *et al*., 2008b; McCulloch *et al*., 2005a), and in the Chilean Lake District, ice recession was underway by ca. 17.8 ka (Moreno *et al*., 2015; Denton *et al*., 1999). The timing is similar to the onset of deglaciation in New Zealand (Rother *et al*., 2015; Putnam *et al*., 2013; Kelley *et al*., 2014; Doughty *et al*., 2015; Schaefer *et al*., 2006). The cause of early, rapid deglaciation in central Patagonia likely stems from many processes. Rapid deglaciation here has been linked to southward migration of the SWWs and regional warming (Boex *et al*., 2013), which could also help to explain the comparatively early deglaciation. Modelling experiments indicate the PIS in central Patagonia is stable in two states, full glacial and full interglacial (Hubbard *et al*., 2005). At these times, the ice sheet is relatively insensitive to changes in climate. However, during deglaciation, the modelling suggests the ice sheet reached a tipping point where it rapidly switched between stable states and deglaciated, losing some 85% of its volume in 800 years (Hubbard *et al*., 2005). Thus, while the trigger for initial deglaciation will relate to an external driver, the feedbacks within the system,

including the change in dynamics associated with ice calving into deep pro-glacial lakes, must play a significant role in the rapidity of ice decline following the LGM.

4.2. The Lateglacial

4.2.1. Western Andes

On the western side of the Andes there are no directly dated Lateglacial ice limits. There are a series of moraines indicating an expansion of the NPI outlet glaciers (San Quintín, San Rafael and Gualas/Reicher Glaciers) to form three piedmont lobes. It has been suggested that these moraines might be correlative (Heusser, 2002). Tentatively dated sedimentological records suggest that Golfo Elefantes remained ice free since ca. 11.3 ka, and thus the moraines deposited along its western edge by the Gualas/Reicher Glacier are probably older than this age (Fernandez *et al*., 2012). The San Rafael Glacier advanced into a pre-existing moraine system during the early Holocene (see section 4.3.1.). The exact timing for the formation of these piedmont lobes remains to be established. The existing evidence suggests the Taitao Peninsula and the Chonos Archipelago likely remained ice free for most of the Lateglacial.

In the marine pollen record, gradual *Nothofagus* forest expansion was recorded from ca. 17.6 cal ka BP, representing a first step of warming (Montade *et al*., 2013). Closed *Nothofagus-Pilgerodendron-Podocarpus* forest developed across the Chonos Archipelago and Taitao Peninsula between 14-13 cal ka BP and showed no reductions in the forest cover once a closed forest became established (Haberle and Bennett, 2004; Bennett, 2000; Lumley and Switsur, 1993). Humid rainforests, once established, tend to be insensitive to smaller climatic changes. However, a high-resolution marine pollen record indicated there was an increase in Magellanic moorland (*Astelia*) at 14.5 cal ka BP, interpreted as a sudden precipitation increase accompanied by a pause in the warming trend and coinciding with the ACR. The subsequent retreat of the Magellanic moorland after 12.8 cal ka BP marks the second warming step during the Lateglacial and provides a strong evidence for the end of the ACR (Montade *et al*., 2013). A Chironomid record from Laguna Stibnite (Taitao Peninsula) shows a peak in abundance of *Podonominae* between 13.1-10.5 cal ka BP, interpreted as indicative of cool and oligotrophic lake waters. The changes in the chironomid assemblages were small, however, and any cooling during this period, coeval with the YD would have been minimal (Massaferro and Brooks, 2002).

4.2.2. Eastern Andes

4.2.2.1. Glacier advances

Evidence for the extent of glaciers during the Lateglacial is sparse on the eastern side of the Andes. Four moraines deposited by Tranquilo Glacier, Cerro San Lorenzo, were dated to the ACR using ^{10}Be (E. Sagredo, personal communication, 2017). These provide the only direct evidence for an ACR glacier re-advance in central Patagonia. A single ^{10}Be age of 14.2 ± 0.7 ka from the Lago Tranquilo cirque moraine, and two ^{10}Be ages of 13.2 ± 0.9 and 12.2 ± 0.8 ka, from boulders on bedrock in the Río Bayo valley have also been reported (Glasser *et al*., 2006). Unlike moraines, exposure ages from

boulders on bedrock do not represent advances or still-stands, but in this case they do suggest that the ice margin withdrew to within ~30 km of the present day margin by ca. 13 ka. Glasser *et al*. (2012) obtained ^{10}Be ages from moraines in several valleys east of the present day NPI (Fig. 2), ranging from ca. 11.4-10.0 ka, which represent advances near the Lateglacial/Holocene transition. Although most of these moraines have apparent early Holocene exposure ages, within uncertainties, they might represent the culmination of YD advances/still-stands (Glasser *et al*., 2012). We note that in certain locations east of the NPI, such Lateglacial advances may be intricately linked with the development of regional lakes that have the potential to complicate surface exposure ages if samples had been submerged.

In contrast, Lateglacial glacier advances are well-documented in southern Patagonia. Robust radiocarbon and cosmogenic nuclide chronologies from Lago Argentino (50° S; Fig. 1) showed that outlet glaciers advanced during the ACR, deposited the Puerto Bandera moraines, and subsequently retreated during the YD, reaching within 20 km of the present day glacier margins by 12.2 ka (Strelin *et al*., 2011; Kaplan *et al*., 2011; Ackert *et al*., 2008). ^{10}Be and radiocarbon chronologies from Torres del Paine (51° S), revealed that the outlet glaciers of the SPI re-advanced during the ACR and ice recession was underway by about 12.5 ka (García *et al*., 2012; Moreno *et al*., 2009; Fogwill and Kubik, 2005). There is geomorphic and stratigraphic evidence for a re-advance of the Última Esperanza lobe (52° S), tentatively assigned to 14.8-12.8 ka (Sagredo *et al*., 2011). In Tierra del Fuego (54.6° S), ^{10}Be ages from cirque moraines showed deposition contemporaneous with the ACR (Menounos *et al*., 2013). A re-advance of the Cordillera Darwin outlet glaciers into the Strait of Magellan, coeval with the ACR, has been suggested by McCulloch *et al*. (2005a, 2005b) . Still-stands or minor re-advances coeval with the YD interrupted the overall ice retreat from the maximum ACR position at numerous sites in southern Patagonia (Strelin *et al*., 2011; Moreno *et al*., 2009; Kaplan *et al*., 2011). A similar pattern of glacier advances culminating at the end of the ACR, followed by retreat during the YD has been documented in New Zealand (Kaplan *et al*., 2010; Kaplan *et al*., 2013; Putnam *et al*., 2010; Turney *et al*., 2007). These glacier advances occurred during the northern hemisphere Bølling/Allerød interstadial.

4.2.2.2. Lake evolution

The over-deepened nature of the glacially-eroded basins in central Patagonia led to the formation of large proglacial lakes as ice retreat progressed. These lakes initially drained eastward into the Atlantic Ocean because the low-lying structural gap in the Andes (48° S) was blocked by the PIS. As ice retreat progressed, several of these lakes are thought to have become interconnected as a large regional lake east of the present NPI (Turner *et al*., 2005; Bell, 2008; Hein *et al*., 2010; Glasser *et al*., 2016; Bourgois *et al*., 2016). The position of ice margins to the west and moraine dams to the east determined the location of low overspill routes and hence controlled the former lake levels (Glasser *et al*., 2016). The retreating ice margin caused a gradual re-organization of the drainage, leading to a final sudden drainage of the lake into the Pacific as the ice sheet separated and the Río Baker Valley opened up (Turner *et al*., 2005; Bell, 2008; Hein *et al*., 2010; Glasser *et al*., 2016). This forced a 200 km migration of the water divide, a major re-

organization of the drainage and released between 160 km^3 and 1150 km^3 of freshwater into the Pacific Ocean (Glasser *et al*., 2016; Hein *et al*., 2010). Therefore, the palaeo-lake history has implications for understanding of the wider deglacial history of the region, the dynamics of glaciers terminating in such lakes, and the impact of freshwater release on the regional oceanic and climate system in the Pacific. However, the timing and sequence of events relating to the evolution of palaeo-lakes in the LBA/LP basins, is the subject of debate.

Evidence of former lake levels in the form of raised shorelines, deltas and beaches has been documented in the LBA, LP and Chacabuco valleys (Turner *et al*., 2005; Bell, 2008; Hein *et al*., 2010; Glasser *et al*., 2016; Bourgois *et al*., 2016). The shorelines can be observed as continuous features at the eastern ends of LBA and LP, but become discontinuous toward the interior of the range. The elevations vary within and between each valley, but there appears to be enough coherence to suggest a series of palaeo-lake levels with an overall tilt toward the east; the tilt and variance are thought to be a consequence of differential isostatic rebound (Turner *et al*., 2005).

Turner *et al*. (2005) mapped three distinct shorelines in the LP and LBA valleys, on the basis of which a three-stage lake evolution was inferred. One shoreline mapped at 654-633 m a.s.l., which is confined to the LP basin, represented an upper lake level which drained eastwards via the Estancia Caracoles channel (475 m). Retreat of the ice margin exposed a part of Río Baker basin, allowing LP to drain into LBA to create a single lake at a lower elevation of 512-489 m a.s.l. and 484-390 m a.s.l. in LP and LBA valley respectively, and leading to the abandonment of the Estancia Caracoles channel. The minimum age for the abandonment of this channel is ca. 13 cal ka BP on the basis of radiocarbon ages from peat within the channel (Turner *et al*., 2005; Mercer, 1976), but probably closer to 17.3 ± 1.1 ka on the basis of a cosmogenic ^{10}Be age for the timing of lake drainage (Hein *et al*., 2010). The above mentioned radiocarbon age is unlikely to be a close minimum age as organic matter is limited and slow to develop in the arid environment east of the Andes. The single pro-glacial lake drained via a channel (near Perito Moreno) eastwards into the Río Deseado and to the Atlantic Ocean. The higher united lake must have formed and drained sometime before ca. 16 cal ka BP, based on the two ^{14}C ages from a kettle hole near Cerro Ataud (Turner *et al*., 2005) or by ca. 17.3 ka, based on the above mentioned ^{10}Be age from a boulder on bedrock (350 m a.s.l.) in the LP valley (Hein *et al*., 2010). A shoreline recorded at 397-375 m a.s.l. and 355-305 m a.s.l. in LP and LBA basins, respectively, provides evidence for a lower united pro-glacial lake. This shoreline is constrained by two ^{10}Be ages from boulders on a delta in Nef Valley (14.2 ± 0.6 and 15.4 ± 0.6 ka), two direct radiocarbon ages obtained from *in situ* organic material from a kame delta at Río Nef (12.7 ± 0.04 cal ka BP) and a lake terrace at Mirador Chile Chico (13.4 ± 0.1 cal ka BP), and several minimum radiocarbon ages from the lake floor (Table 3) (Turner *et al*., 2005).

Three OSL ages ranging from 12.9 to 10.3 ka have been obtained from deltas above LBA at ~400 m a.s.l. (Glasser *et al*., 2016), equivalent to the higher single proglacial lake. However, the ages are significantly younger that the ages for the abandonment of the Estancia Caracoles channel (Turner *et al*., 2005; Mercer, 1976) and for the drainage

Table 3. List of ages associated with former shorelines of a palaeo-lake.

Site and geomorphological context	Shoreline association and age significance	Sample elev. (m)	Dating method*	Age			Sample number	Reference
Rio Nef, boulder on kame delta	lower united lake, direct age	365	10Be**	14195 ± 554			DES/00/C1	Turner *et al.*, 2005
Rio Nef, boulder on kame delta	lower united lake, direct age	368	10Be**	15412 ± 602			DES/00/C2	Turner *et al.*, 2005
					Calibrated age (BP)*			
				14C Age	cal median ±σ	cal range (99.7 %)		
Rio Nef, kame delta	lower united lake, direct age		14C	10780 ± 50	12687 ± 35	12758 - 12555		Turner *et al.*, 2005
Chile Chico Mirrador	lower united lake, direct age		14C	11636 ± 73	13420 ± 77	13717 - 13193		Turner *et al.*, 2005
Cerro Ataud I, kettle hole	lower united lake, min. age		14C	13550 ± 95	16267 ± 157	16795 - 15820		Turner *et al.*, 2005
Cerro Ataud I, kettle hole	lower united lake, min. age		14C	13107 ± 81	15651 ± 158	16069 - 15231		Turner *et al.*, 2005
Cerro Ataud II, kettle hole	lower united lake, min. age		14C	12105 ± 80	13915 ± 106	14242 - 13573		Turner *et al.*, 2005
Cerro Ataud II, kettle hole	lower united lake, min. age		14C	11578 ±71	13372 ± 72	13578 - 13138		Turner *et al.*, 2005
Lago Esmeralda I, kettle hole	lower united lake, min. age		14C	9805 ± 70	11184 ± 121	11596 - 10738		Turner *et al.*, 2005
Lago Esmeralda II, kettle hole	lower united lake, min. age		14C	10975 ± 80	12812 ± 85	13073 - 12680		Turner *et al.*, 2005
Lago Esmeralda III, kettle hole	lower united lake, min. age		14C	10752 ± 87	12654 ± 77	12882 - 12398		Turner *et al.*, 2005
El Maiten, kettle hole	lower united lake, min. age		14C	10472 ± 72	12284 ± 150	12654 - 11943		Turner *et al.*, 2005
Rio Cochrane, kettle hole	lower united lake, min. age		14C	10840 ± 95	12712 ± 85	13025 - 12431		Turner *et al.*, 2005
Cordon Esmeralda, kettle hole	lower united lake, min. age		14C	11205 ± 85	13017 ± 101	13275 - 12729		Turner *et al.*, 2005
Estancia Caracoles palaeochannel	channel abandonment, min. age		14C	11850 ± 75	13635 ± 84	13961 - 13419		Turner *et al.*, 2005
Estancia Caracoles palaeochannel	channel abandonment, min. age		14C	11245 ± 245	13069 ± 226	13849 - 12417		Mercer, 1976
Puente Santa Marta, aeolian sand capping of a delta	300 - 320 m a.s.l	333	OSL	8000 ± 500			PSM01	Glasser *et al.*, 2016
Peninsula Levican, delta	300 - 320 m a.s.l	301	OSL	10200 ±700			PL01	Glasser *et al.*, 2016
Rio Ibanez, delta	300 - 320 m a.s.l	315	OSL	9500 ± 800			RI102	Glasser *et al.*, 2016
Las Mercedes, palaeo-beach	300 - 320 m a.s.l	330	OSL	8500 ± 1100			MCS01	Glasser *et al.*, 2016
Bahia Murta, delta	300 - 320 m a.s.l	315	OSL	10600 ± 900			BMG02	Glasser *et al.*, 2016
Fachinal, delta	300 - 320 m a.s.l	303	OSL	11000 ±700			FD02	Glasser *et al.*, 2016
Jeneneni Valley, delta fragment	300 - 320 m a.s.l	303	OSL	9800 ±700			JV02	Glasser *et al.*, 2016
	300 - 320 m a.s.l	-	OSL	10900 ± 1600			SB01	Glasser *et al.*, 2016
Bertrand, delta fragment	370 - 440 m a.s.l.	396	OSL	12900 ± 2100			BC02	Glasser *et al.*, 2016
Rio Ibanez, flat topped feature	370 - 440 m a.s.l.	396	OSL	10300 ± 900			RI101	Glasser *et al.*, 2016
Puarto Ibanez,delta front foresets	370 - 440 m a.s.l.	396	OSL	11100 ± 200			PI102	Glasser *et al.*, 2016
Chile Chico, delta fragment	370 - 440 m a.s.l.	403	OSL	16800 ± 1500			WCC01	Glasser *et al.*, 2016
Los Tres Hermanos, palaeo-beach	460 - 520 m a.s.l	452	OSL	11800 ± 1200			LTH01	Glasser *et al.*, 2016
Las Mercedes, aeolian sand capping, palaeo-beach	460 - 520 m a.s.l	444	OSL	6500 ± 700			MCS02	Glasser *et al.*, 2016
				12000 ± 1300			MCS02	Glasser *et al.*, 2016

* ^{10}Be - cosmogenic surface exposure dating using ^{10}Be, ^{14}C - radiocarbon dating, OSL - optically stimulated luminescence.
**Exposure ages were calculated with the online calculator formerly known as the CRONUS online calculator (v.2.2; constants v. 2.2.1; Balco *et al.*, 2008), southern South America ^{10}Be production rate (Kaplan *et al.*, 2011), and the time-dependent Lal (1991)/Stone (2000) scaling model, see supplementary table for other scaling models.
***Radiocarbon ages were recalculated using the OxCal 4.3 online tool (Bronk Ramsey, 2009) and the ShCal13 curve (Hogg *et al.*, 2013), range at (99.7%).

of the higher united lake (Hein *et al*., 2010). OSL ages from deltas above LBA at ~300-315 m a.s.l., equivalent to the lower united lake, ranged from 11 to 9.5 ka (Glasser *et al*., 2016), and are also significantly younger than direct and minimum radiocarbon ages for the lower united lake (Turner *et al*., 2005). The persistence of the lower regional proglacial lake until ca. 8.5 ka, proposed on the basis of the two youngest OSL ages from deltas above LBA (Glasser *et al*., 2016), or 6.7 ka as inferred from the absence of volcanic ash on top of the lowest delta at Fachinal (Bell, 2008), appears at odds with the radiocarbon and cosmogenic nuclide age constraints. It is more likely that the final drainage of the lower pro-glacial lake into the Pacific Ocean occurred at ca. 12.7 ka on the basis of direct radiocarbon ages from the shoreline (Turner *et al*., 2005). Yet, several interpretations on the exact sequence and timing of events exist (Turner *et al*., 2005; Bell, 2008; Hein *et al*., 2010; Glasser *et al*., 2016; Bourgois *et al*., 2016) and further work is be required to resolve this.

4.2.2.3. Lateglacial palaeoenvironmental and climate records

Following ice retreat, most records from the eastern side of the Andes indicate an open landscape with sparse scrub-steppe dominated by *Poacea, Asteraceae,* and *Ericaceae* under persistent colder and drier conditions at most sites until ca. 14 cal ka BP (Markgraf *et al*., 2007; de Porras *et al*., 2012; Iglesias *et al*., 2016). Steppe taxa such as *Plantago* and *Acaena* was often present indicating disturbance and unstable post-glacial conditions (de Porras *et al*., 2012; de Porras *et al*., 2014; Markgraf *et al*., 2007; Iglesias *et al*., 2016). Small abundances of hygrophilous arboreal taxa in records from the eastern side of the Andes were interpreted as a long distance transport from forest refugia along the Pacific coast (Markgraf *et al*., 2007; de Porras, 2014). Iglesias *et al*. (2016) inferred ~200 mm annual precipitation required to support the reconstructed vegetation community (44° S 71° W). Subsequently, a gradual increase in *Nothofagus* taxa suggests grass-steppe vegetation with scattered trees and an increase in effective moisture, but still less than modern values (de Porras *et al*., 2012; Markgraf *et al*., 2007; de Porras *et al*., 2014). The pollen record from Lago Los Niños suggests open forest between 14.3-13.2 cal ka BP, with a subsequent trend towards more open landscape and drier conditions until 11.5 cal ka BP (Iglesias *et al*., 2016). Fluctuations of aquatic taxa in pollen records attest for high millennial environmental variability between ca. 14-11 cal ka BP (Markgraf *et al*., 2007; Villa-Martínez *et al*., 2012)

Contrary to the above, wetter and colder conditions throughout the Lateglacial period are inferred from the Lago Augusta and Lago Edita pollen record on the basis of arboreal taxa, such as *Nothofagus*, hygrophilous *Fitzroya*/*Pilgerodendron* and *Drimys* present immediately after the onset of sedimentation and persisting until 11.8 cal ka BP (Villa-Martínez *et al*., 2012; Henríquez *et al*., 2017). The pollen assemblages reflect patches of evergreen forests in an open landscape, likely a forest refugia in Chacabuco Valley (Henríquez *et al*., 2017), sustained by the enhanced influence of the SWW at this latitude. A decline in hygrophilous and cold-resistant taxa at ca. 11.8 cal ka BP is concurrent with an increase in *Nothofagus* and likely reflects warming and reduced precipitation due to the decreased influence of the SWWs.

4.3. Holocene

4.3.1. Western Andes

On the western side, the only evidence of Holocene glacier advances comes from the Rafael Glacier, a large outlet of the NPI. OSL ages from the Tempanos moraines (9.7 ka, 9.3 ka and 5.7 ka) and glacial outwash (7.7 ka and 7.8 ka) suggested that Rafael Glacier was either more extensive between 9.7 ka and 5.7 ka, or advanced multiple times during this time period (Harrison *et al*., 2012). However, non-climatic factors related to calving dynamics may have driven the Holocene fluctuations of Rafael Glacier. Previous sedimentological work demonstrated the complex composition of these moraines, resulting from sediment reworking by a glacier re-advance into its former proglacial area (Glasser *et al*., 2006). Holocene advances of the Rafael Glacier correlate with short term variations in offshore terrigenous sediment input at 10.1-9.1 ka and 7.8-6.5 ka, probably indicating glacier re-advances (Siani *et al*., 2010). Palaeoenvironmental archives, however, indicate warmer (~1° to 2° C above present mean temperature) and drier conditions during the early Holocene, as suggested by forests in the Chonos Archipelago dominated by *Tepualia* and *Weinmannia* between 12.4-6.7 ka (Haberle and Bennett, 2004). Palynological analysis of a marine core recovered off the Taitao Peninsula ~46° S (MD07-3088) showed an increase in heliophytic taxa, such as *Myrtacea* and *Tepualia,* from 11.5 to 7.4 ka, indicating the warmest and driest conditions of the Holocene (Montade *et al*., 2013). This is further supported by a chironomid record from Laguna Stibnite which suggested conditions drier than today between 10.5-7.2 cal ka BP (Massaferro and Brooks, 2002).

With the exception of one OSL date from the Tempanos moraines (see above), no moraines directly dated to the mid-Holocene have been reported. Sedimentological and geochemical analysis of two fjord sediment cores suggested that Gualas Glacier advanced towards the Golfo Elefantes shore between ca. 4 ka and 0.8 ka (Bertrand *et al*., 2012). The chironomid record from Laguna Stibnite suggests a trend towards wetter conditions during the mid-Holocene indicating intermediate precipitation between 7.2-5.2 cal ka BP and higher precipitation between 5.2-2.4 cal ka BP (Massaferro and Brooks, 2002). Slightly cooler and wetter conditions were also inferred from an increase in arboreal taxa, such as *Pilgerodendron,* in the marine pollen record from ca. 7.4 cal ka BP (Montade *et al*., 2013).

4.3.2. Eastern Andes

The Fachinal moraines were deposited on top of a raised delta above LBA and have ^{10}Be and ^{36}Cl ages of 8.9 ka (peak, inner moraine) and 10.9 ka (peak, outer moraine) (Douglass *et al*., 2005). The ages, including repeat measurements, in particular for the outer moraines, show a considerable scatter (Fig. 6). ^{10}Be ages from moraines east of the NPI (Leones and Nef valleys, Lago Negro, Lago Bertrand) might represent early Holocene advances (see section 4.2.2.1) (Glasser *et al*., 2012), correlative to the outer Fachinal moraines.

Palaeoenvironmental records suggest a drier and warmer period in the early Holocene. At ca. 11 ka, most records detected an increase in the frequency and magnitude

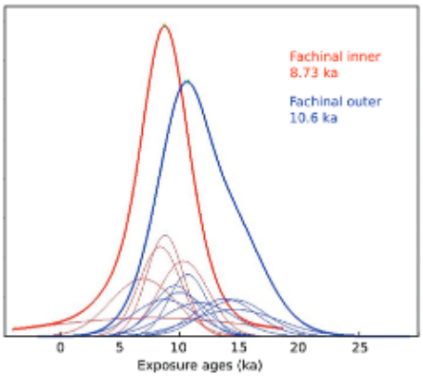

Figure 6. Camel plots summarising distribution of ^{10}Be ages for the inner and outer Fachinal moraines, outliers identified in the original publications were removed. Including re-calculated ^{36}Cl ages (Douglass et al.*, 2005) in the probability distribution (not shown) makes the peak age of the outer Fachinal moraine slightly younger (9.73 ka). Thin lines represent individual Gaussian probability distributions for ^{10}Be ages with 1σ internal error; thick line represents the sum of the individual probability distributions.*

of fires (de Porras *et al*., 2012; de Porras *et al*., 2014; Markgraf *et al*., 2007; Villa-Martínez *et al*., 2012), accompanied by a sudden change from aquatic to a dominance of marsh/bog taxa (de Porras *et al*., 2012), including a short-lived drying of a fen at Mallín Pollux (Markgraf *et al*., 2007). However, the concurrent expansion of *Nothofagus* forest suggests these changes represent an increase in effective moisture, but below modern values, and summers that were drier and/or warmer than present (de Porras *et al*., 2012; de Porras *et al*., 2014; Markgraf *et al*., 2007). The palynological record from the southern side of Lago San Martin is characterized by dominance of *Poaceae- Ephedra - Chenopodiaceaea* taxa between 11.3-9.5 cal ka BP. This pollen assemblage is analogous to modern dwarf-shrub steppe and was interpreted to represent precipitation lower than today, likely around 200 mm a^{-1} (Bamonte and Mancini, 2011). The increased frequency of fires, a peak in laminated carbonate deposition, decline of hygrophilous and cold-resistant taxa and the increase of *Nothofagus* taxa at Lago Augusta at ca. 11.8 cal ka BP was interpreted as a temperature increase and precipitation decrease, driven by a shift in the SWWs (Villa-Martínez *et al*., 2012). A major transgression was documented at Lago Cardiel during early Holocene ca. 11.8 cal ka BP (Gilli *et al*., 2005), attributed to easterly moisture advection to the extra-Andean region due to decreased SWW influence, which would support decreased precipitation within the Andes.

The cosmogenic ^{10}Be ages on moraines in the Río Tranquilo valley, indicate that an outlet glacier of the San Lorenzo ice cap advanced at ca. 5.5 ka (Sagredo *et al*., 2016). Three OSL ages (2.6 ± 0.2 ka, 2.4 ± 0.5 ka and 3.3 ± 0.9 ka) were obtained from glacio-

lacustrine sediments and a section in a terminal moraine of the Leon Glacier (Harrison *et al*., 2008). The OSL ages are, however, inconsistent with ^{10}Be ages obtained from the terminal moraine (1.1 ka and 0.9 ka) (Harrison *et al*., 2008). Several records suggest wetter and/or colder conditions during the mid-Holocene. From 8-3 cal ka BP the Lake Shaman record suggests the highest effective moisture for the whole record (de Porras *et al*., 2012). A shift to colder, periglacial conditions between 7.4-6.5 cal ka BP was inferred from sediment stratigraphy and a pollen record at a high altitude site at ~47° S, followed by drier temperate conditions until 3.7 cal ka BP, and a subsequent shift to more humid, temperate conditions (McCulloch *et al*., 2016). Similarly, a pollen record from Lago San Martin ~49° S indicated a decrease in moisture levels (<300 mm a^{-1}) between 8-3 cal ka BP (Bamonte and Mancini, 2011). At other sites, no major changes in the pollen record were observed once the closed *Nothofagus* forest established (Villa-Martínez *et al*., 2012; Markgraf *et al*., 2007).

There is evidence from both sides of the Andes for Lateglacial/early Holocene advances in central Patagonia (Glasser *et al*., 2012; Harrison *et al*., 2012; Douglass *et al*., 2005). Variations in the terrigenous sediment record, interpreted as a proxy for glacier activity, supports early Holocene (10 - 9 ka) glacier expansion (Siani *et al*., 2010). These glacier advances occurred despite the drier and warmer conditions inferred from the palaeoenvironmental proxies. It also contrasts with well-dated chronologies from southern Patagonia, where there was extensive recession of the Upsala Glacier from its Lateglacial maximum to within the present-day limit by ~9.2 ka (Kaplan *et al*., 2016; Strelin *et al*., 2014; Strelin *et al*., 2011). The SPI outlet glaciers were most extensive between 6.1-4.5 ka (Kaplan *et al*., 2016; Strelin *et al*., 2014; Strelin *et al*., 2011). Model simulations suggested a northward shift of low level SWWs at and before 9 ka, leading to substantial precipitation increases on the western side of Andes and at high elevation north of 49° S (Pollock and Bush, 2013).

5. Discussion and Conclusions

5.1. Local LGM

The LGM is only constrained chronologically at LBA and LP where the Fenix and Río Blanco ice limits represent advances contemporaneous with the global LGM. However, there exists a growing body of evidence from elsewhere in Patagonia and New Zealand to suggest that glaciers reached their maxima earlier in the last glacial cycle, during MIS 3 when southern insolation was more favourable (García *et al*., in review). The MIS 3 advances are coeval with a peak in the EPICA Dome C dust record between ca. 31-37 ka (Lambert *et al*., 2008). Such dust peaks have previously been correlated with glacier advances in southern Patagonia (Sugden *et al*., 2009). There is also a trend of decreasing sea surface temperatures in the marine offshore record, near the coast of Chile (41° S), during the late MIS 3 (Kaiser *et al*., 2005; Lamy *et al*., 2004). The apparent absence of an MIS 3 glacier advance in central Patagonia (with the exception of some tentative evidence; Smedley *et al*., 2016; Hein *et al*., 2010) is therefore puzzling. The absence of this signal in central Patagonia might be due to: 1) lack of discovery 2) the large LBA/LP outlet glaciers failing to respond to this climate signal; 3) calving into

large proglacial lakes that might have decoupled these outlet glaciers from climate; 4) pre-LGM advances were later obliterated by a more extensive LGM advance; or 5) pre-LGM moraines were removed by focused meltwater erosion as a consequence of the over-deepened nature of the big glacial basins of central Patagonia (e.g. Hein *et al*., 2017). Determining the geographic extent of the MIS 3 advance and the global LGM should be a priority for resolving the drivers of southern hemisphere mountain glaciation. Thus, in central and, in particular, northern Patagonia, there is a need to derive detailed glacial chronologies for what are assumed to be LGM and pre-LGM moraines. Ideally, moraines should be targeted for dating in valleys where complication by points 3) and 5) can be avoided. Robust chronologies are required to confidently resolve the occurrence, or absence, of the MIS 3 advance in central Patagonia, to determine its geographic extent relative to the global LGM limits, and to explore the drivers of southern hemisphere glaciation through modelling.

5.2. Lateglacial

The Lateglacial ice marginal positions are poorly constrained and the occurrence of the ACR and/or YD is equivocal in central Patagonia. Only at one site, the Tranquilo Glacier, moraines have been dated to the ACR (E. Sagredo, personal communication, 2017). The offshore pollen record is the only palaeoenvironmental proxy, which firmly shows a vegetation change indicative of cooling coeval with the ACR (Montade *et al*., 2013). Other palaeovegetation proxies, however, do not indicate any significant vegetation changes from which cooling contemporaneous with either the ACR or YD may be inferred. An exception to this is a chironomid record, from which minor cooling at the time of YD was inferred (Massaferro and Brooks, 2002). Proxies from the eastern side of the Andes show high variability in effective moisture during the Lateglacial (15-11 ka), which together with the degree of insensitivity of proxies to minor oscillations in temperature might have masked any less pronounced cooling coeval with either the ACR or YD. Moraines deposited by the eastern outlet glaciers of the NPI, were dated at the Lateglacial/Holocene transition, which might represent YD readvances or stillstands (Glasser *et al*., 2012). Obtaining minimum and/or maximum radiocarbon ages for some of these moraines would provide further chronological control needed to improve dating resolution. Obtaining chronological constrains from undated, likely Lateglacial, moraines on the western side of the Andes, would fill the spatial and temporal gap and help to evaluate the relative extent of glaciers during ACR and YD. On the eastern side of the Andes moraines unaffected by regional lake inundation should be targeted for dating. The existence of the regional pro-glacial lake implies substantial ice mass and ice margin stabilization to maintain the ice damn. The lake was probably in existence since the retreat of ice from the position of the Menucos moraines and the youngest Río Blanco moraines at LP. The inconsistency in the interpretation of radiocarbon and OSL ages from shorelines renders the history of the lake open to debate. Resolving the lake history is important for understanding the wider deglacial history, especially since such lakes may have decoupled glacier response from climate by invoking calving dynamics.

5.3. Holocene

Much of the early work on Holocene glacial advances often relied on single minimum/maximum radiocarbon age from a given locality (see Glasser *et al*., 2004). It is only in last decade and a half that a wider range of dating techniques such as OSL, more robust radiocarbon chronologies, and cosmogenic nuclide dating have been applied to date Holocene glacial advances in Patagonia (e.g. Strelin *et al*., 2011, 2014; Kaplan *et al*., 2016; Harrison *et al*., 2012). Yet, evidence for Holocene glacier advances in central Patagonia remains sparse and poorly constrained. The available evidence suggests that the glaciers in central Patagonia advanced or stabilised at the Lateglacial/Holocene transition, while the contemporary palaeoenvironmental proxies revealed warm and dry conditions throughout central Patagonia. The explanation for this is unclear, within dating uncertainties, these advances might represent Lateglacial events. Alternatively, more easterly penetration of the SWWs and precipitation due to a diminishing NPI could have promoting advances of glaciers in the higher mountains east of the NPI as suggested by modelling experiments (Hubbard *et al*., 2005). There is far less evidence for moraines deposited during the mid-Holocene, with only one moraine (Tranquilo valley) directly dated (Sagredo *et al*., 2016), when palaeoenvironmental records showed colder and/or wetter conditions. The duration of these climatic changes evident from palaeoenvironmental proxies varied between sites. The timing and pattern of Holocene glacial advances in central Patagonia remains elusive. Improvements in cosmogenic nuclide dating methods have enabled increasingly younger surfaces to be dated. In combination with bracketing radiocarbon ages, this approach would provide robust chronological control in order to determine the pattern of Holocene glacier advances.

6. Acknowledgements

We thank the UK Natural Environment Research Council and University of Edinburgh for Monika Mendelova's Ph.D. studentship.

References

Ackert, R., Becker, R.A., Singer, B.S., Kurz, M.D., Caffee, M.W., Mickelson, D.M. 2008. Patagonian Glacier Response during the Late Glacial - Holocene Transition. *Science* 321, 5887, 392-396. https://doi.org/10.1126/science.1157215.

Aravena, J.C., Luckman, B.H. 2009. Spatio-temporal rainfall patterns in 542 Southern South America. *International Journal of Climatology* 29, 2106-2120. http://doi.org/10.1002/joc.1761

Balco, G., Stone, J.O., Lifton, N.A., Dunai, T.J. 2008. A complete and easily accessible means of calculating surface exposure ages or erosion rates from ^{10}Be and ^{26}Al measurements. *Quaternary Geochronology* 3 (3), 174-195. http://doi.org/10.1016/j.quageo.2007.12.001.

Bamonte, F.P., Mancini, M.V. 2011. Palaeoenvironmental changes since Pleistocene-Holocene transition: Pollen analysis from a wetland in southwestern Patagonia (Argentina). *Review of Palaeobotany and Palynology* 165 (1-2), 103-110. http://doi.org/10.1016/j.revpalbo.2011.02.003.

Bell, C.M. 2008. Punctuated drainage of an ice-damned Quaternary lake in Southern South America. *Geografiska Annaler* 90A (1), 1-17. http://doi.org/10.1111/j.1468-0459.2008.00330.x.

Bennett, K.D., Haberle, S.G., Lumley, S.H. 2000. The Last Glacial-Holocene Transition in Southern Chile. *Science* 290, 325-328. https://doi.org/10.1126/science.290.5490.325.

Bertrand, S., Hughen, K.A., Lamy, F., Stuut, J.B.W., Torrejón, F., Lange, C.B. 2012. Precipitation as the main driver of Neoglacial fluctuations of Gualas glacier, Northern Patagonian Icefield. *Climate of the Past* 8 (2), 519-534. http://doi.org/10.5194/cp-8-519-2012.

Boex, J., Fogwill, C., Harrison, S., Glasser, N.F., Hein, A., Schnabel, C., Xu, S. 2013. Rapid thinning of the late Pleistocene Patagonian Ice Sheet followed migration of the Southern Westerlies. *Scientific Reports* 3, 2118. http://doi.org/10.1038/srep02118.

Bourgois, J., Cisternas, M.E., Braucher, R., Bourlès, D., Frutos, J. 2016. Geomorphic Records along the General Carrera (Chile)-Buenos Aires (Argentina) Glacial Lake (46°-48°S), Climate Inferences, and Glacial Rebound for the Past 7-9 ka. *The Journal of Geology* 124 (1), 27-53. http://doi.org/10.1086/687551

Bronk Ramsey, C. 2009. Bayesian Analysis of Radiocarbon Dates. *Radiocarbon* 51 (1), 337-360. https://doi.org/10.1017/S0033822200033865.

Caldenius, C.R.C. 1932. Las glaciaciones cuaternarias en la Patagonia y Tierra del Fuego. *Geografiska Annaler* 14, 1-164. https://www.jstor.org/stable/pdf/519583.pdf.

Carrivick, J.L., Davies, B.J., James, W.H.M., Quincey, D.J., Glasser, N.F. 2016. Distributed ice thickness and glacier volume in southern South America. *Global and Planetary Change* 146, 122-132. http://doi.org/10.1016/j.gloplacha.2016.09.010.

Clapperton, C.M. 1993. Nature of environmental changes in South America at the Last Glacial Maximum. *Palaeogeography, Palaeoclimatology, Palaeoecology* 101 (3-4), 189-208. https://doi.org/10.1016/0031-0182(93)90012-8.

Clark, P.U., Dyke, A.S., Shakun, J.D., Carlson, A.E., Clark, J., Wohlfarth, B., Mitrovica, J.X., Hostetler, S.W., McCabe, A.M. 2009. The Last Glacial Maximum. *Science* 325, 710-714. https://doi.org/10.1126/science.1172873.

Darvill, C.M., Bentley, M.J., Stokes, C.R., Hein, A.S., Rodés, Á. 2015. Extensive MIS 3 glaciation in southernmost Patagonia revealed by cosmogenic nuclide dating of outwash sediments. *Earth and Planetary Science Letters* 429, 157-169. http://doi.org/10.1016/j.epsl.2015.07.030.

Davies, B.J., Glasser, N.F. 2012. Accelerating shrinkage of Patagonian glaciers from the Little Ice Age (~AD 1870) to 2011. *Journal of Glaciology* 58 1063-1084. https://doi.org/10.3189/2012JoG12J026.

Denton, G.H., Lowell, T. V, Heusser, C.J., Schluchter, C., Andersen, B.G., Heusser, L.E., Moreno, P.I., Marchant, D.R. 1999. Geomorphology, stratigraphy, and radiocarbon chronology of LlanquihueDrift in the area of the Southern Lake District, Seno Reloncaví, and Isla Grande de Chiloé, Chile. *Geografiska Annaler Series A Physical Geography* 81A (2), 167-229. http://doi.org/10.1111/1468-0459.00057.

de Porras, M.E., Maldonado, A., Abarzúa, A.M., Cárdenas, M.L., Francois, J.P., Martel-Cea, A., Stern, C.R., Méndez, C., Reyes, O. 2012. Postglacial vegetation, fire and climate dynamics at Central Chilean Patagonia (Lake Shaman, 44°S). *Quaternary Science Reviews* 50, 71-85. http://doi.org/10.1016/j.quascirev.2012.06.015.

de Porras, M.E., Maldonado, A., Quintana, F.A., Martel-Cea, A., Reyes, O., Méndez, C. 2014. Environmental and climatic changes in central Chilean Patagonia since the Late Glacial (Mallín El Embudo, 44°S). *Climate of the Past* 10 (3), 1063-1078. http://doi.org/10.5194/cp-10-1063-2014.

Doughty, A.M., Schaefer, J.M., Putnam, A.E., Denton, G.H., Kaplan, M.R., Barrell, D.J.A., Andersen, B.G., Kelley, S.E., Finkel, R.C., Schwartz, R. 2015. Mismatch of glacier extent and summer insolation in Southern Hemisphere mid-latitudes. *Geology* 43 (5), 407-410. https://doi.org/10.1130/G36477.1.

Douglass, D., Singer, B., Kaplan, M., Mickelson, D., Caffee, M. 2006. Cosmogenic nuclide surface exposure dating of boulders on last-glacial and late-glacial moraines, Lago Buenos Aires,

Argentina: Interpretive strategies and paleoclimate implications. *Quaternary Geochronology* 1 (1), 43-58. http://doi.org/10.1016/j.quageo.2006.06.001.

Douglass, D.C., Bockheim, J.G. 2006. Soil-forming rates and processes on Quaternary moraines near Lago Buenos Aires, Argentina. *Quaternary Research* 65 (2), 293-307. http://doi.org/10.1016/j.yqres.2005.08.027.

Douglass, D.C., Singer, B.S., Kaplan, M.R., Ackert, R.P., Mickelson, D.M., Caffee, M.W. 2005. Evidence of early Holocene glacial advances in southern South America from cosmogenic surface-exposure dating. *Geology* 33 (3), 237-240. https://doi.org/10.1130/G21144.1.

Dowdeswell, J.A., Dowdeswell, E.K., Rodrigo, C., Diaz, J. 2016. Assemblage of glacial and related landforms in the fjords of southern Chile. In: J.A. Dowdeswell, M. Canals, M. Jakobsson, J. Todd, E.K. Dowdeswell, K.A. Hogan (Eds.), Geological Society, London, Memoirs: 131-134. http://www.submarineglacialatlas.com/authors/examples/assemblage/assemblage1oct.pdf.

Dowdeswell, J.A., Vásquez, M. 2013. Submarine landforms in the fjords of southern Chile: Implications for glacimarine processes and sedimentation in a mild glacier-influenced environment. *Quaternary Science Reviews* 64, 1-19. http://doi.org/10.1016/j.quascirev.2012.12.003.

Fernandez, R., Anderson, J., Bertrand, S., Wellner, J. 2012. Gualas Glacier sedimentary record of climate and environmental change, Golfo Elefantes, Western Patagonia (46.5°S). *Holocene* 22 (4), 451-463. https://doi.org/10.1177/0959683611425545.

Fogwill, C.J., Kubik, P.W. 2005. A glacial stage spanning the Antarctic Cold Reversal in Torres del Paine (51°S), Chile, based on preliminary cosmogenic exposure ages. *Geografiska Annaler, Series A: Physical Geography* 87 (2), 403-408. http://doi.org/10.1111/j.0435-3676.2005.00266.x.

García, J.L., Kaplan, M.R., Hall, B.L., Schaefer, J.M., Vega, R.M., Schwartz, R., Finkel, R. 2012. Glacier expansion in southern Patagonia throughout the Antarctic cold reversal. *Geology* 40 (9), 859-862. https://doi.org/10.1130/G33164.1.

García, J.L., Hall, B.L., Kaplan, M.R., Vega, R.M., Strelin, J.A. 2014. Glacial geomorphology of the Torres del Paine region (southern Patagonia): Implications for glaciation, deglaciation and paleolake history. *Geomorphology* 204, 599-616. http://doi.org/10.1016/j.geomorph.2013.08.036.

Garreaud, R., López, P., Minvielle, M., Rojas, M. 2013. Large-scale control on the Patagonian climate. *Journal of Climate* 26 (1), 215-230. http://doi.org/10.1175/JCLI-D-12-00001.1.

Garreaud, R.D. 2009. The Andes climate and weather. *Advances in Geosciences* 22, 3-11. Doi:10.5194 / ADGEO-22-3-2009.

Garreaud, R.D., Vuille, M., Compagnucci, R., Marengo, J. 2009. Present-day South American climate. *Palaeogeography, Palaeoclimatology, Palaeoecology* 281 (3-4), 180-195. http://doi.org/10.1016/j.palaeo.2007.10.032.

Gilli, A., Anselmetti, F.S., Ariztegui, D., Beres, M., McKenzie, J.A., Markgraf, V. 2005. Seismic stratigraphy, buried beach ridges and contourite drifts: the Late Quaternary history of the closed Lago Cardiel basin, Argentina (49°S). *Sedimentology* 52, 1, 1-23. http://doi.org/10.1111/j.1365-3091.2004.00677.x.

Glasser, N.F., Ghiglione, M.C. 2009. Structural, tectonic and glaciological controls on the evolution of fjord landscapes. *Geomorphology* 105, 3-4, 291-302. http://doi.org/10.1016/j.geomorph.2008.10.007.

Glasser, N.F., Harrison, S., Ivy-Ochs, S., Duller, G.A.T., Kubik, P.W. 2006. Evidence from the Rio Bayo valley on the extent of the North Patagonian Icefield during the Late Pleistocene-Holocene transition. *Quaternary Research* 65, 1, 70-77. Doi:http://doi.org/10.1016/j.yqres.2005.09.002.

Glasser, N.F., Harrison, S., Schnabel, C., Fabel, D., Jansson, K.N. 2012. Younger Dryas and early Holocene age glacier advances in Patagonia. *Quaternary Science Reviews* 58, 7-17. http://doi.org/10.1016/j.quascirev.2012.10.011.

Glasser, N.F., Harrison, S., Winchester, V., Aniya, M. 2004. Late Pleistocene and Holocene palaeoclimate and glacier fluctuations in Patagonia. *Global and Planetary Change* 43 (1-2), 79101. http://doi.org/10.1016/j.gloplacha.2004.03.002.

Glasser, N.F., Jansson, K., Mitchell, W.A., Harrison, S. 2006. The geomorphology and sedimentology of the 'Témpanos' moraine at Laguna San Rafael, Chile. *Journal of Quaternary Science* 21 (6), 629-643. http://doi.org/10.1002/jqs.1002.

Glasser, N.F., Jansson, K.N. 2005. Fast-flowing outlet glaciers of the Last Glacial Maximum Patagonian Icefield. *Quaternary Research* 63 (2), 206-211. http://doi.org/10.1016/j.yqres.2004.11.002.

Glasser, N.F., Jansson, K.N., Duller, G.A.T., Singarayer, J., Holloway, M., Harrison, S. 2016. Glacial lake drainage in Patagonia (13-8 kyr) and response of the adjacent Pacific Ocean. *Scientific reports* 6, 21064. http://doi.org/10.1038/srep21064.

Glasser, N.F., Jansson, K.N., Goodfellow, B.W., de Angelis, H., Rodnight, H., Rood, D.H. 2011. Cosmogenic nuclide exposure ages for moraines in the Lago San Martin Valley, Argentina. *Quaternary Research* 75 (3), 636-646. http://doi.org/10.1016/j.yqres.2010.11.005.

Glasser, N.F., Jansson, K.N., Harrison, S., Kleman, J. 2008. The glacial geomorphology and Pleistocene history of South America between 38°S and 56°S. *Quaternary Science Reviews* 27 (3-4), 365-390. http://doi.org/10.1016/j.quascirev.2007.11.011.

Gutiérrez, F., Gioncada, A., González Ferran, O., Lahsen, A., Mazzuoli, R. 2005. The Hudson Volcano and surrounding monogenetic centres (Chilean Patagonia): An example of volcanism associated with ridge-trench collision environment. *Journal of Volcanology and Geothermal Research* 145 (3-4), 207-233. http://doi.org/10.1016/j.jvolgeores.2005.01.014.

Haberle, S.G., Bennett, K.D. 2004. Postglacial formation and dynamics of North Patagonian Rainforest in the Chonos Archipelago, Southern Chile. *Quaternary Science Reviews* 23, 2433-2452. http://doi.org/10.1016/j.quascirev.2004.03.001.

Harrison, S., Glasser, N., Winchester, V., Haresign, E., Warren, C., Duller, G.A.T., Bailey, R., Ivy-Ochs, S., Jansson, K., Kubik, P. 2008. Glaciar León, Chilean Patagonia: late-Holocene chronology and geomorphology. *The Holocene* 18 (4), 643-652. https://doi.org/10.1177/0959683607086771.

Harrison, S. 2004. The Pleistocene Glaciations of Chile. *Developments in Quaternary Sciences* 2, part C, 89-103. https://doi.org/10.1016/S1571-0866(04)80115-5.

Harrison, S., Glasser, N.F., Duller, G.A.T., Jansson, K.N. 2012. Early and mid-Holocene age for the Tempanos moraines, Laguna San Rafael, Patagonian Chile. *Quaternary Science Reviews* 31, 82-92. http://doi.org/10.1016/j.quascirev.2011.10.015.

Hein, A.S., Cogez, A., Darvill, C.M., Mendelova, M., Kaplan, M.R., Herman, F., Dunai, T.J., Norton, K., Xu, S., Christl, M., Rodés, Á. 2017. Regional mid-Pleistocene glaciation in central Patagonia. *Quaternary Science Reviews* 164, 77-94. https://doi.org/10.1016/j.quascirev.2017.03.023.

Hein, A.S., Hulton, N.R.J., Dunai, T.J., Schnabel, C., Kaplan, M.R., Naylor, M., Xu, S. 2009. Middle Pleistocene glaciation in Patagonia dated by cosmogenic-nuclide measurements on outwash gravels. *Earth and Planetary Science Letters* 286 (1-2), 184-197. http://doi.org/10.1016/j.epsl.2009.06.026.

Hein, A.S., Hulton, N.R.J., Dunai, T.J., Sugden, D.E., Kaplan, M.R., Xu, S. 2010. The chronology of the Last Glacial Maximum and deglacial events in central Argentine Patagonia. *Quaternary Science Reviews* 29 (9-10), 1212-1227. http://doi.org/10.1016/j.quascirev.2010.01.020.

Henríquez, W.I., Villa-Martínez, R., Vilanova, I., De Pol-Holz, R., Moreno, P. 2017. The Last Glacial Termination on the eastern flank of the central Patagonian Andes (47°S). *Climate of the Past Discussions* 13, 879-895. http://doi.org/10.5194/cp-13-879-2017.

Heusser, C.J. 2002. On glaciation of the southern Andes with special reference to the Peninsula de Taitao and adjacent Andean cordillera (46°30's). *Journal of South American Earth Sciences* 15 (5), 577-589. http://doi.org/10.1016/S0895-9811(02)00076-7.

Hogg, A.G., Hua, Q., Blackwell, P.G., Niu, M., Buck, C.E., Guilderson, T.P., Heaton, T.J., Palmer, J.G., Reimer, P.J., Reimer, R.W., Turney, C.S.M., Zimmerman, S.R.H. 2013. SHCal13 Southern Hemisphere Calibration, 0-50,000 Years cal BP. *Radiocarbon* 55 (4), 1889-1903. https://doi.org/10.2458/azu_js_rc.55.16783.

Hubbard, A., Hein, A.S., Kaplan, M.R., Hulton, N.R.J., Glasser, N.F. 2005. A Modelling Reconstruction Of The Last Glacial Maximum Ice Sheet And Its Deglaciation In The Vicinity Of The Northern Patagonian Icefield, South America. *Geografiska Annaler, Series A: Physical Geography* 87 (2), 375-391. http://doi.org/10.1111/j.0435-3676.2005.00264.x.

Iglesias, V., Markgraf, V., Whitlock, C. 2016. 17,000 years of vegetation, fire and climate change in the eastern foothills of the Andes (lat. 44°S). *Palaeogeography, Palaeoclimatology, Palaeoecology* 457, 195-208. http://doi.org/10.1016/j.palaeo.2016.06.008.

Kaiser, J., Lamy, F., Hebbeln, D. 2005. A 70-kyr sea surface temperature record off southern Chile (Ocean Drilling Program Site 1233). *Paleoceanography* 20 (4), PA4009. http://doi.org/10.1029/2005PA001146.

Kaplan, M.R., Ackert, R.P., Singer, B.S., Douglass, D.C., Kurz, M.D. 2004. Cosmogenic nuclide chronology of millennial-scale glacial advances during O-isotope stage 2 in Patagonia. *Bulletin of the Geological Society of America* 116 (3-4), 308-321. https://doi.org/10.1130/B25178.1.

Kaplan, M.R., Moreno, P.I., Rojas, M. 2008a. Glacial dynamics in southernmost South America during Marine Isotope Stage 5e to the Younger Dryas chron: a brief review with a focus on cosmogenic nuclide measurements. *Journal of Quaternary Science* 23 (6-7), 649-658. http://doi.org/10.1002/jqs.1209.

Kaplan, M.R., Fogwill, C.J., Sugden, D.E., Hulton, N.R.J., Kubik, P.W., Freeman, S.P.H.T. 2008b. Southern Patagonian glacial chronology for the Last Glacial period and implications for Southern Ocean climate. *Quaternary Science Reviews* 27 (3-4), 284-294. http://doi.org/10.1016/j.quascirev.2007.09.013.

Kaplan, M.R., Schaefer, J.M., Denton, G.H., Barrell, D.J., Chinn, T.J., Putnam, A.E., Andersen, B.G., Finkel, R.C., Schwartz, R., Doughty, A.M. 2010. Glacier retreat in New Zealand during the Younger Dryas stadial. *Nature* 467, 194-197. http://doi.org/10.1038/nature09313.

Kaplan, M.R., Schaefer, J.M., Denton, G.H., Doughty, A.M., Barrell, D.J.A., Chinn, T.J.H., Putnam, A.E., Andersen, B.G., Mackintosh, A., Finkel, R.C., Schwartz, R., Anderson, B. 2013. The anatomy of long-term warming since 15 ka in New Zealand based on net glacier snowline rise. *Geology* 41 (8), 887-890. https://doi.org/10.1130/G34288.1.

Kaplan, M.R., Schaefer, J.M., Strelin, J.A., Denton, G.H., Anderson, R.F., Vandergoes, M.J., Finkel, R.C., Schwartz, R., Travis, S.G., Garcia, J.L., Martini, M.A., Nielsen, S.H.H. 2016. Patagonian and southern South Atlantic view of Holocene climate. *Quaternary Science Reviews* 141, 112-125. http://doi.org/10.1016/j.quascirev.2016.03.014.

Kaplan, M.R., Strelin, J.A., Schaefer, J.M., Denton, G.H., Finkel, R.C., Schwartz, R., Putnam, A.E., Vandergoes, M.J., Goehring, B.M., Travis, S.G. 2011. In-situ cosmogenic ^{10}Be production rate at Lago Argentino, Patagonia: Implications for late-glacial climate chronology. *Earth and Planetary Science Letters* 309 (1-2), 21-32. http://doi.org/10.1016/j.epsl.2011.06.018.

Kelley, S.E., Kaplan, M.R., Schaefer, J.M., Andersen, B.G., Barrell, D.J.A., Putnam, A.E., Denton, G.H., Schwartz, R., Finkel, R.C., Doughty, A.M. 2014. High-precision ^{10}Be chronology of moraines in the Southern Alps indicates synchronous cooling in Antarctica and New Zealand 42,000 years ago. *Earth and Planetary Science Letters* 405, 194-206. http://doi.org/10.1016/j.epsl.2014.07.031.

Lagabrielle, Y., Suárez, M., Rossello, E.A., Hérail, G., Martinod, J., Régnier, M., de la Cruz, R. 2004. Neogene to Quaternary tectonic evolution of the Patagonian Andes at the latitude of the Chile Triple Junction. *Tectonophysics* 385, 211-241. http://doi.org/10.1016/j.tecto.2004.04.023.

Lambert, F., Delmonte, B., Petit, J.R., Bigler, M., Kaufmann, P.R., Hutterli, M.A., Stocker, T.F., Ruth, U., Steffensen, J.P., Maggi, V. 2008. Dust-climate couplings over the past 800,000 years from the EPICA Dome C ice core. *Nature* 452, 616-619. http://doi.org/10.1038/nature06763.

Lamy, F., Kaiser, J., Ninnemann, U., Hebbeln, D., Arz, H.W., Stoner, J. 2004. Antarctic timing of surface water changes off Chile and Patagonian ice sheet response. *Science* 304, 1959-1962. https://doi.org/10.1126/science.1097863.

Lumley, S.H., Switsur, R. 1993. Late Quaternary Chronology of the Taitao peninsula, southern Chile. *Journal of Quaternary Science* 8 (2), 161-165. http://doi.org/10.1002/jqs.3390080208.

Mackintosh, A.N., Barrows, T.T., Colhoun, E.A., Fifield, L.K. 2006. Exposure dating and glacial reconstruction at Mt. Field, Tasmania, Australia, identifies MIS 3 and MIS 2 glacial advances and climatic variability. *Journal of Quaternary Science* 21, 363-376. http://doi.org/10.1002/jqs.989.

Markgraf, V., Whitlock, C., Haberle, S. 2007. Vegetation and fire history during the last 18,000 cal yr B.P. in Southern Patagonia: Mallín Pollux, Coyhaique, Province Aisén (45°41'30"S, 71°50'30" W, 640 m elevation). *Palaeogeography, Palaeoclimatology, Palaeoecology* 254 (3-4), 492-507. Doi:http://doi.org/10.1016/j.palaeo.2007.07.008.

Marrero, S.M., Phillips, F.M., Borchers, B., Lifton, N., Aumer, R., Balco, G. 2016a. Cosmogenic nuclide systematics and the CRONUScalc program. *Quaternary Geochronology* 31, 160-187. http://doi.org/10.1016/j.quageo.2015.09.005.

Marrero, S.M., Phillips, F.M., Caffee, M.W., Gosse, J.C. 2016b. CRONUS-Earth cosmogenic ^{36}Cl calibration. *Quaternary Geochronology* 31, 199-219. http://doi.org/10.1016/j.quageo.2015.10.002.

Massaferro, J., Brooks, S.J. 2002. Response of chironomids to late quaternary environmental change in the Taitao Peninsula, Southern Chile. *Journal of Quaternary Science* 17 (2), 101-111. http://dx.doi.org/10.1002/jqs.671.

McCulloch, R., Bentley, M., Tipping, R., Clapperton, C.M. 2005a. Evidence for Late-Glacial Ice Dammed Lakes In The Central Strait Of Magellan And Bahía Inútil, Southernmost South America. *Geografiska Annaler, Series A: Physical Geography* 87 (2), 335-362. http://doi.org/10.1111/j.0435-3676.2005.00262.x.

McCulloch, R.D., Bentley, M.J., Purves, R.S., Hulton, N.R.J., Sugden, D.E., Clapperton, C.M. 2000. Climatic inferences from glacial and palaeoecological evidence at the last glacial termination, southern South America. *Journal of Quaternary Science* 15 (4), 409-417. http://doi.org/10.1002/1099-1417(200005)15:4<409::AID-JQS539>3.0.CO;2-#.

McCulloch, R.D., Figuerero Torres, M.J., Mengoni Goñalons, G.L., Barclay, R., Mansilla, C. 2016. A Holocene record of environmental change from Rio Zeballos, central Patagonia. *The Holocene*. https://doi.org/10.1177/0959683616678460.

McCulloch, R.D., Fogwill, C.J., Sugden, D.E., Bentley, M.J., Kubik, P.W. 2005b. Chronology of the Last Glaciation in Central Strait of Magellan and Bahía Inútil, Southernmost South America. *Geografiska Annaler, Series A: Physical Geography* 87 (2), 289-312. http://doi.org/10.1111/j.0435-3676.2005.00260.x.

Menounos, B., Clague, J.J., Osborn, G., Davis, P.T., Ponce, F., Goehring, B.M., Maurer, M., Rabassa, J.O., Coronato, A., Marr, R. 2013. Latest Pleistocene and Holocene glacier fluctuations in southernmost Tierra del Fuego, Argentina. *Quaternary Science Reviews* 77, 70-79. http://doi.org/10.1016/j.quascirev.2013.07.008.

Mercer, J.H. 1968. Variations of some Patagonian glaciers since the Late-Glacial. *American Journal of Science* 266 (2), 91-109. http://dx.doi.org/10.2475/ajs.266.2.91.

Mercer, J.H. 1976. Glacial history of southernmost South America. *Quaternary Research* 6 (2), 125-166. https://doi.org/10.1016/0033-5894(76)90047-8.

Mercer, J.H. 1982. Holocene glacier variations in southern South America. *Striae* 18, 35-40.

Mercer, J.H. 1983. Cenozoic glaciation in the Southern Hemisphere. *Annual Review Earth Planetary Sciences* 11, 99-132. http://doi.org/10.1146/annurev.ea.11.050183.000531.

Montade, V., Combourieu Nebout, N., Kissel, C., Haberle, S.G., Siani, G., Michel, E. 2013. Vegetation and climate changes during the last 22,000yr from a marine core near Taitao Peninsula, southern Chile. *Palaeogeography, Palaeoclimatology, Palaeoecology* 369, 335-348. http://doi.org/10.1016/j.palaeo.2012.11.001.

Moreno, P.I., Denton, G.H., Moreno, H., Lowell, T.V., Putnam, A.E., Kaplan, M.R. 2015. Radiocarbon chronology of the last glacial maximum and its termination in northwestern Patagonia. *Quaternary Science Reviews* 122, 233-249. http://doi.org/10.1016/j.quascirev.2015.05.027.

Moreno, P.I., Kaplan, M.R., François, J.P., Villa-Martínez, R., Moy, C.M., Stern, C.R., Kubik, P.W. 2009. Renewed glacial activity during the Antarctic cold reversal and persistence of cold conditions until 11.5 ka in southwestern Patagonia. *Geology* 37 (4), 375-378. https://doi.org/10.1130/G25399A.1.

Pollock, E.W., Bush, A.B.G. 2013. Atmospheric simulations of southern South America's climate since the Last Glacial maximum. *Quaternary Science Reviews* 71, 219-228. http://doi.org/10.1016/j.quascirev.2012.09.019.

Putnam, A.E., Denton, G.H., Schaefer, J.M., Barrell, D.J.A., Andersen, B.G., Finkel, R.C., Schwartz, R., Doughty, A.M., Kaplan, M.R., Schlüchter, C. 2010. Glacier advance in southern middle-latitudes during the Antarctic Cold Reversal. *Nature Geoscience* 3, 700-704. http://doi.org/10.1038/ngeo962.

Putnam, A.E., Schaefer, J.M., Denton, G.H., Barrell, D.J. a., Birkel, S.D., Andersen, B.G., Kaplan, M.R., Finkel, R.C., Schwartz, R., Doughty, A.M. 2013. The Last Glacial Maximum at 44°S documented by a ^{10}Be moraine chronology at Lake Ohau, Southern Alps of New Zealand. *Quaternary Science Reviews* 62, 114-141. http://doi.org/10.1016/j.quascirev.2012.10.034.

Rabassa, J., Clapperton, C.M. 1990. Quaternary Glaciations of the Southern Andes. *Quaternary Science Reviews* 9, 153-174. https://doi.org/10.1016/0277-3791(90)90016-4.

Rabassa, J., Coronato, A. 2009. Glaciations in Patagonia and Tierra del Fuego during the Ensenadan Stage/Age (Early Pleistocene-earliest Middle Pleistocene). *Quaternary International* 210 (1-2), 18-36. http://doi.org/10.1016/j.quaint.2009.06.019.

Rabassa, J., Coronato, A., Bujalesky, G., Salemme, M., Roig, C., Meglioli, A., Heusser, C., Gordillo, S., Roig, F., Borromei, A., Quattrocchio, M. 2000. Quaternary of Tierra del Fuego, Southernmost South America: an updated review. *Quaternary International* 68-71, 217-240. http://doi.org/10.1016/S1040-6182(00)00046-X.

Rabassa, J.O.J., Coronato, A., Martínez, O. 2011. Late Cenozoic glaciations in Patagonia and Tierra del Fuego: an updated review. *Biological Journal of the Linnean Society* 103 (2), 316-335. http://doi.org/10.1111/j.1095-8312.2011.01681.x.

Rivera, A., Benham, T., Casassa, G., Bamber, J., Dowdeswell, J.A. 2007. Ice elevation and areal changes of glaciers from the Northern Patagonia Icefield, Chile. *Global and Planetary Change* 59 (1-4), 126-137. http://doi.org/10.1016/j.gloplacha.2006.11.037.

Rodbell, D.T., Smith, J.A., Mark, B.G. 2009. Glaciation in the Andes during the Lateglacial and Holocene. *Quaternary Science Reviews* 28, 2165-2212. http://doi.org/10.1016/j.quascirev.2009.03.012.

Rojas, M., Moreno, P., Kageyama, M., Crucifix, M., Hewitt, C., Abe-Ouchi, A., Ohgaito, R., Brady, E.C., Hope, P. 2009. The Southern Westerlies during the last glacial maximum in PMIP2 simulations. *Climate Dynamics* 32 (4), 525-548. http://doi.org/10.1007/s00382-008-0421-7.

Rother, H., Shulmeister, J., Fink, D., Alexander, D., Bell, D. 2015. Surface exposure chronology of the Waimakariri glacial sequence in the Southern Alps of New Zealand: Implications for MIS-2 ice extent and LGM glacial mass balance. *Earth and Planetary Science Letters* 429, 69-81. http://doi.org/10.1016/j.epsl.2015.07.033.

Sagredo, E.A., Lowell, T.V., Kelly, M.A., Rupper, S., Aravena, J.C., Ward, D.J., Malone, A.G. 2016. Equilibrium line altitudes along the Andes during the Last millennium: Paleoclimatic implications. *The Holocene*. https://doi.org/10.1177/0959683616678458.

Sagredo, E.A., Moreno, P.I., Villa-Martínez, R., Kaplan, M.R., Kubik, P.W., Stern, C.R. 2011. Fluctuations of the Última Esperanza ice lobe (52°S), Chilean Patagonia, during the last glacial maximum and termination 1. *Geomorphology* 125 (1), 92-108. http://doi.org/10.1016/j.geomorph.2010.09.007.

Schaefer, J.M., Denton, G.H., Barrell, D.J.A., Ivy-Ochs, S., Kubik, P.W., Andersen, B.G., Phillips, F.M., Lowell, T. V., Schlüchter, C. 2006. Near-Synchronous Interhemispheric Termination of the Last Glacial Maximum in Mid-Latitudes. *Science* 312, 1510-1513. https://doi.org/10.1126/science.1122872.

Schaefer, J.M., Putnam, A.E., Denton, G.H., Kaplan, M.R., Birkel, S., Doughty, A.M., Kelley, S., Barrell, D.J.A., Finkel, R.C., Winckler, G., Anderson, R.F., Ninneman, U.S., Barker, S., Schwartz, R., Andersen, B.G., Schluechter, C. 2015. The Southern Glacial Maximum 65,000 years ago and its Unfinished Termination. *Quaternary Science Reviews* 114, 52-60. http://doi.org/10.1016/j.quascirev.2015.02.009.

Siani, G., Colin, C., Michel, E., Carel, M., Richter, T., Kissel, C., Dewilde, F. 2010. Late Glacial to Holocene terrigenous sediment record in the Northern Patagonian margin: Paleoclimate implications. *Palaeogeography, Palaeoclimatology, Palaeoecology* 297 (1), 26-36. http://doi.org/10.1016/j.palaeo.2010.07.011.

Singer, B.S., Ackert, R.P., Guillou, H. 2004. 40Ar/39Ar and K-Ar chronology of Pleistocene glaciations in Patagonia. *Geological Society of America Bulletin* 116 (3-4), 434-450. http://doi.org/10.1130/B25177.1.

Smedley, R.K., Glasser, N.F., Duller, G.A.T. 2016. Luminescence dating of glacial advances at Lago Buenos Aires (~46°S), Patagonia. *Quaternary Science Reviews* 134, 59-73. http://doi.org/10.1016/j.quascirev.2015.12.010.

Stern, C.R. 2004. Active Andean volcanism: its geologic and tectonic setting. *Revista Geológica de Chile* 31 (2), 1-51.

Strelin, J.A., Denton, G.H., Vandergoes, M.J., Ninnemann, U.S., Putnam, A.E. 2011. Radiocarbon chronology of the late-glacial Puerto Bandera moraines, Southern Patagonian Icefield, Argentina. *Quaternary Science Reviews* 30, 19-20, 2551-2569. http://doi.org/10.1016/j.quascirev.2011.05.004.

Strelin, J.A., Kaplan, M.R., Vandergoes, M.J., Denton, G.H., Schaefer, J.M. 2014. Holocene glacier history of the Lago Argentino basin, Southern Patagonian Icefield. *Quaternary Science Reviews* 101, 124-145. http://doi.org/10.1016/j.quascirev.2014.06.026.

Sugden, D.E., Bentley, M.J., Fogwill, C.J., Hulton, N.R.J., McCulloch, R.D., Purves, R.S. 2005. Late-Glacial Glacier Events in Southernmost South America: a Blend of 'Northern' and 'Southern' Hemispheric Climatic Signals ? *Geografiska Annaler, Series A: Physical Geography* 87 (2), 273-288. http://doi.org/10.1111/j.0435-3676.2005.00259.x.

Sugden, D.E., McCulloch, R.D., Bory, A.J.-M., Hein, A.S. 2009. Influence of Patagonian glaciers on Antarctic dust deposition during the last glacial period. *Nature Geoscience* 2 (4), 281-285. http://doi.org/10.1038/ngeo474.

Sylwan, C.A. 1989. *Paleomagnetism, paleoclimate, and chronology of Late Cenozoic deposits in southern Argentina*. Stockholm University.

Toggweiler, J.R., Russell, J.L., Carson, S.R. 2006. Midlatitude westerlies, atmospheric CO_2, and climate change during the ice ages. *Paleoceanography* 21 (2), 1-15. http://doi.org/10.1029/2005PA001154.

Turner, K.J., Fogwill, C.J., McCulloch, R.D., Sugden, D.E. 2005. Deglaciation of The Eastern Flank Of The North Patagonian Icefield And Associated Continental-Scale Lake Diversions. *Geografiska Annaler, Series A: Physical Geography* 87 (2), 363-374. http://doi.org/10.1111/j.0435-3676.2005.00263.x.

Turney, C.S.M., Roberts, R.G., de Jonge, N., Prior, C., Wilmshurst, J.M., McGlone, M.S., Cooper, J. 2007. Redating the advance of the New Zealand Franz Josef Glacier during the Last Termination: evidence for asynchronous climate change. *Quaternary Science Reviews* 26, 3037-3042. http://doi.org/10.1016/j.quascirev.2007.09.014.

Van Daele, M., Bertrand, S., Meyer, I., Moernaut, J., Vandoorne, W., Siani, G., Tanghe, N., Ghazoui, Z., Pino, M., Urrutia, R., De Batist, M. 2016. Late Quaternary evolution of Lago

Castor (Chile, 45.6°S): Timing of the deglaciation in northern Patagonia and evolution of the southern westerlies during the last 17 kyr. *Quaternary Science Reviews* 133, 130-146. http://doi.org/10.1016/j.quascirev.2015.12.021.

Vandekerkhove, E., Bertrand, S., Reid, B., Bartels, A., Charlier, B. 2016. Sources of dissolved silica to the fjords of northern Patagonia (44-48°S): The importance of volcanic ash soil distribution and weathering. *Earth Surface Processes and Landforms* 41 (4), 499-512. http://doi.org/10.1002/esp.3840.

Vanneste, H., De Vleeschouwer, F., Martínez-Cortizas, A., von Scheffer, C., Piotrowska, N., Coronato, A., Le Roux, G. 2015. Late-glacial elevated dust deposition linked to westerly wind shifts in southern South America. *Scientific reports* 5, 11670. http://doi.org/10.1038/srep11670.

Villa-Martínez, R., Moreno, P.I., Valenzuela, M.A. 2012. Deglacial and postglacial vegetation changes on the eastern slopes of the central Patagonian Andes (47°S). *Quaternary Science Reviews* 32, 86-99. http://doi.org/10.1016/j.quascirev.2011.11.008.

Völker, D., Geersen, J., Contreras-Reyes, E., Reichert, C. 2013. Sedimentary fill of the Chile Trench (32-46°S): volumetric distribution and causal factors. *Journal of the Geological Society* 170 (5), 723-736. https://doi.org/10.1144/jgs2012-119.

Warren, C.R., Sugden, D.E. 1993. The Patagonian Icefields: A Glaciological Review. *Arctic and Alpine Research* 25 (4), 316-331. http://doi.org/10.2307/1551915.